THE UNIVERSITY of ADELAIDE

FRP-CONCRETE-STEEL COMPOSITE STRUCTURAL MEMBERS

Yunita Idris

M.Eng (Structural Engineering)

B.Eng. (Civil Engineering)

Thesis submitted to The University of Adelaide

School of Civil, Environmental, and Mining Engineering

In fulfilment of the requirements

For the degree of Doctor of Philosophy

CONTENTS

CONTENTS ..... **I**

ABSTRACT ..... **III**

STATEMENT OF ORIGINALITY ..... **V**

ACKNOWLEDGEMENTS ..... **VII**

CHAPTER 1

INTRODUCTION **1**

CHAPTER 2

SEISMIC BEHAVIOR OF HIGH STRENGTH CONCRETE-FILLED FRP TUBE COLUMNS **5**

CHAPTER 3

SEISMIC BEHAVIOR OF FRP-HIGH-STRENGTH CONCRETE-STEEL DOUBLE-SKIN TUBULAR COLUMNS **53**

CHAPTER 4

BEHAVIOR OF SQUARE FRP-HSC-STEEL DOUBLE-SKIN TUBULAR COLUMNS UNDER COMBINED AXIAL COMPRESSION AND REVERSED-CYCLIC LATERAL LOADING **103**

CHAPTER 5

FLEXURAL BEHAVIOR OF FRP-HSC-STEEL COMPOSITE BEAMS **149**

CHAPTER 6

FLEXURAL BEHAVIOR OF FRP-HSC-STEEL TUBULAR BEAMS UNDER REVERSED CYCLIC LOADING **185**

CHAPTER 7

CONCLUSIONS **231**

REFERENCES **235**

ABSTRACT

The use of fibre reinforced polymer (FRP) composites as a confinement material for concrete has received a great deal of attention over the past two decades. Together with the retrofitting applications, the use of FRP as confinement material in the construction of new high-performance composite members in the form of concrete-filled FRP tubes has become increasingly popular. Following from the research on CFFTs, a new type of composite system, which consists of a steel tube inside, an FRP tube outside and a concrete sleeve sandwiched in between, has received significant recent research attention. These double-skin tubular (DST) beams and columns (referred to as DSTBs and DSTCs) rely on the same FRP tube confinement mechanism that is present in CFFTs, and through the combination of the advantages of the three constituent materials they can be designed to exhibit extremely high structural performance levels. The research reported in this thesis was aimed at investigating the behaviour of CFFT and DST structural members under various loading conditions. To this end, five experimental studies were designed and undertaken at the University of Adelaide.

First, an experimental study was conducted to investigate the seismic performance of high-strength concrete (HSC) CFFT columns, in which the column specimens were tested under combined axial compression and reversed-cyclic lateral loading. The seismic behaviour of the columns was evaluated on the basis of their experimentally recorded moment-lateral drift hysteretic relationships. Following this, four series of experimental studies were conducted on DSTCs and DSTBs, which consisted of tests on: i) circular and square DSTCs under combined axial compression and reversed-cyclic lateral loading, ii) circular and square cantilever DSTBs under reserved-cyclic loading, and iii) circular simply supported DSTBs under monotonically increasing four-point loading. The results of these

studies clearly indicate that DSTCs and DSTBs may provide an attractive alternative to CFFTs for the construction of new high-performance composite structural members. The results also show that the provision of a concrete-filling inside the inner steel tube of DSTCs significantly improves the overall behaviour of these columns.

STATEMENT OF ORIGINALITY

I certify that this work contains no material which has been accepted for the award of any other degree or diploma in my name, in any university or other tertiary institution and, to the best of my knowledge and belief, contains no material previously published or written by another person, except where due reference has been made in the test. In addition, I certify that no part of this work will, in the future, be used in a submission in my name, for any other degree or diploma in any university or other tertiary institution without the prior approval of the University of Adelaide and where applicable, any partner institution responsible for the joint-award of this degree.

I give consent to this copy of my thesis when deposited in the university Library, being made available for load and photocopying, subject to the provisions of the Copyright Act 1968.

The author acknowledges the copyright of published works contained within this thesis resides with the copyright holder(s) of those work.

I also give permission for the digital version of my thesis to be made available on the web, via the University's digital research repository, the Library Search and also through web search engines, unless permission has been granted by University to restrict access for a period of time.

Signed: Date: 02/10/2015

ACKNOWLEDGEMENTS

First and above all, I praise God, the almighty for providing me this opportunity.

My deepest gratitude is to my supervisor, Dr. Togay Ozbakkaloglu for his patience, motivation, immense knowledge and guidance helped me all the time during my research and writing of this thesis. I am also grateful to my co-supervisor Prof. Michael C Griffith for his advice and encouragement.

I acknowledge the financial support from The Government of Aceh, Indonesia through their The Institute for Improvement of Human Resource (LPSDM) Scholarships for sponsoring my study at the University of Adelaide.

My sincere thanks also goes to all academics and technical staff who have helped me with this thesis in their fields of expertise. In particular, I thank Mr. Ian Ogier, Dale Hodson and Gary Bowman who provided technical assistance throughout the experimental program and Ms Barbara Brougham who provided technical reviews of most of the publications presented in this thesis.

I would like to thank my fellow PhD students Ms. Nora Abdullah, Mr. Butje Alfonsius Louk Fanggi, Thomas Vincent, Jian Chin Lim, and Tianyu Xie for their friendship, encouragement, and help. Many thanks also to other PhD students in the School of Civil, Environmental and Mining Engineering who have helped me throughout the course of my study.

Finally and most importantly, I would like to express my gratitude to my husband, Rinaldi, my children, Nadine, Altair and Owais, and my parent for their constant love, support and concern.

CHAPTER 1

INTRODUCTION

Owing to their favourable material properties, fibre reinforced polymer (FRP) has become popular in the construction industry. An important application of FRP is as a confinement material for concrete. Recently, the use of FRP composites in the construction of new high-performance composite columns in the form of concrete-filled FRP tubes (CFFTs) has received significant attention in the research field. Following from the research on CFFTs, a new type of composite system, which consists of a steel tube inside, an FRP tube outside and a concrete sleeve sandwiched in-between had also been proposed. These FRP-concrete-steel double-skin tubular beams and columns (DSTBs and DSTCs) benefit from the same FRP tube confinement mechanism that is present in CFFTs and they offer a long list of advantages. In the construction of these DST structural systems, the use of high-strength concrete (HSC) is particularly attractive, as this ensures that the properties of concrete complements those of the other two high-strength constituents (i.e. steel and FRP) in a composite system that is designed to maximize the advantages offered by each constituent. However, as the research to date on the behaviour of DST structural members has been very limited, additional studies are required to better understand and be able to model the behaviour of these composite structural members.

Research objectives

The main objective of the research presented in this thesis is to establish clear understanding on the structural behaviour of different FRP-steel-concrete composite structural members (i.e. CFFTs, DSTBs and DSTCs) under various loading conditions. To

this end, a series of combined axial compression and reversed cyclic loading tests on CFFTs and DSTCs, reserved cyclic loading tests on cantilever DSTBs, and monotonic four-point loading tests on simply supported DSTBs have been performed to address the identified research gaps.

Thesis overview

This thesis is organized into eight chapters. Chapters 1 and 7 are the introduction and conclusions, whereas each of Chapters 2 to 6 is a manuscript that had been submitted for publication as journal article throughout the course of this study [1-5]. The parameters that are investigated in each of the experimental studies are summarized in Table 1.

As illustrated in Table 1, eleven key parameters on the behavior of CFFT columns, DST columns and beams were identified and investigated in this research program. The main parameters were member cross sectional shape, type of FRP tube, thickness of FRP tube, diameter of steel tube, thickness of steel tube, cross sectional shape of steel tube, concrete strength, presence (or absence) concrete-filling inside the steel tube, axial load ratio, member aspect ratio, and the presence (or absence) of mechanical connectors on steel tube. The performance of the specimens was assessed based their lateral displacement and energy dissipation capacities [1-3, 5]. Performance comparisons of different types of FRP-concrete-steel members (i.e. CFFTs and DSTCs) were also presented in this study [2-3].

Table 1. Summary of publications and test parameters investigated

Publications	Research area	Key parameters										
		Member cross-sectional shape	Type of FRP tube	Thickness of FRP tube	Diameter of steel tube	Thickness of steel tube	Cross sectional shape of steel tube	Concrete strength	Presence (absence) concrete-filling inside steel tube	Axial load ratio	Member aspect ratio	Presence (absence) of mechanical connectors on steel tube
Idris and Ozbakkaloglu [1]	Seismic behaviour of CFFT columns	Yes	Yes	Yes	-	-	-	-	-	Yes	-	-
Ozbakkaloglu and Idris [2]	Seismic behaviour of circular DSTCs	-	Yes	Yes	-	Yes	Yes	Yes	Yes	Yes	-	-
Idris and Ozbakkaloglu [3]	Seismic behaviour of square DSTCs	-	-	-	Yes	Yes	-	-	Yes	Yes	Yes	-
Idris and Ozbakkaloglu [4]	Flexural behaviour of DSTBs	Yes	-	-	Yes	Yes	Yes	-	Yes	-	-	Yes
Idris and Ozbakkaloglu [5]	Cyclic behaviour of cantilever DSTBs	-	-	-	Yes	Yes	-	Yes	Yes	-	-	Yes

References

[1] Idris, Y., and Ozbakkaloglu, T. (2013). “Seismic behavior of square high-strength concrete-filled FRP tube columns.” *Journal of Composites for Construction, ASCE,* 17(6): 04013013.

[2] Ozbakkaloglu, T., and Idris, Y. (2014), “Seismic behavior of FRP-high-strength concrete-steel double skin tubular columns.” *Journal of Structural Engineering, ASCE,* 140(6): 04014019.

[3] Idris, Y., and Ozbakkaloglu, T. (2015). “Behavior of square FRP-HSC-Steel double-skin tubular columns under combined axial compression and reversed-cyclic lateral loading.” *(submitted to Engineering Structures)*.

[4] Idris, Y., and Ozbakkaloglu, T. (2014). “Flexural behavior of FRP-HSC-steel composite beams.” *Thin-Walled Structures,* 80: 207-16.

[5] Idris, Y., and Ozbakkaloglu, T. (2015). “Flexural behavior of FRP-HSC-steel tubular beams under reversed cyclic loading.” *Thin-Walled Structures*, 87: 89-101.

CHAPTER 2

Seismic Behavior of High Strength Concrete-Filled FRP Tube Columns

Yunita Idris and Togay Ozbakkaloglu

School of Civil, Environmental, and Mining Engineering, University of Adelaide, 5000

Journal of Composites for Construction, ASCE (Published)

Statement of Authorship

Title of Paper	Seismic Behaviour of High-Strength Concrete-Filled FRP Tube Columns
Publication Status	● Published ○ Accepted for publication ○ Submitted for publication ○ Publication style
Publication Details	Idris, Y., and Ozbakkaloglu, T. (2013). "Seismic Behavior of High-Strength Concrete-Filled FRP Tube Columns." *Journal of Compositse for Construction*. 18(5): 715-738.

Author Contributions

By signing the Statement of Authorship, each author certifies that their stated contribution to the publication is accurate and that permission is granted for the publication to be included in the candidate's thesis.

Name of Principal Author (Candidate)	Yunita Idris		
Contribution to the Paper	Review of literature, analysis data, and preparation of manuscript		
Signature		Date	22/09/2015

Name of Co-Author	Dr. Togay Ozbakkaloglu		
Contribution to the Paper	Research supervision and review of manuscript		
Signature		Date	23/09/2015

SEISMIC BEHAVIOR OF HIGH-STRENGTH CONCRETE-FILLED FRP TUBE COLUMNS

Yunita Idris and Togay Ozbakkaloglu

ABSTRACT

This paper reports on an experimental program that investigated the seismic behavior of high-strength concrete (HSC)-filled fiber reinforced polymer (FRP) tubes (HSCFFTs), designed to perform as building columns. Five square and one circular concrete-filled FRP tube (CFFT) columns were tested under constant axial compression and reversed-cyclic lateral loading. The main parameters of the experimental study included the axial load level, column cross-sectional shape, concrete strength, amount and type FRP confinement, and FRP tube corner radius. Examination of the test data resulted in a number of significant conclusions with regards to the influence of the investigated column parameters on the performance of CFFT columns. Of primary importance, the results indicate that square HSCFFT columns are capable of developing very high inelastic deformation capacities under simulated seismic loading. The results also indicate that increasing the FRP tube corner radius up to a certain threshold leads to a significant increase in column lateral drift capacities. By contrast, increasing the corner radius beyond that threshold value provides no additional improvement in the hysteretic behavior of square CFFT columns. The influence of the cross-sectional shape is found to be significant, with the circular CFFT exhibiting a larger lateral drift capacity compared with the companion square CFFTs. A set of comparable columns from previous studies has also been included in the discussion to clarify the influence of each parameter on the column behavior. The results of the experimental program are presented together with a discussion on the influence of the main parameters on the seismic behavior of CFFT columns.

KEYWORDS: Fiber-reinforced polymer; High-strength concrete; Confinement; Columns; Tubes; Lateral drift.

INTRODUCTION

During the last two decades, the popularity of high-strength concrete (HSC) in the construction industry has been undergoing a steady growth due to the superior performance and economy offered by the material over normal-strength concrete in a large number of structural engineering applications. However, the use HSC structural members in seismically active regions, where significant inelastic deformability and energy-dissipation capacity are required to resist seismically induced forces, poses a challenge due to the brittle nature of HSC. Thus, the development of effective confinement systems for HSC columns to increase their ductility has become one of the main priorities in the seismic-resistant design of concrete structures.

External confinement of existing concrete columns by fiber-reinforced polymer (FRP) composites has been shown to be an effective method for increasing column ductility by a large number of studies reported on the axial compressive behavior (e.g. Rochette and Labossiere 2000; Pessiki et al. 2001; Lam and Teng 2004; Ilki et al. 2008; Eid et al. 2009; Cui and Sheikh 2010; Kusumawardhaningsih and Hadi 2010; Wu and Wei 2010; Ozbakkaloglu and Akin 2012) and seismic behavior (e.g., Saadatmanesh et al. 1996; Sheikh and Yau 2002; Hosseini et al. 2005; Iacobucci et al. 2003; Ye et al. 2003; Haroun and Elsanadedy 2005; Bousias et al. 2007; Chung et al 2008; Ozcan et al. 2008; Wu et al. 2008; Bournas et al. 2009; Realfonzo and Napoli 2009; Gu et al. 2010; Dai et al. 2012) of FRP-wrapped columns. The previous studies on the use of FRP composites in the construction of new high-performance composite columns in the form of concrete-filled

FRP tubes (CFFTs) have also demonstrated the ability of these columns to exhibit highly ductile behavior under both axial (Mirmiran et al. 1998; Fam and Rizkalla 2001; Hong and Kim 2004; Fam et al. 2005; Ozbakkaloglu and Oehlers 2008a,b; Mohamed and Masmoudi 2010; Park et al. 2011; Ozbakkaloglu 2013a, b, c) and simulated seismic loading (Seible et al. 1996; Yamakawa et al. 2003; Zhu et al. 2006; Ozbakkaloglu and Saatcioglu 2006, 2007; Saatcioglu et al. 2008; Shi et al. 2012; Li et al. 2013; Zohrevand and Mirmiran 2013). Furthermore, the tests conducted by Ozbakkaloglu and Saatcioglu (2006, 2007) on large-scale HSCFFT columns have shown that FRP tube-encased HSC columns are capable of developing very high inelastic deformation capacities under simulated seismic loading. It is evident from the results of the existing studies that the composite CFFT structural system offers an attractive alternative for construction of new earthquake-resistant columns. However, research on the seismic behavior of CFFTs has so far been very limited and additional experimental studies are required to better understand the influence of important column parameters on the seismic behavior of CFFT columns.

To contribute toward this end, this paper reports on the first ever experimental study on the seismic behavior of aramid FRP (AFRP)-confined HSCFFT, which was aimed at investigating the influence of key column parameters on the behavior of HSCFFT columns tested under combined axial compression and reversed-cyclic lateral loading. The main parameters of the study were the axial load level, concrete strength, column cross-sectional shape, amount and type FRP confinement, and FRP tube corner radius. The seismic performances of the columns are evaluated on the basis of the experimentally recorded moment-lateral drift hysteretic relationships. The results of the experimental study are presented and followed by a discussion on the influence of the key column parameters on the performance of the CFFT columns.

EXPERIMENTAL PROGRAM

Test Specimens

A total of six CFFTs were manufactured and tested under constant axial compression and incrementally increasing lateral deformation cycles. The specimens were designed as half-scale cantilever columns that represented the lower portion of a first-story building column with an interstory height of 4 m. Each specimen was designed to have a nominal cross-sectional dimension (D) of 150 mm and a cantilever height of 1.2 m. Lateral cyclic loading was applied to the specimens at a section 200 mm below the column tip, which resulted in a shear span (L) of 1.0 m. Fig. 1 illustrates the geometry of the specimens. The levels of constant axial compression were established to stimulate the loading conditions of typical building columns and they varied from 27% to 42% of the nominal column concentric load capacity (P_o) as reported in Table 1.

Five of the specimens had a square cross-section and they were manufactured using two different grades of HSC. In addition, a companion circular specimen was also manufactured using the higher grade HSC. Each column was fixed into a heavily reinforced concrete footing that was 790 mm in length, 290 mm in width, and 460 mm in height. One of the square columns was confined with a carbon FRP (CFRP) tube, whereas the remaining five columns were provided with AFRP external tubes. Four of the square CFFT columns were designed with a 15-mm FRP tube corner radius (R), whereas the fifth square CFFT had a FRP tube with 30-mm radius corners. The FRP tubes of the specimens were designed on the basis of the previous tests by Ozbakkaloglu and Saatcioglu (2006, 2007) to yield a ductile column behavior without exceeding the 15% lateral drift capacity of the test setup. Fig. 2 illustrates the manufacturing process of the specimens. Table 1 provides a summary of the material and geometric properties of each specimen.

Material Properties

FRP tubes

The FRP tubes were manufactured first to create a simple formwork for concrete. The tubes were manufactured using a manual wet lay-up process, which involved wrapping epoxy resin-impregnated fiber sheets around precision-cut high-density plastic foam moduls in the hoop direction. The FRP sheets were wrapped around the moduls one layer at a time, with an overlap length of 100 mm provided for each layer to prevent premature debonding failure. The overlap region of each subsequent layer was provided on the opposite face at a 180^{o} interval from the previous overlap region. The tubes were manufactured in a manner that the overlap regions formed continuous lines along the height of the columns, which were oriented to correspond to column-side faces. The width of each fiber sheet was 300 mm and a small overlap of approximately 10 mm was provided in the axial direction only to ensure continuity of the tube. The number of layers used in the tubes of each CFFT columns was established as a function of concrete strength and applied axial load level, with the test results reported in Ozbakkaloglu and Saatcioglu (2006, 2007) on HSCFFT columns used to established the baseline-performance estimates. Properties of aramid and carbon fibers used in manufacture of the FRP tubes are shown in Table 2. The table reports both the manufacturer-supplied properties and the ones obtained from the flat coupon tests based on nominal fiber thickness. Manufacturer-supplied properties of the epoxy resin are also given in the same table.

Concrete

Two different concrete mixes were used in the manufacture of the test specimens. Both mixes consisted of crushed bluestone as the coarse aggregate with a nominal maximum

size of 10 mm. Two different water-to-cement ratios of 0.34 and 0.50 were used in the mixes, which resulted in test day compressive strengths of 95 MPa and 62 Mpa, respectively. Silica fume and superplasticizer were added to the 95 MPa mix to achieve the desired level of strength and workability.

Steel reinforcement

Each specimen contained eight 10-mm diameter steel reinforcing bars as the column flexural reinforcement. The arrangement of the steel reinforcement is illustrated in Fig. 1. The number and diameter of reinforcing bars were selected to represent typical reinforcement arrangements and ratios (A_s/A_g) used in the construction of reinforced concrete building columns. The reinforcing bars were provided with standard hooks and they were fully embedded in the concrete footing. All the reinforcing bars were from the same batch and they had yield strength of 600 MPa. Table 3 summarizes the material properties of the steel bars that were obtained from the direct tension tests.

Instrumentation, test setup and loading program

All the column specimens were instrumented with a total of eight linear variable displacement transducers (LVDTs) to measure the lateral displacements, rotations within the plastic hinge region and anchorage slip. Each specimen was also instrumented with strain gauges placed along the length of the steel reinforcing bars and on the FRP tube both in axial and hoop directions. Column lateral displacements were measured by two string pots that were placed at heights of 1.0 and 1.2 m measured from column-footing interface. Column rotations were measured by two LVDTs with 50-mm stroke capacities that were placed on FRP tube at 150 mm from column-footing interface. Anchorage slips were

measured by two 10-mm stroke capcity LVDTs that were placed on FRP tubes 20 mm away from the interface. The acquisition of hoop strain data on FRP tubes was of particular interest to better understand the activation of the confinement mechanism and the development of confining pressures at different sections along the height of the columns. To this end, up to 30 strain gauges with 10-mm gauge lengths were bonded to each FRP tube in the hoop direction at seven different cross sections along the column height that extended up to 300 mm away from the interface. Axial strains of steel reinforcing bars were measured with 5-mm long strain gauges that were placed at sections at 75 mm below and 75 mm above the column-footing interface.

The specimens were tested under the combined effects of a constant axial compression that was applied at the top of the column and incrementally increasing lateral deformation reversals. The columns were first subjected to axial compression that was applied through a hydraulic jack of 1000-kN working capacity. Lateral deformation reversals were then applied through a hydraulic ram with a 1000-kN load capacity and 330 mm stroke, placed at a height that was 1000 mm from the column-footing interface. Fig. 3 illustrates the test setup. The axial load was maintained at the same level throughout the loading history of up to 6 h, and attempts were made to maintain the axial load near constant during the load cycles by limiting the maximum fluctuations from the required axial load to approximately 20 kN in each cycle.

The magnitude of the applied axial compression (P) was determined based on the design axial load level (P/P_o) of the column, which ranged between 27% and 42% of the column nominal axial load capacity (P_o), calculated according to ACI 318-11 (American Concrete Institute 2011) as

$$P_o = 0.85 f'_c \left(A_c - A_s\right) + A_s f_y \quad (1)$$

where f'_c is the cylinder strength of unconfined concrete, A_c is the cross-sectional area of the concrete, A_s is the cross-sectional area of steel reinforcing bars and f_y is the yield strength of the steel reinforcing bars. Eq. (1) incorporates a reduction factor of 0.85 to convert the cylinder strength of the concrete to its in-place strength when used in a structural member, which is in agreement with the factor of 0.9 recommended by Ozbakkaloglu and Saatcioglu (2004) for this purpose.

Following the application of the axial compression, each specimen was then subjected to lateral displacement excursions, consisting of incrementally increasing deformation reversals. Three full cycles were applied at each deformation level starting with 1% lateral drift ratio, calculated by dividing the recorded lateral displacements by column shear span. The lateral deformation reversals were then continually increased to subsequent drift ratios of 2%, 3%, 4%, etc., until the specimen was unable to maintain a significant fraction of its maximum lateral load resistance. The rate of the lateral loading was applied at a constant rate of approximately 0.4 mm/s and the total duration of a typical test was approximately 5-6 h, depending on the lateral displacement capacity of column.

TEST RESULTS

Specimens at the End of Testing

Critical sections of the specimens at the end of testing are shown in Fig. 4, which also shows the damage regions of the specimens after the removal of their FRP tubes. In all the specimen, the testing was terminated when the FRP tube of the specimen ruptured. The fiber rupture took place within a region along the column height that was between 75 mm to 150 mm away from the column-footing interface. In the square CFFTs, this region corresponded to one of the column corners. Shifting of the critical section from the

interface can be attributed to the confining effect of the footing. Similar observations were reported previously in Ozbakkaloglu and Saatcioglu (2006, 2007) for circular and square CFFT columns. The discoloration of the FRP tubes of the columns started around 5% to 7% lateral drift, which was followed by local fiber rupture at the most damaged regions of the columns. Additional increase in the applied lateral displacements beyond these drift levels led to the complete rupture of the FRP tubes and resulting loss in column capacity. The displacements recorded at the same time of FRP tube rupture are used to calculate the maximum lateral drifts ($\delta_{\max}$) given in Table 4. It should be noted that in this study, the column lateral drift capacities ($\delta_{0.8M\max}$) reported in Table 4 were established at the column failure, which defined in the following section, and they were lower than the maximum lateral drifts ($\delta_{\max}$).

Hysteretic behavior

Fig. 5 presents the recorded hysteretic moment (M)-lateral drift (δ) relationships for each column. All the columns showed a flexure dominant behavior with well-rounded hysteresis loops. The majority of the square columns developed their maximum moment capacity around 4%-5% lateral drift, followed by a gradual decrease in the moment capacity with an increase in lateral displacements beyond these levels. It is understood that some strength decay in column resistance can be tolerated in multistory buildings before the column is considered to have failed. In this study, if a column maintained at least 80% of its maximum moment resistance (M_{max}) for three full cycles of deformation, then it was considered to have maintained its seismic resistance at the corresponding deformation level. Once the strength decay exceeded 20% of the maximum moment capacity, the column was

considered to have failed. The lateral drifts corresponding to the column failure are reported in Table 4 as the column lateral drift capacities ($\delta_{0.8Mmax}$).

As evident from Fig. 5, the majority of the columns of this study exhibited a strength decay of over 20% by the time the testing was stopped. This strength decay was caused by the excessive damage sustained by the concrete within the extreme compression region. When the lateral displacements increased beyond 8% lateral drift level, additional strength losses were observed due to the failure of the internal steel reinforcement at the extreme fibers. Column CFFT-3 was the exception, which reached its maximum moment capacity at 5% lateral drift and failed at 9% lateral drift without exhibiting any significant strength decay until failure. The testing of Column CFFT-1 was terminated at 11% lateral drift when the FRP tube of the column ruptured. However, at that displacement level the moment capacity of the column was below 80% of its maximum moment capacity. Beyond 5% drift, the moment capacity of the column started to decrease rapidly and the column lateral drift capacity, corresponding to 20% strength decay, ($\delta_{0.8Mmax}$) was established as 8%. The FRP tube rupture of Column CFFT-2, with 30-mm radius corners, also occurred at a lateral drift of 11%. However, the drift that corresponded to 80% of the maximum moment capacity of the column was lower (i.e. $\delta_{0.8Mmax}$ = 8%) due to strength decay experienced by the column beyond 5% lateral drift. The hysteretic moment-lateral drift relationship of Column CFFT-4, with a 2-layer AFRP tube, started to show strength degradation beyond 3% lateral drift. The lateral drift capacity ($\delta_{0.8Mmax}$) of Column CFFT-4 was established as 6% as the column experienced more than 20% strength decay beyond this point. Column CFFT-5, with a CFRP tube, maintained the maximum moment capacity it attained around 3%-4% lateral drift without a significant decay until the end of 7% lateral drift cycles. After this drift level, however, the column experienced a rapid strength decay failing shortly thereafter. The circular CFFT column (CFFT-6) developed a higher lateral drift capacity

than its square counterparts, maintaining 80% of the maximum moment capacity it attained at 6% lateral drift until 9.5% lateral drift. The key results from the moment-lateral drift relationships of the specimens are tabulated in Table 4. Lateral load (F)-displacement (Δ) envelopes that were obtained by averaging the measurements from pull and push directions after correcting lateral loads for P-Δ effects (i.e. $M = F \times L$) are presented in Fig. 6 for all the specimens.

Column ductility

The ductility factors (μ) of the specimens that were established from Eq. 2 are reported in Table 4.

$$\mu = \frac{\Delta_{0.8M\max}}{\Delta_y} \tag{2}$$

where $\Delta_{0.8Mmax}$ and Δ_y are the lateral displacements at column failure and yield, respectively. The failure displacements ($\Delta_{0.8Mmax}$) were determined in the same manner as the column lateral drift capacities ($\delta_{0.8Mmax}$). The yield displacements were established using the envelope load-displacement curves and by extending a straight line with a slope that is equal to the initial elastic region slope of the curve until the maximum column lateral load capacity (F_{max}). As illustrated in Table 4, the ductility factors of the specimens ranged between 4.5 and 7.1, which indicate ductile column behavior.

Column stiffnesses

Fig. 7 illustrates the variation of average column stiffnesses (K) with lateral drifts for all the specimens, which were obtained from the lateral load-displacement hysteretic

relationships, as $K = F/D$. Based on the imposed boundary conditions of the specimens, the relationship between the sectional flexural stiffness (EI) and column stiffness (K) can be established as:

$$K = \frac{3.E.I}{L^3} \tag{3}$$

where E and I = elastic modulus and moment of inertia of composite section, respectively; and L = shear span of the column.

Column stiffnesses shown in Fig. 7 were determined from the average lateral loads and displacements recorded at a given drift level for the three cycles in the pull and push directions. As expected, the circular column, CFFT-6, exhibited a lower initial stiffness compared with its square counterparts. Likwise, the initial stiffness of column CFFT-3, with lower concrete strength, was lower than that of the rest of the square columns. An interesting observation from Fig. 7 is that the stiffness of the CFRP-confined column, CFFT-5, was lower than companion AFRP-confined column. This difference is believed to have been caused by minor imperfections in the placement of concrete and steel reinforcement during the manufacture of column CFFT-5.

Fig. 7 illustrates the progressive reduction of column stiffnesses with increasing lateral drifts, which is associated with cracking of concrete and yielding of internal steel reinforcement. In all specimens this reduction in stiffness is most significant up to 3-4% lateral drift, and beyond this displacement level stiffness degradation continues at a lower and continually decreasing rate. The major change in the slope of the stiffness curves of the specimens observed at this displacement indicates the large level of plastification experienced by the specimens by this stage of loading. Significantly reduced slopes of the curves beyond this displacement level point to a stabilized column behavior, with the slope

of the curve progressively approaching zero in majority of the specimens just before the termination of the curve.

Column Energy-Dissipation Capacity

The energy-dissipation capacity of each specimen was determined at each cycle by calculating the area under the corresponding lateral load-displacement hyteretic curve. The average energy dissipation capacities of the columns were then calculated for the three consecutive load cycles at a given drift level and are shown in Fig. 8. The figure illustrates that the energy dissipation capacities of the specimens followed a similar trend and, except for the drop observed in the capacity of the circular column, CFFT-6, between the 8% and 9% drift cycles, they monotonically increased until the lateral drift capacities of the specimens ($\delta_{0.8Mmax}$) were attained. The drop observed in CFFT-6 was caused by the combined influence of the strength decay and increased magnitude of pinching observed in the hysteresis curves of the column, which is evident from Fig. 5(f). Similar drops were also observed in the energy capacities of the square columns once the lateral drifts increased beyond the column drift capacities.

The comparison of the energy dissipation capacities of the companion AFRP- and CFRP-confined specimens, CFFT-1 and CFFT-5, in Fig. 8 shows that at a given displacement level the energy dissipation capacity of the AFRP-confined specimen was higher than that of its companion. However, this difference was mostly due to the differences of the lateral load capacities of the columns, which are believed to have been caused by small variations in reinforcement and concrete placement during the fabrication of these specimens as discussed previously. The comparison of the energy dissipation curves of columns CFFT-1 and CFFT-3, which were manufactured using different concrete grades, indicates that until

6% lateral drift the columns exhibited very similar dissipation capacities. Beyond this drift level, however, the specimen with lower concrete strength and higher axial load level (i.e. CFFT-3) started to develop significantly higher energy dissipation capacities than its counterpart, CFFT-1. As can be seen in Fig. 5, this difference was a result of the increased magnitude of strength decay experienced by CFFT-1 beyond this drift level, which was not observed in CFFT-3. As illustrated in Fig. 8, at a given displacement level, the circular column, CFFT-6, developed lower energy dissipation capacities than its square counterparts. This was expected and the difference is due to the lower lateral load capacity of the circular column.

Variation of FRP tube hoop strains along column height

The variation of FRP tube hoop strains was recorded by strain gauges placed on the FRP tube at eight different levels along the column height. Fig. 9 illustrates the variation of the FRP tube strains for each column. The values given in Fig. 9 represent the recorded maximums that were obtained from the larger of the maximum strains recorded in pull and push direction. In some of these strain profiles, the dotted lines were used to represent the predicted strain gauge reading in cases where the actual strain gauge readings were not available due to failure of particular strain gauges. These predictions were based on the observed relationships that were established from the previous cycles between the failed and functioning strain gauges of the same cross section. It was observed that the maximum-recorded strains on the profiles shown in Fig. 9 often corresponded to the loacation of fiber rupture. These regions were located 75 mm (D/2) to 150 mm (D) away from the point where the column joined the footing. The aforementioned strengthening effect of the column footing is also evident from the profiles shown in Fig. 9.

DISCUSSION OF TEST RESULTS

The following sections provide discussions on the influence of the test parameters investigated in this study on the hysteretic moment-lateral drift relationship and plastic hinge behavior of CFFT columns.

Effect of test parameters on column lateral drift capacities

Combined effect of concrete strength and axial load level

It is well established that the column axial load level (P/P_o) significantly influences the cyclic behavior of concrete columns. Similarly, the deformability and overall cyclic behavior the reinforced concrete columns are known to be significantly influenced by the column concrete strength (f'_c). To investigate the combined influence of concrete strength (f'_c) and the axial load level (P/P_o), which in practice represents a case where two columns are loaded under similar axial loads (P), companion columns CFFT-1 and CFFT-3 were manufactured using 95 MPa and 62 MPa concretes, respectively. The axial load levels of the Columns CFFT-1 and CFFT-3 were determined so that the product of concrete strength and axial load level, $f'_c \times P/P_o$, would be the same for these two columns. This resulted in P/P_o ratios of 0.27 and 0.41 for Columns CFFT-1 and CFFT-3, respectively. It can also be seen in Fig. 5 that hysteresis loops of Column CFFT-3 were more well-rounded than those of Column CFFT-1, suggesting that Column CFFT-3 experienced a higher level of plastification compared to Column CFFT-1. Although the FRP tube rupture of Column CFFT-1 occurred at 11% lateral drift, the lateral drift capacity of the column was established as 8%, as discussed previously. By contrast, the lateral drift capacity of Column CFFT-3 was established as 9%, which corresponded to the lateral drift at the time of FRP tube rupture.

As can be seen in Table 1, due to its lower concrete strength, nominal confinement ratio (f_{lu}/f'_c) of Column CFFT-3 was higher than that of Column CFFT-1. The nominal confinement ratio (f_{lu}/f'_c) was calculated by dividing the ultimate confining pressure (f_{lu}), determined from Eq. (4) assuming an idealized uniform confinement distribution, with concrete cylinder strength (f'_c).

$$f_{lu} = \frac{2.E_f.t.\varepsilon_f}{D} \tag{4}$$

where E_f = elastic modulus of fibers; ε_f = ultimate tensile strain of fibers; t = total fiber thickness of the tube; and D = column cross-sectional dimension. Table 1 also shows the actual confinement ratios ($f_{lu,a}/f'_c$) of the specimens that were calculated based on the experimentally determined actual confining pressures ($f_{lu,a}$) at the failure of the specimens. The actual confining pressures ($f_{lu,a}$) were calculated from Eq. (5) using the maximum recorded hoop strains ($\varepsilon_{h,fail}$) at specimen failure that were established from Figure 9.

$$f_{lu,a} = \frac{2.E_f.t.\varepsilon_{h,fail}}{D} \tag{5}$$

As illustrated in Table 1, the actual confinement ratio of Column CFFT-3 was about two times that of Column CFFT-1, and the axial load level of the former column was approximately 50% higher than that of the latter. The similar performance levels of Columns CFFT-1 and CFFT-3 suggest that the favorable influence of the increased confinement ratio of Column CFFT-3 was largely neutralized by the increased P/P_o ratio of the column. A similar observation was previously reported by Ozbakkaloglu and Saatcioglu (2006) for circular CFFT columns.

Effect of FRP tube corner radius

Columns CFFT-1 and CFFT- 2 were compared to study the influence of the ratio of the corner radius to the column cross-sectional dimension (*R/D*). Columns CFFT-1 and CFFT-2 had *R/D* ratios of 1/10 and 1/5 respectively. As evident from Fig. 5, strength decay in Column CFFT-1 started at a lower lateral drift level than that in Column CFFT-2. By contrast, as shown in Table 4, the lateral drift capacities of these columns were identical. It was previously reported by Ozbakkaloglu and Saatcioglu (2007) that a CFFT column with sharp corners (i.e *R/D* = 1/34) performed significantly worse than a companion column with well-rounded corners (i.e. *R/D* = 1/6). By contrast, based on an investigation on the axial compressive behavior of square and rectangular CFFTs with sufficiently well-rounded corners, Ozbakkaloglu (2013a) recently reported that CFFT columns with smaller corner radius (*R/D* = 1/10) tended to have axial stress-strain curves with flatter and longer second branches than CFFT columns with larger corner radius (*R/D* = 1/5). The observations summarized in this section suggest that increasing the corner radius up to a certain threshold *R/D* ratio results in a significant improvement in the column behavior. However, increasing the *R/D* ratio beyond this threshold provides no additional improvement in the hysteretic behavior of square CFFT columns. Additional studies are required to gain further insight into the influence of *R/D* ratio on the lateral cyclic behavior and drift capacities of square and rectangular CFFT columns.

Effect of FRP type

The influence of the type of fibers used in the manufacture of the FRP tubes on the hysteretic behavior of square CFFTs was investigated by comparing columns CFFT-1 and CFFT-5. Column CFFT-1 consisted of an FRP tube formed from three layers of AFRP,

while column CFFT-5 was constructed from four layers of CFRP. The numbers of FRP layers of these columns were established to obtain two comparable columns in terms of the level of confinement. As can be seen in Table 1, Columns CFFT-1 and CFFT-5 had close actual confinement ratios ($f_{lu,a}/f'_c$). The performance of the two columns was compared based on their moment-lateral drift relationships shown in Fig. 5. The FRP-tube rupture of Column CFFT-1 occurred at 11% lateral drift, whereas this took place earlier at 9% lateral drift in Column CFFT-5. The columns developed their maximum moment capacities at the same drift level (i.e. 3% lateral drift), and their lateral drift capacities were established at 20% strength decay as 8% for CFFT-1 and 7% for CFFT-5. As shown in Table 4, these columns had identical yield displacements (Δ_y), and hence the ductility factor (μ) of column CFFT-1 was also higher than that of column CFFT-5. Slightly higher drift capacity of the AFRP-confined CFFT suggests that the higher rupture strain of aramid fibers had a beneficial influence on the lateral drift capacity of the column. This observation is in support of the findings of the studies on the axial compressive behavior of FRP-confined concrete, where it was reported that for a given confinement level the axial deformation capacity of FRP-confined concrete increases with the increase in the ultimate tensile strain of the FRP material (Ozbakkaloglu and Akin 2012).

Effect of amount of confinement

It is well understood that the amount of confinement has a major influence on the lateral drift capacity of CFFT columns. To investigate this influence for AFRP-confined CFFTs, Column CFFT-4, which was companion to Column CFFT-1, was designed with two layers of AFRP. Apart from the difference in the number of FRP layers and resulting confinement ratios ($f_{lu,a}/f'_c$), these columns were identical in all other aspects. As can be seen in Fig. 5,

Column CFFT-4 reached its maximum moment capacity at around 3% lateral drift, started to demonstrate strength degradation after 4% drift, and developed a lateral drift capacity of 6%. As mentioned previously Column CFFT-1, confined with 3 layers of AFRP, started to experience strength decay starting at 5% lateral drift and developed a lateral drift capacity of 8%. This comparison, as expected, indicates that the lateral drift capacities of CFFT columns increase with an increase in the amount of confinement.

Effect of column cross-sectional shape

The influence of the cross-sectional shape of CFFT columns was investigated by comparing the behaviors of Columns CFFT-1, CFFT-2 and CFFT-6. As indicated in Table 4, although the circular column CFFT-6 was tested under a higher axial load level than its square companions, it was able to develop a higher lateral drift capacity of 9.5% versus 8% of the square columns CFFT-1 and CFFT-2. The higher performance of the circular column was expected and it can be attributed to the higher confinement effectiveness of circular FRP tubes over the square ones, as was discussed previously (Ozbakkaloglu and Saatcioglu 2007; Ozbakkaloglu and Oehlers 2008b; Ozbakkaloglu 2013b). It may be worth noting, however, that as evident from Fig. 5 the pinching effect was more pronounced in the hysteresis loops of the circular CFFT than that of the square CFFTs. Similar observation was previously reported by Saatcioglu et.al (2008) for CFRP-confined HSCFFTs. The pinching effect is associated with the concrete crushing, which results in slippage of the reinforcing bar between the crack surfaces when the load is reversed and the compression region becomes the tension region. These observations, therefore, imply that the extent of bar slippage was more significant in circular CFFTs than in square CFFTs.

Influence of Key Parameters on Plastic Hinge Length

Modeling of the plastic hinge region is an important step in predicting the moment-lateral drift hysteretic behavior of a concrete column. In many of the previous experimental studies on conventional reinforced concrete columns (e.g. Bae and Bayrak 2008; Pam and Ho 2009; Liu and Sheikh 2013), plastic hinge lengths were established based on visual observations of the column damage regions. This approach relates the damage in concrete to the longitudinal plastic deformations, rather than measuring the axial strains along the column height continuously, which is challenging particularly after the yielding of the longitudinal steel bars. In the present study, an approach that was previously introduced in Ozbakkaloglu and Saatcioglu (2006, 2007) and that involves the use of recorded hoop strain profiles recorded on FRP tubes were used in establishing the plastic hinge lengths of the specimens. This approach is based on the fact that an intimate relationship exists between the lateral expansion of FRP tube and the level of damage sustained by concrete inside the tube. That is, higher FRP tube hoop strains correspond to the most highly damaged regions of the columns, as the concrete undergoes rapid expansion inside the FRP tube within these regions. The plastic hinge lengths of the specimens that are referred to in this section were established through the hoop strain distribution of the specimen at the final drift cycle, assuming that the region terminated at a height where the recorded hoop strains fell below one third of the maximum recorded strain in that drift cycle. These values are reported in Table 4.

Based on the observations on the behavior of conventional reinforced concrete columns, it was previously reported that an increase in the axial load level results in an increase in the length of the plastic hinge region (Bae and Bayrak 2008; Pam and Ho 2009). Pam and Ho (2009) also reported that an increase in the concrete strength results in an increase in the plastic hinge lengths of conventional columns. The comparison of the hoop strain

distributions of columns CFFT-1 and CFFT-3 in Fig. 9 indicates that column CFFT-3 with f'_c = 62 MPa and P/P_o = 0.41 exhibited a larger plastic hinge length than the companion column CFFT-1 with f'_c = 95 MPa and P/P_o = 0.27. In light of the aforementioned observations on conventional column, this observation indicates that P/P_o ratio had a more significant influence than the concrete strength on the length of the plastic hinge region. It should be noted, however, that this observation is not in agreement with the one reported in Ozbakkaloglu and Saatcioglu (2006), where it was stated that plastic hinge region of circular CFFT columns became more localized with increased axial load levels. Additional experimental studies are required to better understand the influence of the axial load level and concrete strength on the formation and propagation of plastic hinge regions of CFFT columns.

Comparison of the hoop strain profiles of Columns CFFT-1 and CFFT-2 in Fig. 9 indicates that *R/D* ratio had no significant influence on the plastic hinge region lengths of the CFFT columns. This observation suggests that within the range of *R/D* ratios investigated in the present study, the plastic hinge region of CFFT columns is not highly sensitive to the *R/D* ratio. As evident from Fig. 9, the plastic hinge region of Column CFFT-1, which was confined with AFRP, was slightly higher than its companion Column CFFT-5 that was confined with CFRP. This observation points to the possible influence of FRP confinement type on the plastic hinge region. By contrast, this slight difference in the plastic hinge length of the aforementioned columns might have been influenced by other factors and further research is required to gain further insight into the influence of FRP type on the plastic hinge regions of CFFT columns.

Comparison of Test Results with Results of Companion Square FRP-Confined Concrete Columns

The seismic behavior of the CFFT columns of this study was compared with a group of companion columns with similar column parameters, selected from literature to gain additional insight into the influence of important parameters on the performance of CFFTs. The specimens were selected based on a carefully chosen selection criteria, which ensured that the key test parameters [i.e. slenderness ratio (*L/D*), axial load level (P/P_o), and nominal confinement ratio (f_{lu}/f'_c)] remained near constant to enable a meaningful comparison. Furthermore all the specimens included in this section were tested under quasi-static loading and hence were not subjected to high strain-rate effects. Because it was not possible to establish the actual confining pressures ($f_{lu,a}$) for the specimens of the previous studies, the nominal confinement ratios were used in categorizing the specimens. The described process resulted in two groups of companion specimens as shown in Table 5. Each group consisted of specimens with similar nominal confinement ratios (f_{lu}/f'_c) and axial load levels (P/P_o). As can be seen in Table 5, the specimens of each group also had reasonably close column slenderness ratios (*L/D*).

The comparison of lateral drift capacities of the CFFT columns in Group 1 indicates that *R/D* ratio has no significant influence on the column lateral drift capacities. As shown in Table 5, the columns of Group 1 developed very close lateral drift capacities independent of their *R/D* ratios. This observation supports the one previously derived from the comparison of columns CFFT-1 and CFFT-2 that increasing the corner radius beyond a certain threshold value does not result in an increase in lateral drift capacities of CFFTs. By contrast, investigation of the ultimate drift capacities of the columns in Group 2 indicates that *R/D* ratio has a significant influence on the lateral drift capacities of the columns with *R/D* ratios below 0.10. As can be seen in Table 5, lateral drift capacities of

columns with small-radius corners (i.e., RS-6 and ASC-2NS) were significantly lower than those of the columns with sufficiently rounded corners (i.e., S-NL-1-27, CFFT-4 and RS-4). As evident from Table 5, increasing the *R/D* ratio from 0.03 up to 0.09 leads to a significant increase in column lateral drift capacities. Further increase in the *R/D* ratio beyond *R/D* = 0.09 provides no additional increase in column lateral drift capacities, as was also observed in the comparison of the specimens in Group 1.

As discussed previously, comparison of Columns CFFT-1 and CFFT-5 indicate that the type of FRP tube material has only a slight influence of the drift capacities of CFFTs, with specimens confined by a material of higher ultimate tensile strain developing slightly higher lateral drift capacities. With this in mind, comparison of Columns S-NL-1-27 and Column CFFT-4 in Table 5, which had similar *R/D*, f_{lu}/f'_c and P/P_o ratios, indicates that columns made of different strength concretes may develop similar lateral drift capacities, provided that they are designed to have similar nominal confinement ratios (f_{lu}/f'_c).

CONCLUSIONS

This paper has presented the results of an experimental study on the behavior of HSCFFT columns under simulated seismic loading. Based on the results and discussions presented in the paper the following conclusions can be drawn:

- AFRP- and CFRP-confined square HSCFFT columns can develop significantly high lateral drift capacities under simulated seismic loading. However, as expected, the relative performance levels of the square columns have been found to be lower than their circular counterparts.

- Column deformability decreases with an increase in axial load level (P/P_o) and concrete compressive strength (f'_c). It was observed that the detrimental influence of increased P/P_o ratio was neutralized by the favorable influence of the increased confinement ratio (f_{lu}/f'_c) that resulted from a decrease in the concrete strength (f'_c).
- The treatment of the results of this study together with those from the previous studies that reported on the effect of FRP tube corner radius leads to the following conclusion on the influence of tube corner radius: Increasing the corner radius of square CFFTs up to a certain threshold *R/D* ratio results in a significant increase in column lateral drift capacities. By contrast, increasing the corner radius beyond this threshold value does not appear to provide any further improvement in the behavior of these columns. Therefore, there exists a minimum *R/D* ratio that ensures the square columns are sufficiently confined and hence are capable of developing their full lateral deformation capacity.
- CFFTs with FRP tubes made of fibers with higher ultimate tensile strain appear to develop a slightly higher lateral drift capacity than companion CFFTs with FRP tubes constructed of fibers with lower ultimate tensile strain.
- The lateral drift capacities of CFFTs increase with an increase in the amount of confinement.
- The FRP tube rupture of the specimens occurred at a region along the column height that was between 75 mm to 150 mm away from the column-footing interface. Shifting of the critical section from the interface can be attributed to the confining effect of the column footing.
- It was observed that the concrete strength, P/P_o ratio and fiber type of the confining tube had some influence on the plastic hinge length of CFFT columns. No influence of

R/D ratio was evident on the plastic hinge length within the range of ratios investigated.

ACKNOWLEDGEMENTS

The authors would like to thank Messrs. Morizzi, Schulz, Valenzisi, and Wood, who have undertaken the tests reported in this paper as part of their undergraduate theses. This research is part of an ongoing program at the University of Adelaide on FRP-concrete composite columns.

REFERENCES

American Concrete Institute (2011). "Building code requirements for structural concrete and Commentary." *ACI 318-11*, Farmington Hills, MI.

Bae, S. and Bayrak, O. (2008). "Plastic hinge length of reinforced concrete columns." *ACI Struct. J.*, 105(3), 290-300.

Bournas, D.A., Triantafillou, T.C., Zygouris,K., and Stavropoulos, F. (2009), "Textile mortar versus FRP jacketing in seismic retrofitting of RC columns with continuous or lap-spliced deformed bars." *Journal of Composites for Construction*, ASCE, 13(5): 360-371.

Bousias, S., Spathis, A., and Fardis, M.N. (2007), "Seismic retrofitting of columns with lap spliced smooth bars through FRP or concrete jackets." *Journal of Earthquake Engineering*, 11(5), 653-674.

Chung, Y, Park, C and Meyer, C (2008), "Residual seismic performance of reinforced concrete bridge piers after moderate earthquakes." *ACI Structural Journal*, 105(1), 87–95.

Cui, C., and Sheikh, S. A. (2010). “Experimental study of normal- and high-strength concrete confined with fiber-reinforced polymers.” *Journal of Composites for Construction*, ASCE, 14(5), 553-561.

Dai, J.G., Lam, L., and Ueda, T. (2012). “Seismic retrofit of square RC columns with polythylene terephthalate (PET) fibre reinforced polymer composites.” *Construction and Building Materials*, 27(1), 206-217.

Eid, R., Roy, N., and Paultre, P. (2009). “Normal- and high-strength concrete circular elements wrapped with FRP composites.” *Journal of Composites for Construction*, ASCE, 13(2), 113-124.

Fam, A., Schnerch, D. and Rizkalla, S. (2005). "Rectangular filament-wound GFRP tubes filled with concrete under flexural and axial loading: experimental investigation." *Journal of Composites for Construction*, ASCE, 9(1), 25-33.

Fam, A. Z., and Rizkalla, S.H. (2001), “Confinement model for axially loaded concrete confined by circular fiber-reinforced polymer tubes.” *ACI Structural Journal*, 98(4), 451-461.

Gu, D.S., Wu, G., Wu, Z.S., and Wu, Y.F. (2010),”Confinement effectiveness of FRP in retrofitting circular concrete columns under simulated seismic load.” *Journal of Composite for Construction*, ASCE, 14(5), 531-540.

Haroun, M., and Elsanadedy, H. (2005), “Fiber-reinforced plastic jackets for ductility enhancement of reinforced concrete bridge columns with poor lap-splice detailing.” *Journal of Bridge Engineering*, ASCE, 10(6), 749-757.

Hong, W.K., and Kim, H.C. (2004). “Behavior of concrete columns confined by carbon composite tubes.” *Canadian Journal of Civil Engineering*, 31(2), 178–188.

Hosseini, A., Khaloo, A.R, and Fadaee, S. (2005). “Seismic performance of high-strength concrete square columns confined with carbon fiber reinforced polymers (CFRPs).” *Canadian Journal Civ.Eng*., 32: 569-578.

Iacobucci, R.D., Sheikh, S.A., and Bayrak, O. (2003). “Retrofit of square concrete columns with carbon fiber-reinforced polymer for seismic resistance.” *ACI Structural Journal*, 100(6), 785-794.

Ilki, A., Peker, O., Karamuk, E., Demir, C., Kumbasar, N. (2008), “FRP retrofit of low and medium strength circular and rectangular reinforced concrete columns.” *Journal of Material Civil Engineering*, ASCE, 20(2), 169-188.

Kusumawardaningsih, Y., and Hadi, M.N.S. (2010). “Comparative behaviour of hollow columns confined with FRP composites.” *Composite Structures*, 93(1), 198-205.

Lam, L., and Teng, J. G. (2004), “Ultimate condition of fiber reinforced polymer-confined concrete.” *Journal of Composites for Construction*, ASCE, 8(6), 539-548.

Li, B., Zohrevand, P., and Mirmiran, A. (2013). “Cyclic Behavior of FRP Concrete Bridge Pier Frames.” *Journal of Bridge Engineering*, ASCE, 18(5), 429–438.

Liu, J. (2013), “Seismic behaviour of reinforced concrete columns.” Ph.D. thesis, University of Toronto, Canada.

Mirmiran, A., Shahawy, M., Samaan, M., El Echary, H., Mastrapa, J.C., and Pico, O. (1998). “Effect of column parameters on FRP-confined concrete.” *Journal of Composites for Construction*, ASCE, 2(4), 175-185.

Mohamed, H., and Masmoudi, R. (2010) “Axial load capacity of concrete-filled FRP tube columns: experimental versus predictions.” *Journal of Composite for Construction*, ASCE, 14(2): 231-243.

Ozbakkaloglu, T. (2013a). “Axial compressive behavior of square and rectangular high-strength concrete-filled FRP tubes.” *Journal of Composites for Construction*, ASCE, 17(1), 151-161.

Ozbakkaloglu, T. (2013b). “Compressive behavior of concrete-filled FRP tube columns: Assessment of critical column parameters.” *Engineering Structures*, 51, 188-199.

Ozbakkaloglu, T. (2013c). “Concrete-filled FRP tubes: Manufacture and testing of new forms designed for improved performance.” *Journal of Composites for Construction*, ASCE, 17(2), 280-291

Ozbakkaloglu, T., and Akin, E. (2012). “Behavior of FRP-confined normal- and high-strength concrete under cyclic axial compression.” *Journal of Composites for Construction*, ASCE, 16(4), 451-463.

Ozbakkaloglu, T., and Oehlers, D. J. (2008a). “Concrete-filled square and rectangular FRP tubes under axial compression.” *Journal of Composites for Construction*, ASCE, 12(4), 469-477.

Ozbakkaloglu, T., and Oehlers, D. J., (2008b), “Manufacture and testing of a novel FRP tube confinement.” *Engineering Structures*, 30(9), 2448-2459.

Ozbakkaloglu, T. and Saatcioglu, M. (2004). “Rectangular stress block for high-strength concrete.” *ACI Structural Journal*, ASCE, 101(4), 475-483.

Ozbakkaloglu, T. and Saatcioglu, M. (2006). “Seismic behavior of high strength concrete columns confined by fiber-reinforced polymer tubes.” *Journal of Composite Construction*, ASCE, 10(6), 538-549.

Ozbakkaloglu, T. and Saatcioglu, M. (2007),"Seismic performance of square high strength concrete columns in FRP stay in place formwork." Journal of Structural Engineering, ASCE, 133 (1), 44-56.

Ozcan, O., Binici, B., and Ozcebe, G. (2008), "Improving seismic performance of deficient reinforced concrete columns using carbon fiber-reinforced polymers", *Engineering Structures*, 30: 1632-1646.

Pam, H.J. and Ho, J.C.M. (2009), "Length of critical region for confinement steel in limited ductility high-strength reinforced concrete columns." *Engineering Structures*, 31(12), 2896-2908.

Park, J. H., Jo, B. W., Yoon, S. J., and Park, S. K. (2011). "Experimental investigation on the structural behavior of concrete filled FRP tubes with/without steel re-bar." *KSCE J. Civ. Eng*., 15(2), 337-345.

Pessiki, S., Harries, K. A., Kestner, J. T., Sause, R. and Ricles, J. M. (2001). "Axial behavior of reinforced concrete columns confined with FRP jackets." *Journal of Composites for Construction*, ASCE, 5(4), 237-245.

Realfonzo, R., and Napoli, A. (2009). "Cyclic behavior of RC columns strengthened by FRP and steel devices." *Journal of Structural Engineering*, ASCE, 135(10), 1164-1176.

Rochette, P., and Labossiere, P. (2000). "Axial testing of rectangular column models confined with composites." *Journal of Composites for Construction*, ASCE, 4(3), 129-136.

Saadatmanesh, H., Ehsani, M.R., and Jin, L. (1996). "Seismic strengthening of circular bridge pier models with fiber composites," *ACI Structural Journal*, 93(6), 639-647.

Saatcioglu, M., Ozbakkaloglu, T. and Elnabelsy, G. (2008). "Seismic behavior and design of reinforced concrete columns confined with FRP stay-in-place formwork." *ACI Special Publication*, SP257-09, 257, 149-170.

Seible, F., Burgueño, R., Abdallah, M. G., and Nuismer, R. (1996). “Development of advanced composite carbon shell systems for concrete columns in seismic zones.” *Proc., 11th World Conf. Earthquake Engineering*, Pergamon, Elsevier Science, Oxford, Paper No. 1375.

Sheikh, S.A. and Yau, G. (2002),”Seismic behavior of concrete columns confined with steel and fiber-reinforced polymer.” *ACI Structural Journal*, 99(1), 72-80.

Shi, Y., Zohrevand, P., and Mirmiran, A. (2012). “Assessment of Cyclic Behavior of Hybrid FRP Concrete Columns.” *Journal of Bridge Engineering*, ASCE, 10.1061/(ASCE)BE.1943-5592.0000397, 553-563.

Wu, Y. F., Liu, T., and Wang, L.(2008), “Experimental investigation on seismic retrofitting of square RC columns by carbon FRP sheet confinement combined with transverse short glass FRP bars in bored holes”, *Journal of Composites for Construction*, ASCE, 12(1), 53-60.

Wu, Y. F., and Wei, Y. Y. (2010), “Effect of cross sectional aspect ratio on the strength of CFRP-confined rectangular concrete columns, *Engineering Structure*, 32, 32-45.

Yamakawa, T., Zhong, P., and Ohama, A. (2003). “Seismic performance of aramid fiber square tubed concrete columns with metallic and/or non metallic reinforcement.” *Journal of Reinforced Plastic and Composites*, 22(13): 1221 -1237.

Ye, L.P., Zhang, K., Zhao, and Feng, P. (2003). “Experimental study on seismic strengthening of RC columns with wrapped CFRP sheets.” *Construction and Building Materials*, 17, 499-506.

Zhu, Z., Ahmad, I., and Mirmiran, A. (2006). “Seismic performance of concrete-filled FRP tube columns for bridge substructure.” *Journal of Bridge Engineering*, ASCE, 11(3), 359-370.

Zohrevand, P., and Mirmiran A. (2013). “Seismic response of ultra-high performance concrete-filled FRP tube columns.” Journal of Earthquake Engineering, 17(1), 155-170.

Table 1. Properties of Test Specimens

Column	f'_c (MPa)	Cross-sectional shape	R (mm)	R/D	FRP tube fiber type	Number of FRP layers	$\varepsilon_{h,fail}$	f_{lu}/f'_c	$f_{lu,a}/f'_c$	P (kN)	P/P_o
CFFT -1	95	Square	15	0.1	Aramid	3	0.014	0.24	0.14	565	0.27
CFFT -2	95	Square	30	0.2	Aramid	3	0.013	0.24	0.13	582	0.28
CFFT -3	62	Square	15	0.1	Aramid	3	0.020	0.37	0.29	617	0.41
CFFT -4	95	Square	15	0.1	Aramid	2	0.012	0.16	0.08	582	0.27
CFFT -5	95	Square	15	0.1	Carbon	4	0.010	0.25	0.16	595	0.28
CFFT -6	95	Circular	75	0.5	Aramid	3	0.021	0.24	0.20	725	0.42

* f'_c = concrete strength; f_{lu}/f'_c = nominal confinement ratio; $f_{lu,a}/f'_c$ = actual confinement ratio; P = applied axial compression; P/P_o = Axial load level; R = FRP tube corner radius; R/D = corner radius to sectional dimension ratio; $\varepsilon_{h,fail}$ = FRP tube hoop strain at column failure

Table 2. Material Properties of Fiber Sheets and Epoxy Resin Used in FRP tubes

Type	Nominal thickness t_f (mm/ply)	Provided by manufacturers			Obtained from flat FRP coupon tests		
		Tensile strength f_f (MPa)	Ultimate tensile strain, ε_f (%)	Elastic modulus E_f (GPa)	Tensile strength f_{frp} (MPa)	Ultimate tensile strain, ε_{frp} (%)	Elastic modulus E_{frp} (GPa)
Aramid	0.200	2900	2.50	116.0	2663	2.12	125.7
Carbon	0.117	3800	1.55	240.0	3626	1.44	251.0
Epoxy Resin	-	> 50	2.50	> 3	-	-	-

Table 3. Material Properties of Steel Reinforcing Bars

Diameter (mm)	Yield Stress, f_y (MPa)	Yield strain, ε_y (%)	Ultimate strength, f_u (MPa)	Ultimate strain, ε_u (%)	Rupture strain, ε_r (%)
10	600	0.3	760	8.0	10.5

Table 4. Observed column behavior

Column	f'_c (MPa)	P/P_o	M_{max} (kN.m)	Δ_y (mm)	$\Delta_{0.8Mmax}$ (mm)	δ_{max} (%)	δ_{Mmax} (%)	$\delta_{0.8Mmax}$ (%)	μ	Maximum* Damage Region (mm)	Plastic hinge length (mm)
CFFT-1	95	0.27	55.7	13.0	80	11.0	3.0	8.0	6.2	120	200
CFFT-2	95	0.28	53.4	13.2	80	11.0	5.0	8.0	6.1	120	190
CFFT-3	62	0.41	47.4	12.7	90	9.0	5.0	9.0	7.1	130	300
CFFT-4	95	0.27	53.9	13.4	60	8.0	3.0	6.0	4.5	140	220
CFFT-5	95	0.28	49.2	13.0	70	9.0	3.0	7.0	5.8	100	180
CFFT-6	95	0.42	44.3	14.5	95	11.0	7.0	9.5	6.5	130	200

M_{max} = maximum recorded moment (averaged from push and pull directions); $\Delta_{0.8Mmax}$ = failure displacement; Δ_y = yield displacement; $\delta_{0.8Mmax}$ = lateral drift at 20% strength decay (i.e. column lateral drift capacity); δ_{max} = maximum lateral drift; δ_{Mmax} = lateral drift at maximum moment; μ= ductility factor.

*Measured from column-footing interface to the far end of FRP tube rupture region.

Table 5. Test results of companion square FRP-confined concrete columns

Study	Specimen	Type of fiber	D (mm)	L (mm)	L/D	R/D	f'_c (MPa)	f_{lu}/f'_c	P/P_o	$\delta_{0.8Mmax}$ (%)
Group 1										
Present study	CFFT-1	Aramid	150	1000	6.7	0.10	95.0	0.24	0.27	8.0
Present study	CFFT-2	Aramid	150	1000	6.7	0.20	95.0	0.24	0.28	8.0
Present study	CFFT-5	Carbon	150	1000	6.7	0.10	95.0	0.25	0.28	7.0
O&S (2007)	RS-1	Carbon	270	2000	7.4	0.17	90.1	0.26	0.32	8.0
Group 2										
O&S (2007)	RS-6	Carbon	270	2000	7.4	0.03	75.2	0.19	0.34	2.3
Iacobucci et al. (2003)*	ASC-2NS	Carbon	305	1473	4.8	0.05	36.5	0.17	0.33	3.8
Ozcan et al. (2008)*	S-NL-1-27	Carbon	350	2000	5.7	0.09	19.4	0.17	0.27	6.0
Present study	CFFT-4	Aramid	150	1000	6.7	0.10	95.0	0.16	0.27	6.0
O&S (2007)	RS-4	Carbon	270	2000	7.4	0.17	75.2	0.19	0.34	6.0

Note: D = column sectional dimension; f_{lu}/f'_c = nominal confinement ratio; L = shear span length; L/D = column aspect ratio; P/P_o = axial load level; R/D = radius to sectional dimension ratio; $\delta_{0.8Mmax}$ = lateral drift at 20% strength decay (i.e. column lateral drift capacity).

*FRP-wrapped columns

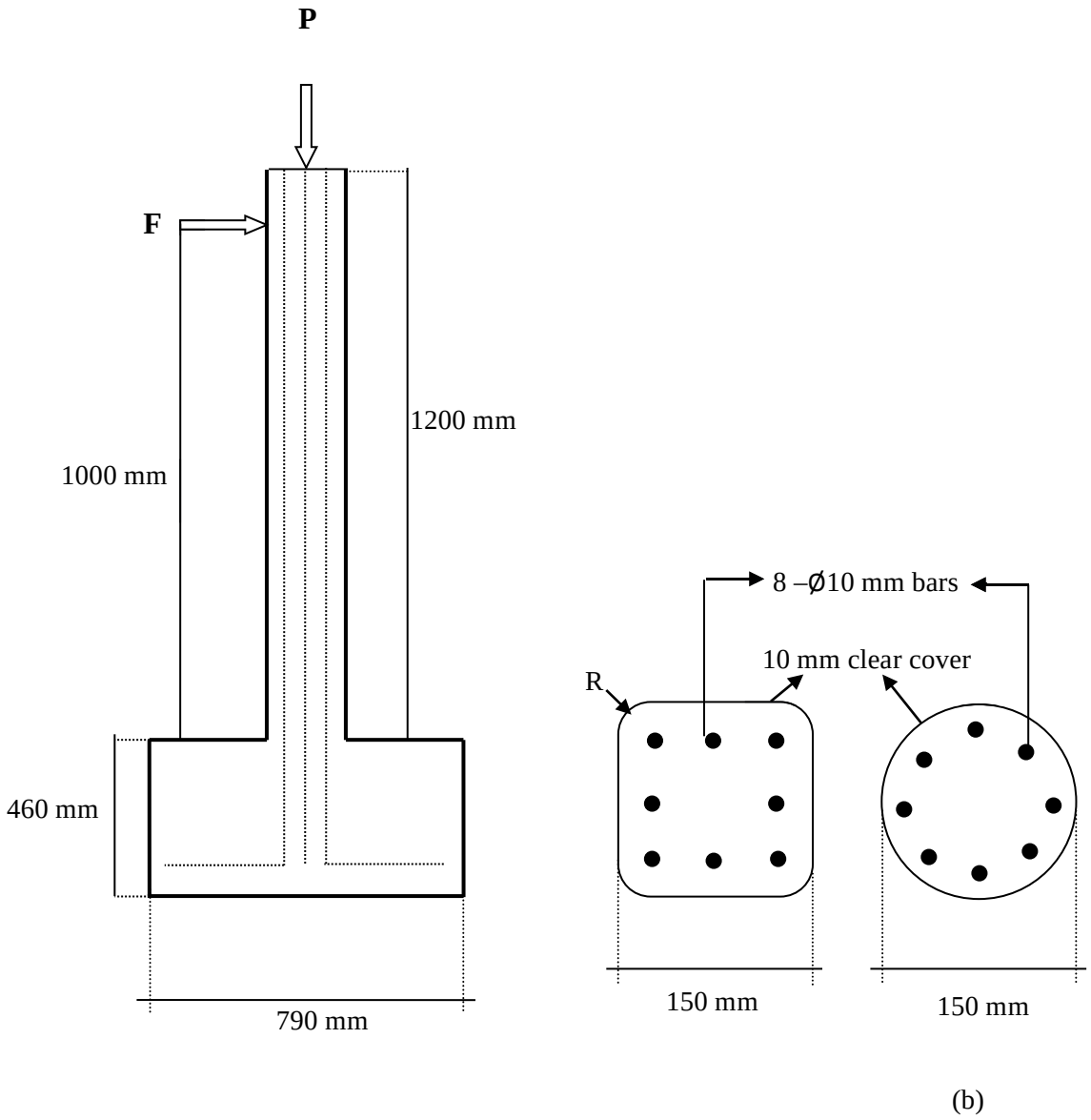

Fig. 1. Column geometry: (a) Square CFFT column, (b) Circular CFFT column

Fig. 2. Manufacturing process of CFFT columns

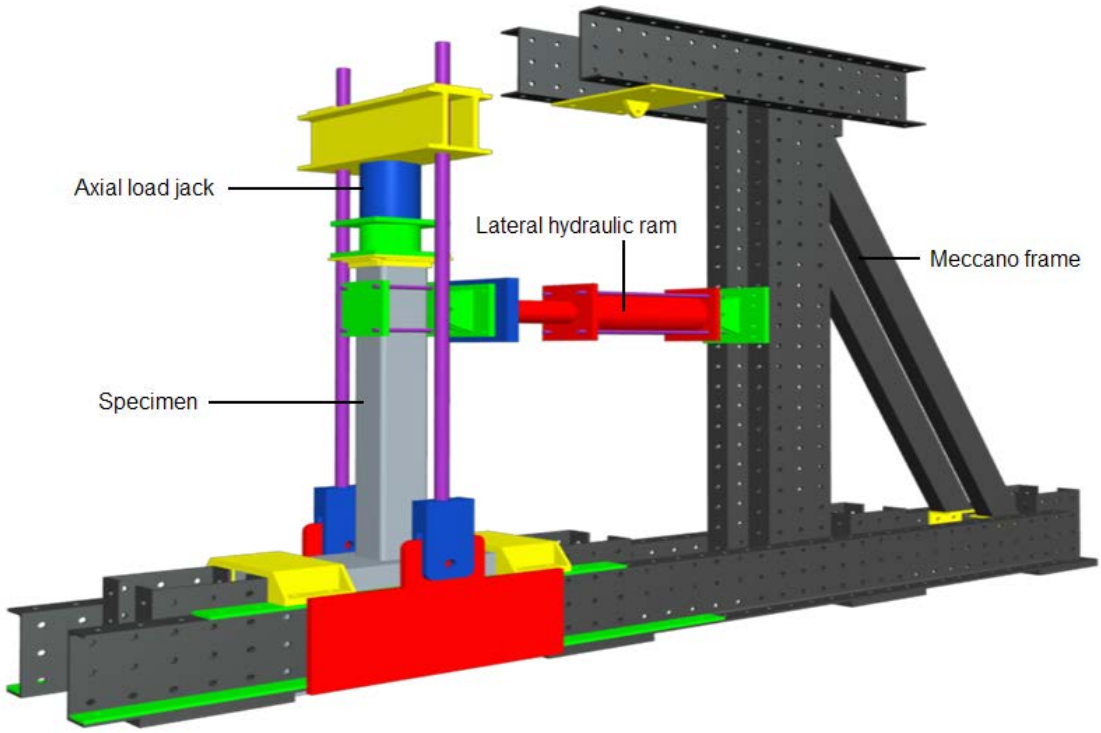

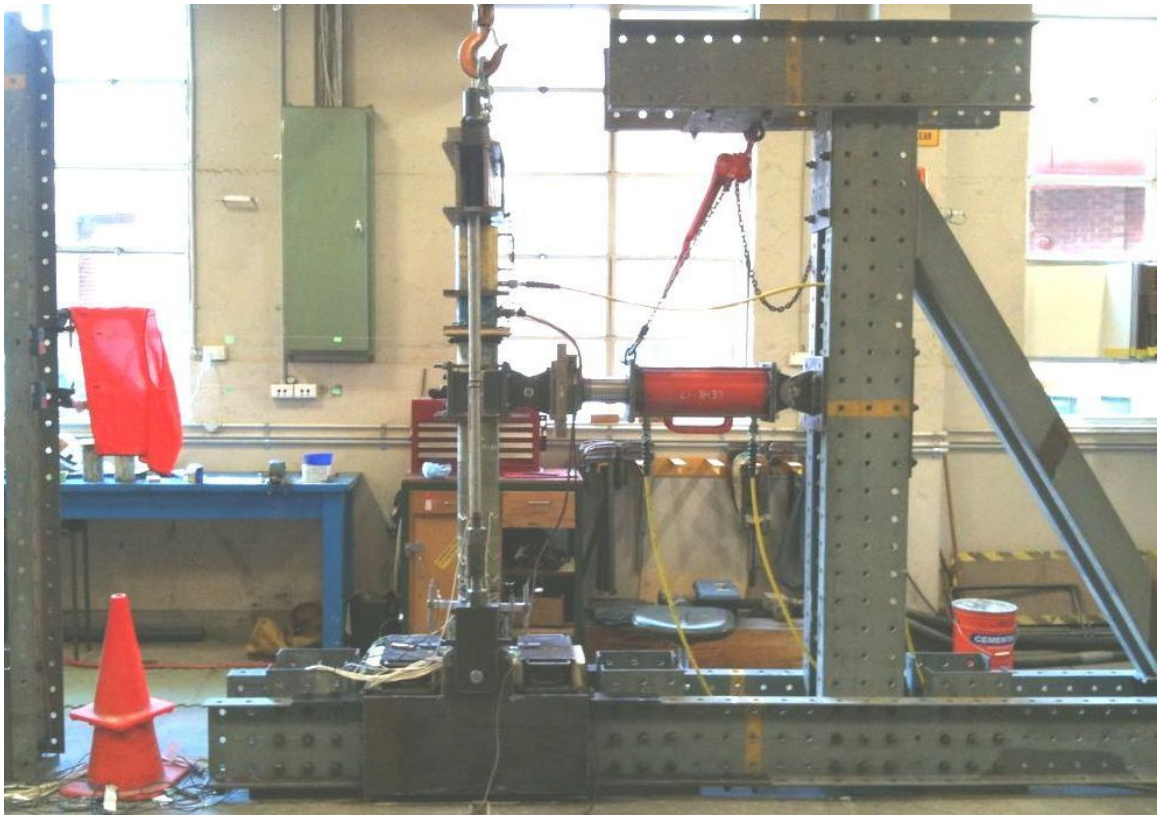

Fig. 3. Column test setup

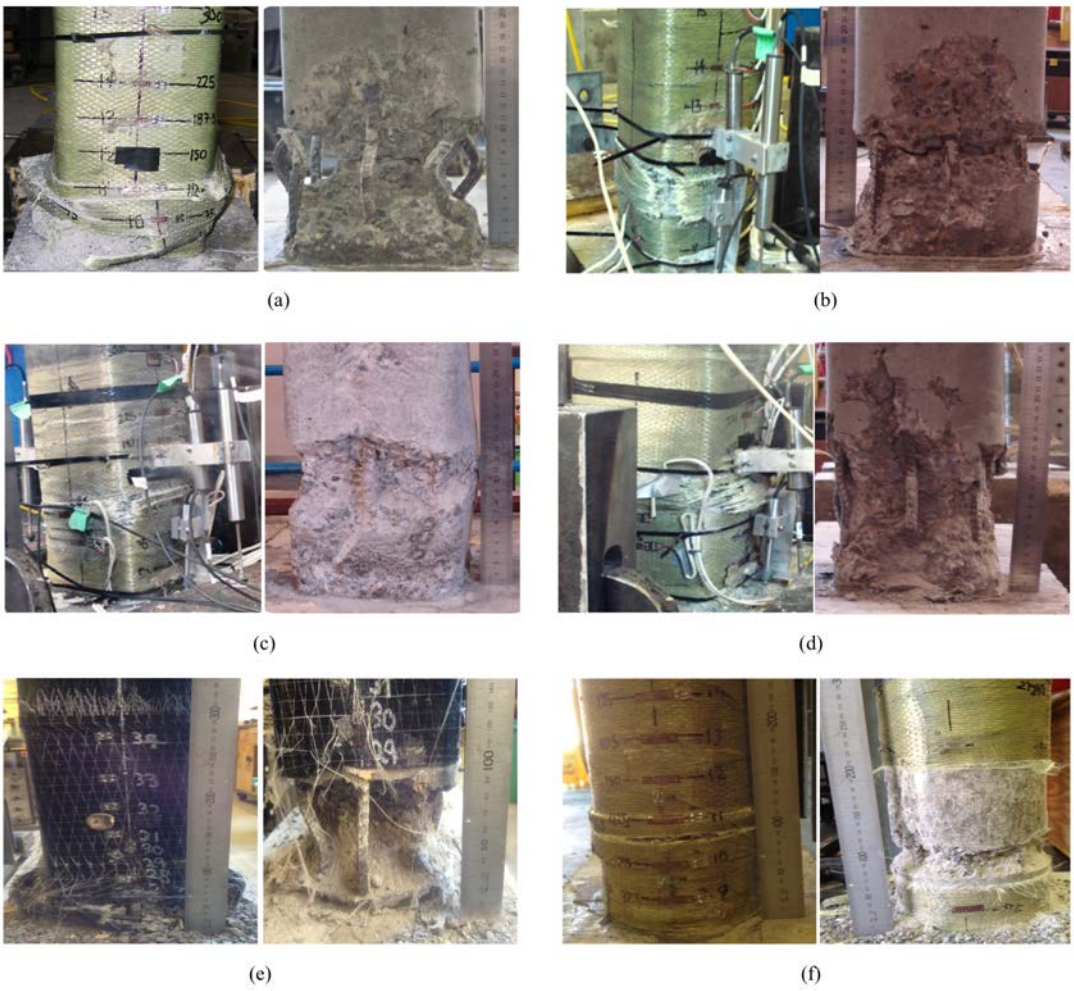

Fig. 4. Plastic hinge regions of columns at the end of testing : (a) CFFT-1, (b) CFFT-2, (c) CFFT-3, (d) CFFT-4, (e) CFFT-5, (f) CFFT-6

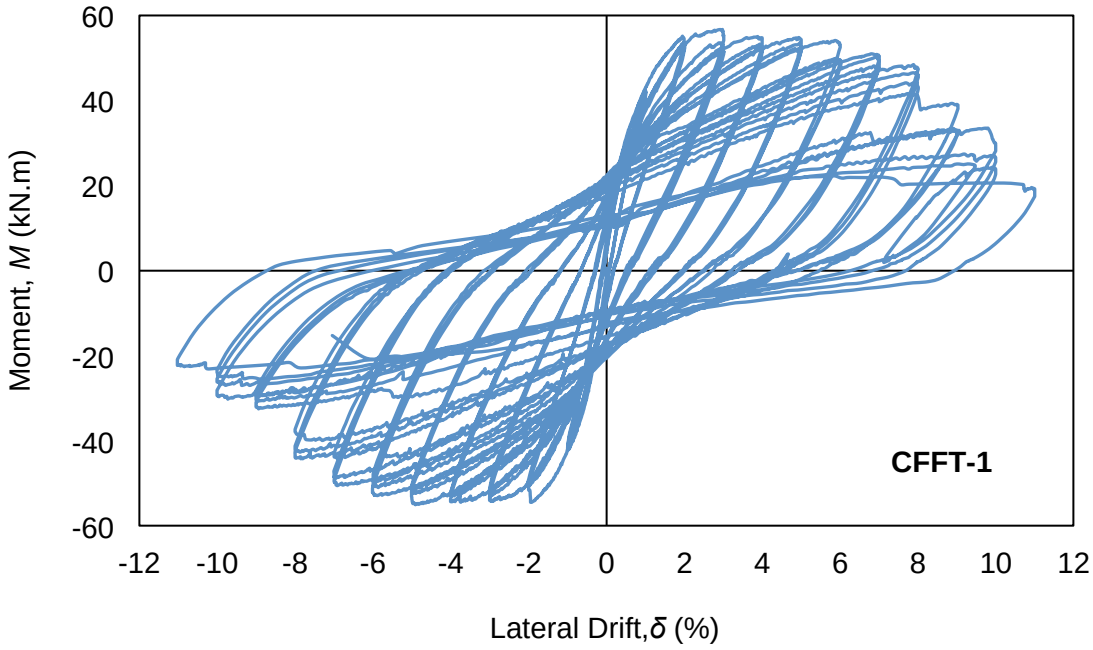
60
40
20
0
-20
-40
-60
-12
-10
-8
-6
-4
-2
0
2
4
6
8
10
12
Moment, M (kN.m)
Lateral Drift,δ (%)
CFFT-1

(a)

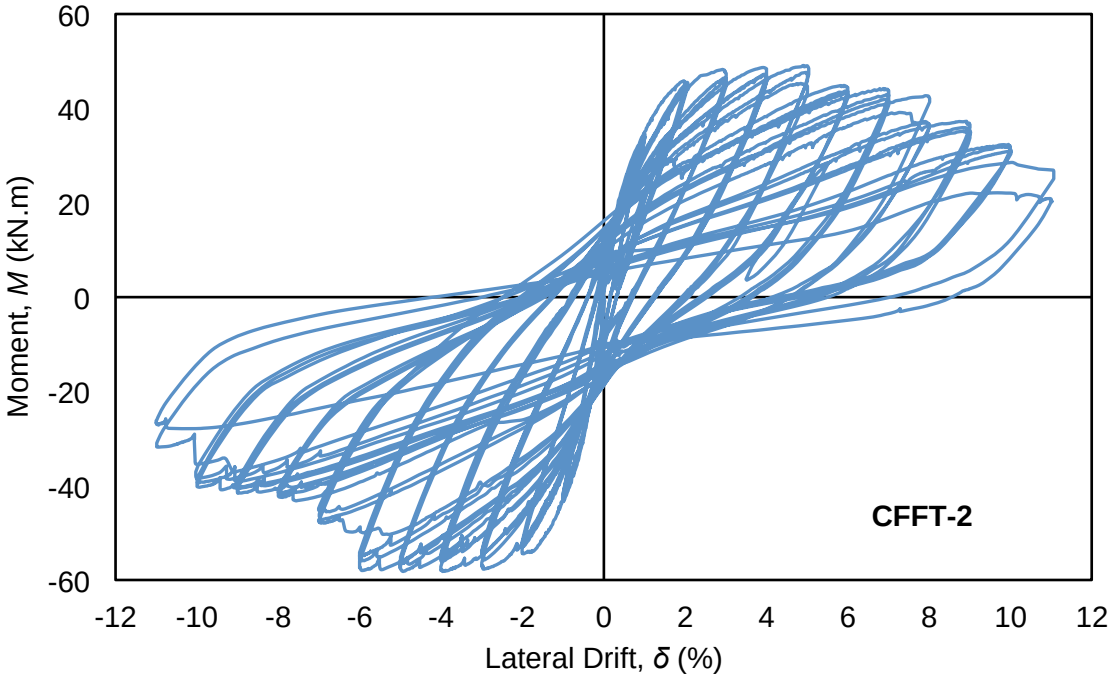
60
40
20
0
-20
-40
-60
-12
-10
-8
-6
-4
-2
0
2
4
6
8
10
12
Moment, M (kN.m)
Lateral Drift, δ (%)
CFFT-2

(b)

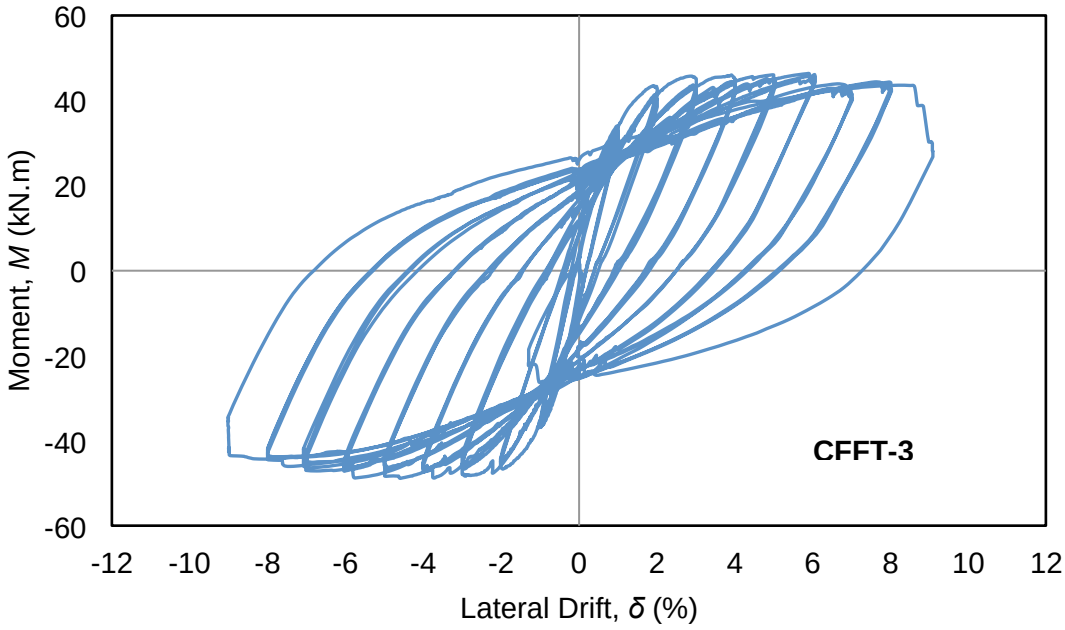
60
40
20
0
-20
-40
-60
-12
-10
-8
-6
-4
-2
0
2
4
6
8
10
12
Moment, M (kN.m)
Lateral Drift, δ (%)
CFFT-3

(c)

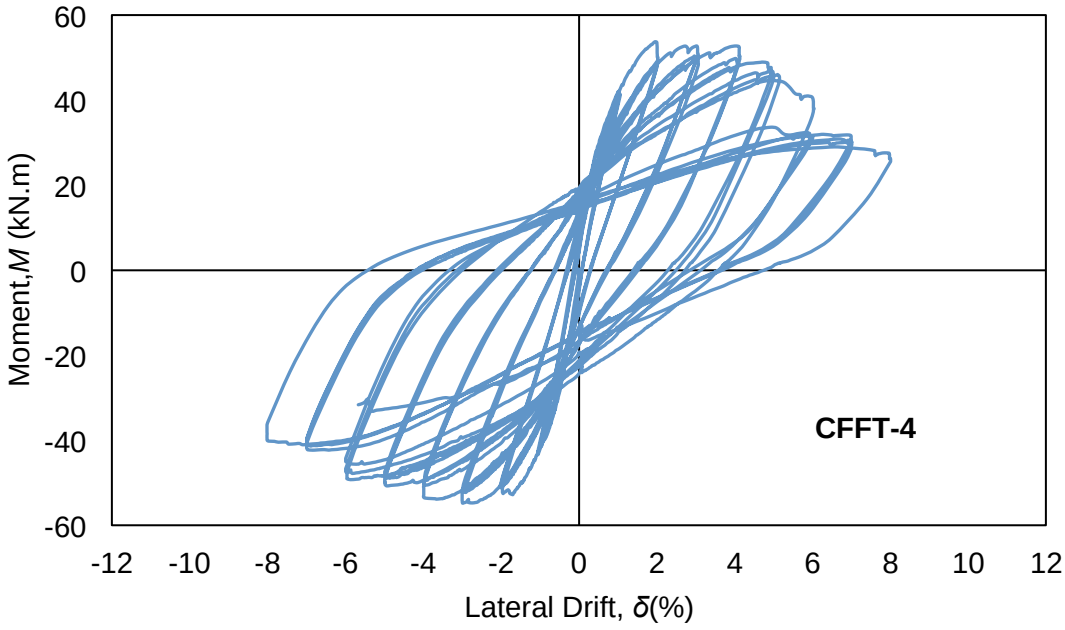
60
40
20
0
-20
-40
-60
-12
-10
-8
-6
-4
-2
0
2
4
6
8
10
12
Moment,M (kN.m)
Lateral Drift, δ(%)
CFFT-4

(d)

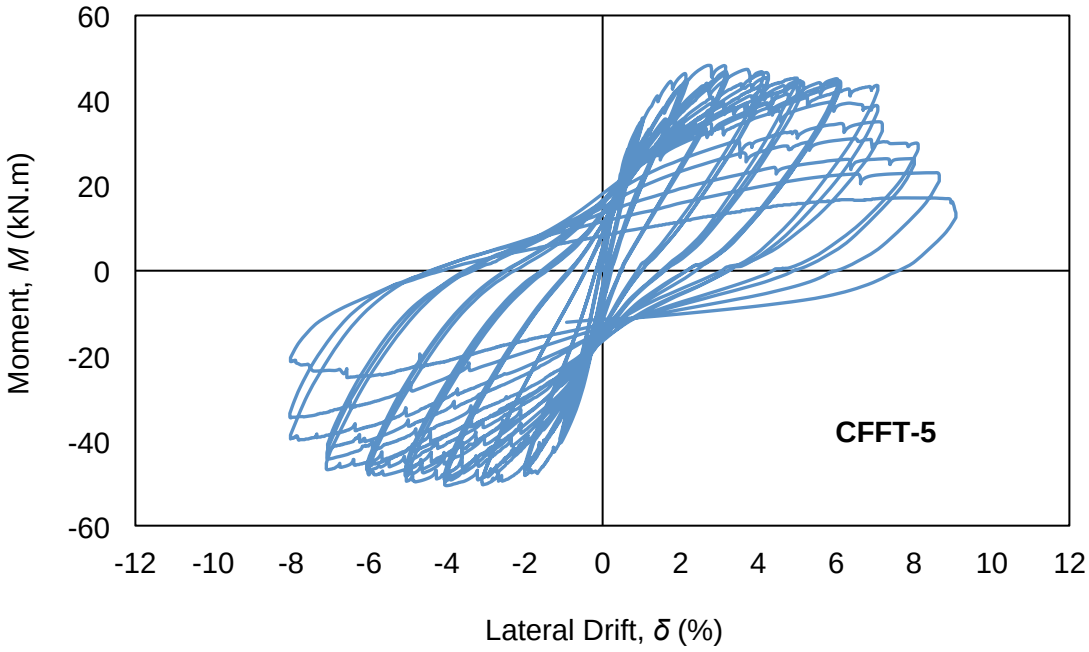

(e)

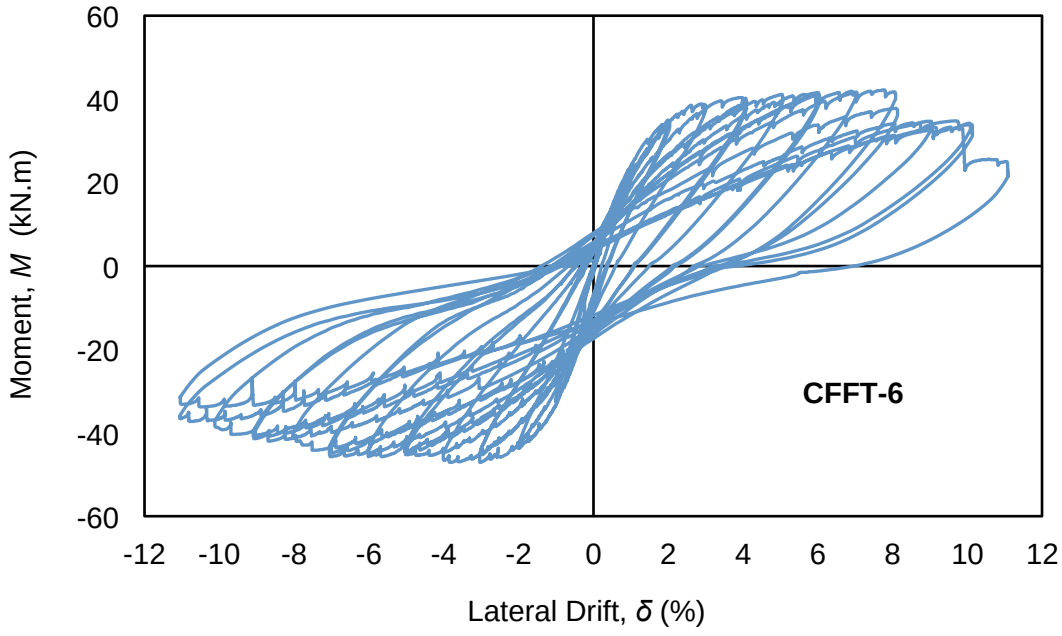

(f)

Fig. 5. Experimentally recorded hysteretic moment-lateral drift relationships: (a) CFFT-1, (b) CFFT-2, (c) CFFT-3, (d) CFFT-4, (e) CFFT-5, (f) CFFT-6

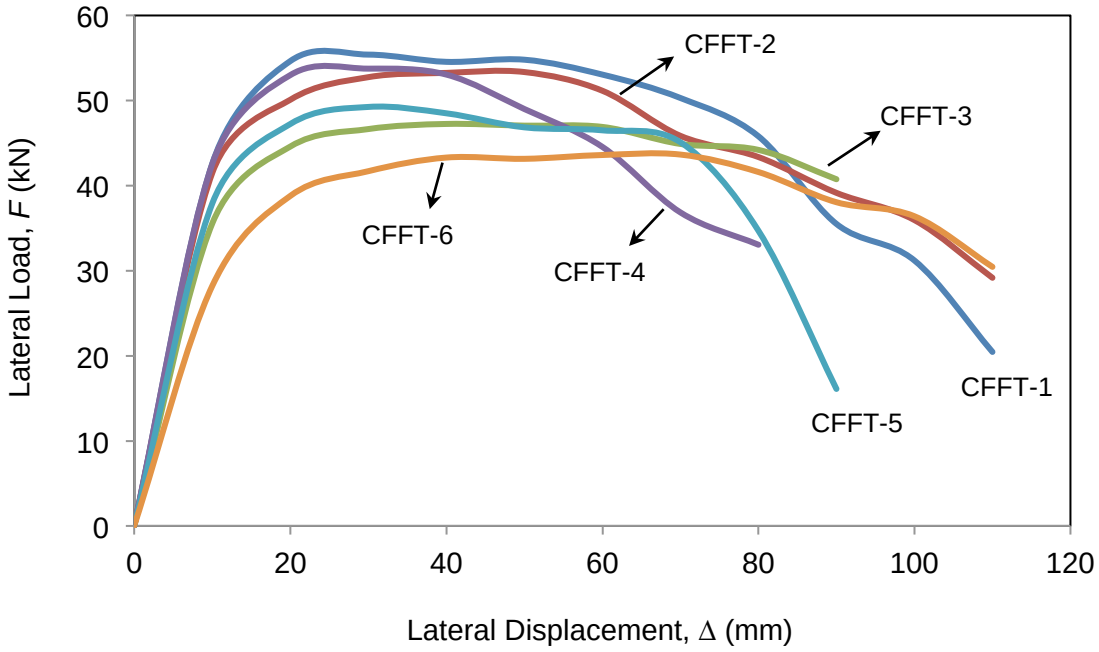

Fig. 6. Envelop curves of column lateral load-displacement relationships

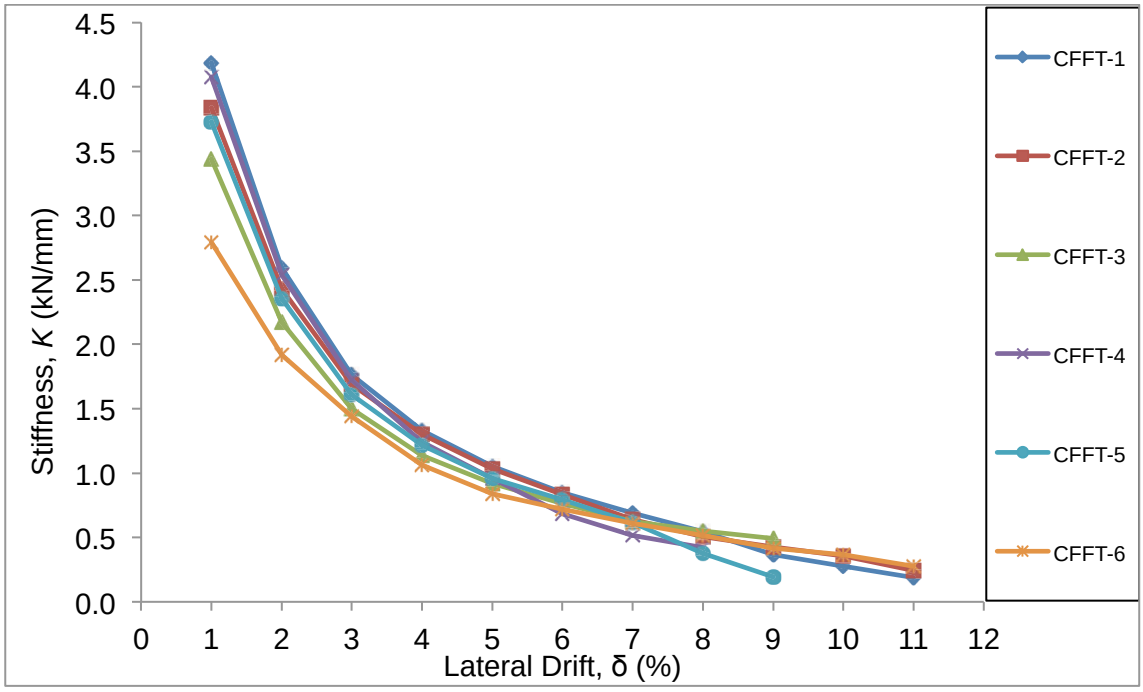

Fig. 7. Variation of column stiffnesses with lateral drifts

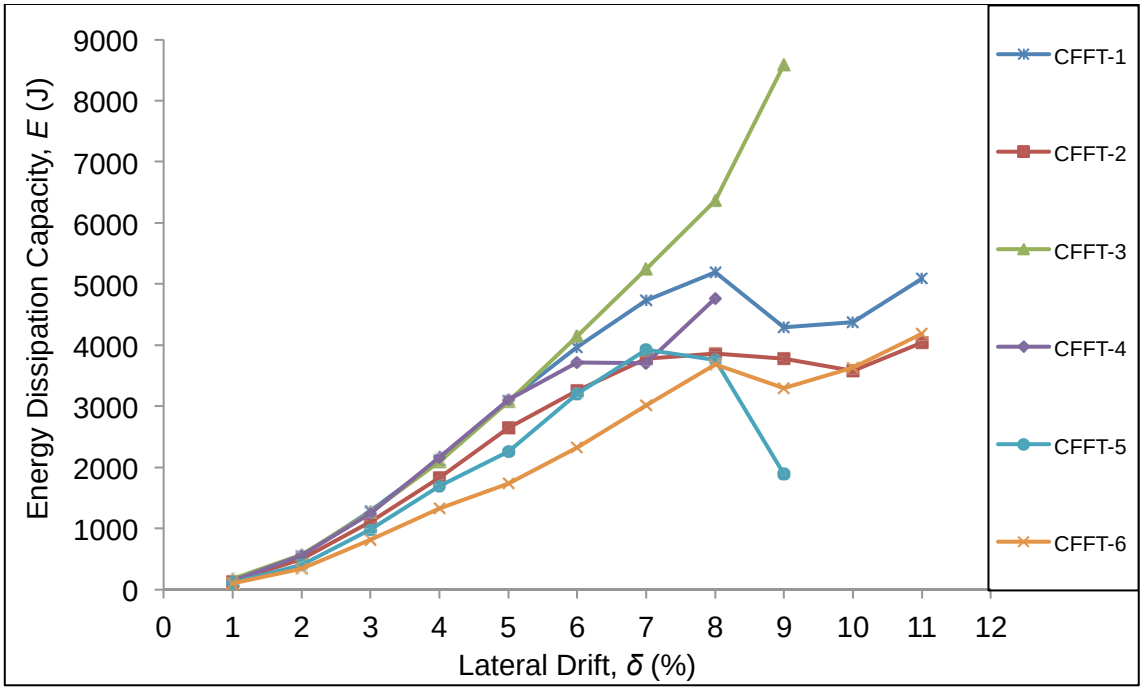

Fig. 8. Column energy dissipation capacities

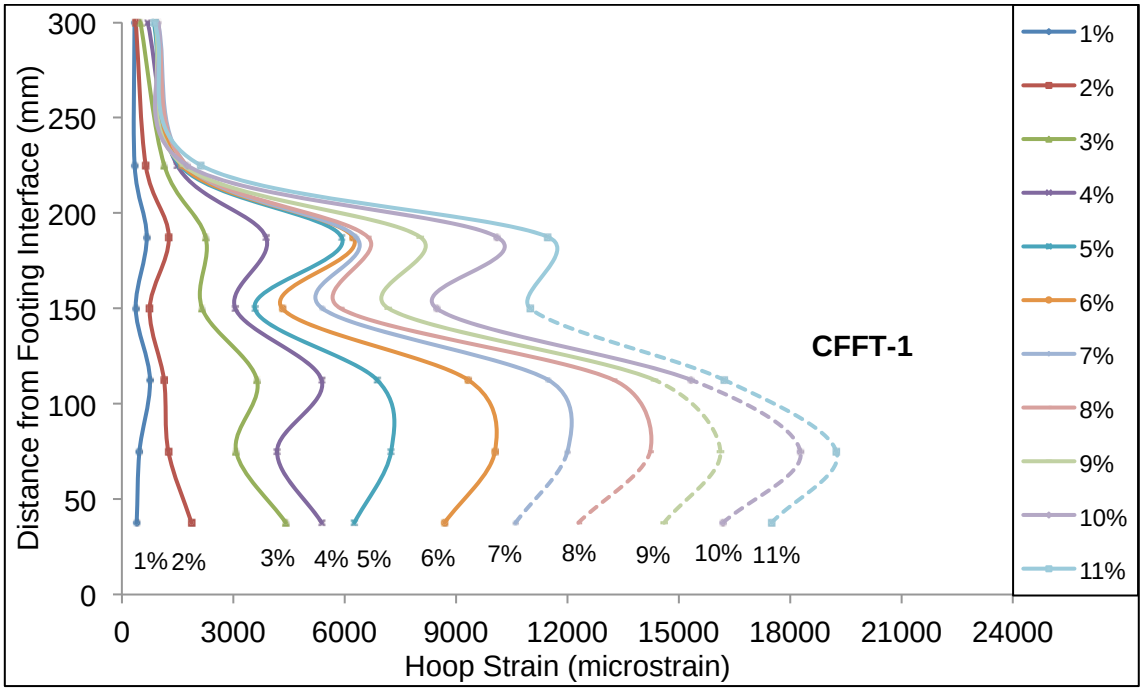
Distance from Footing Interface (mm)
300
250
200
150
100
50
0
0
3000
6000
9000
12000
15000
18000
21000
24000
Hoop Strain (microstrain)
CFFT-1
1%
2%
3%
4%
5%
6%
7%
8%
9%
10%
11%

(a)

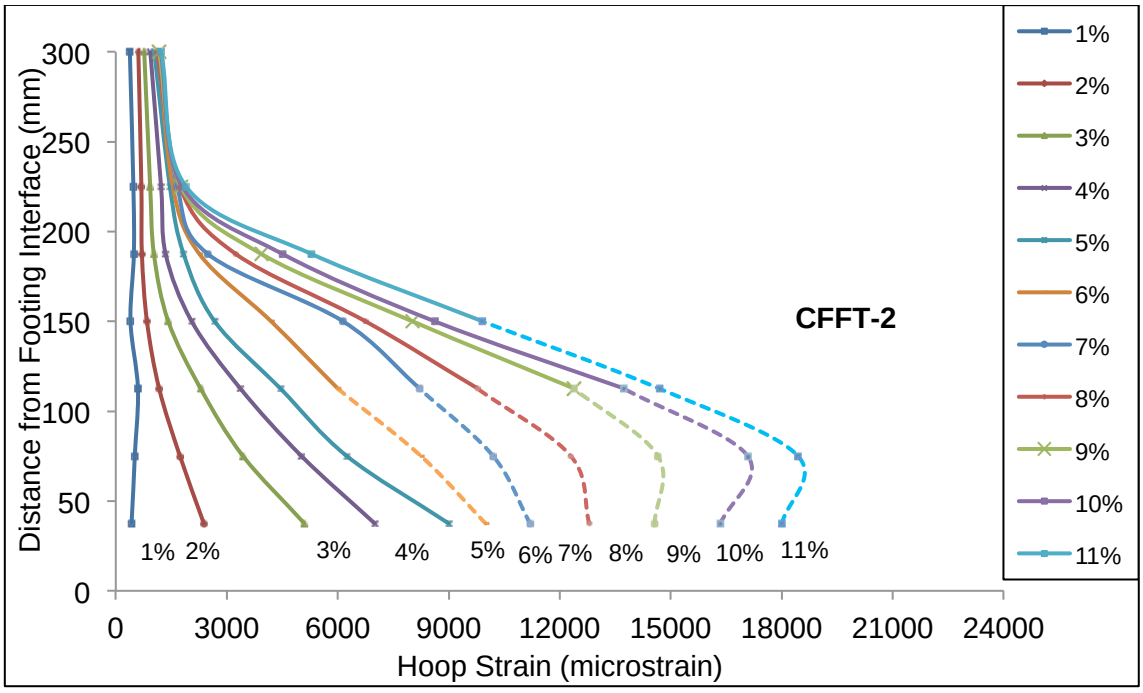
Distance from Footing Interface (mm)
300
250
200
150
100
50
0
0
3000
6000
9000
12000
15000
18000
21000
24000
Hoop Strain (microstrain)
CFFT-2
1%
2%
3%
4%
5%
6%
7%
8%
9%
10%
11%

(b)

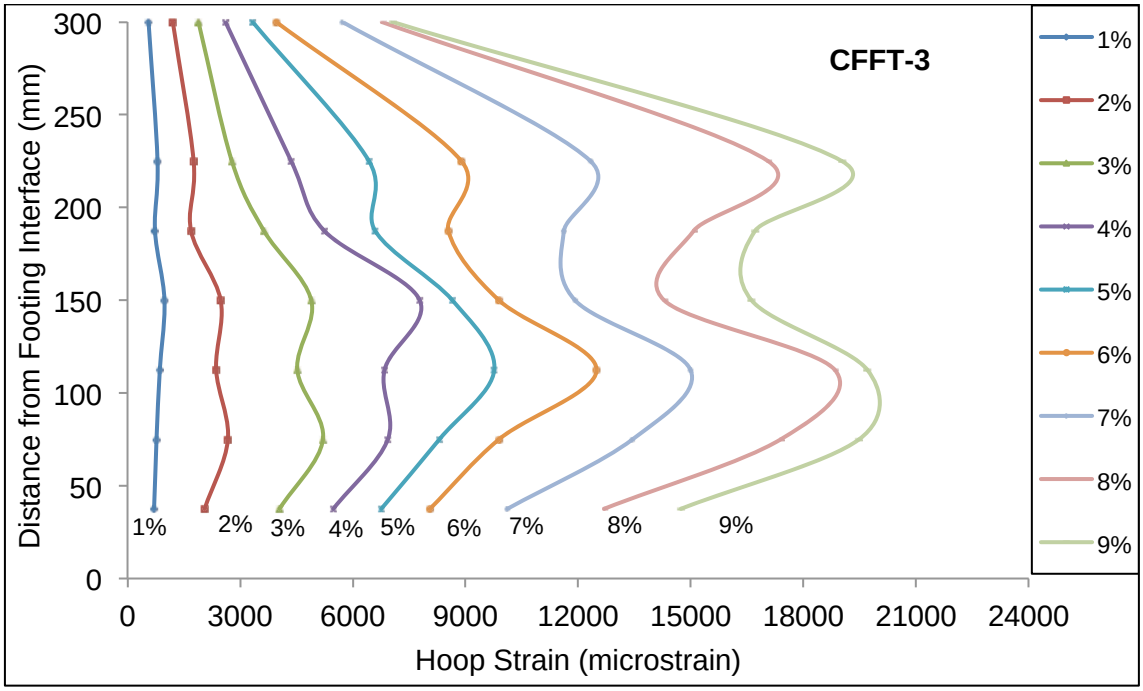
CFFT-3
Distance from Footing Interface (mm)
Hoop Strain (microstrain)
0
50
100
150
200
250
300
0
3000
6000
9000
12000
15000
18000
21000
24000
1%
2%
3%
4%
5%
6%
7%
8%
9%

(c)

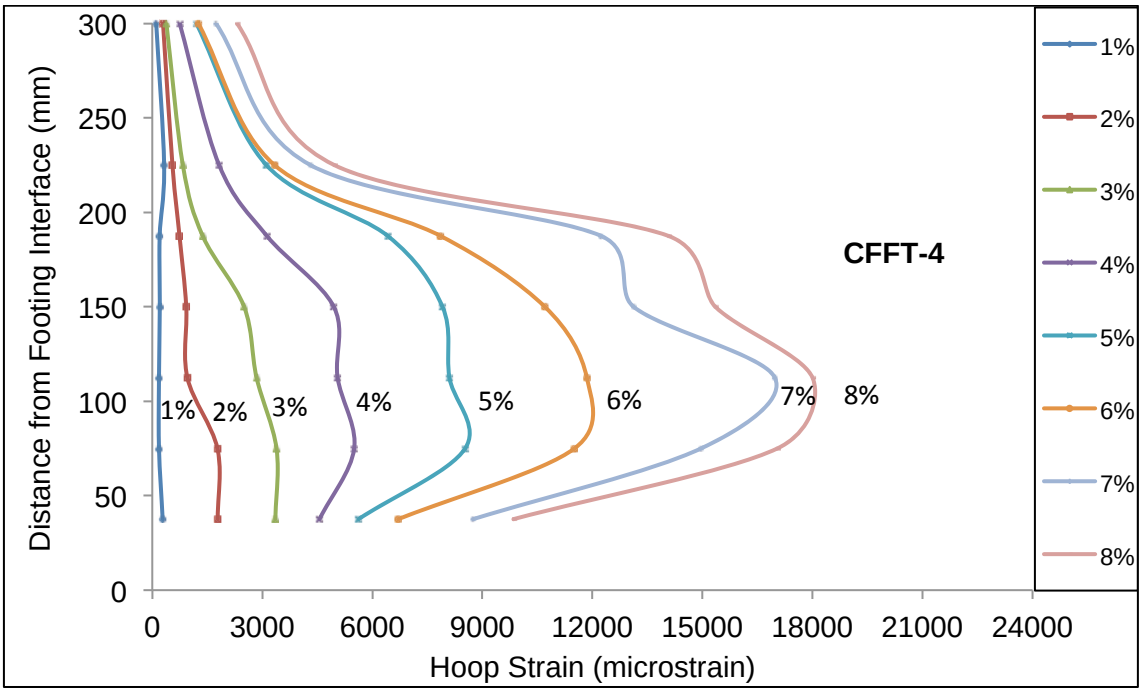
CFFT-4
Distance from Footing Interface (mm)
Hoop Strain (microstrain)
0
50
100
150
200
250
300
0
3000
6000
9000
12000
15000
18000
21000
24000
1%
2%
3%
4%
5%
6%
7%
8%

(d)

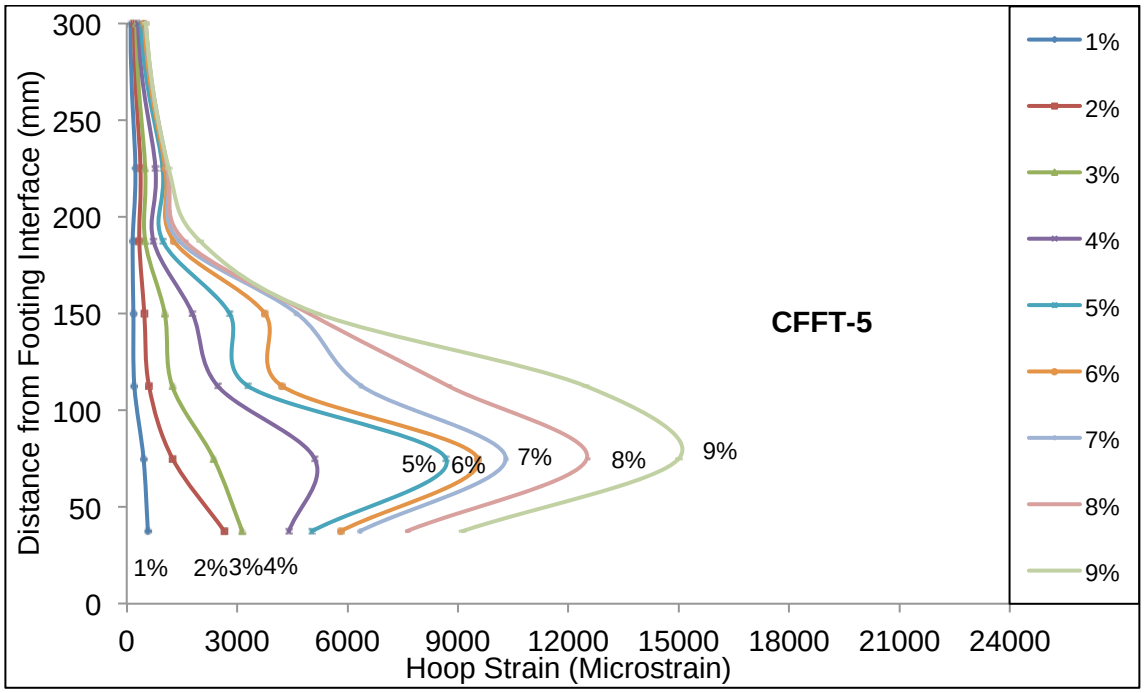

(e)

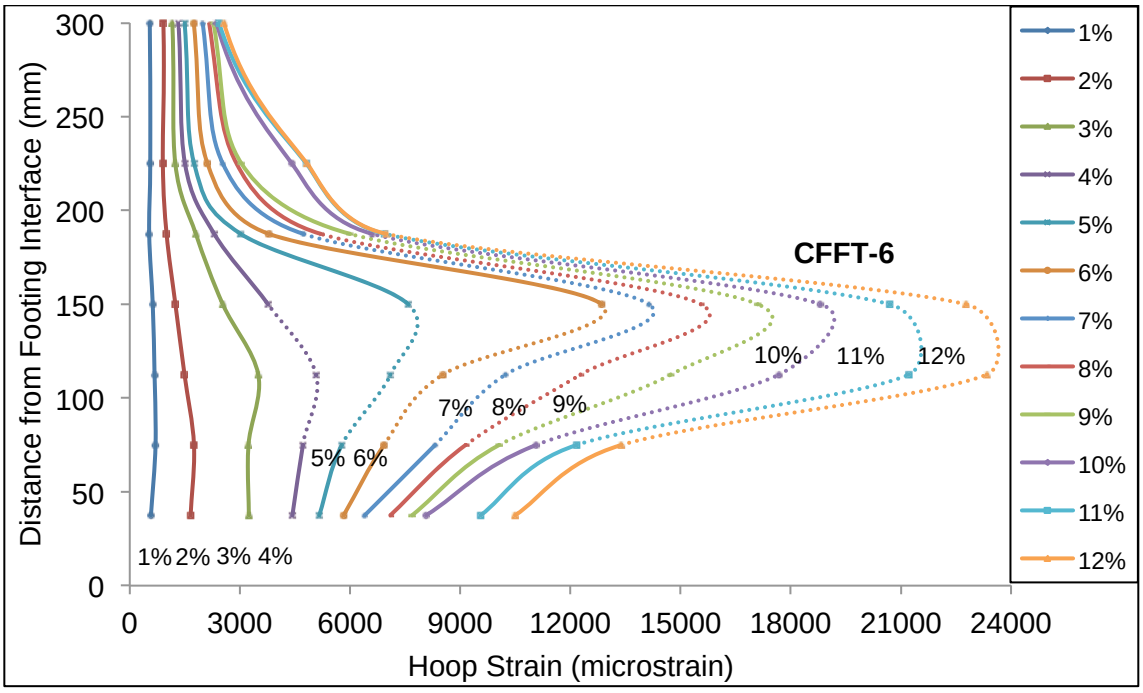

(f)

Fig. 9. Variation of FRP tube hoop strains along column height: (a) CFFT-1, (b) CFFT-2, (c) CFFT-3, (d) CFFT-4, (e) CFFT-5, (f) CFFT-6

CHAPTER 3

Seismic Behavior of FRP-High-Strength Concrete-Steel Double-Skin Tubular Columns

Togay Ozbakkaloglu and Yunita Idris

School of Civil, Environmental, and Mining Engineering, University of Adelaide, 5000

Journal of Structural Engineering, ASCE (Published)

Statement of Authorship

Title of Paper	Seismic Behavior of FRP-High-Strength Concrete-Steel Double-Skin Tubular Columns
Publication Status	● Published ○ Accepted for publication ○ Submitted for publication ○ Publication style
Publication Details	Ozbakkaloglu, T., and Idris, Y. (2014), "Seismic behavior of FRP-high-strength concrete-steel double skin tubular columns." *Journal of Structural Engineering, ASCE*, 140(6): 04014019.

Author Contributions

By signing the Statement of Authorship, each author certifies that their stated contribution to the publication is accurate and that permission is granted for the publication to be included in the candidate's thesis.

Name of Principal Author (Candidate)	Dr. Togay Ozbakkaloglu		
Contribution to the Paper	Research planning and supervision and review of manuscript		
Signature		Date	23/09/2015

Name of Co-Author	Yunita Idris		
Contribution to the Paper	Review of literature, analysis data, and preparation of manuscript		
Signature		Date	22/09/2015

SEISMIC BEHAVIOR OF FRP-HIGH-STRENGTH CONCRETE-STEEL DOUBLE SKIN TUBULAR COLUMNS

Togay OZBAKKALOGLU and Yunita IDRIS

ABSTRACT

This paper reports on an experimental study on the seismic behavior of fiber reinforced polymer (FRP)-concrete-steel double skin tubular (DST) columns. Nine DST and one concrete-filled FRP tube (CFFT) columns that were made of high-strength concrete (HSC) were tested under constant axial compression and reversed-cyclic lateral loading. The main parameters of the experimental study included axial load level, amount and type of FRP confinement, concrete strength, sectional shape and thickness of the inner steel tube, and provision (or absence) of a concrete filling inside the steel tube. Of primary importance, the results indicate that DST columns are capable of developing very high inelastic deformation capacities under simulated seismic loading. The results also indicate that the presence of a concrete filling inside the inner steel tube significantly and positively influences the seismic behavior of DST columns. It is found that the performance of the void-filled DST column is superior to that of a companion CFFT column having identical geometric and material properties apart from the main internal steel reinforcing bars. These early observations suggest that DST columns may provide an attractive alternative to CFFT columns in the construction of new earthquake-resistant columns. No detrimental effect of the increased concrete strength on the displacement capacity of the DST columns is observed, provided that the amount of confinement is increased proportionally with the concrete strength. The influence of the cross-sectional geometry of the inner steel tube is found to be significant, whereas the thickness of the steel tube is found to have only a minor influence on the behavior of DST columns. It is observed that the FRP tube material has some influence on the lateral displacement capacity of DST columns, with the

specimens confined by FRP tubes manufactured using fibers with higher ultimate tensile strains developing slightly higher displacement capacities. Examination of the test results has led to a number of significant conclusions in regards to the influence of the important column parameters on the performance of DST columns. These results are presented together with a discussion of the influence of the main parameters on the seismic behavior of DST columns.

KEYWORDS: Fiber reinforced polymers (FRP); High-strength concrete (HSC); Columns; Confinement; Tubes; Lateral displacement; Concret and masonry structures.

INTRODUCTION

Because of their favorable material properties, fiber reinforced polymer (FRP) composites have become increasingly popular in the construction industry over the last two decades. As an important application of FRP composites, confinement of concrete with externally bonded FRP has received a great deal of attention. A large numbers of experimental studies have been conducted both on the axial compressive (e.g. Mirmiran and Shahawy 1997; Rochette and Labossiere 2000; Pessiki et al. 2001; Lam and Teng 2004; Berthet et al. 2005; Ilki et al. 2008; Eid et al. 2009; Cui and Sheikh 2010; Kusumawardaningsih and Hadi 2010; Wu and Wei 2010; Dai et al. 2012; Ozbakkaloglu and Akin 2012) and seismic behavior (e.g. Saadatmanesh et al. 1996; Sheikh and Yau 2002; Iacobucci et al. 2003; Haroun and Elsanadedy 2005; Hosseini et al. 2005; Chung, et al. 2008; Realfonzo and Napoli 2009; Gu et al. 2010; Ozcan et al 2010) on FRP-wrapped columns to investigate the use of FRP confinement for strengthening existing concrete columns. The use of FRP composites in the construction of new high-performance composite columns in the form of concrete-filled FRP tubes (CFFTs) have also received significant attention, with a number

of resulting studies reported on the axial compressive (Mirmiran et al. 1998; Fam and Rizkalla 2001; Hong and Kim 2004; Fam et al. 2005; Ozbakkaloglu and Oehlers 2008a,b; Mohamed and Masmoudi 2010; Park et al. 2011; Zohrevand and Mirmiran 2011, 2013; Ozbakkaloglu 2013a,b,c) and seismic behavior (Yamakawa et al. 2003; Shao and Mirmiran 2005; Ozbakkaloglu and Saatcioglu 2006, 2007; Saatcioglu et al. 2008; ElGawady et al. 2010; ElGawady and Dawood 2012; Zaghi et al. 2012; Zohrevand and Mirmiran 2012) of CFFT columns.

Very much like FRP, the popularity of high-strength concrete (HSC) in the construction industry has been on a steady incline during the last two decades due to the superior performance and economy offered by HSC over normal-strength concrete (NSC) in a large number of structural engineering applications. The use of HSC in the construction of CFFT columns is particularly attractive because the combination of two high-strength materials (i.e HSC and FRP) results in high-performance columns. The tests conducted by Ozbakkaloglu and Saatcioglu (2006, 2007) on large-scale HSCFFT columns have demonstrated the ability of these columns to exhibit highly ductile behavior under simulated seismic loading.

More recently a new type of composite system was proposed by Teng et al. (2004) in the form of a FRP-concrete-steel double-skin tubular (DST) column. This composite system consists of a steel tube inside, a FRP tube outside with concrete in between, and it combines the advantages of all three materials to achieve a high-performance structural member. A series of axial compression and flexure tests have been conducted by the research group lead by Teng (Teng et al. 2007; Yu et al. 2006; Wong et.al 2008; Yu et al. 2010) to investigate the performance of FRP-concrete-steel DST stub columns and beams. Following these studies, Han et al. (2010) reported on the tests of eight DST beam-columns and Zhang et al. (2012) reported on the tests of six DST columns that were tested

under combined axial compression and lateral cyclic loading. The results of these early tests have demonstrated that the DST beam and column systems provide very effective confinement to concrete, which in turn results in a highly ductile member behavior. However, research on the seismic behavior of DST columns have been extremely limited, with only a single study reported by to date by Zhang et al. (2012). Additional studies are required to better understand and be able to model the behavior of these columns.

To contribute toward this end, the experimental program reported in this paper was aimed at investigating the performance of FRP-HSC-steel DST columns tested under combined axial compression and reversed-cyclic lateral loading. The main parameters of the study included the axial load level, amount and type of FRP confinement, concrete strength, cross-sectional shape and thickness of the inner steel tube, and provision (or absence) of a concrete filling inside the steel tube. The results of the experimental program are first presented, followed by a discussion on the influence of the main test parameters on test results.

EXPERIMENTAL PROGRAM

Test Specimens

Nine DST and one CFFT columns were manufactured and tested under constant axial compression and incrementally increasing lateral displacement reversals. The specimens were designed as cantilever columns that represented the lower portion of a first-story building column between the footing and point of inflection. The columns had a 150-mm circular cross-section and 1.2-m cantilever height and they were fixed into a heavily reinforced concrete footing that was 790 mm in length, 290 mm in width and 460 mm in height. Lateral load was applied to the specimens at a section 200 mm below the column

tip, which resulted in a shear span (L) of 1.0 m. The levels of constant axial compression (P) applied to the specimens were established to simulate loading conditions of typical building columns used in practice and they varied from 34% to 45% of the column nominal concentric load capacity (P_o) as reported in Table 1. The specimens were manufactured using different grades of HSC and they consisted of aramid FRP and carbon FRP external tubes. Table 1 provides a summary of material and geometric properties of the test specimens and Fig. 1 illustrates their geometry.

Material Properties

FRP tube

Aramid fibers were used to manufacture the outer FRP tube in all the specimens except for Column DST-6, which was designed with a CFRP external tube. The tubes were manufactured using a manual wet lay-up process, which involved wrapping epoxy resin impregnated fiber sheets around precision-cut high-density styrofoam moulds in the hoop direction. FRP sheets were wrapped around the moulds one layer at a time, with an overlap length of 100 mm provided for each layer to prevent premature debonding failure. The tubes were oriented such that the overlap regions corresponded to the side faces of the columns, with no overlaps provided along the extreme compression and tension faces. The number of FRP layers used in the tubes of each DSTC column was established as a function of concrete strength and applied axial load level, with the test results reported in Ozbakkaloglu and Saatcioglu (2006, 2007) on HSCFFT columns used to establish baseline performance estimates. Properties of aramid and carbon fibers used in the manufacture of the FRP tubes are shown in Table 2. The table reports both the manufacturer-supplied

properties and the ones obtained from the flat coupon tests based on nominal fiber thickness.

Concrete

Three different HSC mixes were used in the manufacture of the specimens. All the mixes consisted of crushed bluestone as the coarse aggregate with a nominal maximum size of 10 mm, and silica fume added at 8% of the binder content by weight. Water-to-cementations material ratios of the mixes were 0.31, 0.24 and 0.17 which resulted in test day concrete strengths of 95 MPa, 115 MPa and 130 MPa, respectively, as shown in Table 1.

Steel tube and reinforcing bars

All but one DST column specimens were designed to have circular inner steel tubes with an 88.9 mm external diameter, whereas a single specimen was provided with an 89 mm square inner steel tube. Seven of these specimens had inner steel tubes with 3.2 mm wall thickness, and an additional specimen was designed with a 5.5 mm thick internal steel tube. The material properties of the steel tubes were obtained through the testing of steel coupons cut from the original tube. These properties are shown in Table 3 for all the steel tubes. Because the steel tubes were designed as the main reinforcement of the columns, they were fully embedded into the concrete footing apart from a 25-mm clear cover provided between the end of the tube and the base of the footing, which resulted in an embedment length of 435 mm.

In addition to the nine DST columns, a single CFFT column that was reinforced with eight 10 mm steel bars was also tested. These reinforcing bars were designed with hooks to

anchor them fully into the reinforced concrete footing. Table 4 summarizes the material properties of the steel bars that were obtained from the direct tension tests.

Instrumentation, test setup and loading program

All the column specimens were instrumented with linear variable displacement transducers (LVDTs) and strain gauges to measure lateral displacements, rotations of the plastic hinge region, anchorage slip, and axial and hoop strains on both steel and FRP tubes. Column lateral displacements were measured by two string pots that were placed at heights of 1.0 m and 1.2 m measured from column-footing interface. Column rotations were measured by two LVDTs with 50-mm stroke capacities that were placed on FRP tube at 150 mm from column-footing interface. Anchorage slips were measured by two 10-mm stroke capacity LVDTs that were placed on FRP tubes 20 mm away from the interface. The acquisition of hoop strain data on FRP tubes was of particular interest to better understand the activation of the confinement mechanism and development of the confining pressures at different sections along the height of the columns. To this end, up to 30 strain gauges with 10-mm gauges lengths were bonded to each FRP tube in the hoop direction at seven to eight different cross-sections along the column height that extended up to 450 mm away from the interface. Axial and lateral strains of inner steel tubes were measured with 5-mm long strain gauges that were placed at four different cross-sections within a 300-mm long region measured from the interface.

The columns were tested under constant axial compression and incrementally increasing lateral deformation reversals, simulating seismic loading. The columns were first subjected to axial compression. A hydraulic jack with 1,000-kN working capacity combined with a 1,000-kN load cell was placed on the top of the column to apply the axial load. Lateral

deformation reversals were applied through hydraulic ram fitted with a 100-kN load cell that was placed 1,000 mm from the column-footing interface. Fig. 2 illustrates the test setup.

The magnitude of the applied axial compression (P) was determined based on the design axial load level (P/P_o) of the column, which ranged between 34% and 45% of the column nominal axial load capacity (P_o), calculated according to ACI 318-11 (ACI 2011) as

$$P_o = 0.85 f_c^{'} A_c + A_s f_y \quad (1)$$

where f'_c = cylinder strength of unconfined concrete, A_c = net cross-sectional area of concrete, A_s = total cross-sectional area of inner steel tube or reinforcing bars and f_y = yield strength of inner steel tube or reinforcing bars.

Following the application of the axial compression, the specimens were subjected to lateral displacement excursions, consisting of incrementally increasing deformation reversals. Three full cycles were applied at each deformation level, starting with 1% drift ratio and increasing to 2%, 3% etc. in the deformation control mode of the horizontal actuator. Lateral loading continued until the specimen was unable to maintain a significant fraction of its maximum lateral load resistance. The rate of lateral loading was applied at a constant rate of approximately 0.4 mm/sec and the total duration of a typical test was appoximately 5-6 h, depending on the lateral displacement capacity of column.

TEST RESULTS

Failure Modes

Fiber rupture was the failure mode for all but one column. In all columns, the most extensive damage occurred at approximately 60-100 mm above the column-footing interface, which coincided with the location of first fiber rupture. Shifting of the critical section from the interface was attributed to the confining effect of the footing. Similar observations were reported previously for CFFT columns by Ozbakkaloglu and Saatcioglu (2006, 2007) and for conventional steel-confined columns by Sheikh and Khoury (1993). Column DST-9 had no signs of fiber rupture when the testing was stopped at 12% lateral drift, as a result of the column's no longer being able to resist the applied axial compression. Although the fiber rupture was not observed, the hoop strains measured on the FRP tube of the specimen suggested that the rupture of the tube was imminent. Fig. 3 illustrates the most damaged regions of the columns at the end of testing. Table 5 summarizes the maximum recorded capacities and the location of the maximum damage zone of the columns. The damage zones reported in Table 5 were established based on the observed lengths of FRP-tube-rupture regions. The table also reports the locations of inner-steel-tube buckling regions of the DST columns.

Hysteretic Behavior

Experimentally recorded moment-lateral drift hysteretic relationships of the columns are shown in Fig. 4. As evident from the figure, the columns exhibited flexure-dominant response, with well-rounded hysteresis loops. The hysteresis loops of the DST columns indicate no sign of shear effect, as evidenced by the lack of clear pinching of the loops even after the formation of plastic hinges. However, some pinching is evident in the

hysteresis loops of the CFFT column, starting from 6% lateral drift. This is associated with the concrete crushing that resulted in the slippage of the reinforced bar between the crack surfaces when the load was reversed and the compression region of the bar become the tension region.

As illustrated in Fig. 4, Column DST-1 showed no strength decay up to 6% lateral drift, when the column lost more than 20% of its strength just before failure. Similarly, Column DST-3 also demonstrated no strength degradation until its failure, maintaining almost a constant moment capacity starting from 4% lateral drift up to 11% drift cycles when the column eventually failed. Column DST-4, with concrete-filled inner steel tube, also maintained an almost constant moment capacity after 3% lateral drift, demonstrating just a slight gradual decay after 12% lateral drift until 15% drift cycles when the column failed.

Column DST-2 exhibited some strength decay when the lateral deformations were increased from 2% to 3% lateral drift levels. This strength decay was stabilized and partly recovered with the subsequent increase in the deformation levels until the eventual failure of the specimen at the third cycle of 5% lateral drift. It should be noted that a small gap of 20 mm that was provided between the FRP tube and footing of DST-2 appeared to have resulted in an earlier failure of the specimen. This gap was provided only in Specimen DST-2, which was the first specimen that was tested. The main reason behind the provision of the gap was to prevent contact between FRP tube and concrete footing. However, after the observed early failure of DST-2, the gap was eliminated in the remaining specimens.

Column DST-8 started to exhibit some strength decay right after 2% lateral drift, which continued until the eventual failure of the column at 5% drift cycles. Buckling of the inner steel tube within the plastic hinge region observed in Column DST-8 was the primary reason to the earlier failure and inferior hysteretic performance of this column. As evident

from Fig. 4, apart from that of Column DST-9, the moment-lateral drift curves of the specimens followed similar trends in the pull and push directions. Column DST-9, by contrast, started to demonstrate strength decay beyond the 8% lateral drift in the push direction whereas its strength continuously increased in the pull direction until the failure of the column at 12% lateral drift.

Fig. 4 illustrates that Column DST-5, with AFRP tube, and Column DST-6, with CFRP tube, exhibited similar hysteretic moment-drift relationships, except for a slightly higher ultimate drift capacity developed by the AFRP-confined column, DST-5. Neither of these columns exhibited any significant strength degradation. The overall performance of Column DST-7, with a thicker inner steel tube, was similar to that of the companion specimen, Column DST-1, with both columns developing the same lateral drift capacity. Lateral load (F)-displacement (D) envelopes that were obtained by averaging the measurements from pull and push directions after correcting lateral loads for P - Δ effects (i.e., $M = F \times L$) are presented in Fig. 5 for all the specimens.

Measured Column stiffnesses

Fig. 6 illustrates the variation of average column stiffnesses (K) with lateral drifts for all the specimens, which were obtained from the lateral load-displacement hysteretic relationships, as $K = F / \Delta$. Based on the imposed boundary conditions of the specimens, the relationship between the sectional flexural stiffness (EI) and column stiffness (K) can be established as:

$$K = \frac{3.E.I}{L^3} \qquad (2)$$

where E and I = the elastic modulus and moment of inertia of the composite section, respectively, and L = the shear span of the column.

Column stiffnesses shown in Fig. 6 were determined from the average lateral loads and displacements recorded at a given drift level for the three cycles in the pull and push directions. The figure illustrates the progressive reduction of column stiffnesses with increasing lateral drifts, which is associated with cracking of concrete and yielding of internal steel reinforcement. In all specimens this reduction in stiffness is most significant up to 3-4% lateral drift, and beyond this displacement level, stiffness degradation continues at a lower and continually decreasing rate. The major change in the slope of the stiffness curves of the specimens observed at this displacement indicates the large level of plastification experienced by the specimens by this stage of loading. Significantly reduced slopes of the curves beyond this displacement level point to a stabilized column behavior, with the slope of the curve progressively approaching zero in majority of the specimens just before the termination of the curve.

Energy-Dissipation Capacity

The energy-dissipation capacity of each specimen was determined at each cycle by calculating the area under the corresponding lateral load-displacement hyteretic curve. The average energy dissipation capacities of the columns were then calculated for the three consecutive load cycles at a given drift level and are shown in Table 6. The table illustrates that the energy-dissipation capacities of the specimens followed a similar trend and they monotonically increased with lateral drifts, except for the drop observed in the capacity of the CFFT column between the 8% and 9% lateral drift cycles. This drop was caused by the

combined influence of the strength decay and increased magnitude of pinching observed in the hysteresis curves of the CFFT column beyond 8% drift, which is evident from Fig. 4 (j).

A comparison of the energy-dissipation capacities of the companion AFRP and CFRP-confined specimens, DST-5 and DST-6, shows that FRP type had no major influence on the energy dissipation capacities of these columns at a given displacement level. Likewise, similar energy-dissipation capacities of Columns DST-1, with 3.2-mm thick inner steel tube, and DST-7, with 5.5-mm thick tube, indicate that the steel-tube thickness had only a minor influence on the dissipation capacity. A comparison of the energy-dissipation capacities of the filled DST column, DST-4, and CFFT column indicates that at earlier stages of loading the CFFT column exhibited higher capacities, whereas beyond 8% lateral drift this trend reversed with the DST column starting to develop higher capacities. This was caused by the aforementioned strength decay and pinching that were observed in the hysteresis curves of the CFFT column beyond this displacement level. Another interesting observation from Table 6 is that Columns DST-1, with 95-MPa concrete and three layers of FRP, and DST-5, with 115-MPa concrete and four layers of FRP, exhibited similar energy dissipation behavior until the end of 6% lateral drift cycle pointing to similar performance levels of these columns, which is discussed further in the following sections.

Variation of FRP-Tube Hoop Strains along Column Height

The variation of maximum hoop strains recorded on FRP tubes through strain gauges along the column height is shown for each column in Fig. 7. The values given in Fig. 7 represent the recorded maximums that were obtained from the larger of the maximum strains recorded in the pull and push directions. In some of these strain profiles, dotted lines were used to represent the predicted strain gauge readings in cases where the actual strain gauge

readings were not available due to failure of particular strain gauges. These predictions were based on the observed relationships that were established from the previous cycles between the failed and functioning strain gauges of the same cross-section, while also considering the rate of change observed in strains recorded by functioning gauges in every subsequent displacement cycle. As expected, the maximum hoop strain on FRP recorded of each column was lower than the ultimate tensile strain of the fibers. The majority of the specimens developed hoop strains around 80% of the ultimate tensile strain of fibers. This is in agreement with previously reported observation of Ozbakkaloglu and Saatcioglu (2006) on circular HSCFFT columns.

DISCUSSION

The following sections provide discussions on the influence of the test parameters investigated in this study on the hysteretic moment-lateral drift relationship and plastic hinge behavior of the columns. The lateral drift capacities presented in the proceeding discussions were established from recorded lateral drifts at 20% strength decay beyond peak moment resistance (i.e. $\delta_{0.8Mmax}$ in Table 5).

Influence of Test Parameters on Moment-Lateral Displacement Behavior

Effect of Axial Load Level

The influence of the level of axial compression (P/P_o) on lateral displacement capacity of DST columns can be investigated through the comparison of the hysteretic behavior of Columns DST-1 and DST-3 shown in Fig. 4. These specimens had identical material and geometric properties and they were tested under axial load levels of 0.45 and 0.34,

respectively. The comparison illustrates that Column DST-3 failed at a lateral drift that was almost twice that of Columns DST-1. That is, Column DST-1 failed after completing 6% drift cycles; Column DST-3, by contrast, failed at the second cycle of 11% lateral drift. These results indicate that an increase in axial load level results in a significant decrease in the lateral displacement capacity of DST columns. This observation is in agreement with those reported previously by Sheikh and Yau (2002) for FRP-wrapped concrete columns and Ozbakkaloglu and Saatcioglu (2006) for CFFT columns.

Effect of Concrete Strength

To investigate the influence of the concrete strength, Columns DST-1 and DST-5 were designed to have the same level of confinement, which was established through the use of nominal confinement ratio (f_{lu}/f'_c). This ratio was calculated by dividing the ultimate confining pressure (f_{lu}), which was calculated from Eq. (3) assuming a uniform confining pressure distribution, with concrete cylinder strength (f'_c)

$$f_{lu} = \frac{2.f_{fu}.t}{D} \tag{3}$$

where f_{fu} = ultimate tensile strength of fibers; t = total fiber thickness of the tube; and D = diameter of the column measured at concrete core.

To that end, the 95-MPa column, DST-1, was designed with a three-layer FRP tube and the 115-MPa column, DST-5, was provided with a four-layer tube, resulting in similar nominal confinement ratios for these columns. A comparison of the hysteretic behaviors of Columns DST-1 and DST-5 in Fig. 4 indicates that the performance levels of these specimens were fairly close, with the higher strength column, DST-5, exhibiting a slightly better performance. Column DST-1 failed in the final cycle of the 6% drift ratio whereas

Column DST-5 was able to complete two full cycles at 7% lateral drift before failing at the final cycle at this drift level. Furthermore, as expected, Column DST-5 was able to develop a larger maximum moment capacity than DST-1. To further investigate the influence of the concrete strength, a column that was made ultra high-strength concrete, Column DST-9, was also tested. The external tube of DST-9 was made of six layers of AFRP, which resulted in a higher nominal confinement ratio than the two aforementioned specimens. As illustrated in Fig. 4, Column DST-9 performed extremely well, failing at a much higher lateral drift level (third cycle of 12% drift) than Columns DST-1 and DST-5 were able to develop. These observations indicate that using a higher strength concrete has no detrimental influence on the performance of DST columns, provided that the increase in concrete strength is matched by an increase in the amount of confinement.

Effect of Amount of Confinement

The influence of the amount of confinement on the lateral displacement capacities of concrete columns has been studied extensively for both conventional steel reinforcement-confined and FRP-confined concrete columns. To investigate this important parameter for DST columns, two identical columns were designed and tested under the same axial load level. Of the two columns, Column DST-2 was confined with a 2-layer AFRP tube, whereas a 3-layer AFRP tube was used to confine Column DST-3. As expected, an increase in the amount of confinement resulted in an increase in the lateral displacement capacity, with Columns DST-2 and DST-3 failing at 5% and 11% lateral drifts, respectively. However, the difference between the lateral drift capacities of these columns was larger than expected and it can be attributed to the earlier failure of Column DST-2, as discussed previously. Therefore, it would be reasonable to expect that performance

difference between Columns DST-2 and DST-3 would be less significant if the earlier failure of Column DST-2 did not occur.

Effect of Type of Fiber

The influence of different types of FRP confinement was investigated by comparing the hysteretic behaviors of Columns DST-5 and DST-6 shown in Fig. 4. Both columns had the same concrete strength and were tested under the same axial load level, but they were confined with different types of FRP (i.e. aramid and carbon). These columns were designed with almost identical confinement levels, achieved through the use of four layers of aramid fibers in Column DST-5 and five layers of carbon fibers in Column DST-6, which resulted in respective nominal confinement ratios (f_{lu}/f'_c) of 0.27 and 0.26. As shown in Table 5, Column DST-5 developed a slightly higher lateral drift capacity (i.e. 7%) than that of Column DST-6 (i.e. 6%). Higher lateral drift capacity of Column DST-5 over Column DST-6 can be attributed to the higher material ultimate tensile strain of AFRP compared with CFRP. However, as evident from the results given in Table 5, the difference was not very significant.

Effect of inner-Steel Tube Thickness

The influence of the thickness of the internal steel tube was studied through the investigation of two companion specimens, DST-1 and DST-7, which respectively had 3.2 mm and 5.5 mm thick steel tubes. As evident from Fig. 4, these columns developed almost identical lateral drift capacities. However, a closer inspection of Fig. 4 reveals the differences in the overall trends of the recorded hysteresis curves of the two columns. The

figure illustrates that the moment capacity of Column DST-1 remained almost constant after reaching a certain value around 3% of lateral drift. The moment capacity of Column DST-7, by contrast, increased with increasing deformation levels until the final displacement excursion at 6% lateral drift. Furthermore, as expected, Column DST-7 developed a slightly higher maximum moment capacity than Column DST-1. These observations suggest that, within the range considered in this study, the inner steel tube thickness has only a minor influence on the overall hysteretic behavior of DST columns.

Effect of Inner-Steel-Tube Sectional Shape

A square inner steel tube was used in Column DST-8 to examine the influence of the cross-sectional shape of inner steel tube on the lateral drift capacity of DST columns. Column DST-8 failed as a result of buckling of the inner steel tube within the plastic hinge region. This started at early stages of loading around 2% lateral drift and had a major detrimental influence on the overall behavior of the column, as evident from Fig. 4(h). This resulted in a significantly lower performance of Column DST-8 compared to its companion, Column DST-1, with a circular inner steel tube. It is clear from these observations that the sectional shape of the inner steel tube has a significant influence on the behavior of hollow DST columns loaded under a high level of axial compression.

Effect of Filling the Inner Steel Tube with Concrete

Based on the observations on the axial compressive behavior of DST stub columns, Teng et.al (2007) previously reported that the presence of an inner void had no significant influence on the effectiveness of FRP tube confinement. In this study, the effect of filling

the internal void was investigated by observing the relative performance of Columns DST-1 and DST-4. It is evident from Fig. 4 that Column DST-4 with a filled inner steel tube demonstrates a significantly improved hysteretic behavior compared to Column DST-1 with a hollow inner steel tube, developing nearly 2.5 times the lateral drift capacity developed by Column DST-1. The main factor behind the improved behavior of DST-4 was the prevention of the inward buckling of the inner steel tube within the plastic hinge region through the support provided by the concrete filling placed inside it. It was previously reported that the existence of concrete around the inner steel tube prevents it from buckling outward (Wong. et.al 2008). The results of the current study indicate that additional concrete inside the steel tube is equally effective at preventing inward buckling. The result also indicate that buckling of the inner steel tube appears to be playing an important role in the failure of hollow DST columns, with resulting stress concentration causing earlier failure of the FRP tube which leads to the eventual failure of the specimens.

Comparison of DST Column with a Companion CFFT Column

To gain a better insight into the relative performance of DST columns with respect to conventional CFFT columns, as a companion to Column DST-4, a CFFT column was also tested as part of the experimental program. These two columns were identical in every aspect except for the form of the internal steel reinforcement. As evident from Fig. 4, DST column exhibited a much higher inelastic deformation capacity, developing an ultimate lateral drift of 14.5%, compared to 9.5% lateral drift capacity of the CFFT column. Furthermore, Column DST-4 experienced no major strength decay until 14% lateral drift cycle, whereas the CFFT column started to exhibit strength degradation as soon as the 8% lateral drift cycle. Another important observation from the comparison of the hysteresis

curves of DST and CFFT columns in Fig. 4 is that the curves of CFFT column demonstrates some pinching effects whereas the curves of DST column are well-rounded without any clear signs of pinching. These promising observations point to the prospect that DST columns may provide an attractive alternative to CFFT columns in the construction of earthquake-resistant building columns.

Influence of Key Parameters on Plastic Hinge Length

An important step involved in predicting the lateral load-drift behavior of a concrete column is the modeling the plastic hinge region. Formation and propagation of the plastic hinge region of the columns of the present study were determined based on the maximum values of the FRP tube hoop strains at the lateral load direction recorded along the column height, which are illustrated in Fig. 7. In many of the previous experimental studies on conventional reinforced concrete columns (e.g. Bae and Bayrak 2008; Pam and Ho 2009; Liu and Sheikh 2013), lengths of plastic hinge regions were established based on visual observations of the column-damage regions. This approach relates the damage in concrete to the longitudinal plastic deformations, rather than measuring the axial strains along the column height continuously, which is challenging particularly after the yielding of the longitudinal steel bars. In this study, an approach that was previously introduced in Ozbakkaloglu and Saatcioglu (2006, 2007) and that involves the use of recorded hoop-strain profiles recorded on FRP tubes were used in establishing the plastic hinge lengths of the specimens. This approach is based on the fact that an intimate relationship exists between the lateral expansion of FRP tube and the level of damage sustained by concrete inside the tube. That is, higher FRP-tube hoop strains correspond to the most highly damaged regions of the columns, as the concrete undergoes rapid expansion inside the FRP

tube within these regions. The plastic hinge lengths of the specimens that are referred to in this section were established through the hoop-strain distribution of the specimen at the final drift cycle, assuming that the region terminated at a height where the recorded hoop strains fell below one third of the maximum recorded strain in that drift cycle. These values are reported in Table 5. It might be worth noting that, a recent study that investigated the relationships between different damage regions reported that the length of the tension-yielding zone was often larger than that of the compression-damage zone (defined as the plastic hinge region in this study) for a given reinforced concrete member (Zhao et al. 2012).

Based on the hoop-strain distributions shown in Fig. 7, length of the plastic hinge region of Column DST-3, with a P/P_o ratio of 0.34, was established to be slightly higher than that of Column DST-1, with a P/P_o ratio of 0.45. This observation is in agreement with the one reported in Ozbakkaloglu and Saatcioglu (2006) for circular CFFT columns, where it was found that plastic hinge region of the columns became more localized with increased axial load levels. It might be worth noting, however, that these observations are not supporting the ones reported previously for conventional reinforced concrete columns stating that an increase in the axial load level results in an increase in the plastic hinge lengths (Bae and Bayrak 2008; Pam and Ho 2009).

The differences between the observed behaviors can be attributed to the differences in confinement conditions and failure modes of these columns. In the case of hollow DST columns the stress concentrations caused by the inward buckling of the steel tube often corresponds to the most damaged region of the column. Therefore, the influence of the axial load level on the buckling behavior of the inner steel tube needs to be further studied to better understand the effect of this parameter on the formation of the plastic hinge regions in DST columns.

As evident from the comparison of the hoop strain profiles of Columns DST-1 and DST-4 in Fig. 7, concrete filling the inner void significantly influences the progression and length of the plastic hinge region in DST columns. The void-filled column, DST-4, demonstrated a significantly larger plastic hinge length compared to the hollow column, DST-1. This observation, at least partly, explains the much larger lateral drift capacity of Column DST-4 over Column DST-1. Another interesting observation from the comparison of the strain profiles of Columns DST-1, DST-4 and CFFT in Fig. 7 is that the void-filled DST column developed a higher level of plastic hinge propagation compared to the CFFT column. By contrast, the companion hollow DST column had a significantly shorter plastic hinge length than both the void-filled DST and CFFT columns. The aforementioned observations demonstrate the important influence of filling the inner void of the steel tube on the plastic hinge behavior of DST building columns. Further research is required to understand the influence of this important parameter on the behavior of DST bridge columns that are loaded under lower levels of axial compression.

In addition to the aforementioned observations on the influence of axial load level and filling the inner void of the steel tube, it can be seen from the comparison of the strain profiles of Columns DST-5 and DST-6 in Fig. 7 that the length of the plastic hinge region appear not to be sensitive to the type of FRP used in the fabrication of the DST columns.

CONCLUSIONS

This paper has presented the results of an experimental study on the behavior of FRP-HSC-steel DST columns under simulated seismic loading. Based on the results and discussions presented in the paper the following conclusions can be drawn:

- FRP-HSC-steel DST columns are capable of developing highly ductile behavior under simulated seismic loading. This is shown to be true for columns that were made of concretes of up to 130-MPa compressive strengths. Very high confinement effectiveness of DST column system makes it a suitable choice for meeting increased confinement requirements of HSC;
- Very much like conventional reinforced concrete columns, lateral displacement capacity of a DST column is influenced significantly by the level of axial compression acting on the column and it decreases with increasing axial load relative to column concentric capacity (P/P_o);
- Lateral drift capacities of DST columns increase with the amount of confinement, in much the same manner as was observed in conventional steel-confined or FRP-confined concrete columns;
- Using concretes with higher strengths has no detrimental effect on the lateral displacement capacity of DST columns, provided that the increase in concrete strength is matched with an increase in the amount of confinement;
- Benefitting from the higher ultimate tensile strain of the material, DST columns confined by aramid fibers develop slightly higher lateral drift capacities than companion DST columns confined by carbon fibers;
- DST columns provided with a concrete filling inside the steel tube may develop significantly higher lateral drift capacities compared to hollow DST columns. It is observed that the presence of concrete core both prevents the buckling of inner steel tube and increases the length of the plastic hinge region. These observations are derived from the tests of heavily loaded DST building columns reported in this study, and further research is required to understand the influence of filling the void inside the steel tube on the behavior of lightly loaded DST bridge columns;

- Thickness of the internal steel tube influences the trend of the moment-drift hysteretic loops of DST columns, but it appears to have no significant influence on the lateral drift capacities of the columns;
- Hollow square inner steel tubes are susceptible to buckling under high levels of axial compression if used as main internal reinforcement of DST columns. This failure mode leads to a significant reduction in the column ductility making this an unattractive combination for the construction of building columns;
- The DST column with a concrete-filled inner steel tube investigated in this study developed a significantly higher lateral drift capacity and better overall hysteretic response compared to the companion CFFT column. Pinching effects observed in the CFFT column was not present in the companion DST column. These promising observations point to the prospect that DST columns may provide an attractive alternative to CFFT columns in the construction of earthquake-resistant building columns.
- The level of axial load and provision of a concrete filling inside the steel tube are important parameters that influence the plastic hinge length of DST columns. It is observed that a hollow DST column under lighter axial compression develops a slightly larger plastic hinge progression than a more heavily loaded one. It is also observed that the plastic hinge lengths of hollow DST columns are significantly shorter than those of both void-filled DST and CFFT columns.

ACKNOWLEDGEMENTS

The authors would like to thank Messrs. Ganguly, Georgiou, Holm, Koegler, Lo, Loi, Mabarrack and Wilk who have undertaken the tests reported in this paper as part of their

undergraduate theses. This research is part of an ongoing program at the University of Adelaide on FRP-concrete composite columns.

REFERENCES

ACI Committee 318 (2011). "Building Code Requirements for Structural Concrete and Commentary."*ACI 318-11/318R-11,* American Concrete Institute, Farmington Hills, MI, 509.

Bae, S. and Bayrak, O. (2008),"Plastic Hinge Length of Reinforced Concrete Columns." *ACI Structural Journal*, Vol.105, No.3, pp. 290-300.

Berthet, J. F., Ferrier, E., and Hamelin, P. (2005). "Compressive behaviour of concrete externally confined by composite jackets. Part A: Experimental study." *Construction and Building Materials*, Elsevier, 19, 223-232.

Chung, Y, Park, C and Meyer, C (2008), "Residual seismic performance of reinforced concrete bridge piers after moderate earthquakes." *ACI Structural Journal*, 105(1), 87–95.

Cui, C., and Sheikh, S.A. (2010). "Experimental study of normal- and high-strength concrete confined with fiber-reinforced polymers." *Journal of Composites for Construction*, ASCE, 14(5), 553-561.

Dai, J.G., Bai, Y.L., and Teng, J.G. (2011). "Behavior and modeling of concrete confined with FRP composites of large deformability." *Journal of Composites for Construction*., 15(6), 963-973.

Eid, R., Roy, N., and Paultre, P. (2009). "Normal- and high-strength concrete circular elements wrapped with FRP composites." *Journal of Composites for Construction*, ASCE, 13(2), 113-124.

ElGawady, M.A., Booker, A.J, and Dawood, H.M. (2010). "Seismic behavior of posttensioned concrete-filled fiber tubes." *Journal of Composites for Construction*, ASCE, 14(5), 616-628.

ElGawady, M.A., and Dawood, H.M. (2012). “Analysis of segmental piers consisted of concrete filled FRP tubes.” *Engineering Structures*, 38, 142-152.

Fam, A., Schnerch, D. and Rizkalla, S. (2005). "Rectangular Filament-Wound GFRP Tubes Filled with Concrete under Flexural and Axial Loading: Experimental Investigation." *Journal of Composites for Construction*, ASCE, 9(1), 25-33.

Fam, A. Z., and Rizkalla, S.H. (2001), “Confinement model for axially loaded concrete confined by circular fiber-reinforced polymer tubes.” *ACI Structural Journal*, 98(4), 451-461.

Gu DS, Wu G, Wu ZS, Wu YF. (2010). “The confinement effectiveness of FRP in retrofitting circular concrete columns under simulated seismic load.” *Journal of Composites for Construction*, ASCE, 14(5), 531–40.

Han, L.H., Tao, Z., Liao, F.Y., and Xu, Y. (2010), “Tests on Cyclic Performance of FRP-Concrete –Steel Double-Skin Tubular Columns.” *Thin-Walled Structures*, 4, 430-439.

Haroun, M & Elsanadedy, H (2005), “Fiber-Reinforced Plastic Jackets for Ductility Enhancement of Reinforced Concrete Bridge Columns with Poor Lap-Splice Detailing.” *Journal of Bridge Engineering*, ASCE, 10(6), 749-757.

Hong, W.K., and Kim, H.C. (2004). “Behavior of concrete columns confined by carbon composite tubes”, *Canadian Journal of Civil Engineering*, 31(2), 178–188.

Hosseini, A., Khaloo, A.R, and Fadaee, S. (2005). ”Seismic Performance of High-Strength Concrete Square Columns Confined with Carbon Fiber Reinforced Polymers (CFRPs).” *Canadian Journal of Civil Engineering*, 32(3), 569-578.

Iacobucci, R.D., Sheikh, S.A., and Bayrak, O. (2003),”Retrofit of Square Concrete Columns with Carbon Fiber-Reinforced Polymer for Seismic Resistance.” *ACI Structural Journal*, 100(6), 785-794.

Ilki, A., Peker, O., Karamuk, E., Demir, C., Kumbasar, N. (2008). “FRP retrofit of low and medium strength circular and rectangular reinforced concrete columns.” *Journal of Materials in Civil Engineering*, ASCE, 20(2), 169-188.

Kusumawardaningsih, Y., and Hadi M.N.S. (2010). “Comparative behaviour of hollow columns confined with FRP composites.” *Composite Structures*, 93(1), 198-205.

Lam, L., and Teng, J. G. (2004). “Ultimate condition of fiber reinforced polymer-confined concrete.” *Journal of Composites for Construction*, ASCE, 8(6), 539-548.

Liu, J., and Sheikh, S. (2013), “FRP-confined circular columns under simulated seismic loads.” *ACI Structural Journal*, 110(6), 941-952.

Mirmiran, A., and Shahawy, M. (1997). “Behavior of concrete columns confined by fiber composites”, *Journal of Structural Engineering*, ASCE, 123(5), 583-590.

Mirmiran, A., Shahawy, M., Samaan, M., El Echary, H., Mastrapa, J.C., and Pico, O. (1998). “Effect of Column Parameters on FRP-confined Concrete.” *Journal of Composites for Construction*, ASCE, 2(4), 175-185.

Mohamed, H., and Masmoudi, R. (2010) “Axial Load Capacity of Concrete-Filled FRP Tube Columns: Experimental versus Predictions.” *Journal of Composites for Construction*, ASCE, 14(2), 231-243.

Ozbakkaloglu, T. (2013a). “Axial compressive behavior of square and rectangular high-strength concrete-filled FRP tubes.” *Journal of Composites for Construction, ASCE*, 17(1): 151 – 161.

Ozbakkaloglu, T. (2013b). “Compressive behavior of concrete-filled FRP tube columns: Assessment of critical column parameters.” *Engineering Structures*, 51, 188-199.

Ozbakkaloglu, T. (2013c). “Concrete-filled FRP Tubes: Manufacture and Testing of New Forms Designed for Improved Performance.” *Journal of Composites for Construction, ASCE*, 17(2), 280- 291.

Ozbakkaloglu, T., and Akin, E. (2012) “Behavior of FRP-confined normal- and high-strength concrete under cyclic axial compression.” *Journal of Composites for Construction*, ASCE, 16(4), 451-463.

Ozbakkaloglu, T., and Oehlers, D. J., (2008a), “Concrete-filled square and rectangular FRP tubes under axial compression.” *Journal of Composites for Construction,* ASCE, 12(4), 469-477.

Ozbakkaloglu, T., and Oehlers, D. J., (2008b), “Manufacture and testing of a novel FRP tube confinement.” *Engineering Structures*, 30(9), 2448-2459.

Ozbakkaloglu, T. and Saatcioglu, M. (2006),”Seismic Behavior of High Strength Concrete Columns Confined by Fiber-Reinforced Polymer Tubes.” *Journal of Composite Construction*, ASCE, 10(6), 538 – 549.

Ozbakkaloglu, T. and Saatcioglu, M. (2007),”Seismic Performance of Square High Strength Concrete Columns in FRP stay in place formwork.” *Journal of Structural Engineering*, ASCE, 133(1), 44-56.

Ozcan, O., Binici, B., Ozcebe, G. (2010). “Seismic strengthening of rectangular reinforced concrete columns using fiber reinforced polymers.” *Engineering Structures*, 32(4), 964–973.

Pam, H.J. and Ho, J.C.M. (2009), “Length of Critical Region for Confinement Steel in Limited Ductility High-Strength Reinforced Concrete Columns.” *Engineering Structures*, 31, 2896-2908.

Park, J. H., Jo, B. W., Yoon, S. J., and Park, S. K. (2011). “Experimental investigation on the structural behavior of concrete filled FRP tubes with/without steel re-bar.” *KSCE J. Civ. Eng*., 15(2), 337-345.

Pessiki, S., Harries, K. A., Kestner, J. T., Sause, R. and Ricles, J. M. (2001). “Axial behavior of reinforced concrete columns confined with FRP jackets.” *Journal of Composites for Construction*, ASCE, 5(4), 237-245.

Realfonzo, R., and Napoli, A. (2009).”Cyclic Behavior of RC Columns Strengthened by FRP and Steel Devices.” *Journal of Structural Engineering*, ASCE, 135(10), 1164-1176.

Rochette, P., and Labossiere, P. (2000). “Axial Testing of Rectangular Column Models Confined with Composites.” *Journal of Composites for Construction*, ASCE, 4(3), 129-136.

Saadatmanesh, H., Ehsani, M.R., and Jin, L. (1996). "Seismic Strengthening of Circular Bridge Pier Models with Fiber Composites," *ACI Structural Journal*, 93(6), 639-647.

Saatcioglu, M., Ozbakkaloglu, T., Elnabelsy, G. (2008) “Seismic behavior and design of reinforced concrete columns confined with FRP stay-in-place formwork.” *ACI Special Publication*, 257, 149-170.

Shao, Y., and Mirmiran, A. (2005), “Experimental Investigation of cyclic behavior of concrete-filled FRP tubes.” Journal of Composites for Construction, ASCE, 9(3), 263-273.

Sheikh, S.A., and Khoury, S.S. (1993),”Confined Concrete Columns with Stubs.” *ACI Structural Journal*, 90(4), 414-431.

Sheikh, S.A. and Yau, G. (2002),”Seismic Behavior of Concrete Columns Confined with Steel and Fiber-Reinforced Polymer.” *ACI Structural Journal*, 99(1), 72-80.

Teng, J.G., Yu, T., and Wong, Y.L., (2004), “Behavior of hybrid FRP-concrete-steel double-skin tubular columns.” *Proc. 2nd Int. Conf. on FRP Composites in Civil Engineering*, Adelaide, Australia, 811-818.

Teng, J.G., Yu, T., Wong, Y.L., and Dong, S.L. (2007), “Hybrid FRP-Concrete-Steel Tubular Columns: Concept and Behavior.”*Construction and Building Material*, 21(4), 846-854.

Wong, Y.L., Yu, T., Teng, J.G., and Dong, S.L. (2008). “Behavior of FRP-Confined Concrete in Annular Section Columns.” Composites: Part B, 39(3), 451-466.

Wu, Y. F., and Wei, Y. Y. (2010), “Effect of cross sectional aspect ratio on the strength of CFRP-confined rectangular concrete columns, *Engineering Structures*,.32(1), 32-45.

Yamakawa, T., Zhong, P., and Ohama, A. (2003). “Seismic Performance of Aramid Fiber Square Tubed Concrete Columns with Metallic and/or Non Metallic Reinforcement.” *Journal of Reinforced Plastic and Composites*, 22(13), 1221 -1237.

Yu T., Wong, Y.L., Dong, S.L., and Lam E.S.S. (2006). “Flexural Behavior of Hybrid FRP-Concrete-Steel Double Skin Tubular Members.” *Journal of Composites for Construction*, ASCE, 10()5, 443-52.

Yu T, Wong YL, Teng JG. (2010). “Behavior of hybrid FRP-concrete-steel double-skin tubular columns subjected to eccentric compression.” *Advances in Structural Engineering*; 13(5), 961–74.

Zaghi, A. E., Saiidi, M. S, and Mirmiran, A. (2012). “Shake table response and analysis of concrete-filled FRP tube bridge column.” *Composite Structures*, 94(5), 1564-1574.

Zhang, B., Teng, J. G. & Yu, T. (2012). “Behaviour of hybrid double-skin tubular columns subjected to combined axial compression and cyclic lateral loading.” *Sixth International Conference on FRP Composites in Civil Engineering*, Rome, Italy, (1-7).

Zhao, X. M., Wu, Y. F., and Leung, A. Y. T. (2012). “Analyses of plastic hinge regions in reinforced concrete beams under monotonic loading” *Engineering Structures*, 34(1), 466-482.

Zohrevand, P., and Mirmiran A. (2011). “Behavior of ultrahigh-performance concrete confined by fiber-reinforced polymers.” *Journal of Materials in Civil Engineering*, ASCE, 23, 1727-1734

Zohrevand, P., and Mirmiran A. (2012). “Cyclic behaviour of hybrid columns made of ultra high performance concrete and fiber reinforced polymers.” *Journal of Composites for Construction*, ASCE, 16(1), 91-99.

Zohrevand, P., and Mirmiran A. (2013). “Stress-strain model of ultra-high performance concrete confined by fiber reinforced polymers.” *Journal of Materials in Civil Engineering*, ASCE, DOI: 10.1061/(ASCE)MT.1943-5533.0000769, 1822-1829.

Table 1. Properties of test specimens

Column	f'_c (MPa)	FRP tube		Inner steel tube				P (kN)	P/P_o
		Material	n (mm)	Shape	D (mm)	t (mm)	Inner void		
DST-1	95	Aramid	3	Circular	88.9	3.2	Empty	545	0.45
DST-2	95	Aramid	2	Circular	88.9	3.2	Empty	410	0.34
DST-3	95	Aramid	3	Circular	88.9	3.2	Empty	410	0.34
DST-4	95	Aramid	3	Circular	88.9	3.2	Filled	695	0.42
DST-5	115	Aramid	4	Circular	88.9	3.2	Empty	625	0.45
DST-6	115	Carbon	5	Circular	88.9	3.2	Empty	625	0.45
DST-7	95	Aramid	3	Circular	88.9	5.5	Empty	675	0.45
DST-8	95	Aramid	3	Square	89.0	3.5	Empty	570	0.45
DST-9	130	Aramid	6	Circular	88.9	3.2	Empty	690	0.45
CFFT	95	Aramid	3	Eight internal steel reinforcing bars with 10 mm diameter				725	0.42

Note: D = steel-tube diameter; n = number of FRP layers; P/P_o = Axial load level; t = steel-tube thickness.

Table 2. Material properties of fiber sheets used in FRP tubes

Type	Nominal thickness t_f (mm/ply)	Provided by manufacturers			Obtained from flat FRP coupon tests		
		Tensile strength f_f (MPa)	Ultimate tensile strain, ε_f (%)	Elastic modulus E_f (GPa)	Tensile strength f_{frp} (MPa)	Ultimate tensile strain, ε_{frp} (%)	Elastic modulus E_{frp} (GPa)
Aramid	0.200	2900	2.50	116.0	2663	2.12	125.7
Carbon	0.117	3800	1.55	240.0	3626	1.44	251.0

Table 3. Material properties of steel tubes

Steel tubes	Shape	Thickness, t (mm)	Yield Stress, f_y (MPa)	Yield strain, ε_y (%)	Ultimate strength, f_u (MPa)	Ultimate strain, ε_u (%)	Rupture strain, ε_r (%)
Tube 1	Circular	3.2	350	0.17	441	11.1	17.6
Tube 2	Circular	5.5	412.5	0.20	473	7.7	13.1
Tube 3	Square	3.5	425	0.20	498	4.9	15.4

Table 4. Material properties of steel reinforcing bars

Diameter (mm)	Yield Stress, f_y (MPa)	Yield strain, ε_y (%)	Ultimate strength, f_u (MPa)	Ultimate strain, ε_u (%)	Rupture strain, ε_r (%)
10	600	0.3	760	8.0	10.5

Table 5. Observed column behavior

Column	f'_c (MPa)	P/P_o	M_{max} (kN.m)	Failure drift, δ (%)	δ_{Mmax} (%)	$\delta_{0.8Mmax}$ (%)	Max column damage zone (mm)[a]	Steel tube buckling zone (mm)[b]	Plastic hinge length (mm)
DST-1	95	0.45	36.5	6%, cycle 3	6	6	100	100	130
DST-2	95	0.34	28.6	5%, cycle 3	2	5	75	75	110
DST-3	95	0.34	32.6	11%, cycle 2	4	11	115	85	145
DST-4	95	0.42	39.8	15%, cycle 3	9	14.5	150	NA[c]	350
DST-5	115	0.45	40.7	7%, cycle 3	6.5	7	115	75	190
DST-6	115	0.45	42.0	6%, cycle 2	3	6	100	70	180
DST-7	95	0.45	39.7	6%, cycle 1	5	6	100	50	140
DST-8	95	0.45	21.6	5%, cycle 3	2	5	75	75	110
DST-9	130	0.45	41.0	12%, cycle 3	9	11.5	150	220	370
CFFT	95	0.42	43.6	11%, cycle 1	6	9.5	130	-	200

Note *:* M_{max} = maximum recorded moment (averaged from push and pull directions); δ_{Mmax} = lateral drift at maximum moment (averaged from push and pull directions); $\delta_{0.8Mmax}$ = lateral drift at 20% strength decay (averaged from push and pull directions)

[a]Measured from column-footing interface to the far end of FRP-tube-rupture region.

[b]Measured from column-footing interface to the top of steel-tube buckling region.

[c]Buckling was not observed

Table 6. Column energy dissipation capacities

Drift (%)	Energy dissipation capacity (J)									
	DST-1	DST-2	DST-3	DST-4	DST-5	DST-6	DST-7	DST-8	DST-9	CFFT
1	116.9	109.6	132.2	100.6	121.7	109.9	109.2	150.6	128.3	101.9
2	475.7	376.3	365.5	397.8	488.7	424.3	496.4	650.2	575.7	347.2
3	1114.4	889.4	791.9	693.6	1122.3	972.6	1053.1	857.4	839.1	813.2
4	1499.8	1325.0	1273.0	1121.8	1692.3	1546.6	1658.1	1403.4	1221.8	1331.2
5	2184.5	1959.6	1751.7	1554.1	2360.4	2196.4	2293.4	1712.7	1861.8	1738.7
6	3078.7		2191.6	2135.6	3083.9	3277.7	3289.5		2307.3	2319.8
7			2706.5	2500.0	4325.1				3011.4	3012.9
8			3283.4	2959.2					3748.1	3687.5
9			3924.1	3551.9					4478.1	3295.4
10			4459.2	4062.3					5397.8	3632.1
11			5432.0	4686.1					6233.1	4188.4
12				5299.4					7285.9	
13				5785.8						
14				6480.4						
15				7215.1						

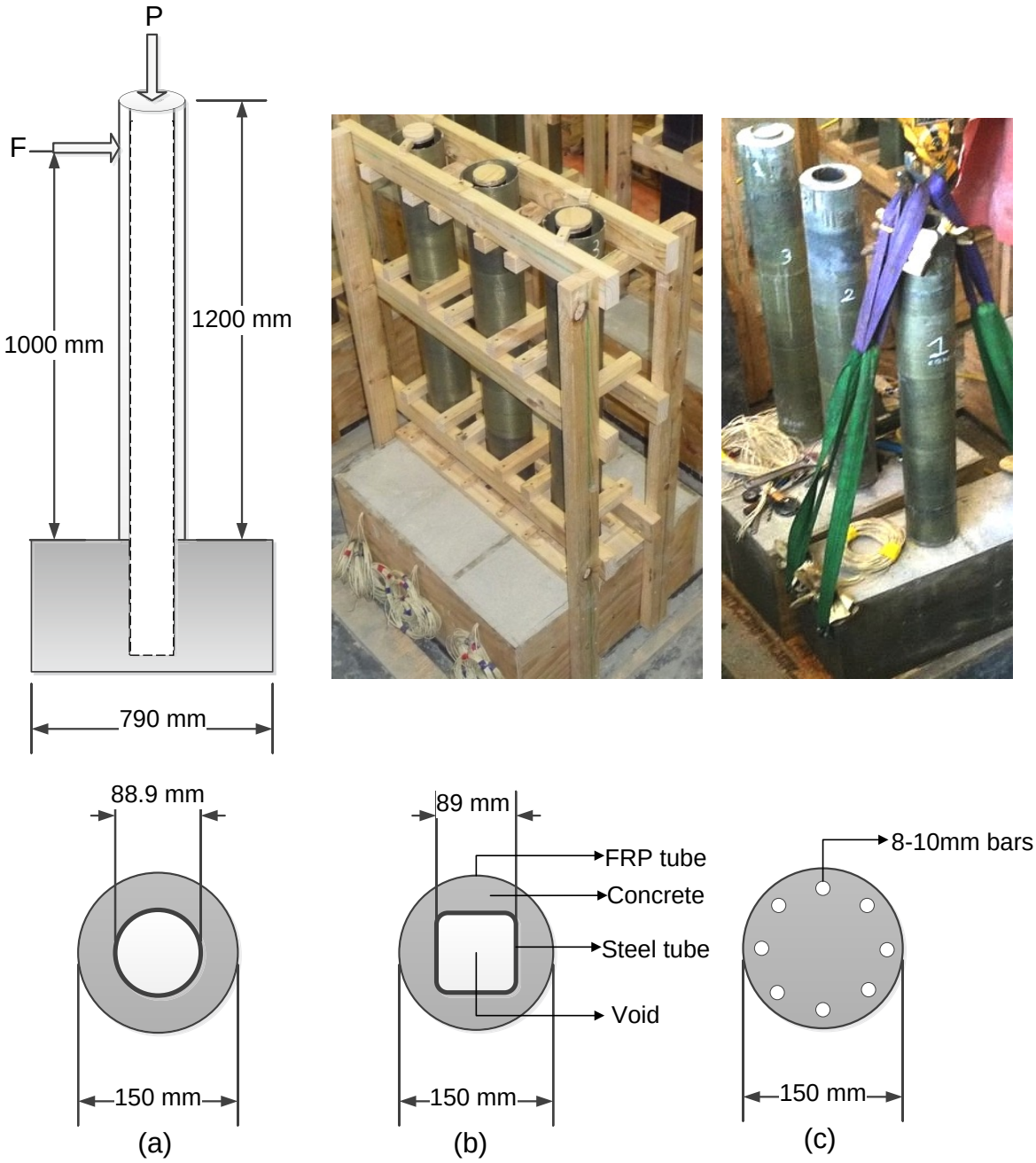

Fig. **1**. Column geometry: (a) DST column with circular inner steel tube; (b) DST column with square inner steel tube; (c) CFFT column

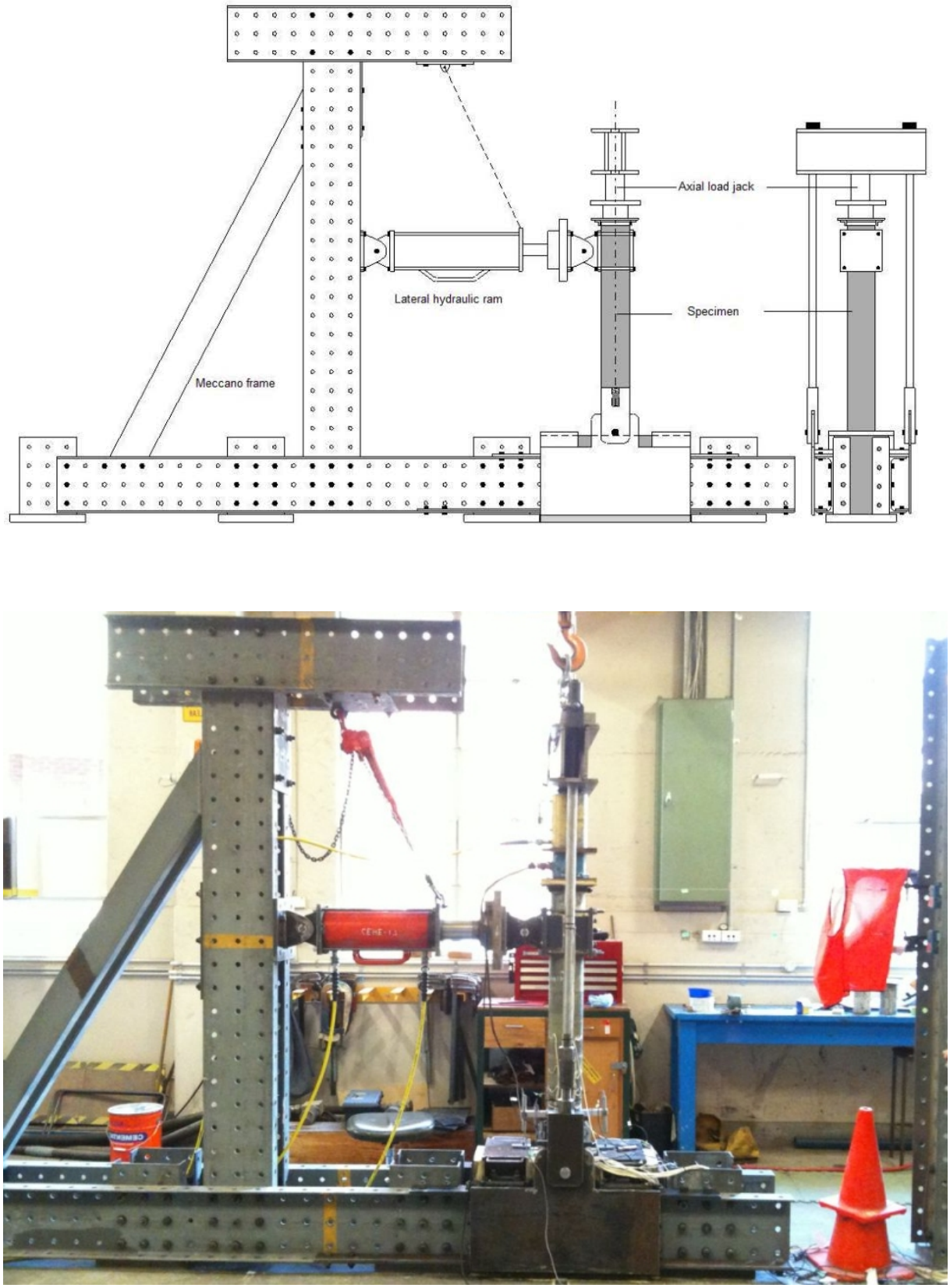

Fig. 2. Column test setup

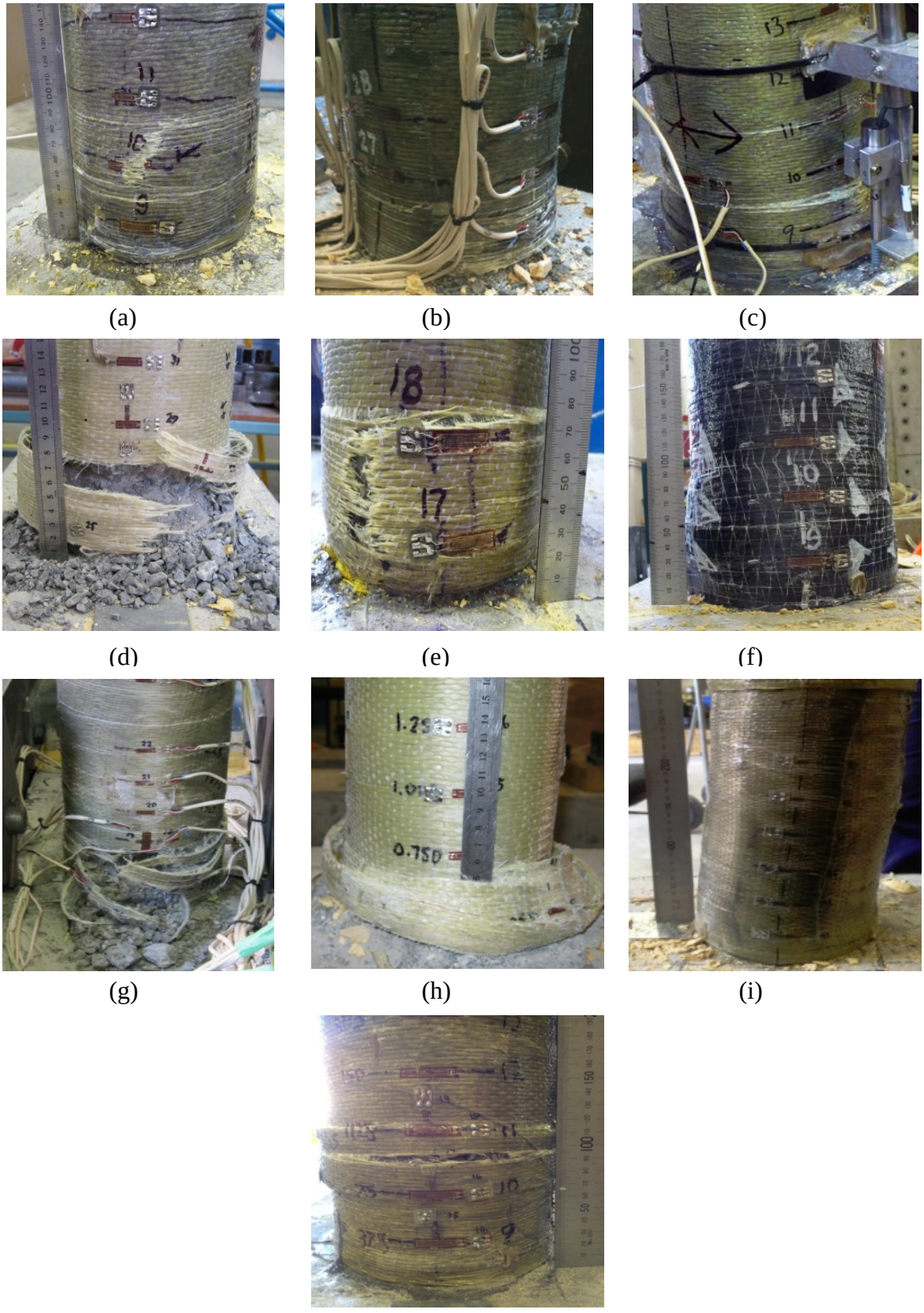

Fig. 3. Plastic hinge regions of columns at the end of testing : (a) DST-1; (b) DST-2; (c) DST-3; (d) DST-4; (e) DST-5; (f) DST-6; (g) DST-7; (h) DST-8; (i) DST-9; (j) CFFT

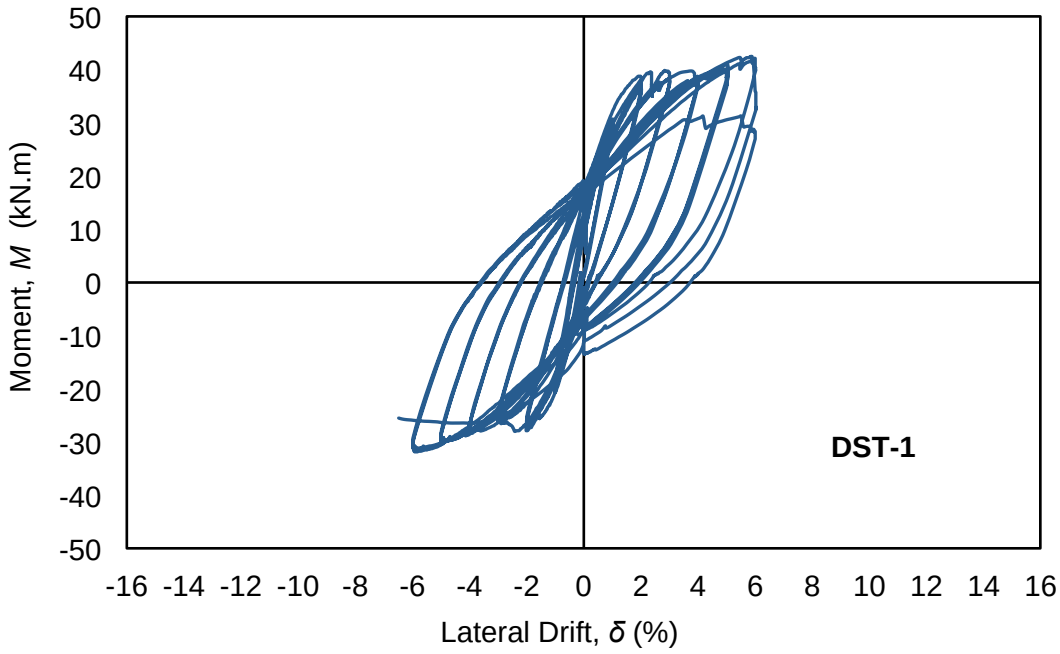
50
40
30
20
10
0
-10
-20
-30
-40
-50
Moment, M (kN.m)
-16 -14 -12 -10 -8 -6 -4 -2 0 2 4 6 8 10 12 14 16
Lateral Drift, δ (%)
DST-1

(a)

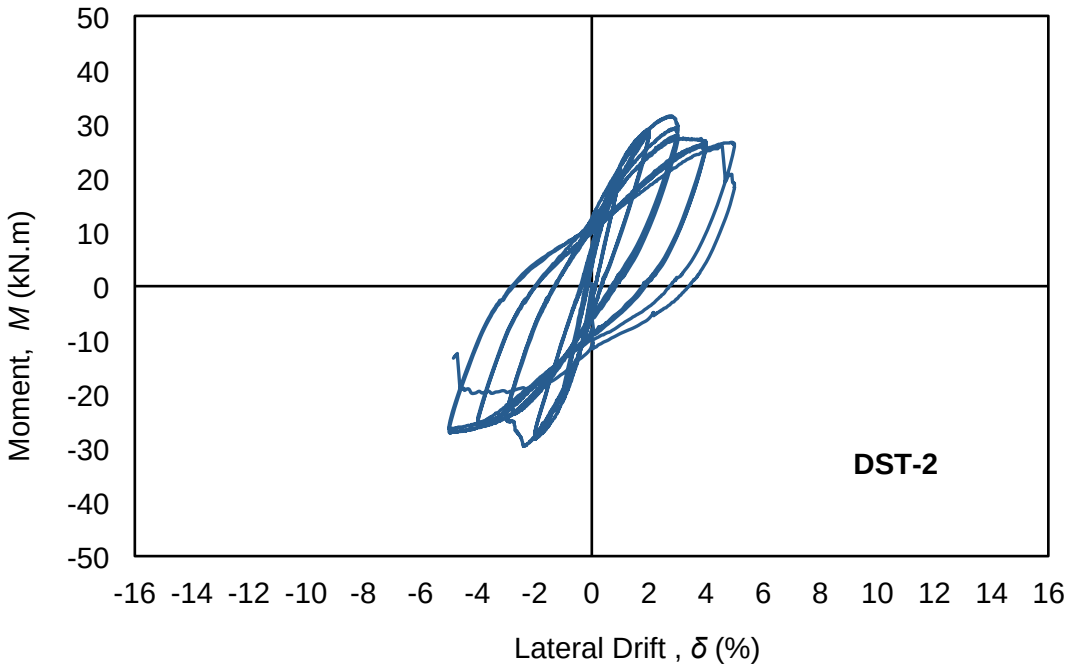
50
40
30
20
10
0
-10
-20
-30
-40
-50
Moment, M (kN.m)
-16 -14 -12 -10 -8 -6 -4 -2 0 2 4 6 8 10 12 14 16
Lateral Drift , δ (%)
DST-2

(b)

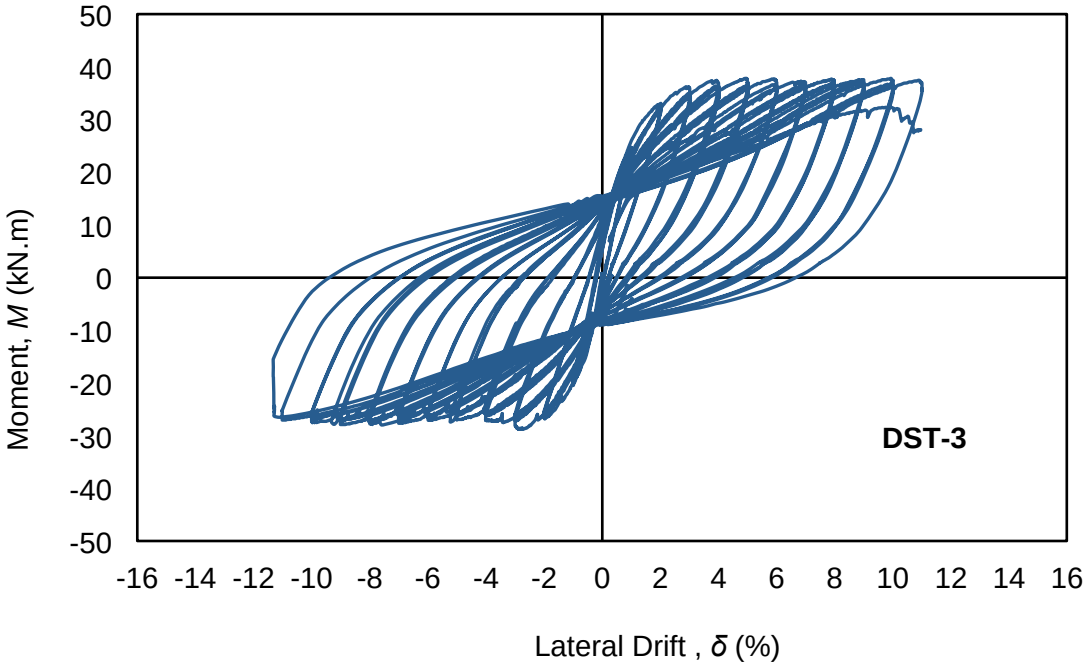
50
40
30
20
10
0
-10
-20
-30
-40
-50
-16 -14 -12 -10 -8 -6 -4 -2 0 2 4 6 8 10 12 14 16
Moment, M (kN.m)
Lateral Drift , δ (%)
DST-3

(c)

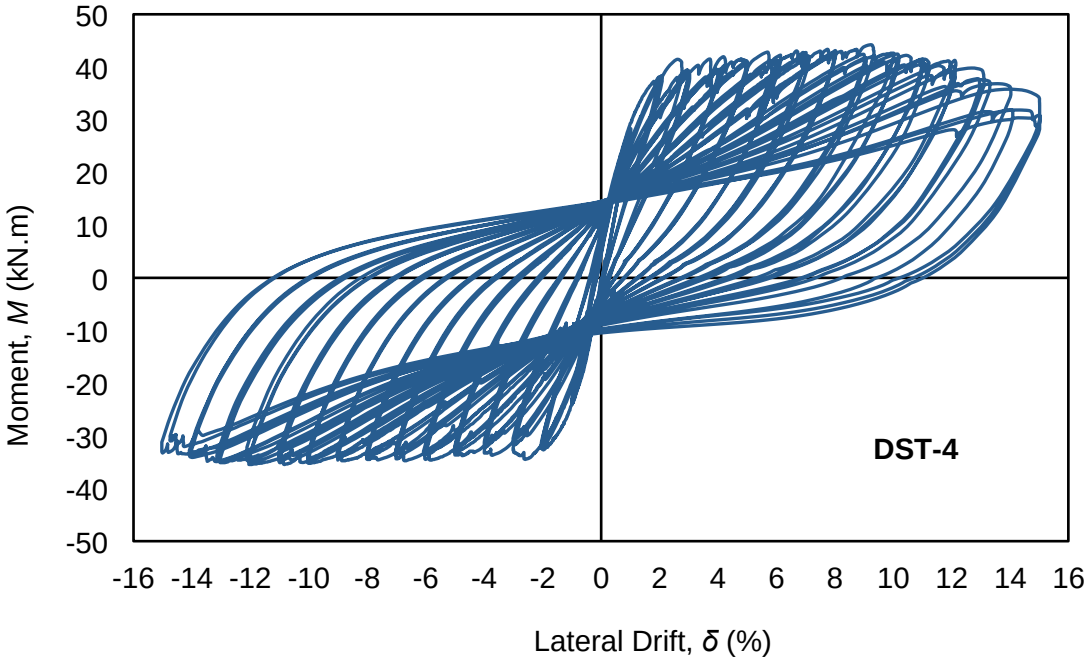
50
40
30
20
10
0
-10
-20
-30
-40
-50
-16 -14 -12 -10 -8 -6 -4 -2 0 2 4 6 8 10 12 14 16
Moment, M (kN.m)
Lateral Drift, δ (%)
DST-4

(d)

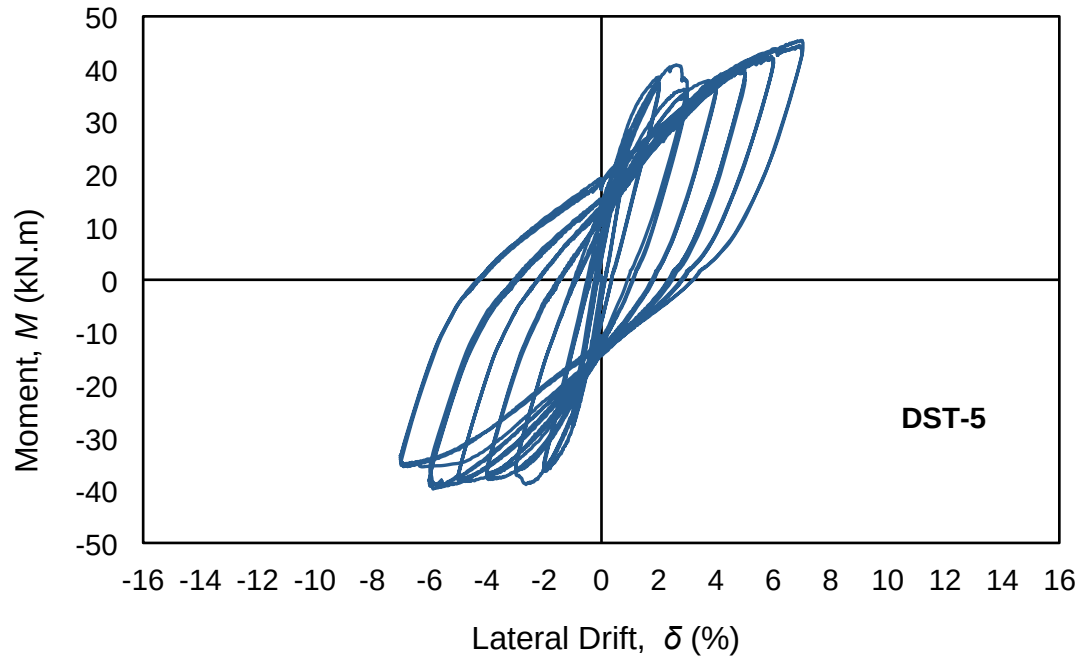
50
40
30
20
10
0
-10
-20
-30
-40
-50
-16 -14 -12 -10 -8 -6 -4 -2 0 2 4 6 8 10 12 14 16
Moment, M (kN.m)
Lateral Drift, δ (%)
DST-5

(e)

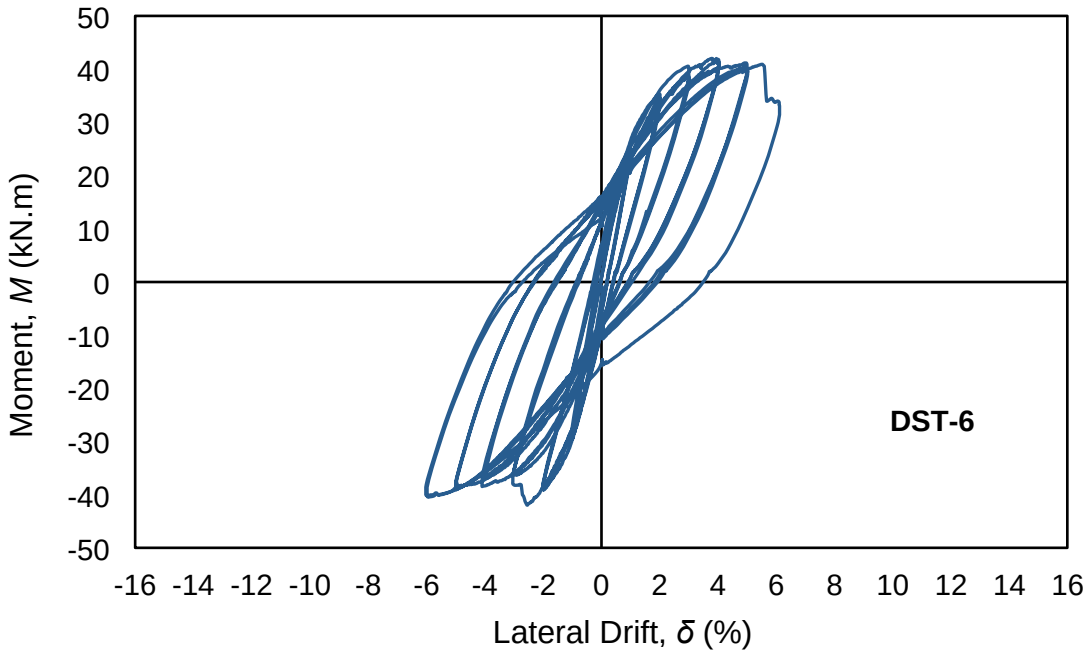
50
40
30
20
10
0
-10
-20
-30
-40
-50
-16 -14 -12 -10 -8 -6 -4 -2 0 2 4 6 8 10 12 14 16
Moment, M (kN.m)
Lateral Drift, δ (%)
DST-6

(f)

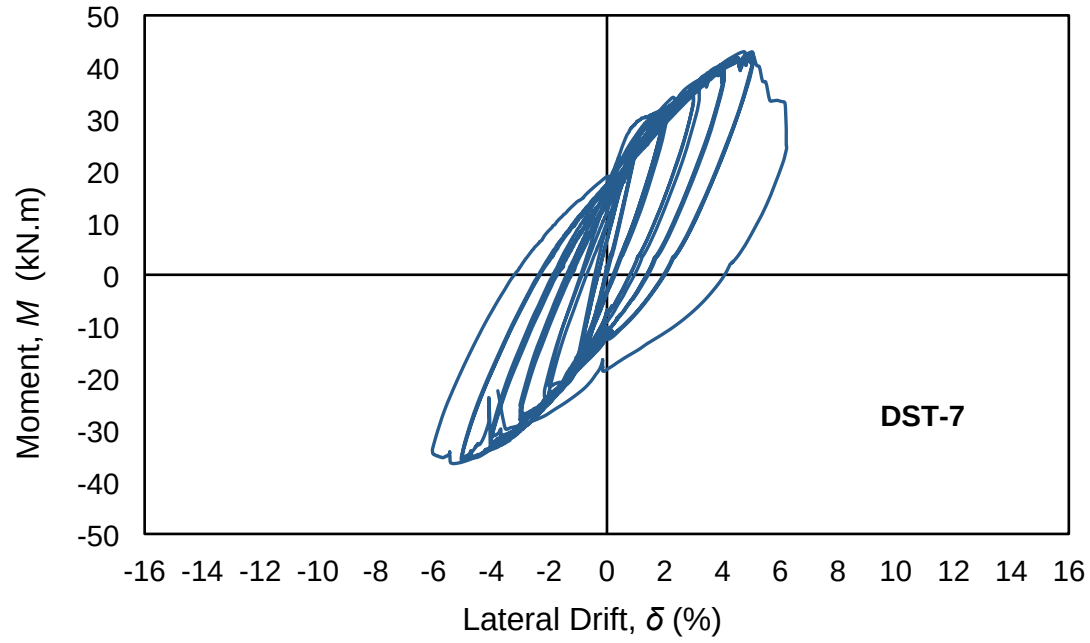
50
40
30
20
10
0
-10
-20
-30
-40
-50
Moment, M (kN.m)
-16 -14 -12 -10 -8 -6 -4 -2 0 2 4 6 8 10 12 14 16
Lateral Drift, δ (%)
DST-7

(g)

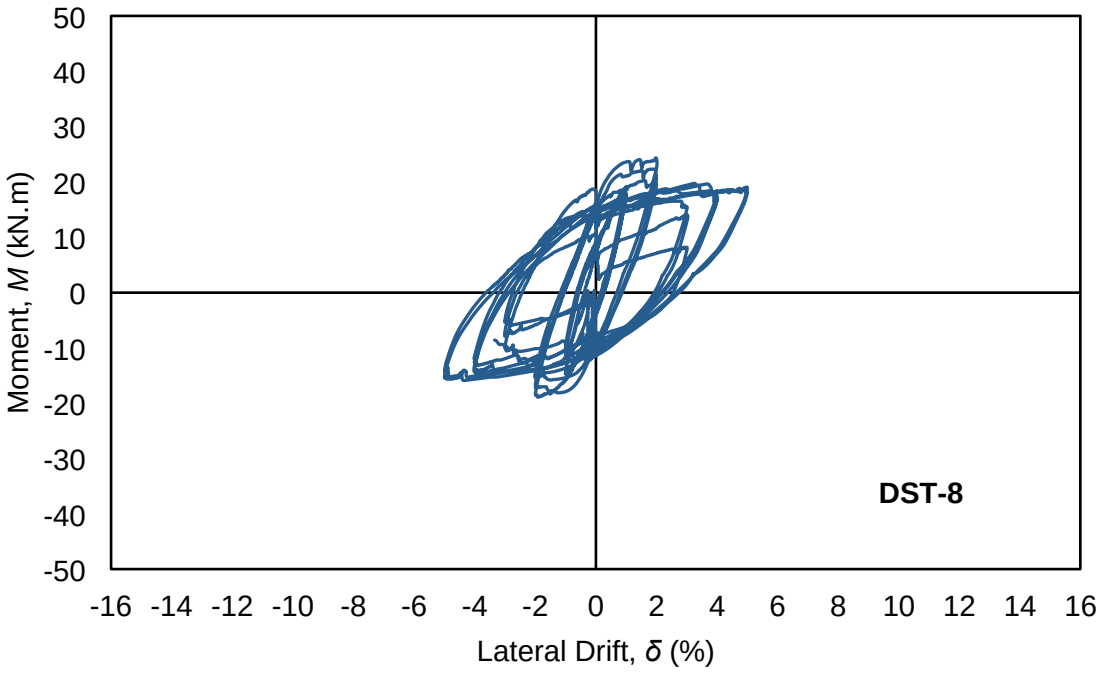
50
40
30
20
10
0
-10
-20
-30
-40
-50
Moment, M (kN.m)
-16 -14 -12 -10 -8 -6 -4 -2 0 2 4 6 8 10 12 14 16
Lateral Drift, δ (%)
DST-8

(h)

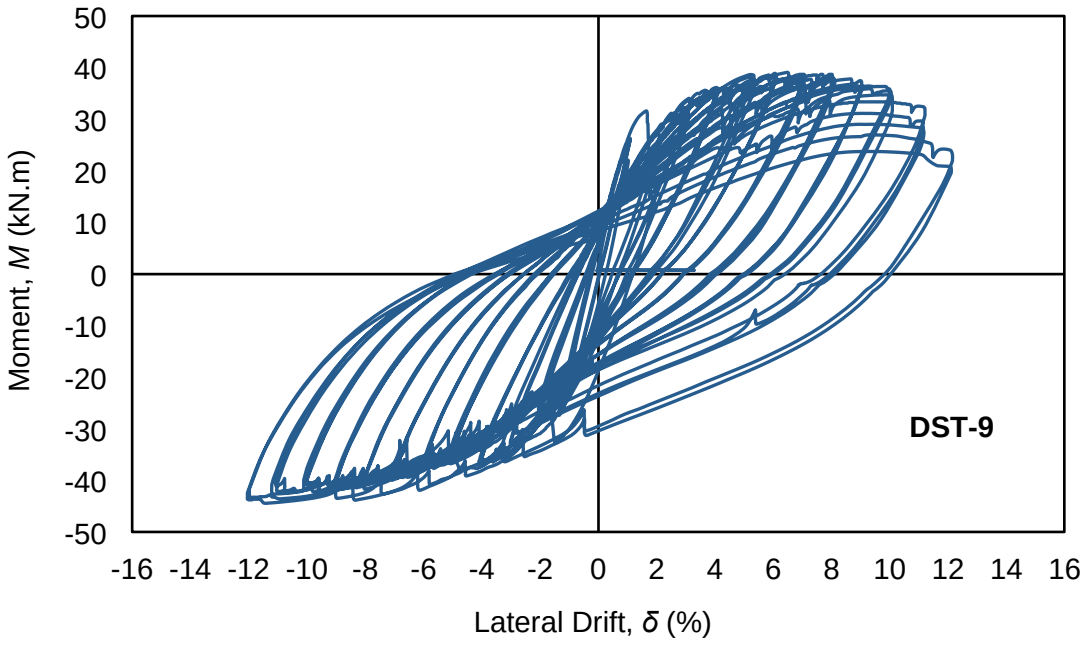

(i)

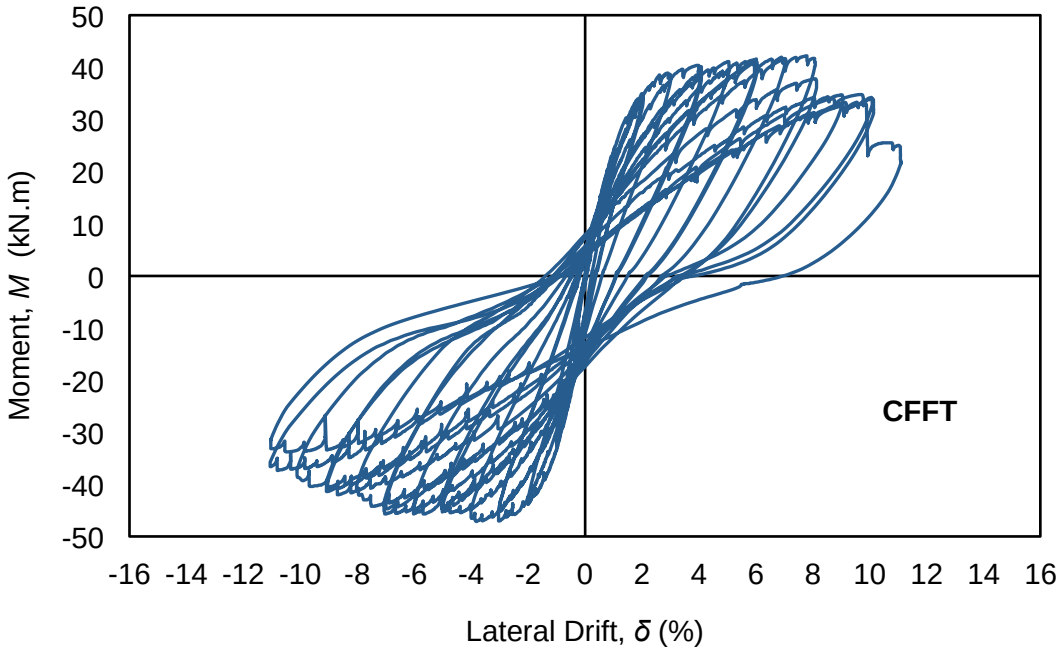

(j)

Fig. 4. Experimentally recorded hysteretic moment-lateral drift relationships: (a) DST-1; (b) DST-2; (c) DST-3; (d) DST-4; (e) DST-5; (f) DST-6; (g) DST-7; (h) DST-8; (i) DST-9; (j) CFFT

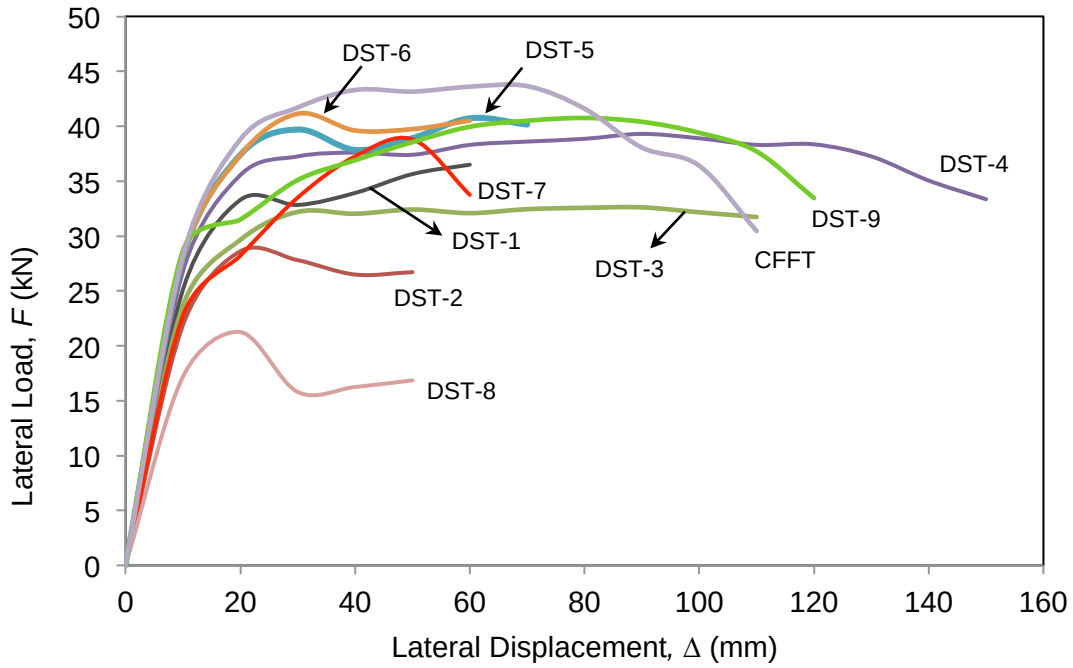

Fig. 5. Envelop curves of column lateral load-displacement relationships

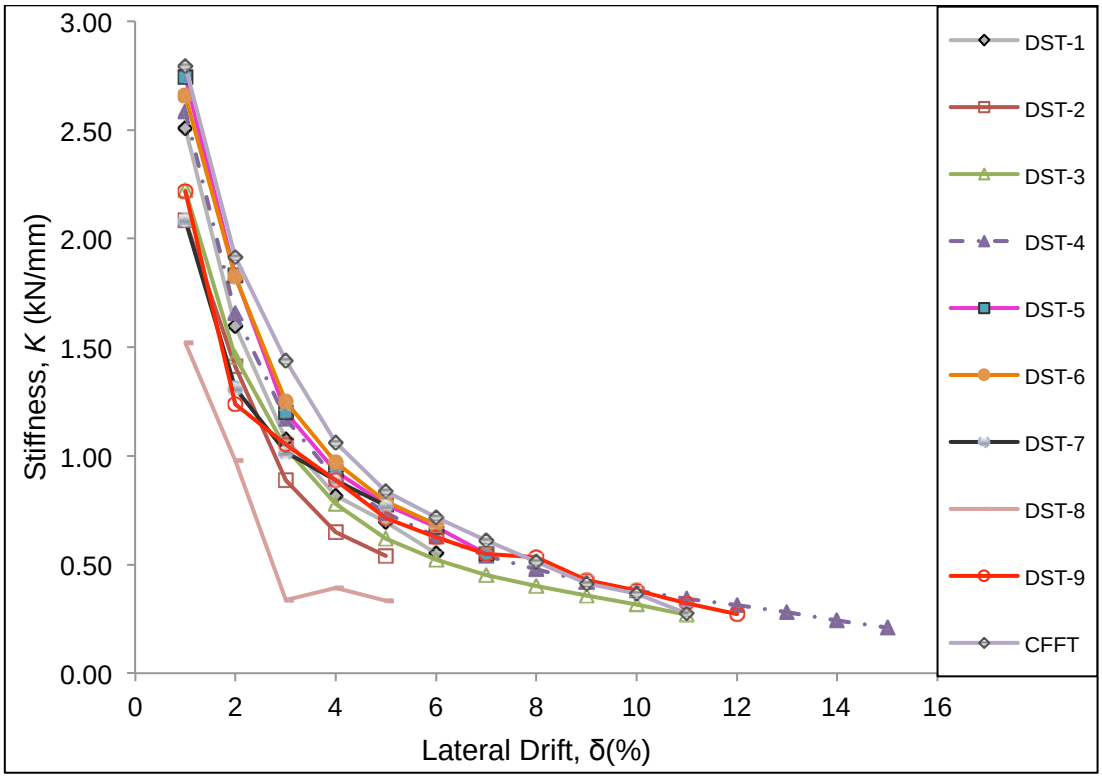

Fig. 6. Variation of column stiffnesses with lateral drifts

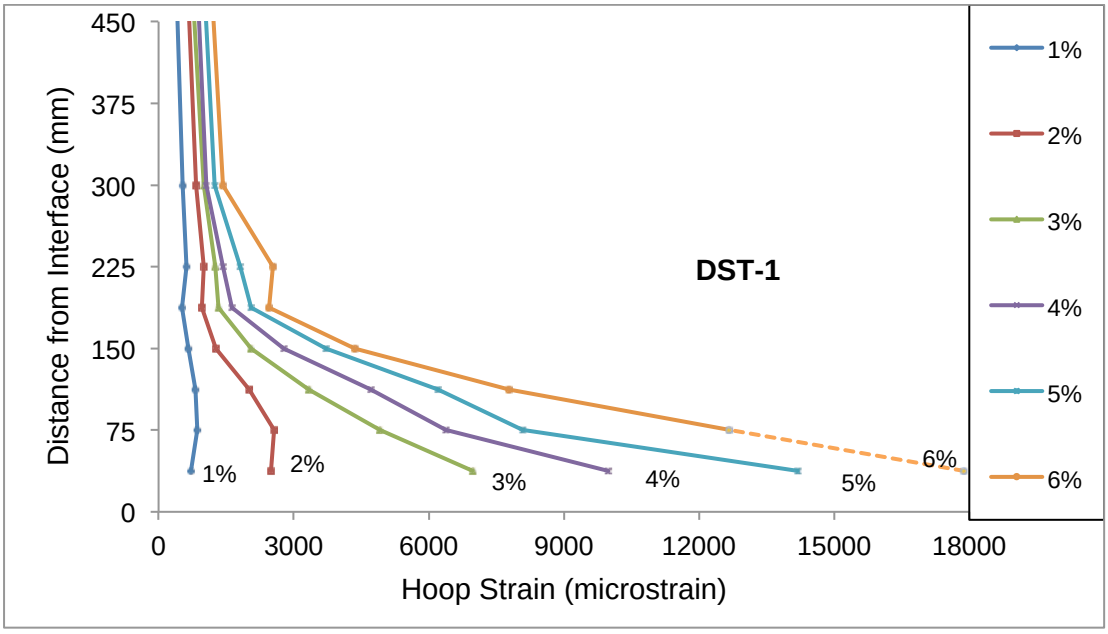
DST-1
Distance from Interface (mm)
Hoop Strain (microstrain)
0
75
150
225
300
375
450
0
3000
6000
9000
12000
15000
18000
1%
2%
3%
4%
5%
6%

(a)

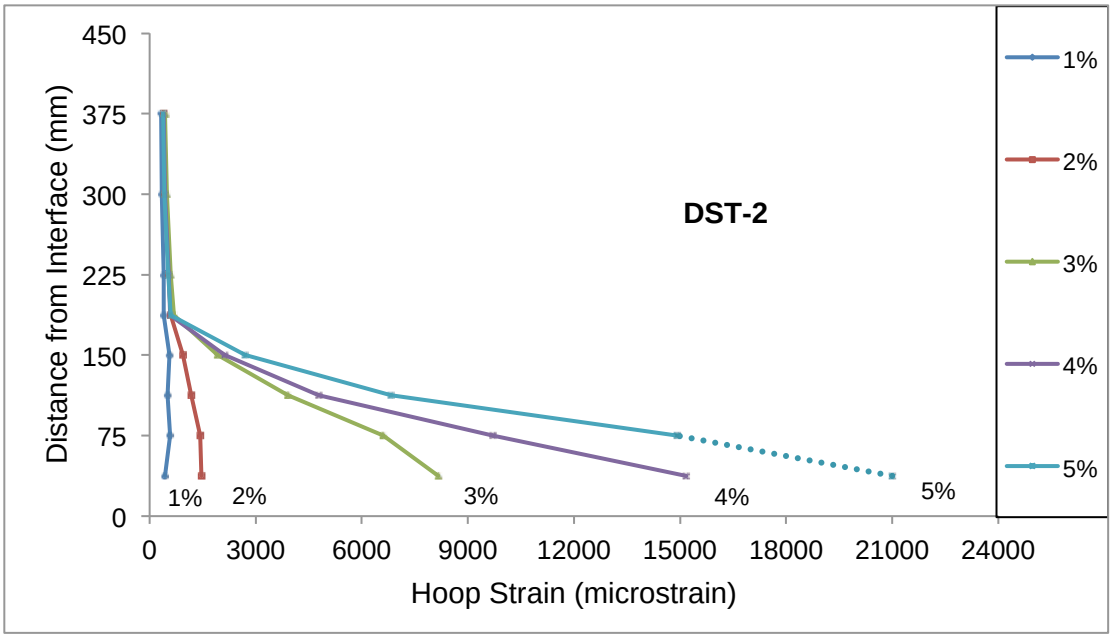
DST-2
Distance from Interface (mm)
Hoop Strain (microstrain)
0
75
150
225
300
375
450
0
3000
6000
9000
12000
15000
18000
21000
24000
1%
2%
3%
4%
5%

(b)

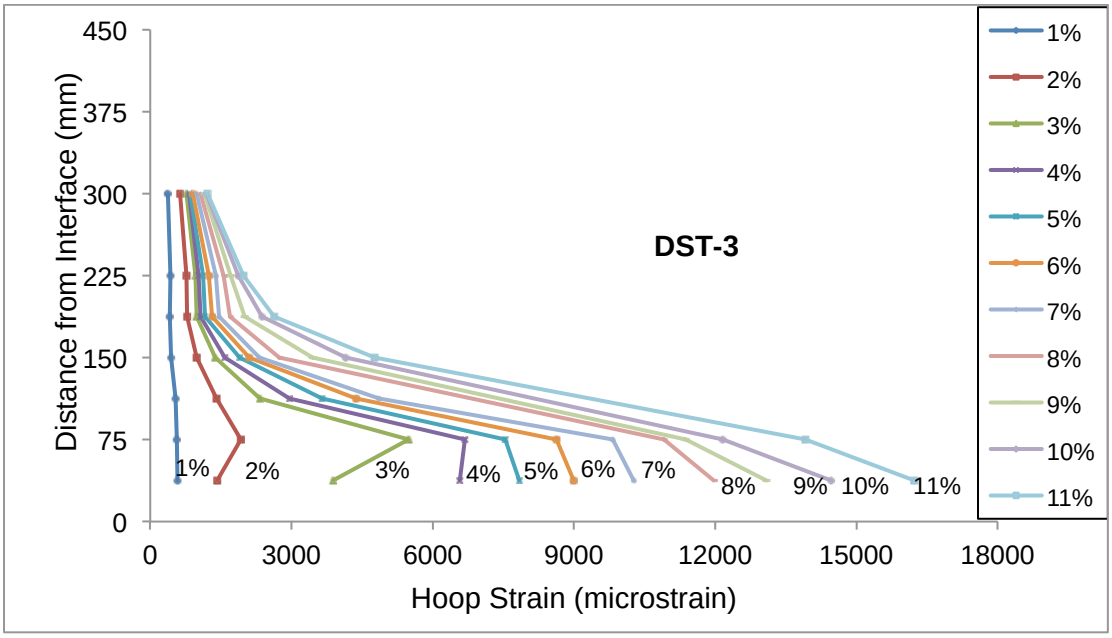
DST-3
Distance from Interface (mm)
Hoop Strain (microstrain)
0
75
150
225
300
375
450
0
3000
6000
9000
12000
15000
18000
1%
2%
3%
4%
5%
6%
7%
8%
9%
10%
11%

(c)

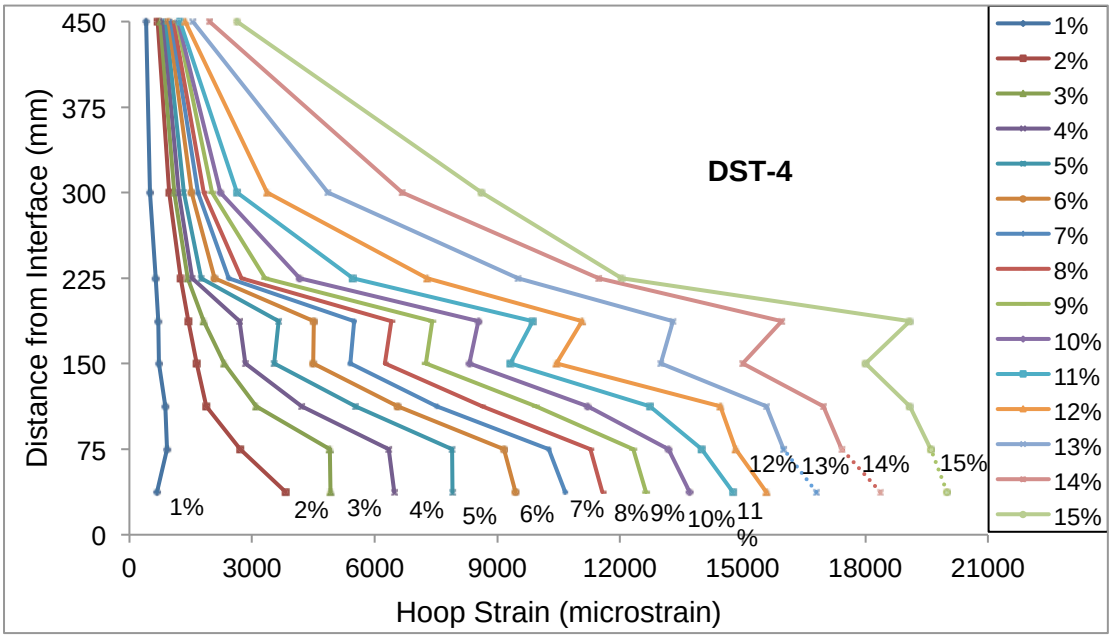
DST-4
Distance from Interface (mm)
Hoop Strain (microstrain)
0
75
150
225
300
375
450
0
3000
6000
9000
12000
15000
18000
21000
1%
2%
3%
4%
5%
6%
7%
8%
9%
10%
11%
12%
13%
14%
15%

(d)

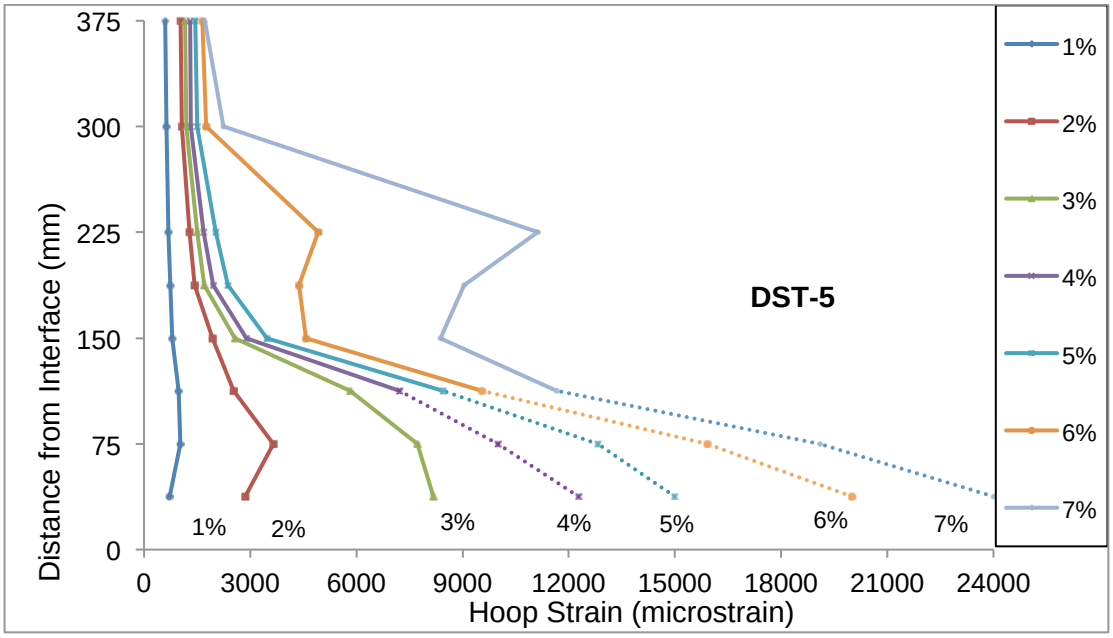
DST-5
Distance from Interface (mm)
Hoop Strain (microstrain)
0
75
150
225
300
375
0
3000
6000
9000
12000
15000
18000
21000
24000
1%
2%
3%
4%
5%
6%
7%

(e)

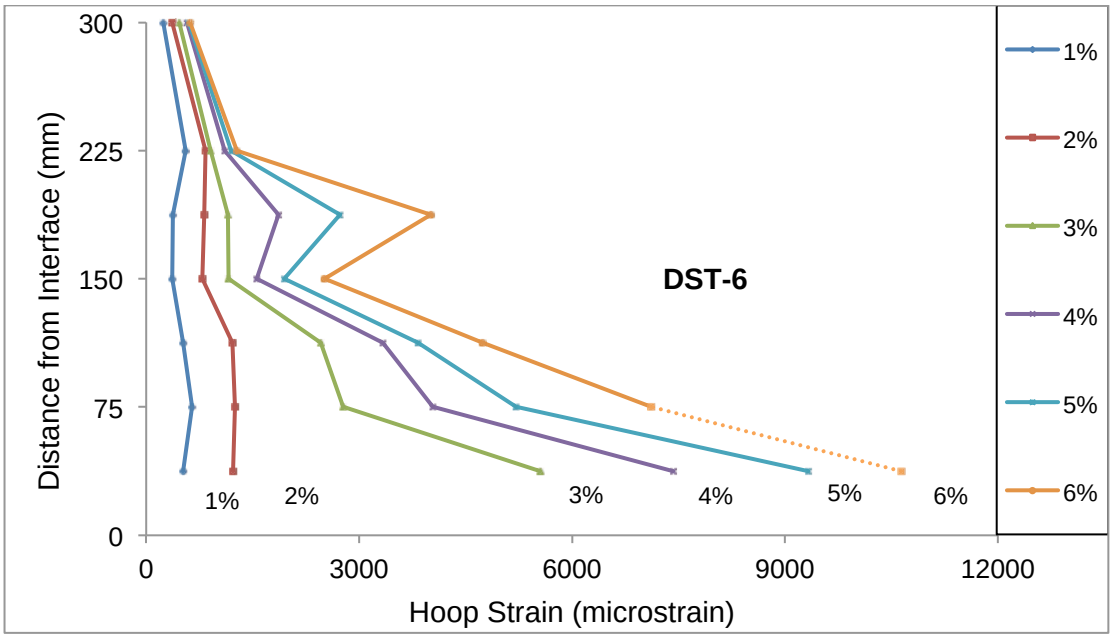
DST-6
Distance from Interface (mm)
Hoop Strain (microstrain)
0
75
150
225
300
0
3000
6000
9000
12000
1%
2%
3%
4%
5%
6%

(f)

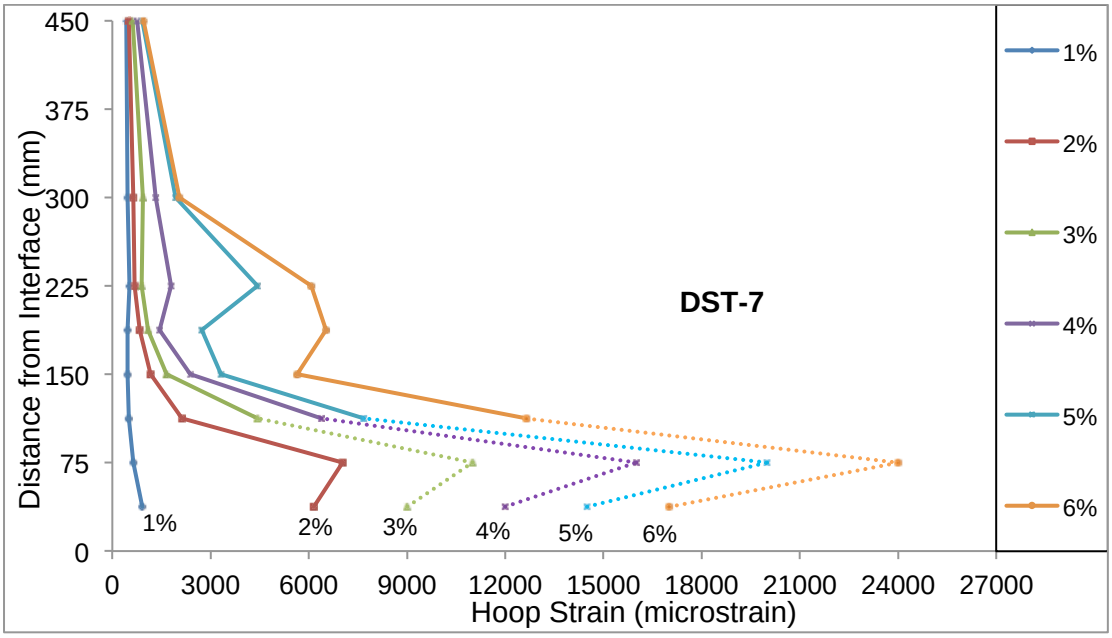
DST-7
Distance from Interface (mm)
Hoop Strain (microstrain)
0
75
150
225
300
375
450
0
3000
6000
9000
12000
15000
18000
21000
24000
27000
1%
2%
3%
4%
5%
6%

(g)

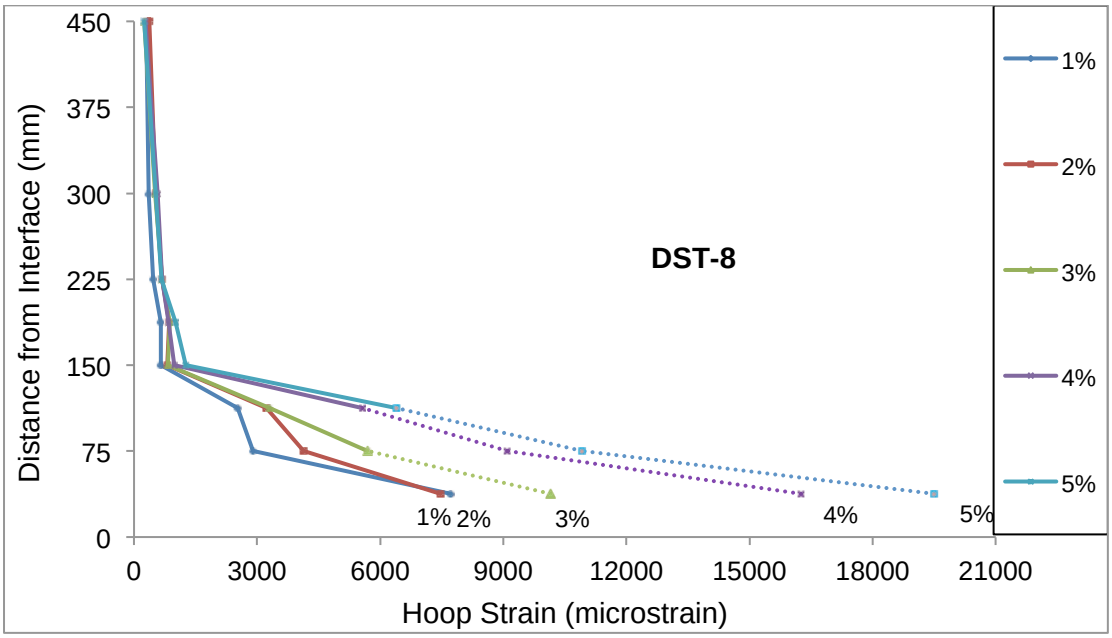
DST-8
Distance from Interface (mm)
Hoop Strain (microstrain)
0
75
150
225
300
375
450
0
3000
6000
9000
12000
15000
18000
21000
1%
2%
3%
4%
5%

(h)

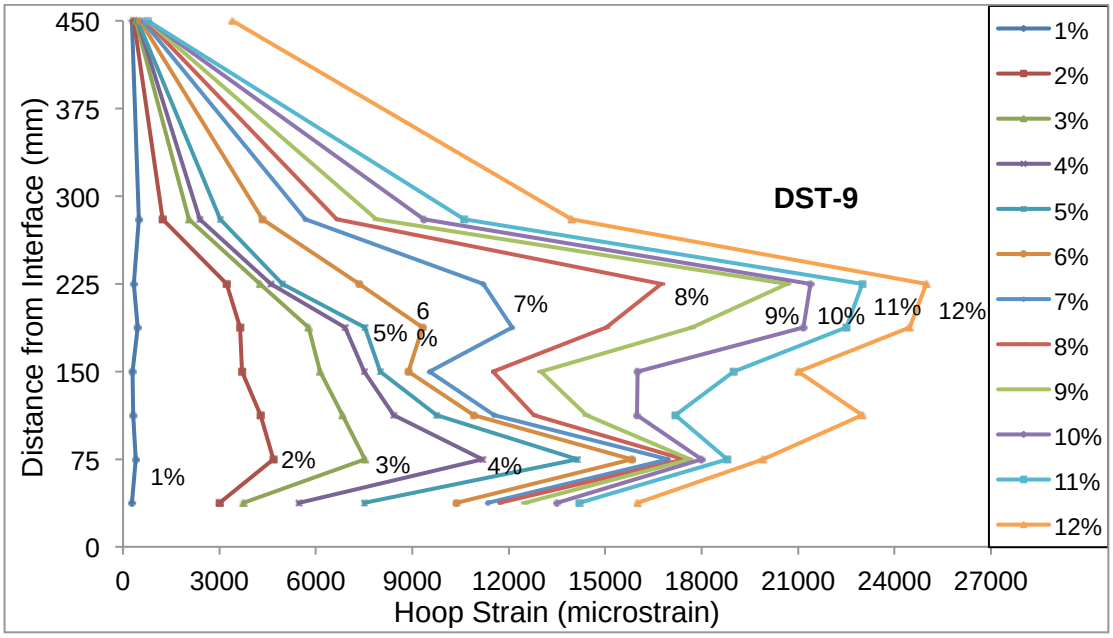

(i)

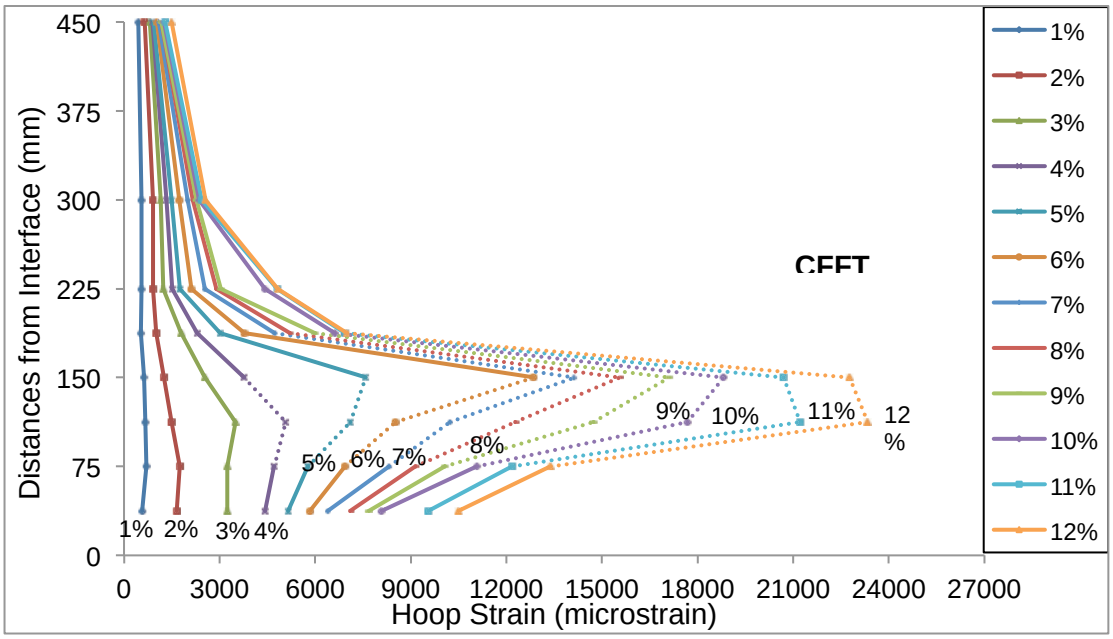

(j)

Fig. 7. Variation of FRP tube hoop strains along column height: (a) DST-1; (b) DST-2; (c) DST-3; (d) DST-4; (e) DST-5; (f) DST-6; (g) DST-7; (h) DST-8; (i) DST-9; (j) CFFT

CHAPTER 4

Behavior of Square FRP-HSC-Steel Double-Skin Tubular Columns under Combined Axial Compression and Reversed-Cyclic Lateral Loading

Yunita Idris and Togay Ozbakkaloglu

School of Civil, Environmental, and Mining Engineering, University of Adelaide, 5000

Engineering Structures (Submitted)

Statement of Authorship

Title of Paper	Behavior of Square FRP-HSC-Steell Double Skin Tubular Columns under Combind Axial Compression and Reversed-Cyclic Lateral Loading
Publication Status	○ Published ○ Accepted for publication ● Submitted for publication ○ Publication style
Publication Details	Idris, Y., and Ozbakkaloglu, T. (2015). "Behavior of square FRP-HSC-Steel double-skin tubular columns under combined axial compression and reversed-cyclic lateral loading." *(submitted to Engineering Structures)*

Author Contributions

By signing the Statement of Authorship, each author certifies that their stated contribution to the publication is accurate and that permission is granted for the publication to be included in the candidate's thesis.

Name of Principal Author (Candidate)	Yunita Idris		
Contribution to the Paper	Review of literature, analysis data, and preparation of manuscript		
Signature		Date	22/09/2015

Name of Co-Author	Dr. Togay Ozbakkaloglu		
Contribution to the Paper	Research supervision and review of manuscript		
Signature		Date	23/09/2015

BEHAVIOR OF SQUARE FRP-HSC-STEEL DOUBLE-SKIN TUBULAR COLUMNS UNDER COMBINED AXIAL COMPRESSION AND REVERSED-CYCLIC LATERAL LOADING

Yunita IDRIS and Togay OZBAKKALOGLU

ABSTRACT

This paper presents an experimental study on seismic behavior of square fiber reinforced polymer (FRP)-concrete-steel columns. Six FRP-concrete-steel double-skin tubular columns (DSTCs) that were manufactured using high-strength concrete (HSC) were tested under combined axial compression and reversed-cyclic lateral loading. The main parameters under investigation were the axial load level, size of inner steel tube, provision (or absence) of a concrete-filling inside the steel tube, and the column aspect ratio. The results indicate that, in general, square DSTCs exhibit very ductile behavior under combined axial compression and reversed-cyclic lateral loading. However, important influence of the axial load level on the column behavior is evident, with an increase in the load level leading to a significant decrease in the lateral deformation capacity of DSTCs. The results also indicate that a DSTC with a larger inner steel tubes exhibits lower lateral displacement capacity than that of a companion DSTC with a smaller inner steel tube. It is shown, however, that provision of a concrete-filling inside the inner steel tube leads to a significant increase in the lateral deformation capacity of a DSTC with a larger inner steel tube to a level that is higher than that seen in a companion DSTC with a smaller hollow inner steel tube. These results are presented together with accompanying discussions on the influence of the investigated parameters on the seismic behavior of square DSTCs.

KEYWORDS: Columns; High-strength concrete (HSC); Fiber reinforced polymer (FRP); Confinement; Tubes; Lateral displacement; Plastic hinge.

1. Introduction

As was demonstrated in a recent review by Ozbakkaloglu et al. [1], the use of fiber reinforced polymer (FRP) composites as a confinement material for concrete has received a great deal of attention over the past two decades. Initially research focused on the use of the material in retrofitting applications of concrete columns [e.g. (2-7)]. More recently, the focus has turned to the application of FRP composites for the development of new high-performance composite structural systems. As one of the most promising of these structural systems, concrete-filled FRP tubes (CFFTs) have been investigated extensively, with a large number of studies reporting on compressive [e.g. (8-13)], flexural [e.g. (14,15)] and seismic [e.g. (16-20)] behavior of CFFT beams and columns.

Following from the research on CFFTs, a new type of composites system, which consists of an inner steel tube, an outer FRP tube and a concrete-filling in between the two tubes (and if preferred, inside the steel tube), has received significant recent research attention. These FRP-concrete-steel double-skin tubular (DST) beams and columns benefit from the same FRP tube confinement mechanism that is present in CFFTs and they offer a long list of advantages, including: i) improved structural performance, ii) improved durability that prolongs the design life, thereby reducing the cost of structural maintenance and urban renewal, iii) significant improvements to the ease of construction that results in reduced construction costs, iv) significant reduction to carbon footprint through more efficient use of materials that reduces both the required amount of raw materials and generation of construction and demolition waste. In the construction of DST structural systems, the use of high-strength concrete (HSC) is particularly attractive, as this ensures that the properties of concrete complements those of the other two high-strength constituents (i.e. steel and FRP) in a composite system that is designed to maximize the advantages offered by each constituent. A large number of experimental studies that were recently undertaken on

composite members manufactured using FRP-concrete-steel DST system demonstrated the performance advantages offered by this system under various loading conditions, including monotonic [21-26] and cyclic [27, 28] axial compression, flexure [29-31], and combined axial compression and lateral load reversals [32-34].

The two studies reported to date on the seismic behavior of circular DST columns (DSTCs) [Refs. 33, 34] illustrated the ability of these columns to develop very high inelastic deformation capacities under combined axial compression and lateral reversed-cyclic loading. Findings of these studies were complemented by those of the studies reported on the behavior of DST beams [Refs. 29-31] and beam-columns [Ref. 32] that were tested under lateral reversed-cyclic loading. Given that the focus of both of the existing studies on the seismic column behavior were on circular DSTCs, there is a need for new studies that examine the seismic behavior of square DSTCs as a natural extension of the existing studies.

This paper reports on such an experimental study, which was designed to investigate the performance of square FRP-HSC-steel DSTCs under simulated seismic loading. The main parameters of this study were the axial load level (P/P_o), column aspect ratio (L/D), size of inner steel tube, and provision (or absence) of a concrete-filling inside the steel tube. The results of the experimental program are first presented, followed by discussions on the influence of the main test parameters on the observed column behavior. In the final part of the paper, the performance of the square DSTCs of the present study is compared with those of two companions circular DSTCs and a square CFFT from previous studies.

2. Experimental Program

2.1 Test specimens

Six square DSTCs were manufactured and tested under constant axial compression and incrementally increasing lateral displacement reversals. The specimens were designed as the lower portion of a first-story building column between the footing and point of inflection and they were fixed into a heavily reinforced concrete footing that was 790 mm in length, 290 mm in width and 460 mm in height. The specimens had a nominal cross sectional dimension of 150 mm and five of them had a cantilever height of 1.2 m and one of 0.6 m. Lateral loads were applied to the specimens by an actuator at a section 150 mm or 200 mm below the tip of the column, which resulted in a column shear span length (L) of 450 mm for one and 1000 mm for five of the specimens. The specimens were manufactured using a HSC mix with a target compressive strength of 95 MPa, and they were enclosed by aramid FRP (AFRP) external tubes. Table 1 provides a summary of material and geometric properties of the test specimens and Fig. 1 illustrates their geometry.

2.2. Materials

2.2.1. FRP tubes

FRP tubes of all specimens were manufactured using a unidirectional aramid fiber sheet with a 0.3 mm nominal fiber thickness. The tubes were manufactured using a manual wet lay-up process, which involved wrapping epoxy resin impregnated fiber sheets around precision-cut high-density polystyrene foam molds in the hoop direction. The epoxy resin was applied to the fiber sheet at a coverage rate of 0.6 L/m^2, which resulted in a ply thickness of 0.9 mm for the resulting FRP composite. The FRP tube of each specimen was

composed of two layers of FRP sheets, which were wrapped around the molds one layer at a time, with an overlap length of 100 mm provided for each layer to prevent premature debonding failure. Overlap regions of the two subsequent layers were located 180-degree apart from each other around the perimeter of the tube. Before the pouring of concrete the finished tubes were oriented such that overlap regions corresponded to the side faces of the columns with respect to the direction of the applied lateral load. Table 2 shows the manufacturer supplied properties of the unidirectional fiber sheets used in the fabrication of the FRP tubes. Material properties of the FRP composites, established through flat coupon tests that were undertaken in accordance with ASTM standard D3039M-08 [35], are also reported in the same table.

2.2.2. Concrete

A single HSC mix was used in the manufacture of the column specimens. The mix consisted of crushed bluestone as the coarse aggregate with a nominal maximum size of 10 mm. Silica fume was added to the mix at 8% of the binder content by weight. A low water-to-cementations material ratio of 0.29 was used to achieve the design concrete strength of 100 MPa. The mix was designed to exhibit a high workability to ensure its proper placement inside the DST columns. This was achieved through the use of a polycarboxyclic ether polymer-based superplasticizer at a rate of 20 kg per m^3. The test day concrete strength of each specimen is shown in Table 1. Column foundations were cast using a concrete mix with 40 MPa design strength that was ordered from a local concrete supplier.

2.2.3. Steel tubes

Two circular steel tubes with different external diameters (D_s) and thicknesses (t_s) were used in the fabrication of the DSTCs. Four of the specimens (i.e. DSTCs 1 to 4) were provided with an inner steel tube of 88.9-mm diameter and 3.2-mm wall thickness. The remaining two specimens (i.e. DSTCs 5 and 6) had an inner steel tube that was 114.3 mm in diameter and 6.0 mm thick walls. In one of these specimens (i.e. DSTC-6), the inner steel tube was filled with concrete. The material properties of the steel tubes were determined by testing steel coupons cut from the original tube. The results of these tests are given in Table 3.

2.3 Specimen preparation

Fig. 2 illustrates the manufacturing process of the specimens. Firstly, the internal steel tubes were fixed into a heavily reinforced foundation cage. The manufacturing process then continued with the concrete pouring of the column foundation. Previously prepared FRP tubes were then placed outside the steel tubes to serve as confining reinforcement for the columns, while also functioning as a formwork during the pour of the column concrete. Column concrete was subsequently poured into the space between the external FRP and inner steel tube, except in DSTC-6, which also received concrete inside its inner steel tube. Concrete was compacted thoroughly by a combination of internal rodding and external vibration to ensure its proper placement inside the specimens with no major air voids or honey combing.

2.4. Instrumentation, test setup and loading program

All the column specimens were instrumented with variable differential transformers (LVDTs) and strain gauges to measure lateral displacements, rotations of the plastic hinge region, anchorage slips, and axial and hoop strains on both steel and FRP tubes. Column lateral displacements were measured by two string pots that were placed at heights corresponding to the point of application of the lateral load (i.e. 0.45 m or 1.0 m from the column-footing interface) and at the tip of the column. Column rotations were measured by two LVDTs with 50-mm stroke capacities that were placed on the FRP tube at 150 mm from the column-footing interface. Anchorage slips were measured by two LVDTs with a 30-mm stroke capacity that were placed on the FRP tube 40 mm away from the interface. The acquisition of hoop strain data on FRP tubes was of particular interest to gain important insights into the activation of the confinement mechanism and development of confining pressures at different sections along the height of the columns. To this end, up to 33 strain gauges with 10-mm gauge lengths were bonded on each FRP tube in the hoop direction at seven to eight different cross-sections along the column height that extended up to 450 mm away from the footing interface. Axial strains of inner steel tubes were measured with 5-mm long strain gauges that were placed at four different cross-sections within a 375-mm long region measured from the interface.

The columns were tested under constant axial compression and incrementally increasing lateral deformation reversals, simulating seismic loading. The columns were first subjected to axial compression. A hydraulic jack with a 1000-kN working capacity and a load cell with the same capacity were placed on top of the column to apply the axial load. Lateral deformation reversals were applied through a hydraulic ram with a 500-kN load and 511-mm stroke capacity. Fig. 3 illustrates the test setup.

The magnitude of the applied axial compression (P) was determined based on the design axial load level (P/P_o) of the columns, which ranged between 14% and 42% of the column nominal axial load capacity (P_o), calculated according to ACI 318-11 [36] as:

$$P_o = 0.85 f_c^{'} A_c + f_y A_s \quad (1)$$

where f'_c = cylinder strength of unconfined concrete, f_y = yield strength of inner steel tube, A_c = net cross-sectional area of concrete, and A_s = total cross-sectional area of inner steel tube.

Following the application of the axial compression, specimens were subjected to lateral displacement excursions, consisting of incrementally increasing deformation reversals. Three full cycles were applied at each deformation level, starting with 1% drift ratio which was progressively increased to 2%, 3% etc. in the deformation control mode of the horizontal actuator. The lateral load was applied at a displacement rate of approximately 0.2 mm to 0.4 mm/sec depending on the column height, and the loading continued until the specimen was unable to maintain a significant fraction of its maximum lateral load resistance. A typical test took five to six hours to complete, depending on the lateral displacement capacity of the column.

3. Test Results

3.1. Failure modes

FRP tube rupture was the failure mode for all but one column, DSTC-1, which experienced a tension failure of its inner steel tube. Fig. 4 illustrates the regions of most extensive column damage at the end of testing. As can be seen in the figure, the most extensive damage regions extended 40 mm to 140 mm away from the column-footing interface. It

can also be seen in Fig. 4 that in specimens that failed due to FRP tube rupture the location of this rupture corresponded to one of the column corners. Table 4 summarizes the maximum recorded column capacities, as well as maximum damage zone locations and plastic hinge lengths of the columns. The damage zones reported in Table 4 were established based on observed heights of FRP tube rupture regions, whereas the plastic hinge lengths reported in the same table were established based on hoop strain distributions of the specimen at the final drift cycle (presented later in the paper), assuming that the plastic hinge region terminated at a height where recorded hoop strains fell below one-third of the maximum recorded strain in that drift cycle.

It can be seen in Fig. 4 that DSTC-1 had no sign of fiber rupture by the time of failure, as its failure was governed by the rupture of its inner steel tube in tension at a height of 40 mm from the column-footing interface. As illustrated in Fig. 4, the removal of FRP tubes of DSTCs 2 to 6 revealed that the most extensive concrete damage occurred at a region that started 30 to 40 mm above the column footing interface and extended up to 140 mm. Shifting of the critical column section from the interface can be attributed to the confining effect of the footing. Similar observations were reported previously for both square and circular CFFT columns [16, 17, 20] and for circular DST columns [33]. As can be seen in Fig.4, removal of the crushed concrete revealed that inner steel tubes of DSTCs 2 to 5 experienced local buckling within the maximum damage region. The figure shows that the buckling experienced by the inner steel tube of DSTC-5 was particularly severe. It can also be seen in the same figure that the concrete-filled inner steel tube of DSTC-6 experienced an outward bulging instead of a local buckling experienced by inner steel tubes of the hollow DSTCs that failed in compression (i.e. DSTCs 2-5).

3.2. Hysteretic Behavior

Fig. 5 shows the experimentally recorded hysteretic moment-lateral drift relationships of the specimens. As can be seen from the figure, all of the columns exhibited a flexure-dominant response. Some pinching is evident in the hysteresis loops of column DSTC-1 starting from 4% lateral drift, as the lightly loaded column started to experience anchorage slip and shear effects after it sustained significant flexural damage. It can also be seen in Fig. 5 that the column maintained almost a constant moment capacity of 30.6 kNm before it failed at 12% lateral drift.

As illustrated in Fig. 5, DSTC-2 with a P/P_o ratio of 0.28 exhibited no strength decay up to 9% lateral drift when the column reached its maximum moment capacity of 39.8 kNm and subsequently failed. The companion column DSTC-3 with P/P_o = 0.42, on the other hand, started to experience strength decay after developing its maximum moment capacity of 46.2 kNm at 2% lateral drift, and it failed at 4% lateral drift. The comparison of the behavior of these two specimens serves to highlight the significant influence of the axial load level on the seismic behavior of square DST columns. It is also worth noting that a slight pinching effect that was evident in the hysteretic curves of DSTC-2 was not seen in DSTC-3 in the presence of a higher axial compression the column was tested under.

DSTC-4, with an aspect ratio (*L/D*) of 3.0, also exhibited some strength decay starting at 4% lateral drift until its failure at 6% lateral drift. The comparison of the hysteric behavior of this column to that of its companion with an *L/D* of 6.7 (i.e. DSTC-2) indicates that the higher shear forces resisted by the shorter column had a detrimental influence on the overall column behavior under lateral displacement excursions, resulting in a lower lateral drift capacity.

As can be seen in Fig. 5, DSTCs 5 and 6 with larger inner steel tubes (i.e. D_s = 114.3 mm) exhibited more well-rounded hysteretic curves than those of the companion column (DSTC-2) with a smaller inner steel tube (i.e. D_s = 88.9 mm), indicating that the effect of shear was less pronounced in the former specimens. This observation also suggests that the concrete was more effectively confined in DSTCs 5 and 6 than it was in DSTC-2. On the other hand, as can be seen in Fig.5, DSTC-5 exhibited a lower lateral drift capacity compared to that of DSTC-1. This can be attributed to the early failure of the inner steel tube of the former specimen, which was contributed by the lower lateral restraint provided by the thinner layer of concrete to the steel tube against buckling. A similar observation was previously reported in Idris and Ozbakkaloglu [31] based on the behavior of DST beams under lateral cyclic loading.

As can be seen in Fig. 5, DSTC-6 with a concrete-filled inner steel tube developed a significant higher lateral drift capacity compared to that of the companion column DSTC-5 with a hollow inner steel tube. This improvement was mainly due to the prevention of the internal buckling of inner steel tube within the plastic hinge region in DSTC-6, through the support provided by the concrete placed inside the tube. This observation is in agreement with that previously reported in Ozbakkaloglu and Idris [33] for circular DSTCs.

To help establishing relative performances of the specimens, Fig. 6 presents the moment (M)-lateral drift (δ) envelope of each specimen, which was obtained by averaging the maximum moments from pull and push directions at each lateral drift level. As can be seen in the figure, the majority of the DST columns exhibited very high lateral drift capacities without any significant strength degradation, except for DSTC-3, which developed a relatively low lateral displacement capacity under the heavy axial compression it was subjected to.

3.3. Measured column stiffness

Fig. 7 illustrates the variation of the average column stiffness (K) with the lateral drift for all specimens. Member stiffness curves shown in Fig. 7 were established from the average lateral loads (F) and displacements (D) recorded at a given drift level for the three cycles in the pull and push direction, with the stiffness calculated as $K = F/\Delta$. As evident from the figure, all specimens exhibited a progressive reduction in their stiffness with an increase in the lateral drift, which is associated with cracking of concrete and yielding of the internal steel tube. In all specimens this reduction in stiffness was most significant up to 2 to 4% lateral drift, and beyond this displacement level stiffness degradation continued at a lower and continuously decreasing rate.

It can be seen in Fig.7 that, as expected, the shorter column DSTC-4 with an aspect ratio (L/D) of 3 exhibited a significantly higher stiffness compared to those of the remaining columns with L/D = 6.7. The figure also shows that DSTCs with a larger inner steel tube (i.e. DSTCs 5 and 6) had a higher stiffness than that of the companion specimen, DSTC-2, with a smaller inner steel tube. Furthermore, the presence of the concrete filling in DSTC-6 resulted in an increase in the column stiffness compared to that of its companion, DSTC-5. Finally the comparison of the curves of DSTCs 1 to 3 in Fig. 7 indicates that an increase in the axial load level resulted in an increase in the column stiffness, contributed by the increase in the column lateral load capacity.

3.4. Energy dissipation capacity

The energy dissipation capacity of each specimen was determined at each drift cycle by calculating the area enclosed within the corresponding lateral load-displacement hysteretic loop. The average energy dissipation capacities of the columns were then calculated for the

three consecutive load cycles at a given drift level, and they are shown in Fig. 8. As can be seen in Fig. 8, owing to their higher lateral load capacity, at a given lateral drift level DSTCs with larger inner steel tubes (DSTCs 5 and 6) exhibited higher energy dissipation capacities than those of the DSTCs with smaller inner steel tubes. It can also be seen in the figure that DSTCs 5 and 6 had similar energy dissipation capacities until the failure of DSTC-5 at 6% lateral drift, beyond which dissipation capacity of DSTC-6 continuously increased until the failure of the column at 11% lateral drift. The comparison of energy dissipation capacities of DSTCs 1 to 3 in Fig. 8 indicates that an increase in the axial load level resulted in an increase in the energy dissipation capacity at a given lateral drift level. This increase, once again, can be explained by higher lateral load capacities of the specimens that were tested under a higher axial compression. It can also be seen in Fig. 8 that the shorter column DSTC-4 developed a slightly higher energy dissipation capacity at each lateral drift level compared to that of its companion, DSTC-2. This can be attributed to the slightly higher moment capacity of the former specimen, which was the result of slightly higher compressive strength of the column compared to that of DSTC-2.

3.5. Measured column rotations

Total column rotations within the plastic hinge region were determined using the measurements of the two LVDTs that were placed on the specimens at 150 mm away from the column-foundation interface. Rotations of the specimens were also determined at 40 mm away from the column-foundation interface by the two LVDTs that were placed at this region. The measurements obtained at these two levels were used together to establish column rotations due to anchorage slip/yield penetration and flexure. Table 5 shows the total column rotations measured within a 150-mm long region from the column base (θ_{TPh}), flexural rotations measured within the same region (θ_{fPh}), and the rotations due to

anchorage slip/yield penetration ($\theta_{a.s}$). The results shown in Table 5 indicate that a significant proportion of the total plastic hinge region rotation (i.e. 37%), and the resulting lateral displacement, of DSTC-1 was caused by the yield penetration of its inner steel tube. This is attributable to the light axial compression load of the column (i.e. P/P_o = 0.14) and is responsible for the pinching effects that were present in the moment-lateral drift relationship of DSTC-1, as was discussed previously. The results shown in Table 5 also indicate that anchorage slip/yield penetration was responsible for approximately 20% of the total plastic hinge region rotations of the remaining columns that were tested under higher axial compression (i.e. $P/P_o \geq 0.28$). Although much lower than that of DSTC-1, this $\theta_{a.s}/\theta_{TPh}$ ratio represents a relatively large contribution of anchorage slip/yield penetration to total rotations/displacements. Therefore, based on these observations it is recommended that in future studies special effort is made to obtain rotations and displacements due to slip/penetration and report these values alongside the total column rotations and displacements.

3.6. Variation of FRP tube hoop strains along column height

The variation of maximum hoop strains recorded by strain gauges placed on FRP tubes along the column height is shown for each specimen in Fig. 9. The values given in Fig. 9 represent the recorded maximums that were obtained from the larger of the maximum strains recorded in the pull and push direction. Strain profiles shown in Fig. 9 provide value information as to the formation and progression of plastic hinge regions, which is discussed in detail later in the paper. It can be seen in Fig. 9 that in all specimens maximum hoop strains were recorded within a region along the specimen height that was 37.5 mm to 150 mm away from the column-footing interface, which corresponded to the maximum column damage region as discussed earlier. Consistent with the findings of

previous studies on CFFTs [16, 17, 20] and DSTCs [33], maximum hoop strains shown in Fig.9 were lower than the ultimate tensile strain of the fibers, with all but one column (i.e. DSTC-1) developing maximum hoop strains of around 70% of the ultimate fiber tensile strain. As can be seen in Fig. 9, the maximum hoop strain developed by DSTC-1 was around one half of those of the remaining specimens. This can be explained by the failure mode of this column (i.e. inner steel tube rupture), which, as was discussed previously, differed from that of the rest of the columns (i.e. FRP tube rupture). The lower axial compression level of DSTC-1 resulted in the failure of the column due to inner steel tube rupture, and as a result the full capacity of the FRP tube could not be developed.

4. Effect of Test Parameters on Observed Column Behavior

The following sections provide discussions on the influence of the test parameters investigated in this study on the lateral drift capacity and plastic hinge region behavior of square DSTCs. In these discussions the lateral drift capacity of the specimens is defined as the drift that corresponds to 20% strength decay beyond the peak moment resistance (i.e. $\delta_{0.8Mmax}$ in Table 4).

4.1. Column lateral drift capacity

4.1.1. Effect of axial load level

Effect of axial load level (P/P_o) on the column drift capacity can be investigated by comparing drift capacities ($\delta_{0.8Mmax}$) of DSTCs 1 to 3 in Table 4, which were tested under axial load levels of 0.14, 0.28 and 0.42, respectively. As is evident from the table, drift capacities of the columns decreased with an increase in the axial load level. This

observation is in agreement with those previously reported in studies on both CFFTs [16, 17, 20] and DSTCs [33] that the column lateral drift capacity is highly sensitive to and it decreases with an increase in P/P_o. However, it is worth noting that, as discussed earlier, DSTC-1 exhibited a different failure mode than DSTCs 2 and 3. Furthermore, as was also discussed previously, anchorage slip/yield penetration component of the lateral displacement was much higher in DSTC-1 than that seen in DSTCs 2 and 3. Therefore, a direct comparison of DSTC-1 with DSTCs 2 and 3 to gain insights into the influence of axial load level on the flexural deformations capacity of the columns would not be appropriate. On the other hand, DSTCs 2 and 3 exhibited the same failure mode and, as shown in Table 5, the slip/penetration component of their total rotations/displacements was similar. Therefore, a reduction in the lateral drift capacity from 9% (in DSTC-2) to 4% (in DSTC-3) with an increase in P/P_o from 0.28 to 0.42 is directly attributable to the influence of P/P_o on the flexural behavior of DSTCs, and this comparison highlights the significance of this influence for hollow square DSTCs.

4.1.2. Effect of inner steel tube size

A comparison of the behaviors of DSTC-2 and DSTC-5 in Fig.5 illustrate that an increase in the diameter and thickness of the inner steel tube resulted in a decrease in the lateral drift capacity. Although both columns exhibited a flexural dominant behavior, as can be seen in Fig. 5, hysteretic curves of DSTC-5 were more well-rounded than those of DSTC-2. The more well-rounded curves of DSTC-5 suggest that the concrete was more effectively confined in this specimen and the shear had no major effect on the behavior even after concrete sustained significant damage under combined axial compression and flexure. On the other hand, DSTC-5 exhibited a lower lateral drift capacity compared to that of DSTC-

2, which is caused by the earlier buckling of its inner steel tube. This can be attributed to the lower lateral restraint provided to the inner steel tube of DSTC-5 by the surrounding concrete layer, which was significantly thinner than that in DSTC-2.

4.1.3. Effect of concrete-filling inner steel tube

The effect of concrete-filling the inner steel tube was investigated by comparing relative performances of DSTC-5 and DSTC-6. As can be seen in Fig. 5, DSTC-6 with a filled inner steel tube developed a significantly higher lateral drift capacity compared to that of its companion, DSTC-5, with a hollow inner steel tube. The improvement seen in the lateral displacement capacity of the concrete-filled DSTC can be attributed to the prevention of the inward buckling failure of the inner steel tube through the support provided by the concrete placed inside the tube. This observation is in agreement with that previously reported in Ozbakkaloglu and Idris [33] for circular DSTCs, where it was shown that, under an axial load level of P/P_o = 0.42, the lateral displacement capacity of a concrete-filled DSTC was 2.5 times that of a companion DSTC with a hollow inner steel tube. It is clear from these results that under higher axial load levels (i.e. $P/P_o \geq 0.28$), which are typically expected in critical building columns, concrete-filled DSTCs exhibit a significantly better performance compared to that of companion hollow DSTCs.

4.1.4. Effect of column aspect ratio

The influence of aspect ratio (*L/D*) on the lateral drift capacity of DSTCs can be investigated through the comparison of responses of DSTC-2 and DSTC-4. As can be seen in Fig. 5 and Table 4, a reduction in the column aspect ratio from 6.7 (DSTC-2) to 3.0

(DSTC-4) resulted in a fairly large decrease in the lateral drift capacity from 9% to 6%. Similar observations were previously reported with regard to the influence of the column aspect ratio on the lateral displacement capacity of both conventional [37, 38] and FRP-confined concrete columns [16], and the decrease in the displacement capacity associated with a decrease in *L/D* can be attributed to increased shear effects that result from a decrease in *L/D.*

4.2. Comparisons with companion specimens

In this section the square DSTCs of the present study are compared with a companion square CFFT and two companion circular DSTCs from previous studies to gain additional insights as to relative performances of these specimens.

To establish the relative performance of square DSTCs compared to square CFFTs, the concrete-filled DSTC of the present study, DSTC-6, was compared with a companion square CFFT (i.e. CFFT-1[a] in Table 6). As can be seen from Tables 1 and 6, these two columns had almost the same geometric and material properties and confinement levels, and they were tested under very similar axial load levels. The comparison indicates that the filled DSTC developed a higher lateral drift capacity (i.e. 11%) than that of the companion CFFT (8%). This observation is in agreement with that previously reported in Ozbakkaloglu and Idris [33] based on the comparison of a circular concrete-filled DSTC and a companion circular CFFT. Consistent with the finding of the present study, the said study too reported that the circular filled DSTC exhibited an approximately 50% higher lateral drift capacity than that of the companion CFFT. Above observations indicate that both square and circular concrete-filled DSTCs exhibit a performance advantage over that of companion CFFTs with the same sectional geometry.

To establish the influence of cross-sectional shape on the performance of DSTCs, one of the hollow square DSTCs of the present study, DSTC-3, was compared with a companion hollow circular DSTC (i.e. DST-1^b in Table 6). Once again, as is evident from Tables 1 and 6, these columns shared very close geometric, material, confinement and loading properties. It can be seen from Tables 1 and 6 that the square column, DSTC-3, developed a lateral drift capacity of 4% compared to 6% drift capacity developed by the companion circular column, DST-1^b. To complement this comparison, DSTC-2 of the present study was compared with another companion circular specimen, DST-3^b shown in Table 6. Although these columns had very close geometric, material and confinement properties, the circular column DST-3^b was tested under a higher axial load level (i.e. P/P_o = 0.34) compared to that of the companion square column, DSTC-2 (P/P_o= 0.28). The results of this comparison indicates that, despite its higher axial load level, DST-3^b developed a higher lateral drift capacity (i.e. 11%) than that of DSTC-2 (i.e. 9%). Previous studies on FRP-confined concrete columns clearly established that due to the higher confinement effectiveness of their cross-sections, under a similar level of confinement, circular columns outperform their square counterparts [16, 17, 20]. The observations presented in this section indicate that column cross-sectional shape affects the behavior of DSTCs in much the same manner as it does the behavior of conventional FRP-confined concrete columns.

4.3. Column plastic hinge region

Formation and propagation of the plastic hinge region of the specimens of the present study were investigated based on a similar approach that was used previously in Refs. [16,17,20,33], which involved the use of the column hoop strain profiles previously shown in Fig.9. This approach is based on the intimate relationship that exists between the lateral

expansion of FRP tube and the level of damage sustained by the concrete inside the tube. As a result, the most highly damaged regions of the columns correspond to higher FRP hoop strains, as within these regions the concrete undergoes rapid expansion inside the FRP tube. The plastic hinge regions of the specimens that are referred to in this section were established using hoop strain distributions of the specimens at the final drift cycle, assuming that the region terminated at a height where the recorded hoop strains fell below one third of the maximum recorded strain in that drift cycle. These values are reported in Table 4.

The comparison of the plastic hinge lengths of DSTCs 1 and 3 in Table 4 indicates that an increase in the column axial load level from P/P_o=0.14 to P/P_o=0.28 resulted in a significant increase in the column plastic hinge length. On the other hand, as evident from the comparison of the plastic hinge lengths of DSTCs 2 and 3, a further increase in P/P_o ratio from 0.28 to 0.42 did not result in any major change in the plastic hinge length. As was discussed previously DSTC-1 experienced a different failure mode (i.e. steel tube rupture) than that of DSTCs 2 and 3 (i.e. FRP tube rupture). The lower plastic hinge length of DSTC-1 can be attributed to its failure mode, associated with its lower axial load level, which did not allow the full development of the plastic hinge region. DSTCs 2 and 3, which both exhibited compression failure by FRP tube rupture, developed very similar plastic hinge lengths, suggesting that the axial load level had no major influence on the length of the plastic hinge region. To place the findings of the present study into broader context, it is worth comparing these results with those of previous studies that investigated the effect of axial load level. It was reported by Bae and Bayrak [38] and Pam and Ho [39] for conventional square reinforced concrete columns and by Idris and Ozbakkaloglu [20] for square CFFTs that an increase in the axial load level resulted in an increase in the column plastic hinge length. On the other hand, it was shown in Ozbakkaloglu and

Saatcioglu [17] for square CFFTs and in Ozbakkaloglu and Idris [33] for circular DSTCs that the column plastic hinge region became more localized with an increase in the axial load level. It is evident from the above summary that additional targeted studies are required to fully understand the complex influence of the P/P_o ratio on the formation and progression of plastic hinge regions of confined concrete columns in general and of DSTCs in particular.

As can be seen from the comparison of DSTCs 2 and 5 in Table 4, an increase in the size of the inner steel tube resulted in a decrease in the column plastic hinge length. As noted previously, failures of these specimens were initiated by the buckling of their inner steel tubes. This took place at a region closer to the column-footing interface in DSTC-5 than in DSTC-2, which explains the lower plastic hinge length of the former. The reduced plastic hinge length of DSTC-5 contributed to the lower lateral drift capacity of this column compared to that of its companion, DSTC-2, as discussed previously.

The comparison of the hoop strain profiles of DSTCs 5 and 6 in Fig. 9 indicates that provision of a concrete-filling inside the steel tube significantly influenced the progression and length of the plastic hinge region. As a result, as can be seen in Table 4, concrete-filled DSTC-6 exhibited a significantly larger plastic hinge region length compared to that of its hollow counterpart, DSTC-5. This can be explained by the different failure modes of inner steel tubes of these specimens. As discussed previously, stress concentrations on the FRP tube that resulted from the inward buckling of the inner steel tube was the main trigger for the failure of DSTC-5. In the filled DSTC, the prevention of the inward buckling of the inner steel tube through the support provided by the concrete-filling inside the tube enabled further progression of the plastic hinge region, resulting in an increased plastic hinge length. Therefore, both the increased plastic hinge length and delayed column failure achieved through prevention of inner steel tube buckling contributed to the significantly

higher lateral drift capacity of the filled DSTC (DSTC-6) over that of its hollow counterpart (DSTC-5). These observations are in agreement with those previously reported in Ozbakkaloglu and Idris [33] for circular DSTCs.

5. Conclusions

This paper has presented the results of an experimental study on square FRP-HSC-steel double-skin tubular columns that were subjected to combined axial compression and cyclic lateral loading. Based on the results and discussions presented in the paper the following conclusion can be drawn:

1. Square FRP-HSC-steel double-skin tubular columns can be designed to exhibit a very ductile behavior under combined axial compression and cyclic lateral loading.
2. Similar to that of conventional and FRP-confined concrete columns, lateral displacement capacity of a DST column is influenced significantly by and it decreases with the level of axial load acting on the column (P/P_o). It should be noted, however, that below a certain axial load level DSTCs may experience relatively large anchorage slips and their failure mode changes from compression failure through FRP tube rupture to tension failure of inner steel tube.
3. It is found that a DSTC with a larger and thicker inner steel tube exhibited a more well-rounded hysteretic curve compared to that of a companion DSTC with a smaller inner steel tube. On the other hand, it is observed that an increase in the tube diameter resulted in a decrease in the lateral drift capacity of the hollow DSTC, which is caused by an earlier buckling of the inner steel tube.
4. DSTCs manufactured with concrete-filled inner steel tubes develop significantly higher lateral drift capacities compared to those of the companion hollow DSTCs. By

preventing the buckling of inner steel tube, the presence of concrete core both delays the column failure and increases the length of the plastic hinge region. This observation is applicable to columns that exhibit compression failure, and the influence of concrete filling inner steel tube is expected to be less significant in columns under lighter axial compression. However, this needs to be verified in future studies.

5. A decrease in the column aspect ratio leads to a decrease in the lateral drift capacity of DSTCs, which is attributable to increased shear effects that result from a decrease in the aspect ratio.
6. Comparisons of the results of the present study with those of the previous studies indicate that concrete-filled square DSTCs exhibit higher lateral displacement capacities compared to those of companion square CFFTs. These comparisons also indicate that lateral displacement capacities of square DSTCs are lower than those of companion circular DSTCs.
7. Plastic hinge lengths of DSTCs are affected by the axial load level, inner steel tube size, and presence of a concrete-filling inside inner steel tube. An increase in axial load level, if it leads to a change in the column failure mode from tension to compression, leads to an increase in the plastic hinge length. Dimensions of inner steel tube influences the plastic hinge length through the influence it has on buckling behavior of the tube. Provision of a concrete-filling inside inner steel tube significantly increases the progression and length of the plastic hinge region.

6. References

[1] Ozbakkaloglu, T., Lim, J. C., and Vincent, T. (2013). “FRP-confined concrete in circular sections: Review and assessment of stress-strain models.” *Engineering Structures*, 49: 1068-1088.

[2] Lignola, G. P., Prota, A., Manfredi, G., and Cosenza E. (2007). “Experimental performance of RC hollow columns confined with CFRP.” *Journal of Composite for Construction, ASCE*, 11(1): 42–49.

[3] Rousakis, T., and Karabinis, A. (2008). “Substandard reinforced concrete members subjected to compression: FRP confining effects.” *Materials and Structures*, 41(9): 1595 – 1611.

[4] Ilki, A., Peker, O., Karamuk, E., Demir, C., and Kumbasar, N. (2008). “FRP retrofit of low and medium strength circular and rectangular reinforced concrete columns.” *Journal of Materials in Civil Engineering*, 20(2): 169–188.

[5] Kusumawardaningsih, Y., and Hadi, M. N. S. (2010). “Comparative behavior of hollow columns confined with FRP composites.” *Composite Structures*, 93(1): 198-205.

[6] Wu, Y. F., and Wei, Y. Y. (2010), “Effect of cross sectional aspect ratio on the strength of CFRP-confined rectangular concrete columns.” *Engineering Structures*. 32(1): 32-45.

[7] Wang, Z, Wang, D., Smith, S. T., and Lu, D. (2012), “Experimental testing and analytical modeling of CFRP-confined large circular RC columns subjected to cyclic axial compression.” *Engineering Structures*, 40: 64-74.

[8] Fam, A. Z., and Rizkalla, S. H. (2001). Behavior of axially loaded concrete-filled circular fiber-reinforced polymer tubes. *ACI Structural Journal*, 98(3): 280-289.

[9] Mirmiran, A., Shahawy, M., & Beitleman, T. (2001). Slenderness limit for hybrid FRP-concrete columns. *Journal of Composites for Construction*, 5(1): 26-34.

[10] Ozbakkaloglu, T. (2013). “Compressive behavior of concrete-filled FRP tube columns: Assessment of critical column parameters.” *Engineering Structures*, 51: 188-199.

[11] Lim, J. C., and Ozbakkaloglu, T. (2014). “Influence of silica fume on stress–strain behavior of FRP-confined HSC.” *Construction and Building Materials*, 63: 11-24.

[12] Vincent, T. and Ozbakkaloglu, T. (2015). “Influence of slenderness on stress-strain behavior of concrete-filled FRP tubes: experimental study.” *Journal of Composites for Construction*, 19(1): 04014029.

[13] Xie, T. and Ozbakkaloglu, T. (2015),"Behavior of steel fiber-reinforced high-strength concrete-filled FRP tube columns under axial compression" *Engineering Structures*, 90: 158-171.

[14] Davol, A., Burgueno, R., and Seible, F. (2001), "Flexural Behavior of Circular Concrete Filled FRP Shells." *Journal of Structural Engineering*, 127(7): 810-7.

[15] Cole, B., and Fam, A. (2006), "Flexural load testing concrete filled FRP tubes with longitudinal steel and FRP rebar." *Journal of Composite for Consturction, ASCE*, 10(2):161-71.

[16] Ozbakkaloglu, T. and Saatcioglu, M. (2006),"Seismic Behavior of High Strength Concrete Columns Confined by Fiber-Reinforced Polymer Tubes." *Journal of Composite Construction, ASCE*, 10(6): 538-49.

[17] Ozbakkaloglu, T. and Saatcioglu, M. (2007), "Seismic Performance of Square High Strength Concrete Columns in FRP stay in place formwork." *Journal of Structural Engineering, ASCE*, 133(1): 44-56.

[18] ElGawady, M.A., Booker, A.J, and Dawood, H.M. (2010). "Seismic behavior of posttensioned concrete-filled fiber tubes." *Journal of Composites for Construction, ASCE*, 14 (5): 616-628.

[19] Zohrevand, P., and Mirmiran A. (2012). "Cyclic behaviour of hybrid columns made of ultra high performance concrete and fiber reinforced polymers." *Journal of Composites for Construction, ASCE*, 16(1): 91-99.

[20] Idris, Y., and Ozbakkaloglu, T. (2013). "Seismic behavior of square high-strength concrete-filled FRP tube columns." *Journal of Composites for Construction, ASCE*, 17(6): 04013013.

[21] Wong, Y.L., Yu, T., Teng, J.G., and Dong, S.L. (2008). "Behavior of FRP-Confined Concrete in Annular Section Columns." *Composites: Part B*, 39: 451-66.

[22] Louk Fanggi, B.A., and Ozbakkaloglu, T. (2013). "Compressive behavior of aramid FRP-HSC-Steel double-skin tubular columns." *Construction and Building Materials*, 48: 554-65.

[23] Yu, T. and Teng, J. G. (2013). “Behavior of hybrid FRP-Concrete-Steel double-skin tubular columns with a square outer tube and a circular inner tube subjected to axial compression.” *Journal of Composites for Construction, ASCE*, 17(2): 271-79.

[24] Ozbakkaloglu, T., and Louk Fanggi, B. A. (2014). “Axial compressive behavior of FRP-concrete-steel double-skin tubular columns made of normal- and high-strength concrete.” *Journal of Composites for Construction, ASCE,* 18(1): 04013027.

[25] Ozbakkaloglu, T., and Louk Fanggi, B.A. (2015). "FRP–HSC–steel composite columns: behavior under monotonic and cyclic axial compression." *Materials and Structures*. 48(4): 1075-1093.

[26] Louk Fanggi, B. A., and Ozbakkaloglu, T. (2015). “Square FRP-HSC-Steel composite columns: Behavior under axial compression.” *Engineering Structures,* 92: 156-171.

[27] Yu, T., Zhang, B., Cao, Y. B., and Teng, J. G. (2012). “Behavior of hybrid FRP-concrete-steel double-skin tubular columns subjected to cyclic axial compression.” *Thin-Walled Structures,* 61: 196-203.

[28] Albitar M., Ozbakkaloglu, T., and Louk Fanggi, B.A. (2015). “Behavior of FRP-HSC-Steel Double-Skin Tubular Columns under Cyclic Axial Compression.” *Journal of Composites for Construction,* ASCE. 19(2), 04014041.

[29] Yu, T., Wong, Y., Teng, J., Dong, S., and Lam, E. (2006). ”Flexural Behavior of Hybrid FRP-Concrete-Steel Double-Skin Tubular Members.” *Journal of Composites for Construction, ASCE,* 10(5): 443-452.

[30] Idris, Y., and Ozbakkaloglu, T. (2014). “Flexural behavior of FRP-HSC-steel composite beams.” *Thin-Walled Structures,* 80: 207-16.

[31] Idris, Y., and Ozbakkaloglu, T. (2015). “Flexural behavior of FRP-HSC-steel tubular beams under reversed cyclic loading.” *Thin-Walled Structures,* 87: 89-101.

[32] Han, L. H., Tao, Z., Liao, F. Y., and Xu, Y. (2010). “Tests on cyclic performance of FRP-concrete-steel double-skin tubular columns.” *Thin-Walled Structures,* 48(6): 430-439.

[33] Ozbakkaloglu, T., and Idris, Y. (2014), “Seismic behavior of FRP-high-strength concrete-steel double skin tubular columns.” *Journal of Structural Engineering, ASCE*, 140(6): 04014019.

[34] Zhang, B., Teng, J. G., and Yu, T. (2015). “Experimental behavior of hybrid FRP-concrete-steel double-skin tubular columns under combined axial compression and cyclic lateral loading.” *Engineering Structures*, 99: 214-231.

[35] ASTM D3039/D3039M-8. (2008). “Standard test method for tensile properties of polymer matrix composite materials.” *ASTM D3039/D3039M-8*, West Conshohocken, PA, 13.

[36] American Concrete Institute. (2011). “Building code requirements for structural concrete and commentary (318R-11).” *ACI 318-11*, Farmington Hills, MI.

[37] Panagiotakos, T. B., and Fardis, M. N. (2001). “Deformations of reinforced concrete members at yielding and ultimate” *ACI Structural Journal*, 98(2): 135-148.

[38] Bae, S., and Bayrak, O. (2008). “Plastic hinge length of reinforced concrete columns.” *ACI Structural Journal*, 105(3): 290-300.

[39] Pam, H. J. and Ho, J. C. M. (2009). “Length of critical region for confinement steel in limited ductility high-strength reinforced concrete columns” *Engineering Structures*, 31(12): 2896-2908.

Table 1. Properties of test specimens

Column	f'_c (MPa)	FRP tube		Inner steel tube			P (kN)	P/P_o	L (mm)	L/D
		Material	t_f (mm)	D_s (mm)	t_s (mm)	Inner void				
DSTC-1	95	Aramid	0.6	88.9	3.2	Empty	227	0.14	1000	6.7
DSTC-2	92	Aramid	0.6	88.9	3.2	Empty	443	0.28	1000	6.7
DSTC-3	95	Aramid	0.6	88.9	3.2	Empty	682	0.42	1000	6.7
DSTC-4	100	Aramid	0.6	88.9	3.2	Empty	474	0.28	450	3.0
DSTC-5	100	Aramid	0.6	114.3	6.0	Empty	533	0.28	1000	6.7
DSTC-6	91	Aramid	0.6	114.3	6.0	Filled	685	0.28	1000	6.7

f'_c = compressive strength of unconfined concrete, t_f = total nominal fiber thickness of FRP tube, D_s = steel tube diameter, t_s = steel tube thickness, P/P_o = Axial load level, L = shear span length, L/D = aspect ratio

Table 2. Material properties of fiber sheets and epoxy resin used in FRP tubes

Type	Nominal fiber thickness (mm/ply)	Provided by manufacturers			Obtained from flat FRP coupon tests		
		Tensile strength f_f (MPa)	Ultimate tensile strain, ε_f (%)	Elastic modulus E_f (GPa)	Tensile strength f_{frp} (MPa)	Ultimate tensile strain, ε_{frp} (%)	Elastic modulus E_{frp} (GPa)
Aramid	0.300	2600	2.20	118.0	2390*	1.86	128.5*
Epoxy Resin	-	>50	2.50	>3			

*Calculated based on nominal thickness of fibers

Table 3. Material properties of steel tubes

Tube	Shape	D (mm)	Yield Stress, f_y (MPa)	Ultimate Tensile Stress, f_u (MPa)	Ultimate Tensile Strain, ε_u (%)	Rupture strain, ε_r (%)
Tube 1	Circular	114.3	436	490	10.1	19.4
Tube 2	Circular	88.9	375	464	12.9	17.6

Table 4. Observed column behavior

Column	f'_c (MPa)	P/P_o	M_{max} (kN.m)	Failure drift, δ (%)	δ_{Mmax} (%)	$\delta_{0.8Mmax}$ (%)	Maximum damage region[a] (mm)	Plastic hinge length[b] (mm)
DSTC-1	95	0.14	30.6	12%, cycle 2	11	12	40	130
DSTC-2	92	0.28	39.8	9%, cycle 2	9	9	100	180
DSTC-3	95	0.42	46.2	4%, cycle 2	3	4	130	190
DSTC-4	100	0.28	44.7	6%, cycle 2	4	6	100	180
DSTC-5	100	0.28	61.8	6%, cycle 3	3	6	100	150
DSTC-6	91	0.28	73.1	11%, cycle 1	4	11	140	210

M_{max} = maximum recorded moment (averaged from push and pull directions), δ_{Mmax} = lateral drift at maximum moment (averaged from push and pull directions), $\delta_{0.8Mmax}$ = lateral drift at 20% strength decay (averaged from push and pull directions), defined as lateral drift capacity in this paper.

[a] Measured from column-footing interface to the far end of FRP tube rupture region

[b] Established based on the hoop strain profiles recorded along the column height shown in Fig.9 at failure drift (i.e. hoop strains within this region corresponded to at least one-third of the maximum recorded hoop strain)

Table 5. Column rotations at failure

Column	Θ_{TPh} (rad)	Θ_{fPh} (rad)	$\Theta_{a.s}$ (rad)	$\Theta_{a.s}/\Theta_{TPh}$
DSTC-1	0.135	0.084	0.051	0.37
DSTC-2	0.094	0.078	0.016	0.17
DSTC-3	0.039	0.032	0.007	0.18
DSTC-4	0.071	0.051	0.017	0.24
DSTC-5	0.070	0.058	0.012	0.17
DSTC-6	0.095	0.068	0.022	0.23

Θ_{TPh} = total rotation at 150 mm from the base,

Θ_{fPh} = flexural rotation at 150 mm from the base,

$\Theta_{a.s}$ = rotation due to anchorage slip/yield penetration

Table 6. Companion columns from previous experimental studies

Column	Cross-section	L/D	$f'c$ (MPa)	t_f (mm)	D_s/t_s	Inner void	P/P_o	M_{max} (kN.m)	Failure drift, δ (%)	δ_{Mmax} (%)	$\delta_{0.8Mmax}$ (%)
CFFT-1[a]	Square	6.7	95	0.6	N/A	N/A	0.27	55.7	11	3	8
DST-1[b]	Circular	6.7	95	0.6	88.9/3.2	Hollow	0.45	36.5	6	6	6
DST-3[b]	Circular	6.7	95	0.6	88.9/3.2	Hollow	0.34	37.2	11	4	11

[a]Idris and Ozbakkaloglu (2013), [b]Ozbakkaloglu and Idris (2014)

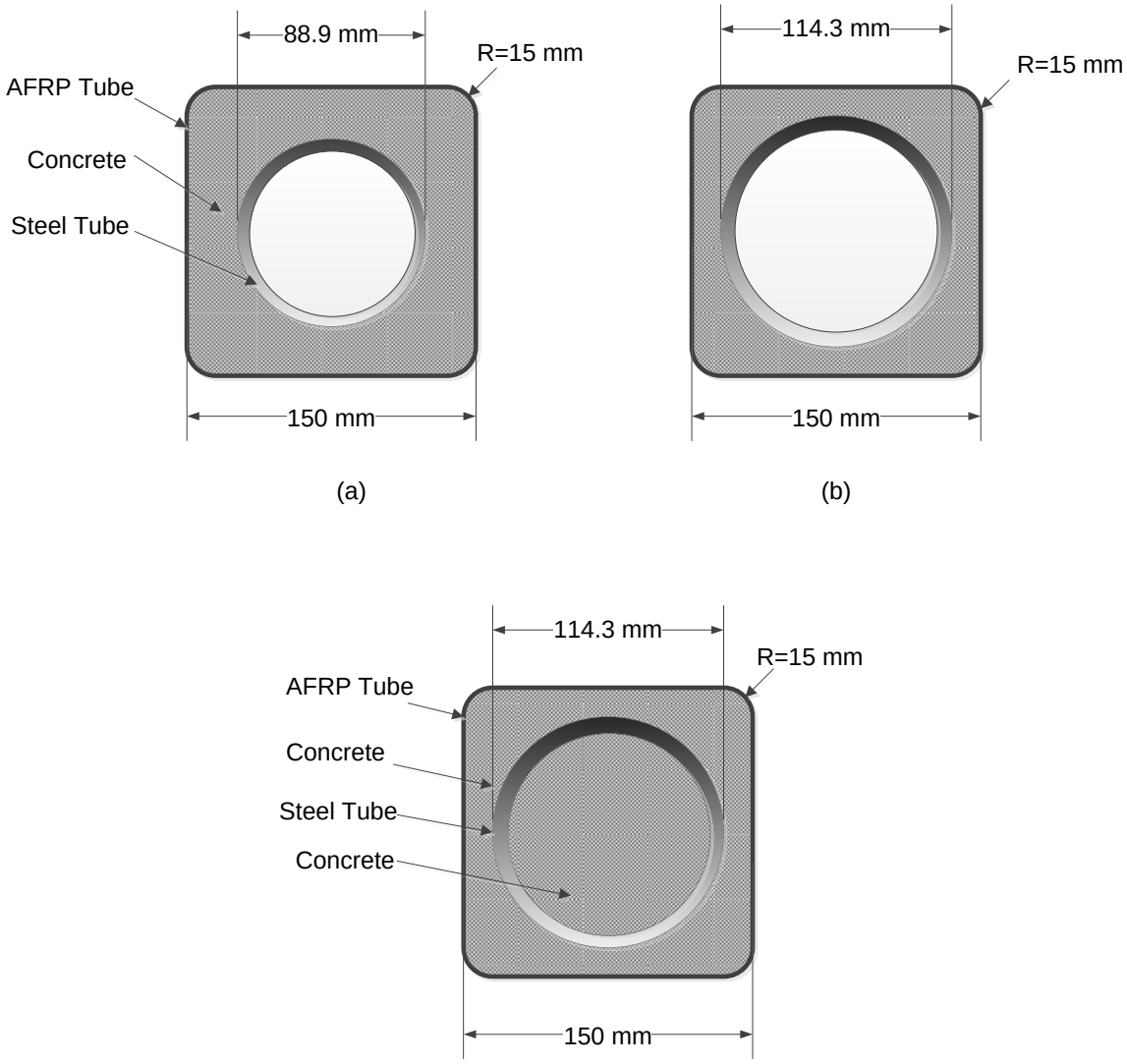

Fig. **1**. Column cross-sections: (a) DSTC-1, DSTC-2, DSTC-3 and DSTC-4, (b) DSTC-5, (c) DSTB-6.

(a)

(b)

(c)

(d)

Fig. 2. Manufacturing process: (a) Steel tube and foundation cage; (b) Concrete pour of the foundation; (c) Column concrete pour; (d) Finished column specimen

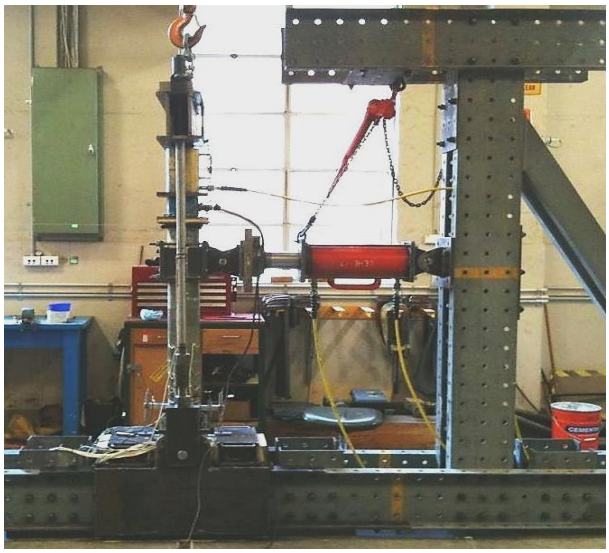

(a)

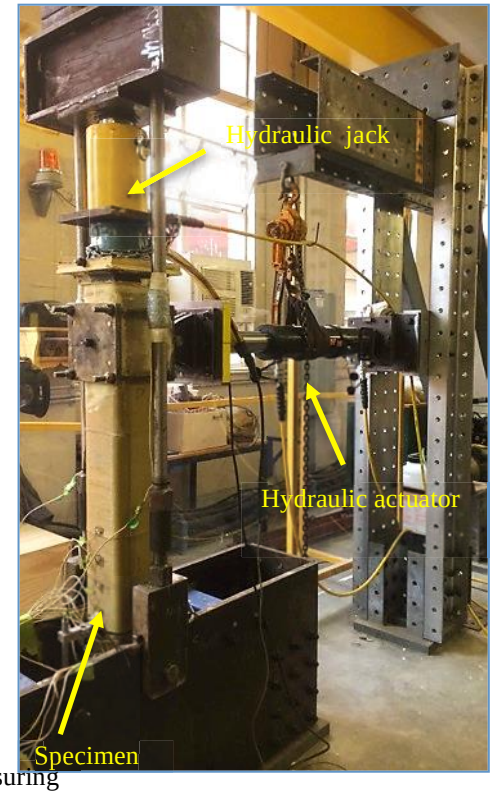

(b)

(c)

Fig. 3. Test setup: (a), (b) Column test setup; (c) LVDT arrangement

(a)

(b)

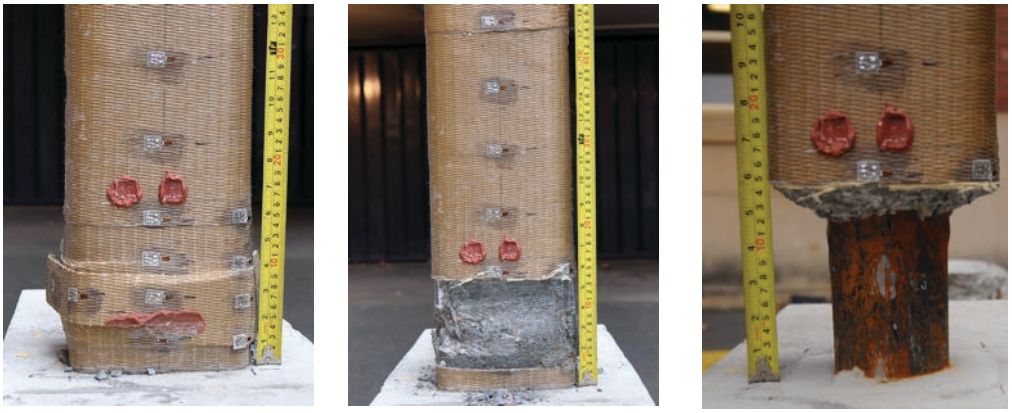

(c)

(d)

(e)

(f)

Fig. 4. Specimen damage regions: (a) DSTC-1; (b) DSTC-2; (c) DSTC-3; (d) DSTC-4; (e) DSTC-5; (f) DSTC-6.

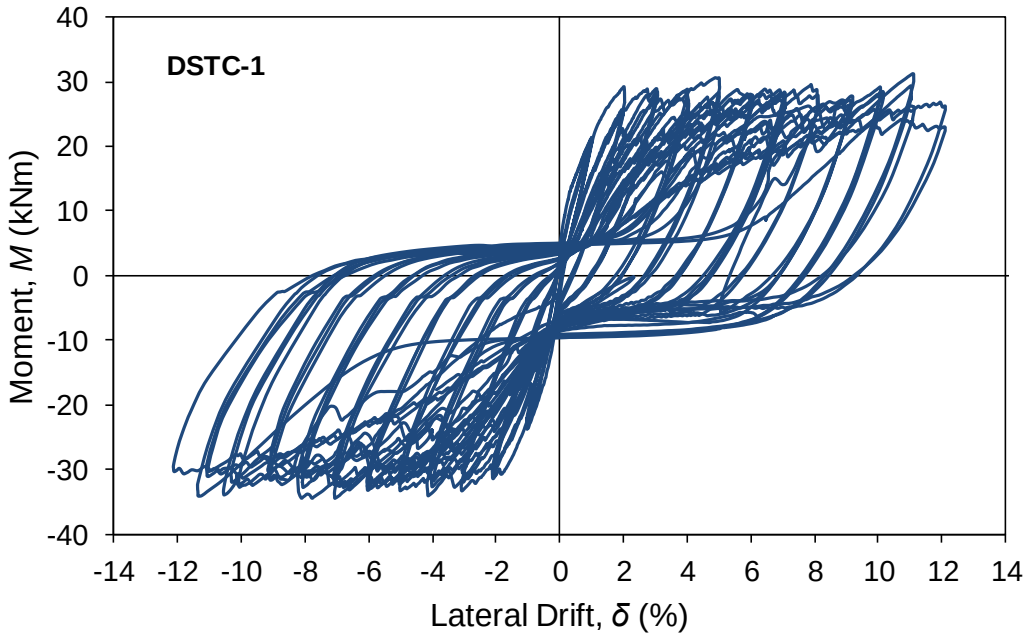
DSTC-1
Moment, M (kNm)
Lateral Drift, δ (%)
40
30
20
10
0
-10
-20
-30
-40
-14 -12 -10 -8 -6 -4 -2 0 2 4 6 8 10 12 14

(a)

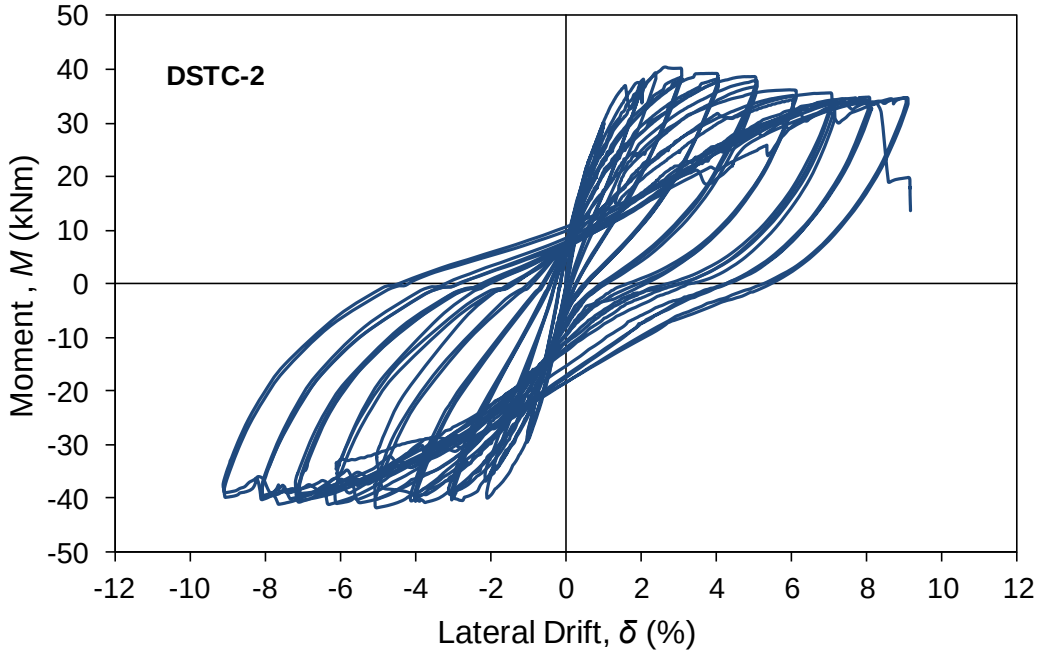
DSTC-2
Moment , M (kNm)
Lateral Drift, δ (%)
50
40
30
20
10
0
-10
-20
-30
-40
-50
-12 -10 -8 -6 -4 -2 0 2 4 6 8 10 12

(b)

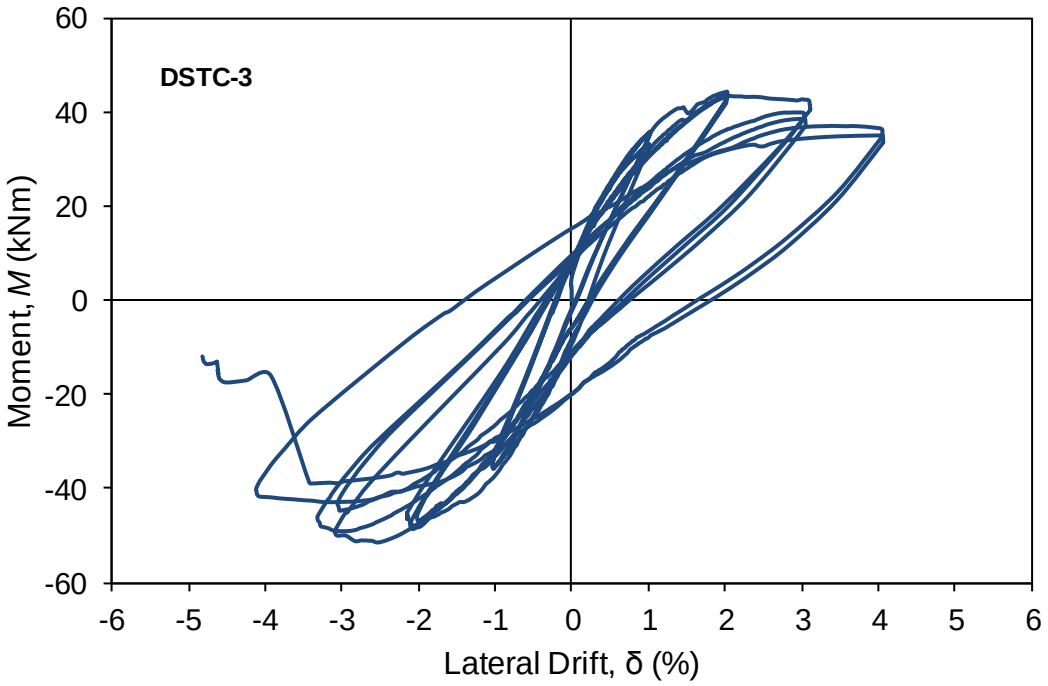
DSTC-3
Moment, M (kNm)
Lateral Drift, δ (%)
60
40
20
0
-20
-40
-60
-6
-5
-4
-3
-2
-1
0
1
2
3
4
5
6

(c)

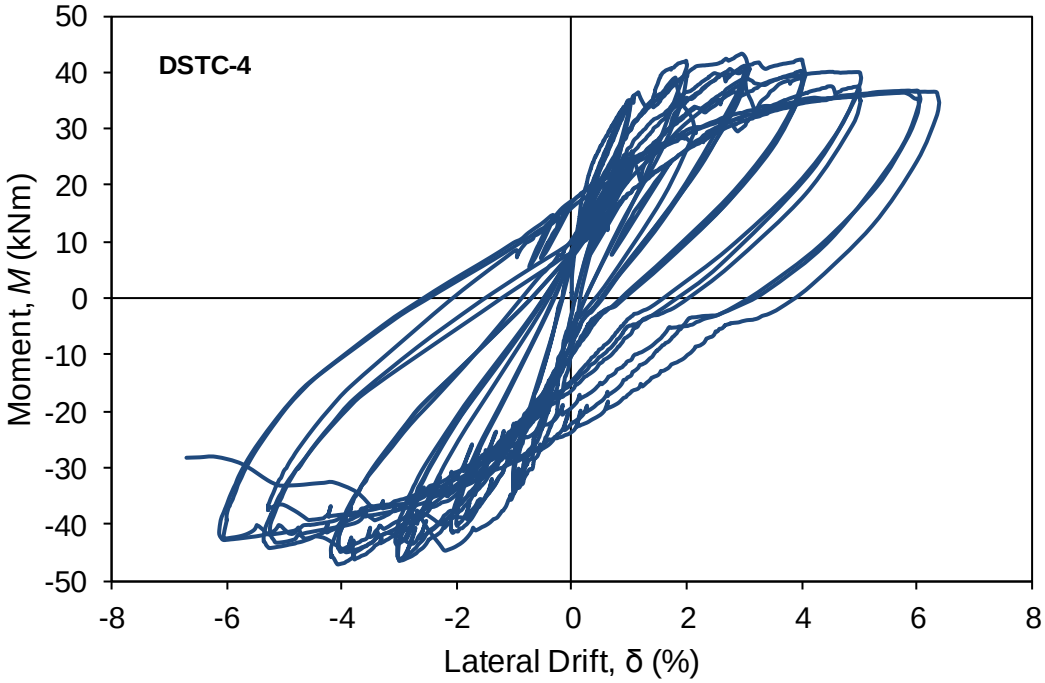
DSTC-4
Moment, M (kNm)
Lateral Drift, δ (%)
50
40
30
20
10
0
-10
-20
-30
-40
-50
-8
-6
-4
-2
0
2
4
6
8

(d)

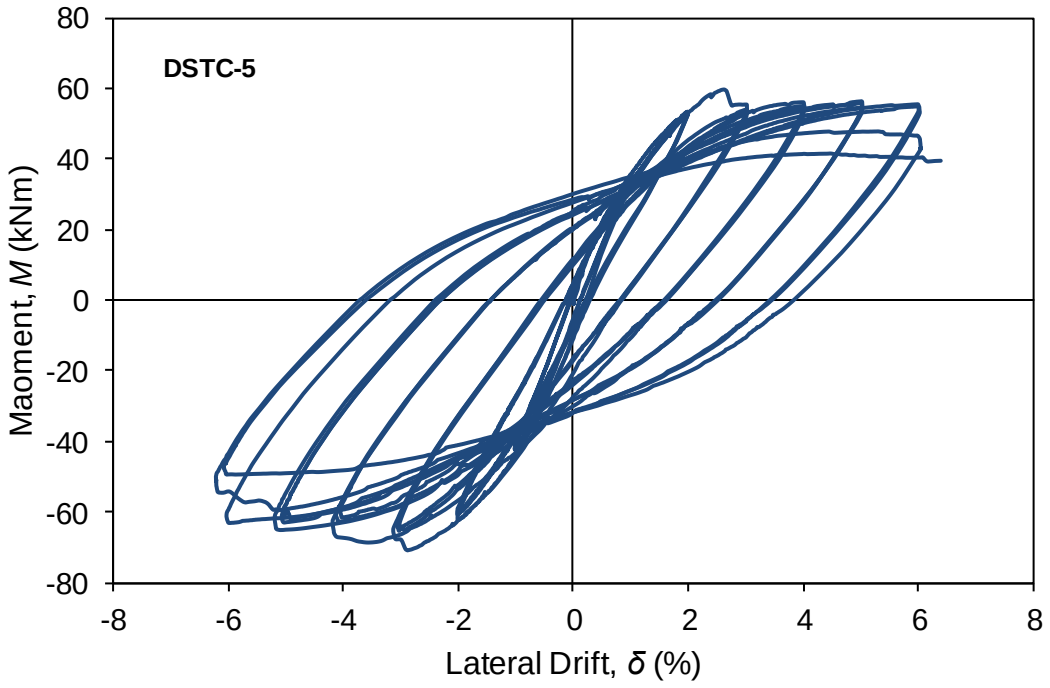

(e)

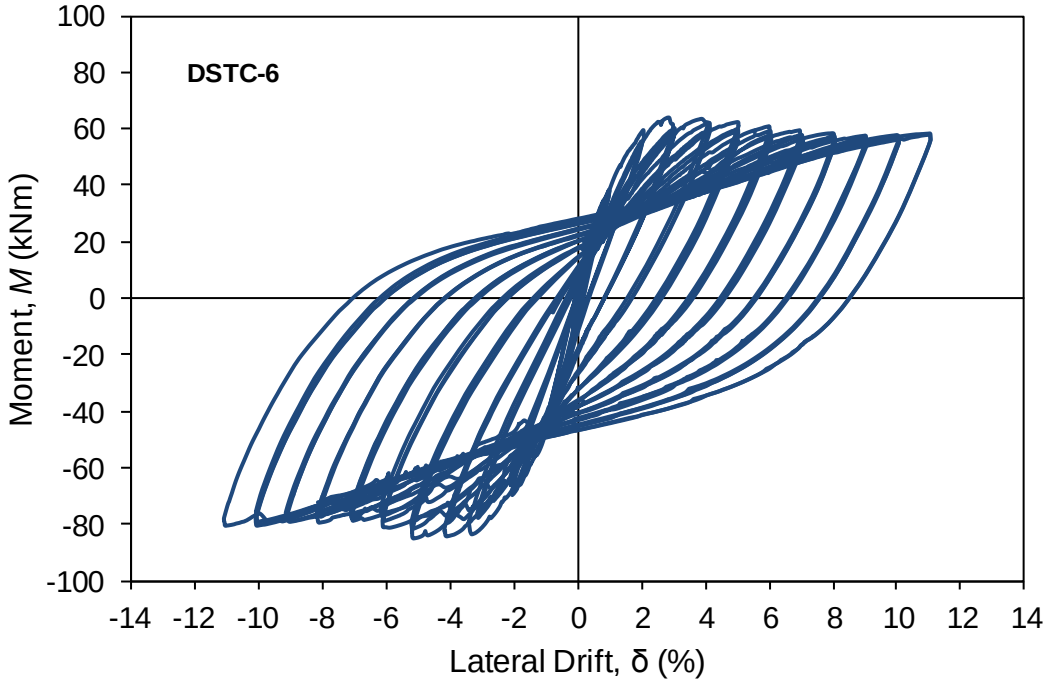

(f)

Fig. 5. Hysteretic moment-lateral drift relationships of columns: (a) DSTC-1; (b) DSTC-2; (c) DSTC-3 (d) DSTC-4; (e) DSTC-5; (f) DSTC-6.

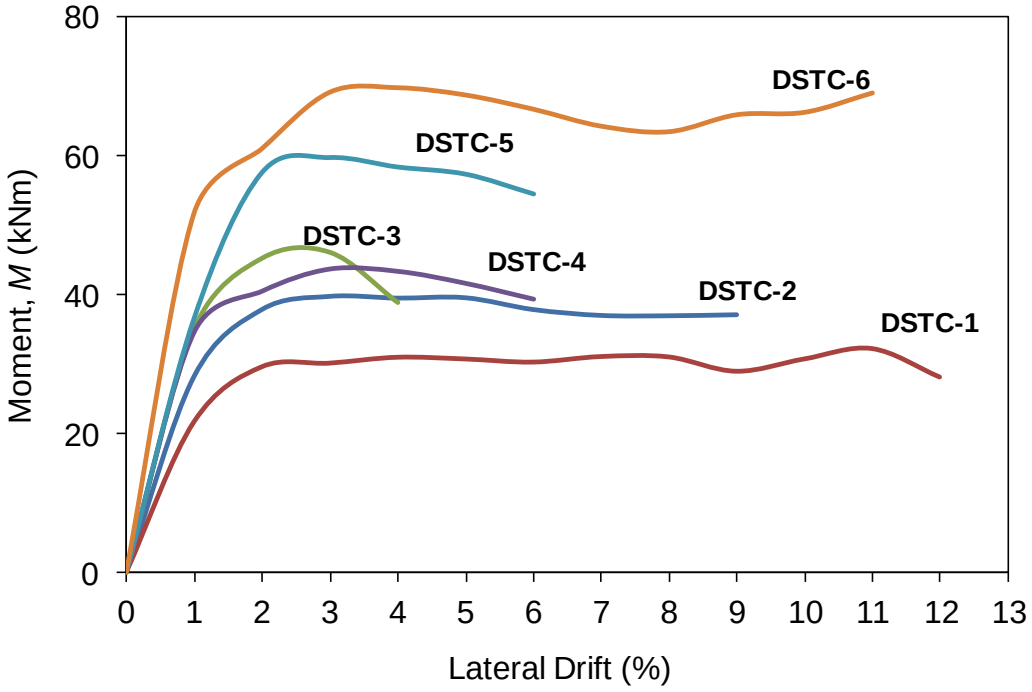

Fig. 6. Envelope curves of column moment-lateral drift relationships

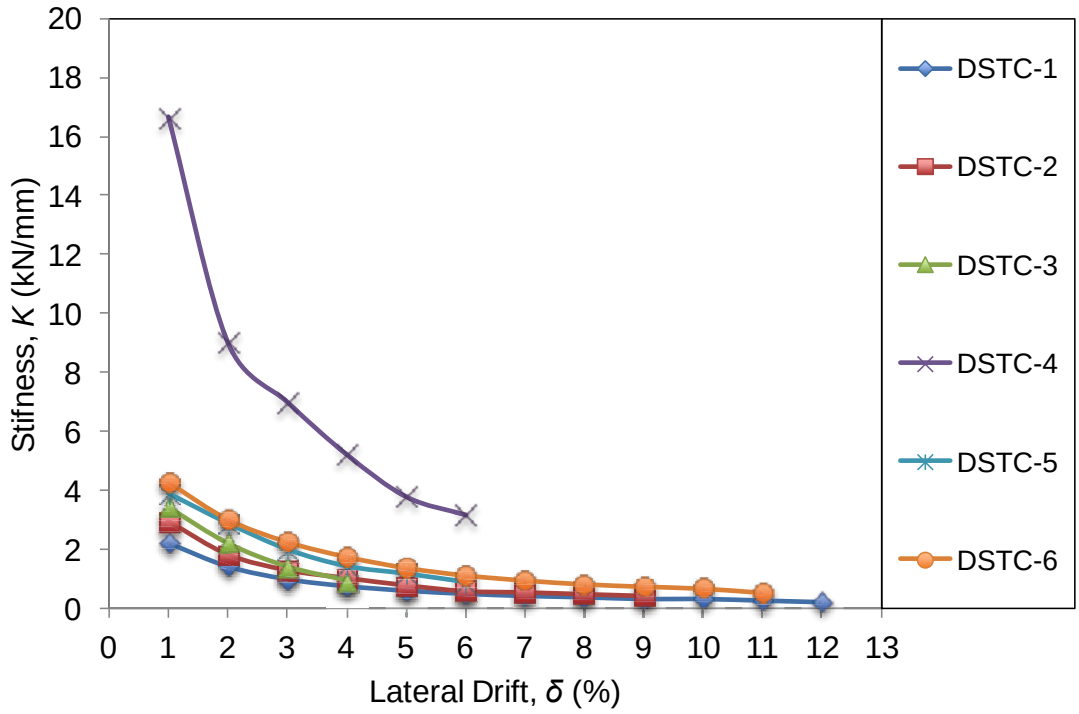

Fig. 7. Variations of column stiffness with lateral drift

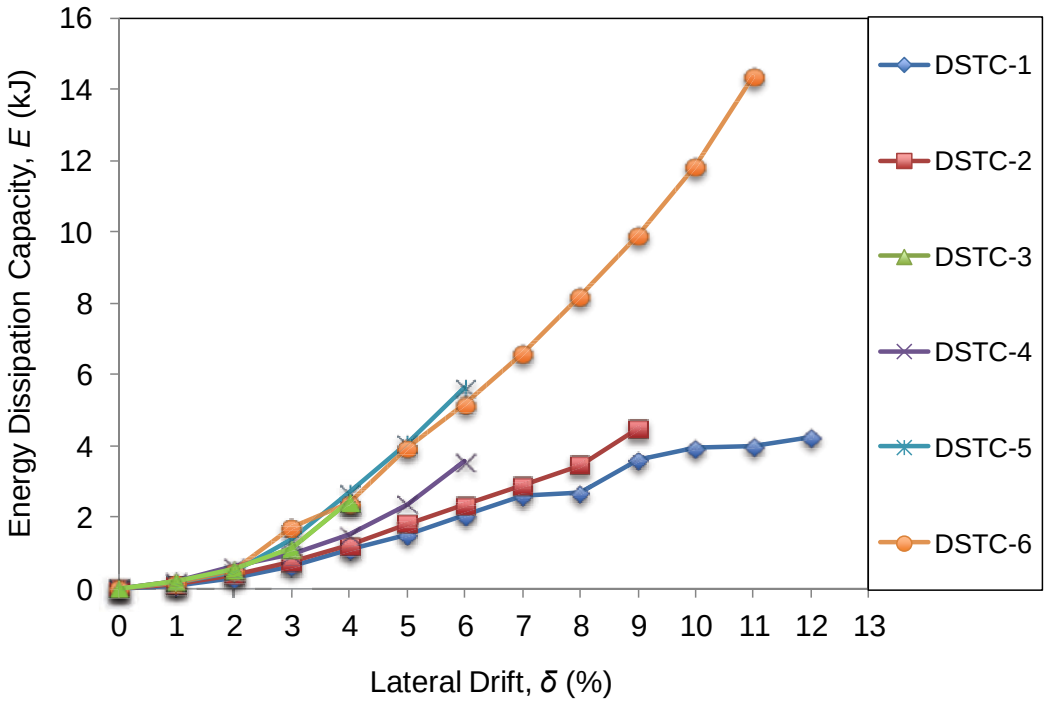

Fig. 8. Column energy dissipation capacity

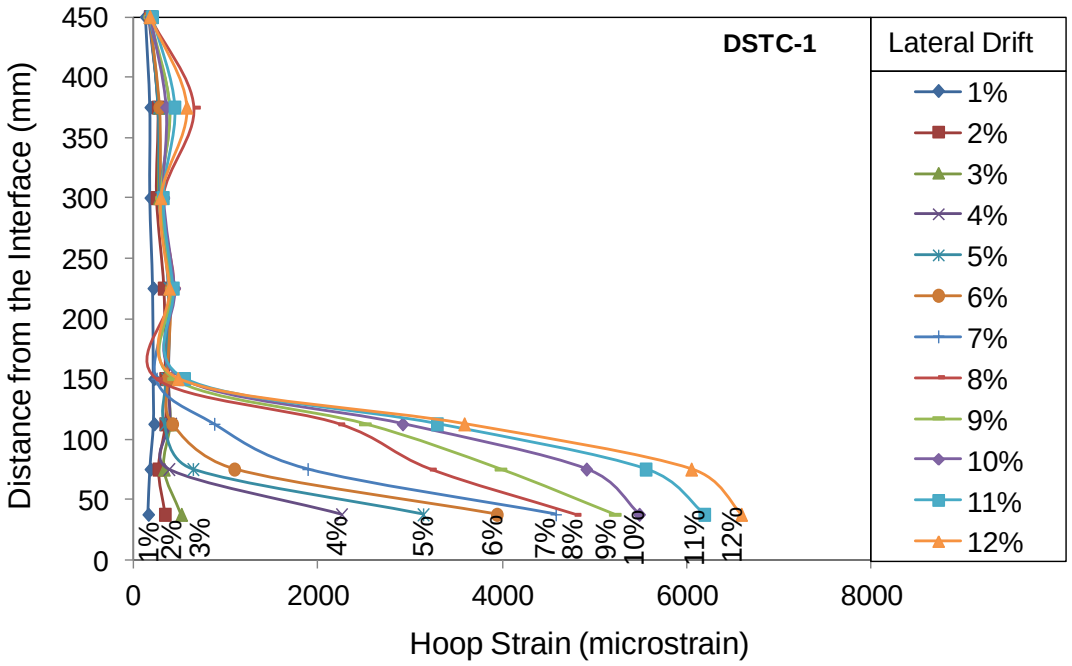
DSTC-1
Lateral Drift
1%
2%
3%
4%
5%
6%
7%
8%
9%
10%
11%
12%
Distance from the Interface (mm)
Hoop Strain (microstrain)
0
50
100
150
200
250
300
350
400
450
0
2000
4000
6000
8000

(a)

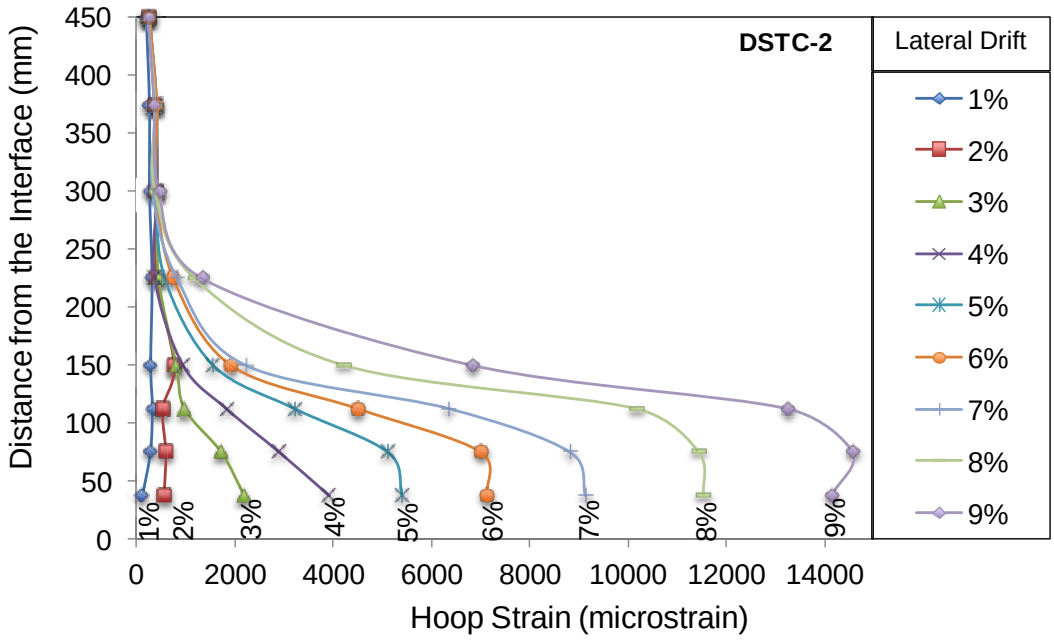
DSTC-2
Lateral Drift
1%
2%
3%
4%
5%
6%
7%
8%
9%
Distance from the Interface (mm)
Hoop Strain (microstrain)
0
50
100
150
200
250
300
350
400
450
0
2000
4000
6000
8000
10000
12000
14000

(b)

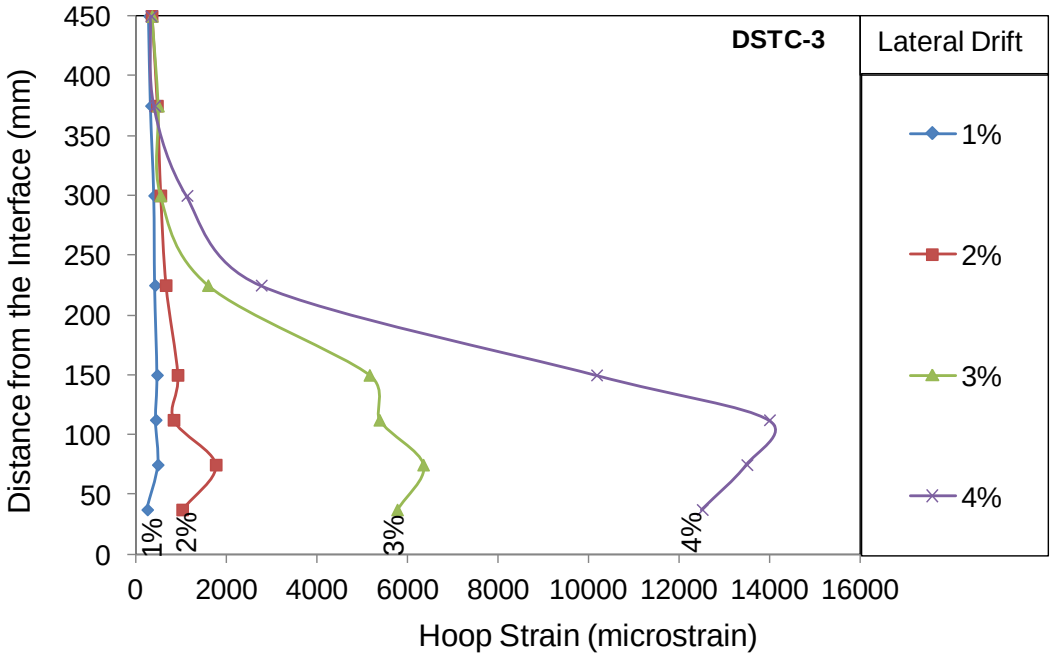
DSTC-3
Lateral Drift
1%
2%
3%
4%
Distance from the Interface (mm)
Hoop Strain (microstrain)
0
50
100
150
200
250
300
350
400
450
0
2000
4000
6000
8000
10000
12000
14000
16000

(c)

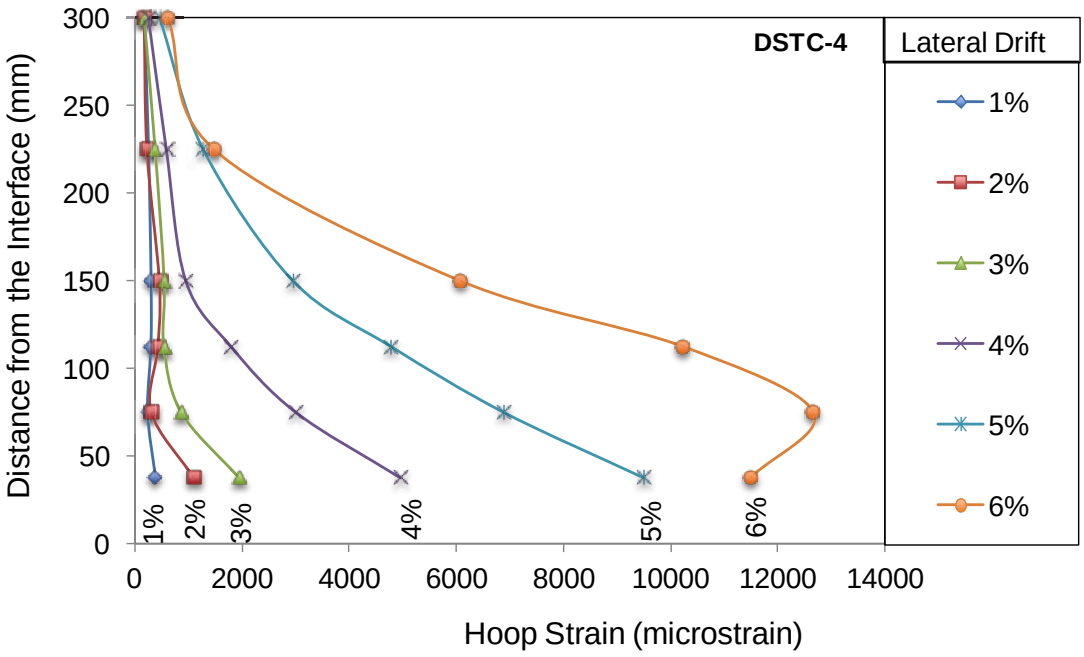
DSTC-4
Lateral Drift
1%
2%
3%
4%
5%
6%
Distance from the Interface (mm)
Hoop Strain (microstrain)
0
50
100
150
200
250
300
0
2000
4000
6000
8000
10000
12000
14000

(d)

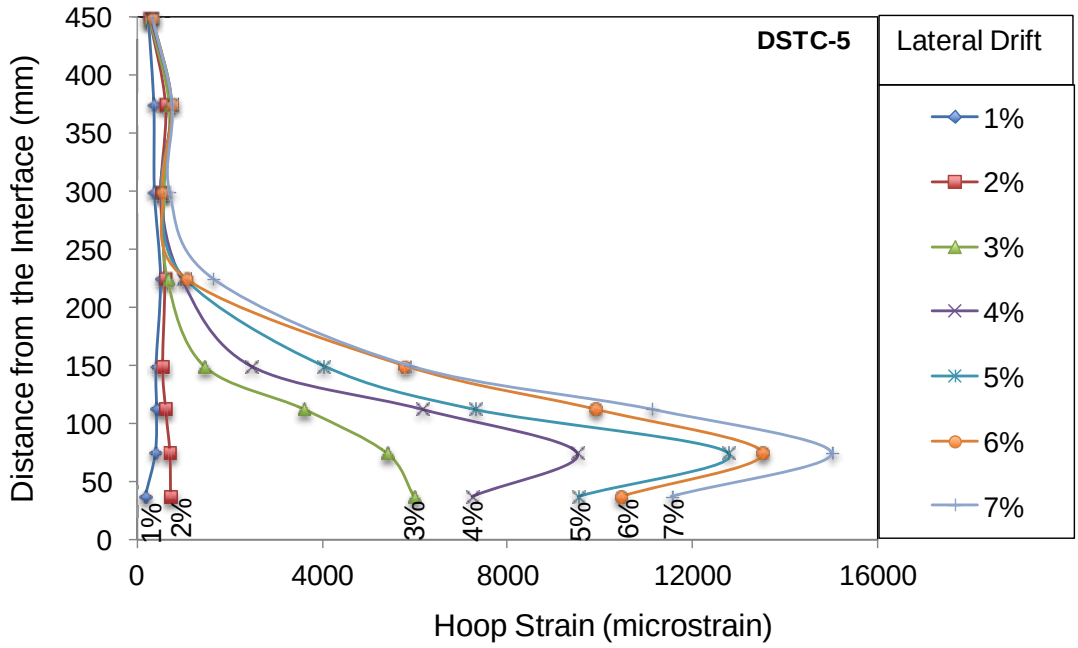

(e)

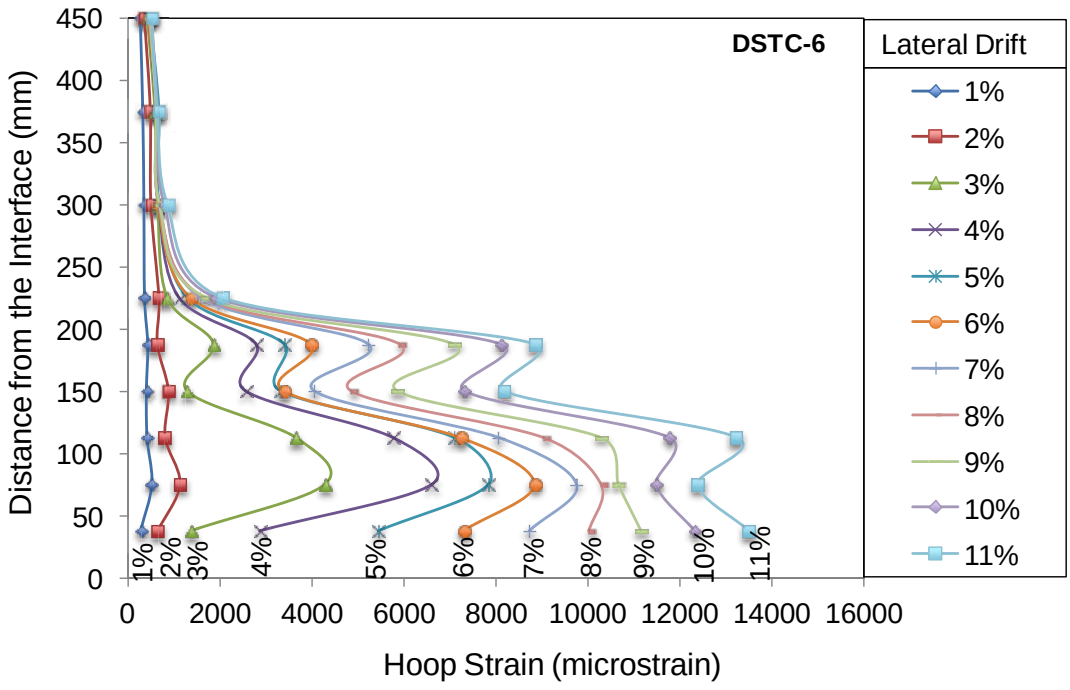

(f)

Fig. 9. Variation of FRP tube hoop strains along the length of column: (a) DSTC-1; (b) DSTC-2; (c) DSTC-3; (d) DSTC-4; (e) DSTC-5; (f) DSTC-6.

CHAPTER 5

Flexural Behavior of FRP-HSC-Steel Composite Beams

Yunita Idris and Togay Ozbakkaloglu

School of Civil, Environmental, and Mining Engineering, University of Adelaide, 5000

Thin-Walled Structures (Published)

Statement of Authorship

Title of Paper	Flexural Behavior of FRP-HSC-Steel Composite Beams
Publication Status	● Published ○ Accepted for publication ○ Submitted for publication ○ Publication style
Publication Details	Idris, Y., and Ozbakkaloglu, T. (2014). "Flexural behavior of FRP-HSC-steel composite beams." *Thin-Walled Structures*, 80: 207-16.

Author Contributions

By signing the Statement of Authorship, each author certifies that their stated contribution to the publication is accurate and that permission is granted for the publication to be included in the candidate's thesis.

Name of Principal Author (Candidate)	Yunita Idris		
Contribution to the Paper	Review of literature, analysis data, and preparation of manuscript		
Signature		Date	22/09/2015

Name of Co-Author	Dr. Togay Ozbakkaloglu		
Contribution to the Paper	Research supervision and review of manuscript		
Signature		Date	23/09/2015

FLEXURAL BEHAVIOR OF FRP-HSC-STEEL COMPOSITE BEAMS

Yunita IDRIS and Togay OZBAKKALOGLU

ABSTRACT

This paper reports on an experimental study on the flexural behavior of fiber reinforced polymer (FRP)-high-strength concrete (HSC)-steel composite beams. Seven double-skin tubular beam (DSTBs) and a concrete-filled FRP tube (CFFT) with an internal steel I-beam were tested as simply supported beams in four-point bending. The main parameters of the experimental study included the cross-sectional shapes of inner steel reinforcement and external FRP tube, concrete strength, presence (or absence) of concrete filling inside the steel tube, and effects of the use of mechanical connectors on the inner steel tube. The results indicate that DSTBs are capable of developing very high inelastic flexural deformations. However, the results also indicate that slip between the concrete and the steel tube of the DSTB can be relatively large, unless the bond between concrete and steel tube is enhanced through the use of mechanical connectors. The results of the beam tests illustrate that the flexural behavior of DSTBs is influenced significantly by the diameter and thickness of the inner steel tube. Concrete-filling the inner steel tube and increasing the concrete strength increase the flexural capacity of DSTBs without affecting their overall ductility. Furthermore, the shape of the inner steel tube influences both the flexural capacity of DSTBs and the occurrence of slippage between the concrete and the inner steel tube. It is shown that the bond slip between the concrete and inner steel tube can be prevented through the use of mechanical connectors. These results are presented together with a discussion on the influence of the main parameters on the flexural behavior of DSTBs.

KEYWORDS: Fiber reinforced polymer (FRP); High-strength concrete (HSC); Beams; Confinement; Flexure; Displacement capacity.

1. Introduction

The use of FRP composites in the form of concrete-filled FRP tubes (CFFTs) for the construction of new high-performance structural members has received significant recent attention, with large numbers of studies reporting on the axial compressive [1-14] and seismic behavior [15-20] of CFFT columns. The flexural behavior of CFFTs has also been the focus of a number of studies [21-24], and a few studies have reported on the flexural behavior of CFFT beams reinforced with steel or FRP bars [25-26].

Following research on CFFTs, a new type of composite system was proposed by Teng et al. (27) in the form of a FRP-concrete-steel double-skin tubular (DST) column (DSTC). This composite system consists of an outer FRP tube enclosing a hollow steel tube with concrete sandwiched in between the FRP and steel components. The resulting column combines the advantages of all three materials to achieve a high-performance structural member. A series of experimental studies have been conducted on the axial compressive behavior of DSTCs [28-33]. The results of these tests have demonstrated that the concrete in DSTCs is confined very efficiently, which in turn results in a highly ductile member behavior. A few studies have also reported on the lateral cyclic behavior of DSTCs that were tested under combined axial compression and lateral deformation reversals [34-36]. Reinforcing the findings of the studies on the compressive behavior of CFFTs, these studies revealed that DSTCs exhibit very high inelastic deformation capacities under simulated seismic loading. To date, only a single study has reported on the flexural behavior of DST beams (DSTBs) [37], which was concerned with the behavior NSC

DSTBs manufactured with circular glass FRP external tubes. In agreement with the findings of the studies on DSTCs, Yu et al. [37] reported that DSTBs exhibit a very ductile response under flexure. It was also noted, however, that significant slip occurred between the inner steel tube and surrounding concrete of DSTBs.

Along with the studies on DST beams and columns, a number of studies have also been carried out on a different type of FRP-concrete-steel composite system that comprises CFFTs with inner steel I-beams. These early studies on the axial compressive [38-40] and flexural behavior [41] of this composite system demonstrated some of its desirable properties, including a highly ductile behavior.

As, to date, only a single study has dealt with the flexural behavior of DSTBs and no study has reported on the flexural behavior of HSC DSTBs, additional studies are required to better understand and be able to model the flexural response of these composite beams. To contribute towards this end, this paper presents the first experimental study on the flexural behavior of HSC DSTBs. The study was aimed at investigating the influence of key parameters on the flexural behavior of DSTBs, with particular emphasis placed on the interface-slip behavior between steel tube and surrounding concrete. In addition, to establish relative performances of the two aforementioned composite systems, the behavior of a FRP-HSC-steel beam that was composed of a CFFT and an inner steel I-beam was also experimentally investigated. The main parameters of the study included the cross-sectional shapes of inner steel reinforcement and external FRP tube, concrete strength, presence (or absence) of concrete filling inside the steel tube, and effects of the use of mechanical connectors to enhance the bond between the steel tube and surrounding concrete. Flexural behaviors of the beams were evaluated using the recorded load-mid-span deflection relationships, with additional data provided by the load-slip relationships measured at the ends of the specimens.

2. Experimental program

2.1. Test specimens

Six DSTBs with circular external FRP tubes and a DSTB with a square FRP tube were manufactured and tested as simply supported beams in a four-point bending setup under monotonic loading. In addition, a single specimen that was composed of a circular CFFT and an inner steel I-beam (i.e. I-CFFT) was also tested under the same loading conditions. Each of the specimens was designed as a flexural beam with a 150-mm cross-section. The corners of the square CFFT were rounded with a 30-mm radius (R). The span, measured between the centre lines of the supports, was 1.3 m, and the length of the constant moment region between the two point loads was 0.3 m. Seven of the specimens were manufactured using HSC and one with normal strength concrete (NSC). All of the specimens were confined with aramid FRP (AFRP) external tubes. Five of the specimens were reinforced with circular inner steel tubes, two with square inner steel tubes, and one with a steel I-beam. Of the five specimens that were reinforced with circular inner steel tubes, three were reinforced with tubes 114.3 mm in diameter and two with 76.1 mm diameter tubes. One of the smaller-diameter specimens was provided with shear studs along the inner steel tube. Table 1 provides a summary of material and geometric properties of the test specimens, and Fig. 1 illustrates their geometry.

The process of DSTB manufacture started with the manufacturing of the outer FRP tube, followed by placing the inner steel tube inside the FRP tube, which functioned as a stay-in-place form during the concrete pour. Concrete mixtures were poured in the space between FRP tube and the inner steel tube, except for DSTB-3 where the concrete was also poured inside the inner steel tube. The process of beam manufacture is illustrated in Fig. 2, with the properties of each material used in the process supplied in the following section.

3. Material properties

3.1. FRP tubes

Aramid fibers were used to manufacture the outer FRP tube in all the specimens. The tubes were manufactured using a manual wet lay-up process, which involved wrapping epoxy resin impregnated fiber sheets around precision-cut high-density styrofoam moulds in the hoop direction. FRP tubes of HSC DSTBs and I-CFFT were made of 2 layers of FRP, whereas the tube of NSC DSTB had a single layer of FRP. FRP sheets were wrapped around the moulds one layer at a time, with an overlap length of 100 mm provided for each layer to prevent premature debonding. The overlap region of each subsequent layer was provided on the opposite face at a 180-degree interval from the previous overlap region. The tubes were manufactured in a manner that the overlap regions formed continuous lines along the length of DSTBs, which were oriented to correspond to the side faces of the beams. The width of each fiber sheet was 300 mm and a small overlap of around 10 mm was provided along the axial direction only to ensure continuity of the tube. The epoxy resin was applied at the fiber sheet coverage rate of 0.6L/m^2, which resulted in a ply thickness of 0.8 mm for the resulting FRP composite. Table 2 provides the properties of aramid sheets and epoxy resin used in the fabrication of the FRP tubes.

3.2. Concrete

Two different concrete mixes were used in the manufacture of the specimens, namely the HSC mix and NSC mix. Both mixes consisted of crushed bluestone as the coarse aggregate with a nominal maximum size of 10 mm. Superplasticizer and silica fume, added at 8% of the binder content by weight, were used in the HSC mix. Test day concrete strengths of the specimens were obtained through concrete cylinders tests. As shown in Table 1, test day

strengths of the HSC mixes varied slightly between 82 and 92 MPa, and the strength of the NSC mix was established as 42 MPa.

3.3. Steel tubes

Five of the DSTBs had circular inner steel tubes with two different external diameters (i.e. 114.3 and 76.1 mm) and thicknesses (i.e. 6.02 and 3.2 mm). One of the DSTBs with 76.1 mm circular inner steel tube (i.e. DSTB-7) was manufactured with additional steel rings made of 8-mm diameter steel reinforcement, which were welded on the steel tube along its length at 80-mm spacing. Two of the specimens had a 100 mm square inner steel tube with a thickness of 6 mm. I-CFFT was constructed with an I-beam steel section with a 125 mm height, a flange width of 65 mm, a web thickness of 5 mm, and a tapered flange that varied from 8.5 mm to 5.5 mm in thickness. The exact dimension of the steel I-beam section is shown in Fig. 1. The material properties of the steel tubes were determined by testing five steel coupons cut from the original tube. The coupon specimens of the steel I-beam were cut from the web section as the flanges were tapered. Material properties of inner steel sections, established from coupon tests, are reported in Table 3 together with the properties of 8-mm diameter bars used in DSTB-7, established from direct tension tests.

3.4. Instrumentation, test setup and loading program

The specimens were instrumented with linear variable displacement transformers (LVDTs) at mid-span, the point of application of concentrated loads, and at the mid-distance between loading points and supports to record the vertical displacements along the beam. Furthermore the specimens were instrumented with 2 additional LVDTs at both ends of

specimen to measure the slippage at steel tube-concrete and FRP tube-concrete interfaces. The acquisition of hoop strain data on FRP tubes was of particular interest to better understand the activation of the confinement mechanism and strain distribution at mid-span, two loading points and at mid-distance between loading points and supports. As illustrated in Fig. 3c, 12 strain gauges were bonded to each FRP tube in the hoop direction, and 10 strain gauges were placed axially.

To observe the behavior of the inner steel reinforcement (i.e. steel tubes and I-beam), 10 strain gauges were placed axially at the: i) mid-span, ii) two loading points and iii) one of the sections in the mid-distance between the support and the adjacent loading point (i.e. Section A in Fig. 3c). The 1.3 m long beams were tested using a four-point bending setup. The load was transferred from the actuator to the test beam through a steel loading beam at two locations spaced 0.3 m apart. The load was applied monotonically in displacement control at a rate of 1 mm/minute. The test setup and instrumentation is illustrated in Fig. 3.

4. Test results

4.1. Specimens at the end of testing

The tests of all of the specimens were stopped after excessive deformation of the specimens, at which point it was no longer possible to maintain symmetrical loading conditions. Fig. 4 illustrates the condition of each specimen after testing, including the most damaged region of the concrete after the removal of FRP tube shell, and the condition of the inner steel reinforcement after the removal of both the FRP tube and concrete.

None of the DSTBs demonstrated any sign of FRP tube rupture. The gap opening along the longitudinal axis of the FRP tubes was observed, which was caused by significant inelastic

deformation experienced by the specimens along their mid-span regions. Removal of the FRP tube revealed that the concrete inside the most damaged regions was cracked in several locations along the beam length within the tension region, as shown in Fig. 4. The number and spacing of the concrete cracks were observed to be slightly different for each beam. The presence of mechanical connectors in DSTB-7 resulted in the localization of tension cracking, where the beam developed a single major crack at a location where the inner steel tube exhibited significant plastic deformation. This formation can be attributed to the stronger concrete-steel tube interface bond of DSTB-7, and resulting restraint provided by the inner steel tube against the opening of cracks in concrete. Fig. 4 also shows the condition of the inner steel reinforcements after the removal of the FRP shell and surrounding concrete. As evident from the figure, inner steel reinforcements of all specimens exhibited significant plastic deformation along the constant moment regions of the beams.

4.2. Load – deflection relationships

All of the specimens showed an almost bi-linear load-deflection relationship with a smooth transition region, as shown in Fig. 5. The majority of the specimens exhibited an almost flat second branch with only a slight decrease in their flexural strengths. The specimen with an inner steel I-beam (I-CFFT), on the other hand, showed a monotonically ascending load-deflection relationship throughout its loading history.

Table 3 provides the recorded data corresponding to the important coordinates of the load-deflection relationships, namely the peak load (P_{peak}), recorded mid-span deflection at the peak load (Δ_{peak}), mid-span deflection at ultimate (Δ_{ult}) where testing was stopped, load at ultimate (P_{ult}), and steel tube slip. Peak moment (M_{peak}) and moment at ultimate (M_{ult}),

which were calculated from the recorded loads, are also provided in Table 3. A detailed discussion on the influences of the test parameters on the trends of the load-deflection relationships of the DSTBs is provided later in the paper.

4.3. Load – slip relationship

4.3.1. Load – slip relationship between concrete and FRP tube

The slips between the FRP tube and concrete were measured by LVDTs that were attached to the FRP tube surface, with the stroke pointed to the concrete section as shown in Fig. 3b. Fig. 6 illustrates he FRP tube-concrete load-slip relationships of the specimens.

As evident from Fig. 6, the slip between FRP tube and concrete was insignificant, with a maximum recorded value of 0.06 mm. This finding is in agreement with the one previously reported in Yu et al. [37], and it can be attributed to the fiber orientation of FRP tubes, which resulted in minimal axial stiffness of the tubes. It might be worth noting that no slippage data was provided for DSTB-3, DSTB-5 and DSTB-6 because of the absence of the instrumentation on these specimens.

4.4. Load – slip relationship between concrete and steel tube

The slips between the concrete and the steel tube for each specimen was measured by LVDTs that were attached to the surface of the FRP tubes with the stroke pointed to the inner steel tube, as illustrated in Fig. 3b. These readings were then corrected for FRP tube-concrete slips to obtain the slippage between the steel tube and concrete. The load-slip relationship of each column is provided in Fig. 7. In DSTB-3, with concrete-filled inner

steel tube, the load-slip relationship between the steel tube and the inner concrete core was also measured and shown in Fig. 7. In each specimen, the majority of the slippage occurred beyond 75% of maximum recorded load (P_{peak}), prior to which slippage was minimal.

The maximum recorded slip among all specimens was around 9 mm, which was observed in DSTB-2, with a 76.1-mm diameter inner steel tube. Increasing the diameter of the inner steel tube to 114.3 mm reduced slippage by around 40%, with DSTB-1 exhibiting 5.5 mm slippage. As illustrated in Fig. 7, there was almost no interface-slip in DSTB-7, which was constructed with a 76.1-mm inner steel tube that was fitted with steel rings. This can be attributed to the increase in the bond strength between the steel tube and concrete due to the mechanical interlock provided by the steel rings, very much like it was observed in the case of deformed bars in concrete (e.g. [42]). Fig. 7 also illustrates that the specimen with an inner steel I-beam (I-CFFT) exhibited almost negligible interface-slip compared to the specimens having inner steel tubes with no mechanical anchors. This can be explained by the increased relative surface area of the steel I-beam section and the way the steel section was surrounded by the concrete.

As can be seen in Fig. 7, the DSTBs with square inner steel tubes (DSTB-5 and DSTB-6) showed slightly smaller interface-slips than the circular inner steel tube DSTB with a similar cross-sectional area (DSTB-1). Almost identical slips observed in DSTB-5 and DSTB-6 indicates that the cross-sectional shape of the external steel tube had no major influence on the slip behavior of these specimens. It can also be seen in Fig. 7 that the DSTB-4, manufactured with a NSC, exhibited a slightly larger interface-slip than the companion HSC specimen, DSTB-1. Fig. 7 also illustrates that the specimen with a concrete-filled inner steel tube (DSTB-3) exhibited a slightly smaller slip that the companion specimen with a hollow inner steel tube (DSTB-1). It can be observed in Fig. 7 that the slip at the interface of the steel tube and inner concrete core that was surrounded

by it was negligible. This full bond behavior can be attributed to the high frictional forces developed at this interface, which resulted from the confining forces exerted by the steel tube to the core concrete.

5. Analysis and discussion

5.1. Influence of test parameters on beam behavior

5.1.1. Effect of diameter and thickness of inner steel tube

The effect of the diameter and thickness of the inner steel tube on the flexural behavior of the DSTBs was investigated by comparing DSTB-1 and DSTB-2. DSTB-1 was reinforced with an inner steel tube 114.3-mm in diameter and 6.02-mm in thickness, whereas DSTB-2 was reinforced with a 76.1-mm diameter inner steel tube with 3.2-mm thickness. DSTB-1 developed a peak load (P_{peak}) of 153.2 kN at 80.8 mm mid-span deflection, whereas DSTB-2 was able to sustain a peak load (P_{peak}) of only 38.8 kN at 57.9 mm mid-span deflection. These specimens exhibited load-deflection curves with similar trends, both exhibiting almost flat second branches.

5.1.2. Effect of cross- sectional shape of inner steel tube

The effect of cross-sectional shape of inner steel tube was investigated by comparing the behaviors of DSTB-1 (circular inner steel tube) and DSTB-5 (square inner steel tube). The inner steel tubes of these specimens were similar in thickness and cross-sectional area, which resulted in similar reinforcement ratios (A_s/A_c) as shown in Table 1. As can be seen in Fig. 5, load-deflection curve of DSTB-5 started exhibiting a slow and steady decline

after the attainment of the peak load of 170.4 kN at 41.6 mm mid-span deflection. As illustrated in Table 4, the peak load of DSTB-1 (i.e. 153.2 kN) was lower than that of DSTB-5, but it was attained at a higher mid-span deflection (i.e. 80.8 mm). The higher flexural capacity of DSTB-5 can be attributed to its more efficient inner steel reinforcement placement, with more reinforcement near the extreme tension and compression fibers.

The influence of different forms of inner steel reinforcement was also investigated by comparing I-CFFT with DSTB-3, with a concrete-filled inner circular steel tube. I-CFFT exhibited an ascending second branch in its load-deflection curve, whereas DSTB-3 had a curve with a slightly descending second branch. The peak load of DSTB-3 was 190.5 kN, and it was recorded at 75.3 mm mid-span deflection, whereas I-CFFT reached 165.6 kN of peak load at 89.5 mm mid-span deflection. The higher load capacity of DSTB-3 can be attributed to the higher reinforcement ratio (A_s/A_c) of the specimen, as shown in Table 1. The hardening type response of I-CFFT compared to the softening response of DSTB-3 suggests that the specimen with an inner steel I-beam had a more favorable neutral axis depth progression compared to the specimen with an inner circular tube resulting in increased moment capacities with increasing deformations.

5.1.3. Effect of FRP tube sectional shape

The effect of the sectional shape of the FRP tube was investigated by comparing DSTB-5 (circular FRP tube) with DSTB-6 (square FRP tube). These specimens were reinforced with identical square inner steel tubes, and they both exhibited load-deflection curve with slightly descending second branches. The peak load of DSTB-5 was 170.4 kN and it was recorded at 41.6 mm mid-span deflection, whereas DSTB-6 reached 179.6 kN of peak load

at 29.5 mm mid-span deflection. As expected, due to its larger cross-sectional area the square DSTB exhibited a higher moment capacity. Similar trends of the load-deflection relationships of these specimens suggest that both the circular and the square tube with 30-mm radius of corners provided sufficient confinement leading to a ductile behavior.

5.1.4. Effect of filling the inner steel tube with concrete

The effect of filling the inner steel tube with concrete can be ascertained by comparing the behavior of DSTB-1, which had a hollow inner steel tube with that of DSTB-3, with a concrete-filled inner steel tube. In a similar trend, both specimens showed an almost flat second branch in their load-deflection curves. Due to the increased area of concrete, a higher peak load was recorded for DSTB-3 (190.5 kN at 75.3 mm mid-span deflection) than DSTB-1 (153.2 kN at 80.8 mm of mid-span deflection). These observations indicate that concrete filling of inner steel tube can enhance the flexural capacity of DSTBs, without affecting their ductility.

5.1.5. Effect of concrete strength

The effect of concrete strength on the flexural behavior of the DSTBs was investigated by comparing DSTB-1, which was made of 92 MPa of concrete mix, with DSTB-4 manufactured using 42 MPa concrete. The FRP tubes of these specimens were manufactured using different numbers of FRP layers according to the strength of the concrete to ensure the specimens had similar nominal confinement ratios (f_{lu}/f'_c), which were calculated by dividing the ultimate confining pressure (f_{lu}) with concrete cylinder strength (f'_c) :

$$f_{lu} = \frac{2.f_{fu}.t_f}{D} \quad (1)$$

where f_{fu} = ultimate tensile strength of fibers, t_f = total fiber thickness of the FRP tube, and D = internal diameter of the FRP tube. DSTB-1 was, therefore, confined by two layers of AFRP, whereas DSTB-4 was confined by a single layer of AFRP, which resulted in the nominal confinement ratios (f_{lu}/f'_c) of 0.15 and 0.17, respectively.

As mentioned previously, DSTB-1 exhibited a load-deflection relationship with an almost flat second branch, with peak load of 153.2 kN attained at 80.8 mm mid-span deflection. Likewise, the load-deflection relationship of DSTB-4 shown in Fig. 5 illustrates an almost flat post peak behavior, with the peak load of 141.9 kN was attained at 60.6 mm mid-span deflection. The higher maximum load capacity of DSTB-1 over DSTB-4 was expected, and it can be attributed to the higher concrete strength of the former specimen. These results indicate that NSC and HSC DSTBs with similar confinement levels (i.e. f_{lu}/f'_c) develop similar inelastic load-deflection behaviors.

5.1.6. Effect of using mechanical connectors

The effect the use of mechanical connectors, in the form of steel rings welded on the inner steel tubes, on the flexural behavior of the DSTBs was investigated by comparing DSTB-2 and DSTB-7. Both beams were reinforced with a 76.1-mm diameter inner steel tube, except that the steel inner tube of DSTB-7 was designed with additional steel rings made of 8-mm diameter steel reinforcement with a yield strength of 546 MPa. These rings were welded on the steel tube at 80-mm spacing along its length to increase the bond between the steel tube and concrete. As can be seen in Fig. 5, DSTB-2 and DSTB-7 exhibited an almost identical trend in their load-deflection curves, except DSTB-7 experienced a rapid

decline in its capacity around 80 mm mid-span deflection, suggesting that the eventual failure of the specimen was near. Such a declined was not observed in DSTB-2.

As evident from Table 4, the addition of mechanical connectors provided a significant increase in specimen flexural capacity, with peak load increasing from 38.8 kN in DSTB-2 to 67.7 kN in DSTB-7. As discussed previously, a significant reduction of slip was recorded for the specimen fitted with the connectors, which changed the partial interaction behavior observed in DSTB-2 to full interaction behavior. The significant portion of the increase in the flexural capacity can be attributed to this change in the bond behavior of the steel tube-concrete interface. In addition, steel rings increased the overall cross-sectional area of the steel reinforcement by approximately 20%, which in turn resulted in a further increase in the flexural capacity of DSTB-7.

5.2. Analysis of progression of neutral axis depths

The locations of the neutral axes were established using the maximum strains recorded at the mid-span on the extreme compression and tension fibers of the inner steel tube, established based on the load-axial strain relationships shown in Fig. 8. It is worth noting that the recorded strains were limited to the valid strain gauges readings and it was not possible to obtain complete load-strain curves for all specimens. For this reason the mid-span deflections corresponding to the maximum recorded strains are also provided in Fig. 8. Fig. 9 illustrates variation of the normalized neutral axis depths (c/D) with the applied load for all the specimens. The figure illustrates that the neutral axis depths of the specimens initially decreased, and later stabilized at a value below 0.5 in all the specimens.

Fig. 9 illustrates that the *c/D* values of DSTB-5 with NSC was higher than the companion HSC specimens, DSTB-1. This was expected, as in the presence of higher strength concrete sectional force equilibrium is attained at a lower neutral axis depth. The investigation of the neutral axis depths of DSTB-2 and DSTB-7 in Fig. 9 indicates that the neutral axis depth increased with the presence of the mechanical connectors. This can be explained by increased tension forces of the latter specimen resulting from an increased bond at its concrete-steel tube interface due to the presence of mechanical connectors.

The comparison of neutral axis depths of DSTB-5 and DSTB-6 in Fig. 9 shows that DSTB-6 with a square FRP tube had a lower *c/D* ratio until the final stages of testing compared to the companion specimen with a circular FRP tube. This can be attributed to the increased concrete cross-sectional area of the square specimen in the compression zone. The comparison of I-CFFT with DSTB-3, with a concrete-filled inner steel tube, in Fig. 9 indicates that I-CFFT had a higher *c/D* ratio than DSTB-3. This can be explained by the influence of the slightly lower concrete strength of the former specimen and more efficient placement of its inner steel reinforcement, with more reinforcement placed closer to the extreme fibers.

CONCLUSIONS

This paper has presented the results of an experimental study on the flexural behavior of FRP-concrete-steel composite beams. Based on the results presented in the paper, the following conclusions can be drawn:

1. DSTBs exhibit excellent load–deflection behaviors with high inelastic deformations and minimal strength degradations. However, relatively large slips can occur at the

concrete-steel tube interface of DSTBs, unless the interface bond is enhanced through the use of mechanical connectors.

2. Like DSTBs, the composite CFFT with an inner steel I-beam investigated in this study is capable of developing a very ductile flexural behavior. Furthermore, unlike DSTBs, this composite system exhibits very little to no slippage at the concrete-steel tube interface.
3. NSC and HSC DSTBs with similar confinement levels (f_{lu}/f'_c) develop similar inelastic load-deflection behaviors.
4. FRP tube shape has only a minor influence on the flexural behavior of DSTBs, with companion square and circular specimens demonstrating load-deflection curves with similar general trends.
5. Flexural capacities of DSTBs can be further enhanced through concrete-filling of their inner steel tubes. No detrimental influence of concrete-filling was observed on the ductility of DSTBs.
6. It is observed that increasing the diameter of the inner steel and concrete strength both result in reduced interface-slip between concrete and steel tube, and that DSTBs with square inner steel tubes experiences slightly smaller interface-slips compared to the companion circular tubes.
7. Mechanical connectors welded on the hoop direction of the inner steel tube eliminate slippage, which in turn results in a significant increase in the flexural capacity of the DSTB. Therefore, the use of mechanical connectors can be considered as an efficient means for reducing the relatively large slippage that occurs between concrete and inner steel tube of DSTBs.

Because the majority of the specimens of the present study were manufactured with HSC, it is suggested that above conclusions be considered applicable only to HSC DSTBs until their validity is verified for NSC specimens through additional tests.

ACKNOWLEDGMENTS

The authors would like to thank Messrs. Cai, Wang, Xie and Ms. Tu, who have undertaken the tests reported in this paper as part of their undergraduate theses. This research is part of an ongoing program at the University of Adelaide on FRP-concrete composite members.

REFERENCES

[1] Mirmiran, A., Shahawy, M., Samaan, M., El Echary, H., Mastrapa, J.C., and Pico, O. (1998). "Effect of Column Parameters on FRP-confined Concrete." *Journal of Composites for Construction, ASCE*, 2, 4, 175-185.

[2] Fam, A. Z., and Rizkalla, S.H. (2001), "Confinement model for axially loaded concrete confined by circular fiber-reinforced polymer tubes." *ACI Structural Journal*, 98(4), 451-461.

[3] Hong, W.K., and Kim, H.C. (2004). "Behavior of concrete columns confined by carbon composite tubes", *Canadian Journal of Civil Engineering*, 31(2), 178–188.

[4] Fam, A., Schnerch, D. and Rizkalla, S. (2005). "Rectangular Filament-Wound GFRP Tubes Filled with Concrete under Flexural and Axial Loading: Experimental Investigation." *Journal of Composites for Construction, ASCE*, 9(1), 25-33.

[5] Ozbakkaloglu, T., and Oehlers, D. J., (2008a), "Concrete-filled square and rectangular FRP tubes under axial compression." *Journal of Composites for Construction, ASCE*, 12, (4), 469-477.

[6] Ozbakkaloglu, T., and Oehlers, D. J., (2008b), "Manufacture and testing of a novel FRP tube confinement." *Engineering Structures*, 30(9), 2448-2459.

[7] Mohamed, H., and Masmoudi, R. (2010) "Axial Load Capacity of Concrete-Filled FRP Tube Columns: Experimental versus Predictions." *J. Compos. Constr., ASCE*, 14(2), 231-243.

[8] Park, J. H., Jo, B. W., Yoon, S. J., and Park, S. K. (2011). "Experimental investigation on the structural behavior of concrete filled FRP tubes with/without steel re-bar." *KSCE J. Civ. Eng*., 15(2), 337-345.

[9] Ozbakkaloglu, T. (2013a). "Axial compressive behavior of square and rectangular high- strength concrete-filled FRP tubes." *Journal of Composites for Construction, ASCE*, 17(1), 151-161.

[10] Ozbakkaloglu, T. (2013b). "Compressive behavior of concrete-filled FRP tube columns: Assessment of critical column parameters." *Engineering Structures,* 51, 188-199.

[11] Ozbakkaloglu, T. (2013c). "Concrete-filled FRP Tubes: Manufacture and Testing of New Forms Designed for Improved Performance." *Journal of Composites for Construction, ASCE*, 17(2), 280- 291.

[12] Ozbakkaloglu, T. (2013d). "Behavior of square and rectangular ultra high-strength concrete-filled FRP tubes under axial compression." *Composites B: Engineering*, 54, 97-111.

[13] Vincent, T. and Ozbakkaloglu, T. (2013a). "Influence of concrete strength and confinement method on axial compressive behavior of FRP confined high-and ultra high-strength concrete." *Composites Part B: Engineering*, 50, 413-428.

[14] Vincent, T. and Ozbakkaloglu, T. (2013b). "Influence of fiber orientation and specimen end condition on axial compressive behavior of FRP-confined concrete" *Construction and Building Materials*, 47, 814-826.

[15] Yamakawa, T., Zhong, P., and Ohama, A. (2003). "Seismic Performance of Aramid Fiber Square Tubed Concrete Columns with Metallic and/or Non Metallic Reinforcement." *Journal of Reinforced Plastic and Composites*, 22(13), 1221 -1237.

[16] Zhu, Z., Ahmad, I., and Mirmiran, A. (2006). "Seismic performance of concrete-filled FRP tube columns for bridge substructure." *Journal of Bridge Engineering*, ASCE, 11(3), 359-370.

[17] Ozbakkaloglu, T. and Saatcioglu, M. (2006),"Seismic Behavior of High Strength Concrete Columns Confined by Fiber-Reinforced Polymer Tubes." *Journal of Composite Construction, ASCE*, 10(6), 538 – 549.

[18] Ozbakkaloglu, T. and Saatcioglu, M. (2007),"Seismic Performance of Square High Strength Concrete Columns in FRP stay in place formwork." *Journal of Structural Engineering, ASCE*, 133(1), PP. 44-56.

[19] Saatcioglu, M., Ozbakkaloglu, T., Elnabelsy, G. (2008) "Seismic behavior and design of reinforced concrete columns confined with FRP stay-in-place formwork." *ACI SP257*, 149-170.

[20] Idris, Y., and Ozbakkaloglu, T. (2013). "Seismic behaviour of square high –strength concrete-filled FRP tube columns." *Journal of Composites for Construction, ASCE,* 10.1061/(ASCE)CC.1943-5614.0000388.

[21] Mirmiran, A., Shahawy, M., El Khoury, C., and Naguib, W. (2000). "Large beam-column tests on FRP-filled composite tubes." ACI Structural Journal, 97(2), 268-276.

[22] Davol, A., Burgueno, R., and Seible, F. (2001). Flexural behaviour of circular concrete filled FRP shells." *Journal of Structural Engineering, ASCE*, 12(7), pp. 810-817.

[23] Fam, A.Z., and Rizkalla, S.H. (2002), "Flexural behavior of concrete filled fiber-reinforced polymer circular tubes." *Journal of Composites Construction, ASCE*, 6(2), 123-132.

[24] Fam, A.Z., and Rizkalla, S.H. (2003), "Large scale testing and analysis of hybrid concrete/composite tubes for circular beam-column applications." *Construction Building Materials*, 17, 507-516.

[25] Cole, B., and Fam, A. (2006). “Flexural load testingof concrete filled FRP tubes with longitudinal steel and FRP rebar.” *Journal of Composite Construction*, *ASCE*, 10(2), 161-171.

[26] Fam, A., Cole, B., and Mandal, S. (2007). “Composite tubes as an alternative to steel spirals for concrete members in bending and shear.” *Construction Building Material*, 21, 347-355.

[27] Teng, J.G., Yu, T., and Wong, Y.L. (2004). “Behavior of hybrid FRP-concrete-steel double-skin tubular columns.” *Proc. 2nd Int. Conf. on FRP Composites in Civil Engineering*, Adelaide, Australia, 811-818.

[28] Wong, Y.L., Yu, T., Teng, J.G., and Dong, S.L. (2008). “Behavior of FRP-Confined Concrete in Annular Section Columns.” *Composites: Part B*, 39, 451-466.

[29] Teng J.G., Yu, T., and Wong, Y.L. (2010) “Hybrid FRP-concrete-steel double-skin tubular structural members.” *Proceedings, The Fifth International Conference on FRP Composites in Civil Engineering, 27-29 September, Beijing, China*, 26-32.

[30] Yu T, Wong YL, Teng JG. (2010). “Behavior of hybrid FRP-concrete-steel double-skin tubular columns subjected to eccentric compression.” *Advances in Structural Engineering*, 13(5), 961–74.

[31] Louk Fanggi, B. A. and Ozbakkaloglu, T. (2013). “Compressive behaviour of aramid FRP-HSC-steel double-skin tubular columns.” *Construction Building Material*, 48, 554-565.

[32] Ozbakkaloglu, T., and Louk Fanggi, B. (2013), “FRP-HSC-stee; composite columns: behavior under monotonic and cyclic axial compression.” *Mater. Struct.,* http://dx.doi.org/10.1617/s11527-013-0216-0

[33] Ozbakkaloglu, T., and Louk Fanggi, B. (2013), “Axial compressive behavior of FRP-concrete-steel double-skin tubular columns made of normal-and high-strength concrete.” *Journal of Composites for Construction, ASCE*. doi/abs/10.1061/(ASCE)CC.1943-5614.0000401

[34] Han, L.H., Tao, Z., Liao, F.Y., and Xu, Y. (2010), "Tests on Cyclic Performance of FRP-Concrete –Steel Double-Skin Tubular Columns." *Thin-Walled Structures*, 4, 430-439.

[35] Zhang, B., Teng, J. G. & Yu, T. (2012). "Behaviour of hybrid double-skin tubular columns subjected to combined axial compression and cyclic lateral loading." *Sixth International Conference on FRP Composites in Civil Engineering* (pp. 1-7). Rome, Italy.

[36] Ozbakkaloglu, T., and Idris, Y. (2013). "Seismic behavior of FRP-high-strength concrete-steel double skin tubular columns." *Journal of Structural Engineering, ASCE,* 04014019, http://dx.doi.org/10.1061/(ASCE)ST.1943-541X.0000981.

[37] Yu T., Wong, Y.L., Dong, S.L., and Lam E.S.S. (2006). "Flexural Behavior of Hybrid FRP-Concrete-Steel Double Skin Tubular Members." *Journal of Composites for Construction ASCE*, 10(5), 443-52.

[38] Karimi, K., Tait, M.J., and El-Dakhakhni, W.W. (2011a). "Testing and modelling of a novel FRP-encased steel-concrete composite column." *Composite Structures,* 93, 1463-1473.

[39] Karimi, K., El-Dakhakhni, W.W., and Tait, M.J. (2011b). "Performance enhancement of steel columns using concrete-filled composite jackets." *Journal of performance of constructed facilities, ASCE*, 25(3), 189-201.

[40] Karimi, K., Tait, M.J., and El-Dakhakhni, W.W. (2012). "Influence of slenderness on the behaviour of a FRP-encased steel-concrete composite column." *Journal of Composite for Construction, ASCE*, 16(1), 100-109.

[41] Zakaib, S. and Fam, A. (2012). "Flexural Performance and Moment Connection of Concrete-Filled GFRP Tube–Encased Steel I-Sections." *J. Compos. Constr.,* 16(5), 604–613.

[42] Park, R., and Paulay, T. (1975). *Reinforced concrete structures*, Wiley, New York.

Table 1. Properties of test specimens

Specimens	f'_c (MPa)	FRP tube		Inner steel tube				A_s/A_c
		Shape	n	Shape	D (mm)	t_s (mm)	Inner void	
DSTB-1	92	Circular	2	Circular	114.3	6.02	Empty	0.28
DSTB-2	92	Circular	2	Circular	76.1	3.2	Empty	0.06
DSTB-3	91	Circular	2	Circular	114.3	6.02	Filled	0.13
DSTB-4	42	Circular	1	Circular	114.3	6.02	Empty	0.28
DSTB-5	84	Circular	2	Square	100	6	Empty	0.27
DSTB-6	84	Square	2	Square	100	6	Empty	0.18
DSTB-7	91	Circular	2	Circular	76.1	3.2	Empty	0.07[a]
I-CFFT	82	Circular	2	Steel I-beam	As in Fig.1		-	0.10

f'_c = concrete strength, n = number of FRP layers, D = diameter of steel tubes, t_s = thickness of steel tubes, A_s/A_c = reinforcement ratio.

[a]includes the area of additional mechanical connectors

Table 2. Material properties of fiber sheets and epoxy resin used in FRP tubes

Type	Nominal thickness t_f (mm/ply)	Provided by manufacturers			Obtained from flat FRP coupon tests		
		Tensile strength f_f (MPa)	Ultimate tensile strain, ε_f (%)	Elastic modulus E_f (GPa)	Tensile strength f_{frp} (MPa)	Ultimate tensile strain, ε_{frp} (%)	Elastic modulus E_{frp} (GPa)
Aramid	0.200	2600	2.50	118.0	2390	1.86	128.5
Epoxy Resin		>50	2.50	>3			

Table 3. Material properties of inner steel sections

Steel section	Designation	Yield stress, f_y (MPa)	Ultimate tensile stress, f_u (MPa)	Ultimate tensile strain, ε_u (%)	Rupture strain, ε_r (%)
Tube 1	114.3 mm circular	436	490	9.5	19.4
Tube 2	76.1 mm circular	398	483	6.9	22.0
Tube 3	100 mm square	411	470	7.7	16.5
I-beam	125 TFB	418	498	6.4	15.7
Steel rings	8-mm diameter bars	546	612	8.1	18.5

Table 4. Test results

Specimens	P_{peak} (kN)	M_{peak} (kNm)	Δ_{peak} (mm)	P_{ult} (kN)	M_{ult} (kNm)	Δ_{ult} (mm)	Steel tube slip (mm)
DSTB-1	153.2	38.3	80.8	152.4	38.1	82.6	5.6
DSTB-2	38.8	9.7	57.9	38.3	19.2	84.7	9.0
DSTB-3	190.5	47.6	75.3	188.8	94.4	81.5	4.0
DSTB-4	141.9	35.4	60.6	140.2	70.1	79.5	6.6
DSTB-5	170.4	42.6	41.6	162.8	81.4	65.5	4.1
DSTB-6	179.6	44.9	29.5	161.2	80.6	90.1	4.1
DSTB-7	67.7	16.9	24.3	63.7	31.9	87.1	0.008
I-CFFT	165.6	41.4	89.5	165.6	82.8	89.5	0.004

P_{peak} = peak load, Δ_{peak} = recorded mid-span deflection at the peak load, Δ_{ult} = mid-span deflection at ultimate, P_{ult} = load at ultimate, M_{peak} = peak moment, M_{ult} = moment at ultimate.

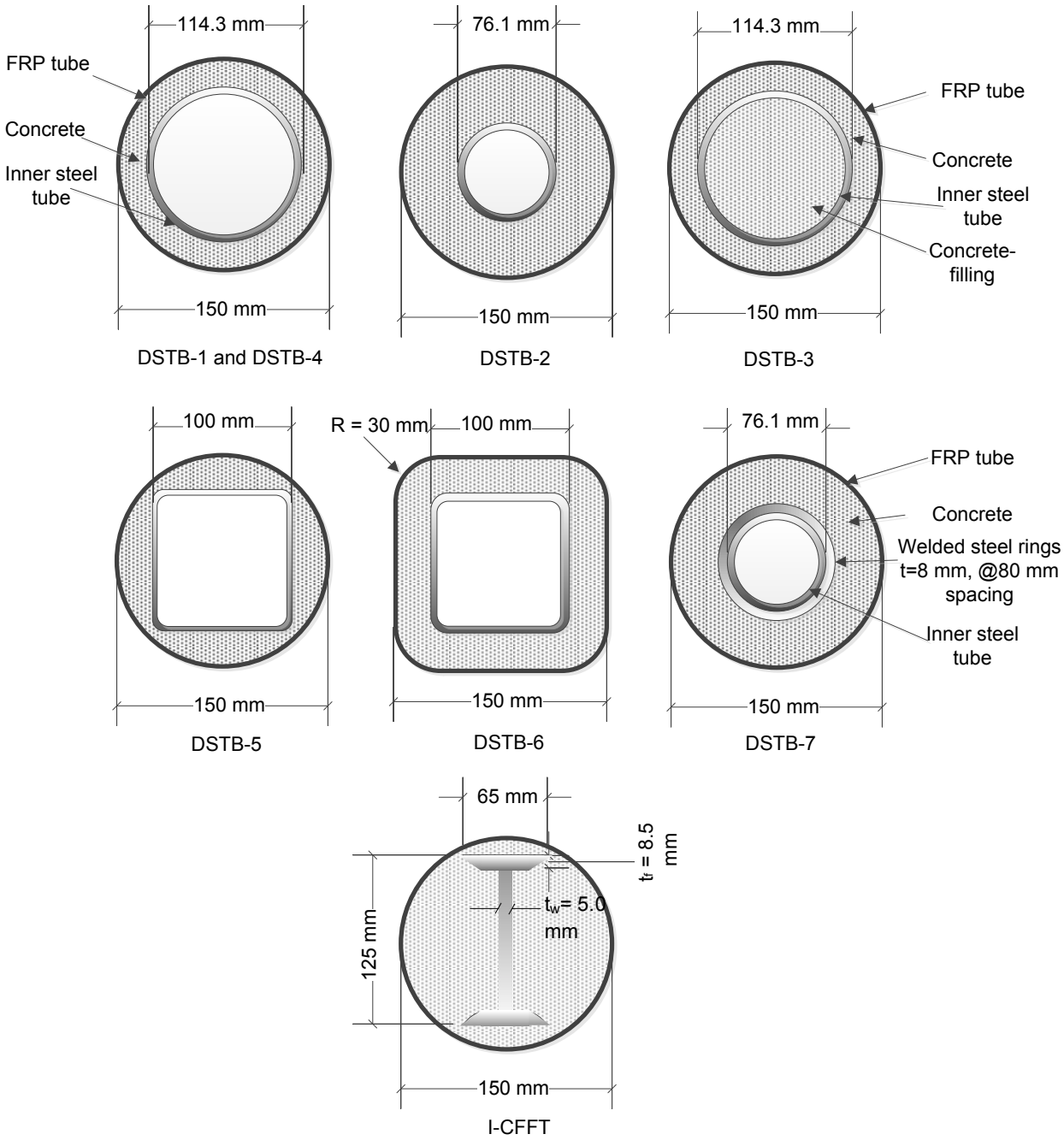

Fig. 1. Cross-sections of test specimens

(a)

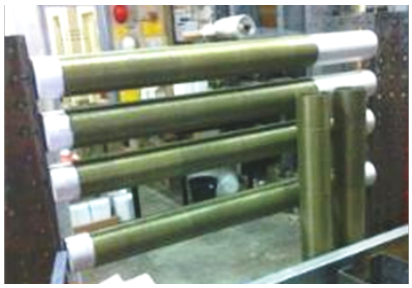

(b)

(c)

(d)

Fig. 2. Manufacturing process: (a) steel tubes; (b) manufacturing of FRP tubes; (c) specimens before concrete pouring; (d) specimens after concrete pouring

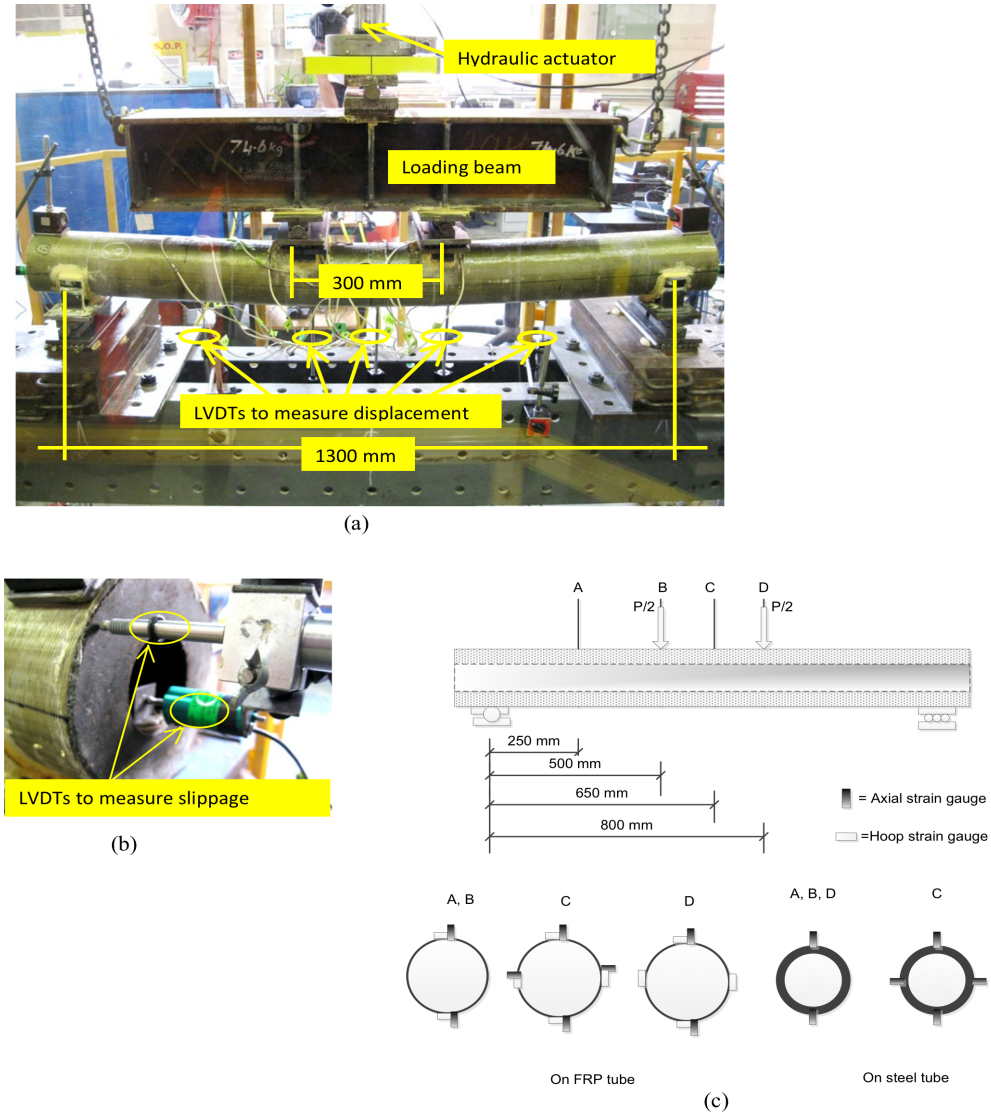

Fig. 3. Test setup and instrumentation: (a) Illustration of the test set-up; (b) Locations of LVDTs used to measure slips; (c) Strain gauge locations

(a) DSTB-1

(b) DSTB-2

(c) DSTB-3

(d) DSTB-4

(g) DSTB-5

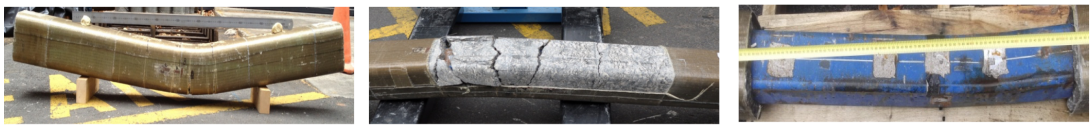

(h) DSTB-6

(h) DSTB-7

(i) I-CFFT

Fig. 4. Specimens after testing

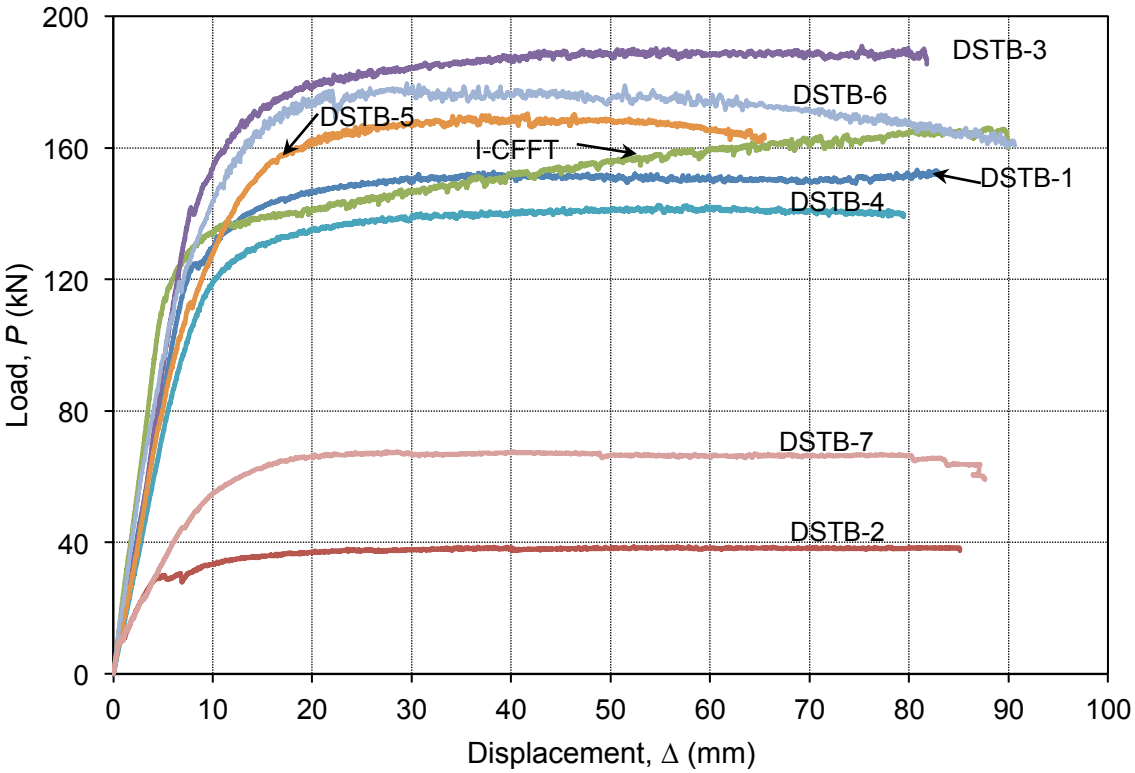

Fig. 5. Load–mid-span deflection relationships of DSTBs

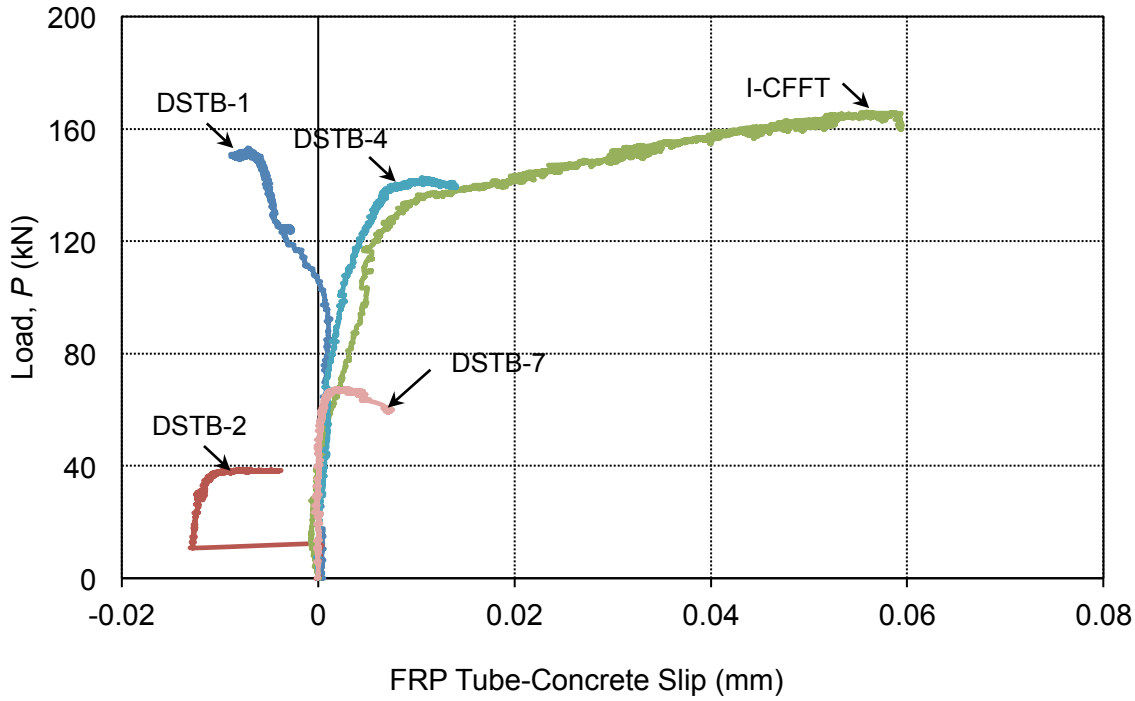

Fig. 6. Load–slip relationships measured between FRP tube and concrete

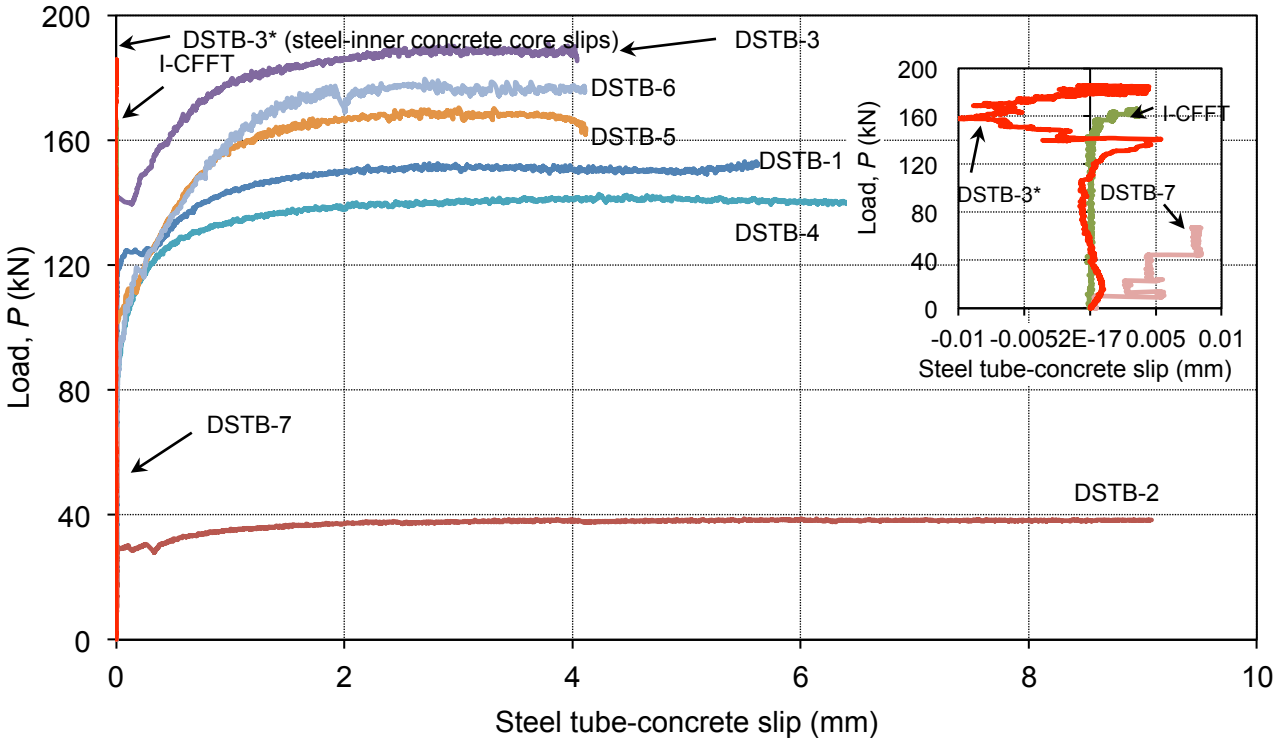

Fig. 7. Load–slip relationships between concrete and steel tube

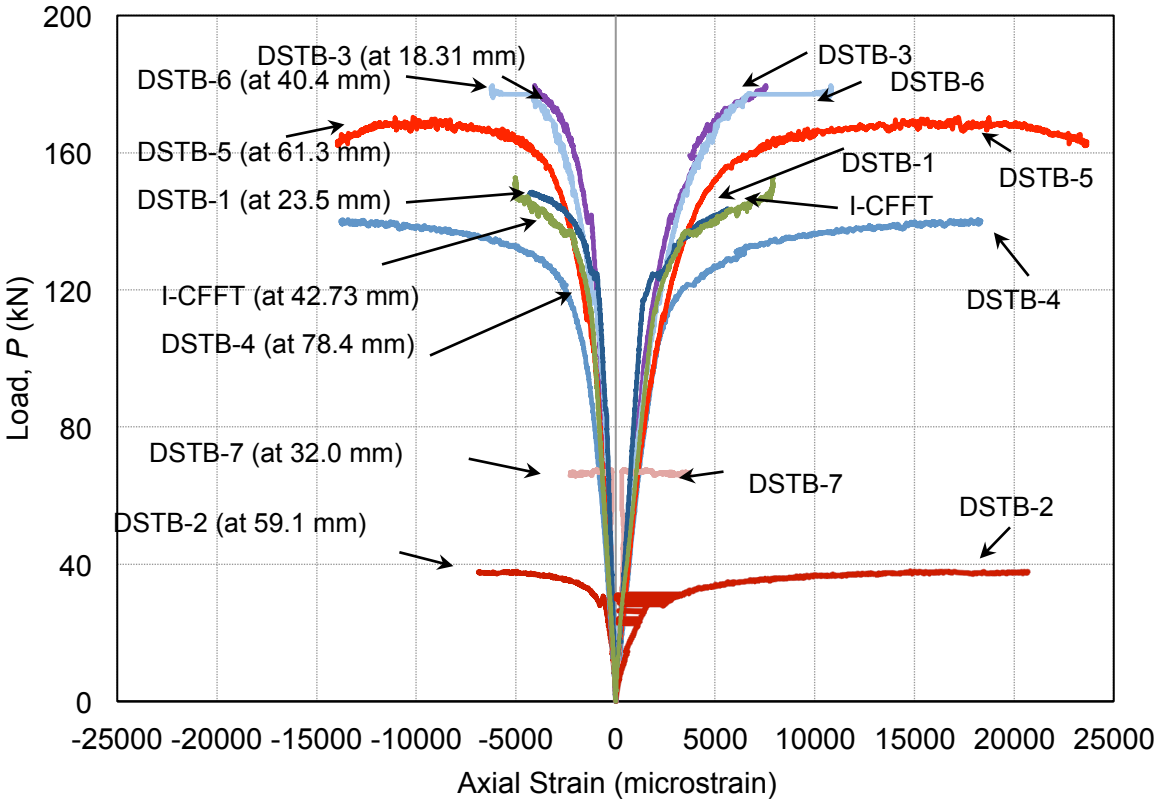

Fig. 8. Steel tube axial strains measured at beam mid-span

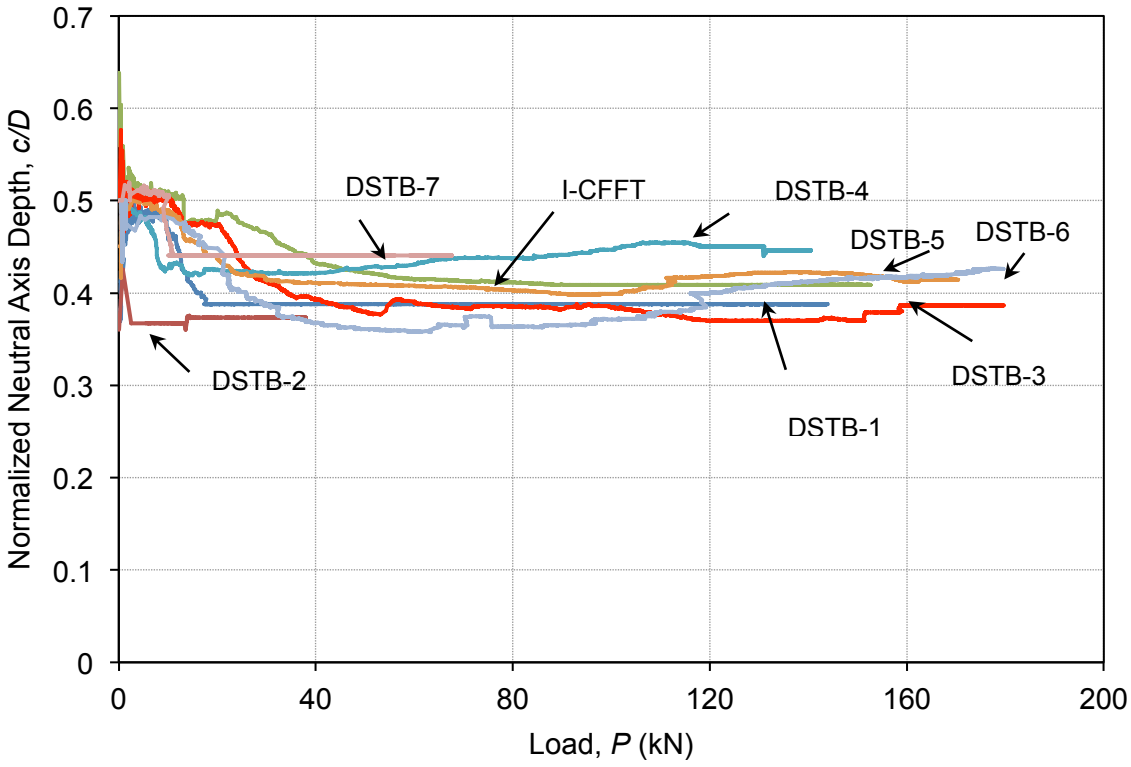

Fig. 9. Variation of neutral axis depths

CHAPTER 6

Flexural Behavior of FRP-HSC-Steel Tubular Beams under Reversed Cyclic Loading

Yunita Idris and Togay Ozbakkaloglu

School of Civil, Environmental, and Mining Engineering, University of Adelaide, 5000

Thin-Walled Structures (Published)

Statement of Authorship

Title of Paper	Flexural Behavior of FRP-HSC-Steel Tubular Beams under Reversed Cyclic Loading
Publication Status	● Published ○ Accepted for publication ○ Submitted for publication ○ Publication style
Publication Details	Idris, Y., and Ozbakkaloglu, T. (2015). "Flexural behavior of FRP-HSC-steel tubular beams under reversed cyclic loading." *Thin-Walled Structures*, 87: 89-101

Author Contributions

By signing the Statement of Authorship, each author certifies that their stated contribution to the publication is accurate and that permission is granted for the publication to be included in the candidate's thesis.

Name of Principal Author (Candidate)	Yunita Idris		
Contribution to the Paper	Review of literature, analysis data, and preparation of manuscript		
Signature		Date	22/09/2015

Name of Co-Author	Dr. Togay Ozbakkaloglu		
Contribution to the Paper	Research supervision and review of manuscript		
Signature		Date	23/09/2015

FLEXURAL BEHAVIOR OF FRP-HSC-STEEL DOUBLE SKIN TUBULAR BEAMS UNDER REVERSED-CYCLIC LOADING

Yunita IDRIS and Togay OZBAKKALOGLU

ABSTRACT

This article presents an experimental study on the cyclic behavior of fiber reinforced polymer (FRP)-concrete-steel double skin tubular (DST) cantilever beams, referred to in this paper as DSTBs. Four DSTBs constructed of high-strength concrete (HSC) were tested under reversed-cyclic lateral loading. The main parameters under investigation were the size of the inner steel tube, the provision (or absence) of a concrete filling inside the steel tube, and the installation of mechanical connectors in the form of steel rings welded on the inner steel tube. The results indicate that DSTBs exhibit very ductile behavior under reversed-cyclic lateral loading. The results also indicate that the DSTBs with larger inner steel tubes exhibit lower lateral displacement capacities compared to their counterparts with smaller inner steel tubes. It was observed that installation of mechanical connectors on the inner steel tube and concrete-filling the tube both influence the overall behavior and lateral displacement capacity of the DSTBs. Furthermore, the results show that through the use of mechanical connectors the slippage at the interface between the steel tube and surrounding concrete sleeve can be completely eliminated.

KEYWORDS: FRP-concrete-steel composite members; Cantilever beams; Fiber reinforced polymer (FRP); High-strength concrete (HSC); Confinement; Lateral displacement.

1. Introduction

As was demonstrated in a recent review by Ozbakkaloglu et al. [1], the use of fiber reinforced polymer (FRP) composites as a confinement material has received a great deal of attention over the past two decades. Together with the retrofitting applications [e.g. (2-6)] the use of fiber reinforced polymer (FRP) composites in the construction of new high-performance composite members in the form of concrete-filled FRP tubes (CFFTs) has become increasingly popular, with a large number of studies that have been reported on the compressive [e.g. (7-13)], flexural [e.g. (14-16)] and seismic behavior [17-21] of CFFT beams and columns. Following from the research on CFFTs, a new type of composite system, which consists of a steel tube inside an FRP tube with a concrete sleeve sandwiched in between, has received significant recent research attention. These double-skin tubular beams and columns (referred to as DSTBs and DSTCs) rely on the same FRP tube confinement mechanism that is present in CFFTs, and through the combination of the advantages of the three constituent materials they can be designed to exhibit extremely high structural performance levels. A large number of experimental studies have recently been undertaken on these composite members by groups led by Teng in Hong Kong [e.g. (22-24)] and the second author in Australia [e.g. (25-29)]. The results of these studies have shown some of the performance advantages offered by this composite system under various loading conditions.

A recent study by Ozbakkaloglu and Idris [28], where the behavior of DSTCs manufactured with high-strength concrete (HSC) was investigated under combined axial compression and lateral load reversals, illustrated the ability of these columns to develop very high inelastic deformation capacities under simulated seismic loading. In agreement with the observations on the behavior of DSTCs, the two studies reported to date on the behavior of DSTBs have shown that these composite beams exhibit very ductile flexural

behavior under four point bending [29,30]. However, no study has been reported to date on the behavior of cantilever DSTBs under reversed-cyclic loading, and addressing this gap formed the aim of the experimental study presented in this article.

The experimental program reported in this paper was designed to investigate the performance of FRP-HSC-steel DSTBs subjected to reversed-cyclic lateral loading. The study investigated the influences of: i) varying the size of the inner steel tube, ii) concrete-filling the steel tube, and iii) installing mechanical connectors on the steel tube. The results of the experimental program are first presented, followed by a discussion on the influence of the main test parameters on the beam behavior.

2. Experimental program

2.1. Test Specimens

Four cantilever DST beams (DSTBs) were manufactured and tested under incrementally increasing lateral displacement reversals. The specimens had 150 mm circular cross-sections and they were 1.2 m long. The inner steel tube of each specimen was groove welded to a 300 x 300 mm steel plate. Lateral loads were applied to the specimens by an actuator at a section 200 mm below the tip of the cantilever, which resulted in a shear span (L) of 1.0 m. The specimens were manufactured using a HSC mix with target compressive strength of 100 MPa, and they were enclosed by aramid FRP external tubes. Table 1 provides a summary of material and geometric properties of the test specimens and Fig. 1 illustrates their geometry.

2.2. Materials and specimen preparation

2.2.1. FRP tubes

Aramid fibers were used to manufacture the outer FRP tube in all the specimens. The tubes were manufactured using a manual wet lay-up process, which involved wrapping epoxy resin impregnated fiber sheets around precision-cut high-density styrofoam moulds in the hoop direction. The FRP tubes of each DSTB were made from two layers of FRP. The sheets were wrapped around the moulds one layer at a time, with an overlap length of 100 mm provided for each layer on opposite sides of the beam to prevent premature debonding. The overlap region of each subsequent layer was located on the opposite face at a 180-degree interval from the previous overlap. The tubes were manufactured so that the overlap regions formed continuous lines along the length of the DSTBs, corresponding to the side faces of the beams. The width of each fiber sheet was 300 mm, and a small overlap of around 10 mm was provided along the axial direction only to ensure the continuity of the tube. The epoxy resin was applied to the fiber sheet at a coverage rate of 0.6L/m^2, which resulted in a ply thickness of 0.8 mm for the resulting FRP composite.

Table 2 provides the manufacturer supplied properties of the unidirectional fiber sheets used in the manufacture of the FRP tubes. The material properties of the FRP composites, established through flat coupon tests where the specimens were loaded in accordance with ASTM standard D3039M-08 [31], are also reported in Table 2.

2.2.2. Concrete

A single HSC mix was used in the manufacture of the specimens. The mix consisted of crushed bluestone as the coarse aggregate with a nominal maximum size of 10 mm. Silica

fume was added to the mix at 8% of the binder content by weight and a low water-cementations material ratio of 0.27 was used to achieve the design concrete strength of 100 MPa. To ensure proper placement of the concrete inside DSTBs, it was crucial for the mix to have a high workability. This was achieved through the use of a polycarboxylic ether polymer-based superplasticizer at a rate of 20 kg per m^3. The mix proportions of the concrete mix are shown in Table 3. The result of slump flow test that was undertaken to establish the workability of the fresh concrete is also supplied in the same table, with the test-day concret strength of each specimen given in Table 1. The difference in the strengths of the specimen pairs DSTB-1&2 and DSTB-3&4 was caused by the difference in concrete curing age of the specimens of these two pairs by the time of testing.

2.2.3. Steel tubes

Two circular steel tubes with different external diameters (D_s) and thicknesses (t_s) were used in the fabrication of the specimens. Two of the specimens were provided with a 114.3-mm diameter inner steel tube with a wall thickness of 6.0 mm (DSTBs 1 and 2). For one of these specimens, the inner steel tube was filled with concrete (DSTB-2). The remaining two specimens had inner steel tubes with a 76.1 mm diameter and 3.2 mm thick walls (DSTBs 3 and 4). Additional steel rings with an 8 mm diameter were welded onto the steel tube of one of these specimens at 80-mm spacing along the specimen length (DSTB-4) to serve as mechanical connectors. The aim of the use mechanical connectors along the steel tube was to prevent slippage between the inner steel tube and surrounding concrete in the longitudinal direction, thereby the composite system enable to develop a full interaction behavior. This should not be confused with the use of steel rings to improve

confinement efficiency of concrete-filled steel tubes, which was investigated in a number of previous studies [32,33].

Prior to their use, all of the steel tubes were carefully checked to ensure that they were free of imperfections. The material properties of the steel tubes were determined by testing five steel coupons cut from the original tube. The results of these tests are reported in Table 4, together with the properties of the steel rings established from direct tension tests.

2.2.4. Preparation of DSTBs

Fig. 2 illustrates the manufacturing process of the specimens. Firstly, the internal steel tubes were welded onto 300 x 300 mm steel plates, which were used to connect the DSTBs to the loading frame of the test setup. The previously prepared FRP tubes were then placed outside the steel tubes to form a confining shell and they also functioned as a formwork during the concrete pour. The concrete was filled in layers with each layer compacted thoroughly through combined internal rodding and external vibration. As can be seen from the cross-sections of Specimens DSTB-1 and DSTB-2 in Fig. 2, the use of a highly workable concrete mix its placement through the procedure described above enabled proper placement of concrete inside the specimens with no major air void or honey combing.

2.3. Instrumentation, test setup and loading program

Fig. 3 illustrates the test setup. The specimens were tested as a cantilever with a 1000 mm span length measured from the loading point to the fixed end. The specimens were connected to the rigid steel frame through a fixed connection, which was formed by

securing the steel end-plates to which the specimens were welded onto to the frame with four corner bolts. The cyclic loading was applied using a 500-kN capacity hydraulic cylinder with 511 mm stroke capacity.

The deflections were measured using two string pots that were placed at the load point (1 m from the steel plate) and at the edge of the beam (1.2 m). Two 30-mm stroke capacity linear variable differential transformer (LVDTs) that were placed on the FRP tube at 35 mm from the steel end-plate at two opposite faces corresponding to the extreme tension/compression fibers to measure the gap opening at the base and rotations caused by slippage and extension of the steel tube at this location. Rotations of the cantilever beam within the potential plastic hinge region were measured by two LVDTs with 50 mm stroke capacities that were placed at a section of 150 mm from the steel plate.

The specimens were also instrumented with two additional LVDTs at their ends, which were used to measure the slippage at steel tube-concrete and FRP tube-concrete interfaces as illustrated in Fig. 3 (b). The acquisition of hoop strain data on FRP tubes was of particular interest in terms of understanding the activation of the confinement mechanism and development of the confining pressures at different sections along the DSTBs. To this end, up to 23 strain gauges with 5 mm gauge lengths were bonded to each FRP tube in the hoop direction at eight different cross sections along the length of the beam that extended up to 450 mm away from the specimen fixed end. The axial strains of the inner steel tubes were measured with 12 5-mm long strain gauges placed at six different cross-sections within the same 450-mm long region.

3. Test results

3.1. Specimens at the end of testing

The condition of the specimens at the end of testing is illustrated in Fig. 4. All of the specimens failed as a result of tension rupture of their inner steel tubes. As evident from Fig. 4, except for DSTB-4, where FRP tube fiber rupture was observed, the FRP tubes of the remaining three specimens exhibited no signs of damage.

As illustrated in Fig. 5, DSTB-1, with a 114.3-mm diameter inner steel tube, showed a sudden loss of strength after attaining its maximum lateral load capacity at 6% lateral drift ($\delta=\Delta/L_s$). The specimen failed due to the rupture of the inner steel tube near its base at 7% lateral drift. The companion specimen DSTB-2, with a concrete-filled 114.3-mm diameter inner steel tube, behaved similarly to DSTB-1, failing due to the rupture of the inner steel tube near the specimen base after attaining its lateral load capacity at 6% lateral drift.

DSTB-3, with a smaller inner steel tube (i.e. D_s = 76.1 mm) reached its maximum lateral load at 4% lateral drift, beyond which the specimen maintained its lateral load capacity, exhibiting only a slight strength decay before it failed at 12% lateral drift. The failure of the specimen was due to the rupture of the inner steel tube at a section 35 mm away from the specimen fixed end. The companion specimen DSTB-4, which was manufactured with an inner steel tube with mechanical connectors, behaved similarly to DSTB-3, developing its maximum lateral load at 4% lateral drift and exhibiting only a slight strength decay before failed at 10% lateral drift. At failure, DSTC-4 exhibited signs of local FRP tube rupture at a section approximately 70 mm away from the specimen base, which also corresponded to the rupture failure location of the inner steel tube.

3.2. Hysteretic Behavior

The experimentally recorded hysteretic lateral load-drift relationships of the columns are shown in Fig. 5. Under lateral cyclic loading, specimens are often considered to have failed once the strength decay exhibited by the specimen exceeds 20% of the lateral load capacity of the specimen. As all of the specimens of the present study maintained over 80% of their lateral load capacities until their failure, the lateral displacement and drift capacities of the specimens were considered to be equal to the maximum lateral displacements and drifts recorded at specimen failure (Δ_{max} and δ_{max}), which are shown in Table 5. As can be seen in Table 5, DSTBs with larger diameters (i.e. D_s = 114.3 mm) exhibited higher lateral loads but lower lateral drift capacities (δ_{max}) than DSTBs with smaller diameters (i.e. D_s = 76.1 mm). The higher lateral load capacities of the specimens with larger inner steel tubes were expected, and their lower drift capacities were contributed by three factors: i) their slightly lower steel tube rupture strain (ε_r), ii) the slightly larger distance between the neutral axis and extreme steel tube tension fibers at their cross-section, and iii) their lower plastic hinge region length. The first two factors resulted in lower sectional curvatures of these specimens at ultimate, and the third factor, which is discussed later in the paper, further magnified this effect and led to their lower displacement capacities as shown in Table 5.

As illustrated in Fig. 5a and b, DSTB-1 and DSTB-2 exhibited very similar hysteretic lateral load-lateral drift relationships. DSTB-1, with a hollow inner steel tube, developed its maximum lateral load capacity of 31.9 kN at 6% lateral drift and failed at the third cycle of 7% lateral drift. DSTB-2, with a concrete-filled inner steel tube, reached its maximum lateral load of 33.9 kN at 6% lateral drift and failed at the third cycle of the same lateral drift level.

The hysteretic lateral load-lateral drift relationships of DSTB-3 and DSTB-4 were also very similar to each other, except that DSTB-3, with mechanical connectors, exhibited a higher lateral load capacity than that of DSTB-4 (i.e F_{max} = 14.7 kN versus F_{max} = 11.8 kN). Both DSTBs 3 and 4 reached their maximum load at 4% lateral drift, and maintained over 80% of their lateral load capacities until their failures at 12% and 10% lateral drift levels, respectively.

To enable comparisons of the overall behaviors of the specimens, Fig. 6 presents the lateral load (F)-displacement (Δ) envelopes of the specimens, which were obtained by averaging the maximum recorded load at each displacement level from pull and push directions.

3.3. Measured beam stiffness

Fig. 7 illustrates the variation of the average beam stiffness (K) with lateral drifts for all the specimens. The stiffness was obtained from the hysteretic lateral load-displacement relationships, as $K = F/\Delta$. Member stiffness curves illustrated in Fig. 7 were determined from the average lateral loads and displacement recorded at a given drift level for the three cycles in the pull and push directions. As expected, the specimens with larger inner steel tubes (DSTB-1 and DSTB-2) exhibited greater stiffness than their counterparts with smaller inner steel tubes (DSTB-3 and DSTB-4). Likewise, the specimen with a concrete-filled inner steel tube (i.e. DSTB-2) developed a higher lateral load capacity and initial stiffness compared to those of the companion specimen with a hollow inner steel tube (i.e. DSTB-1).

Fig. 7 illustrates the progressive reduction of the specimen stiffness with increasing lateral drift, associated with the concrete cracking and the yielding of the internal steel tube. As evident from Fig. 7, the curves of DSTBs 1 and 2 exhibited an almost constant slope throughout the response history. The curves of DSTBs 3 and 4, on the other hand, displayed the most significant change of slope up to 4% lateral drifts, beyond which the stiffness degradation continued at a lower and continually decreasing rate. The major change in the slope of the stiffness curves of the specimens indicates the large level of plastification experienced by the specimens during the corresponding stage of loading. Significantly reduced slopes of the curves of DSTBs 3 and 4 at later stages of loading indicates a stabilized beam behavior, with slopes of the curves progressively approaching zero just before the termination of the curve.

3.4. Energy dissipation capacity

Fig. 8 illustrates the energy dissipation capacities of each specimen. The energy dissipation capacity in each cycle was obtained by calculating the area enclosed under the corresponding lateral load-displacement hysteretic loop. The average energy dissipation capacities of the DSTBs were then calculated for the three consecutive load cycles at a given drift level. Fig. 8 illustrates that the energy dissipation curves of the specimens divided them naturally into two groups. Specimens with larger inner steel tubes (DSTBs 1 and 2) exhibited an almost identical dissipation curves until the failure of DSTB-2 at 6% lateral drift. Owing to their lower lateral load capacities, DSTBs 3 and 4 with smaller inner steel tubes, displayed lower energy dissipation capacities than those of DSTBs 1 and 2. As can be seen from Fig. 8, contributed by its higher lateral load capacity, DSTB-4 with mechanical connectors showed a slightly higher energy dissipation capacity than that of the

companion specimen DSTB-3 until 9% lateral drift level, before exhibiting softening at its failure drift of 10%.

3.5. Load-slip relationships

3.5.1. Load-slip behavior at concrete-FRP tube interface

The load-slip relationship between the FRP tube and concrete was obtained from the LVDTs mounted on the FRP tube at the free end of the beam, with the stroke pointed to the concrete section. Fig. 9 illustrates these relationships for all of the specimens. As evident from the figure, the specimens experienced practically no slippage at their concrete-FRP tube interfaces.

3.5.2. Load-slip behavior at concrete-steel tube interface

The slips between the steel tube and concrete were measured by the LVDTs that were mounted on the FRP tubes at the free end of the beam, with the stroke pointed to the inner steel tube. These readings were then corrected for the FRP tube-concrete slips to obtain the slippage between the steel tube and concrete surrounding it. The load-slip relationship of each specimen is shown in Fig. 10.

Fig. 10 illustrates that only one of the specimens (i.e. DSTB-3) exhibited significant slippage at its concrete-steel tube interface. As can be seen from the figure, an increase in the diameter of the inner steel tube from 76.1 mm to 114.3 mm resulted in a significant reduction in slip, with less than 0.06 mm maximum slippages recorded in both DSTB-1 and DSTB-2. The same observation was also noted in Idris and Ozbakkaloglu [29], where

the behavior of DSTBs was investigated under four point bending. Fig. 10 also shows that the mechanical connecters eliminated the slippage between the steel tube and surrounding concrete, with DSTB-4 showing a maximum slippage of 0.02 mm compared to nearly 2 mm slippage observed in its companion, DSTB-3, without the connectors.

For DSTB-2, with a concrete-filled inner steel tube, the slips between the inner concrete core and the surrounding steel tube were also monitored. The recorded data indicated that there was no the slippage at the inner concrete core-steel tube interface of the specimen.

3.6. Tension gap opening at specimen base

Fig. 11 illustrates the lateral load-tension gap opening relationships of each specimen. The gap formed between the fixed steel end plate and base of the specimen was measured by LVDTs mounted on FRP tubes on either side of the beam 35 mm away from the steel end plate (refer to Fig. 3). The gap opening is caused by elongation of the steel tube under flexural stresses and, if any, slippage between the steel tube and the concrete sleeve. To allow a comparison among the specimens, envelope load-gap opening curves of the specimens averaged from the LVDTs mounted on the opposite beam faces are also shown in Fig. 12.

As illustrated in Fig. 12, the average tension gap opening of DSTB-1 at 7% lateral drift was 7.4 mm. The average tension gap opening of DSTB-2 at 6% lateral drift was 5.4 mm, which was slightly lower than the tension gap opening of DSTB-1 at 6% drift (i.e. 5.8 mm). As mentioned previously, these specimens experienced almost no slippage at their steel tube-concrete interfaces; therefore, the recorded gap openings were exclusively due to extension of their steel tubes under flexure. It was observed that at the end of the test DSTB-3 exhibited quite a large gap opening at its base. Due to instrumentation challenges

experienced during the testing of DSTB-3, the bottom LVDT readings were valid up to 7% lateral drift. However, the top LVDT readings of the specimen indicated a gap opening of 10.5 mm at 11% lateral drift cycle just before the failure of the specimens at 12% drift. The LVDT readings for the companion specimen DSTB-4 were valid up to 8% lateral drift, which indicated a tension gap opening of 5.8 mm at that drift level. This is significantly lower than the 7.7 mm gap opening shown by the top LVDT of DSTB-3 at 8% lateral drift cycle. The higher gap opening of DSTB-3 was due to the additional displacements caused by slippage experienced at concrete-inner steel tube interface of the specimens, which was prevented in DSTB-4 through the use of mechanical connectors, as discussed previously.

3.7. Measured beam rotations

The base rotations of the specimens were determined using the readings of the two LVDTs that were placed on the specimen 35 mm away from the specimen fixed end. Fig. 13 illustrates the lateral load-base rotation relationships of the specimens. DSTB-1 developed a base rotation of 0.054 radians, averaged from pull and push directions, at 7% lateral drift, whereas DSTB-2 exhibited a base rotation of a 0.041 radians at 6% lateral drift. These very high base rotations indicate that the majority of the plastic deformations of these specimens took place within a short segment up to 35 mm away from the specimen base. The aforementioned failure location of these specimens further reinforces this observation. As mentioned previously, in DSTB-3 and DSTB-4, the LVDT readings required for the calculation of the base rotations were available only up to 7% and 8% lateral drift cycles, respectively. At these drift levels DSTBs 3 and 4, respectively, exhibited average base rotations of 0.042 and 0.036 radians. It is worth nothing that the asymmetric curves

exhibited by DST-3 beyond the 3% drift cycle is believed to have been contributed by the slip deformations experienced by this specimen, as discussed previously.

In addition to the base rotations, the rotations within the potential beam plastic hinge region were also calculated using the measurements form the two LVDTs placed 150 mm away from the steel end plate. Fig. 14 illustrates the lateral load-plastic hinge rotation relationships of DSTBs 3 and 4. It was not possible to obtain the plastic hinge rotations of DSTBs 1 and 2 due to problems encountered with the measurements from one of their LVDTs. Fig. 14 shows that DSTBs 3 and 4 and developed plastic hinge rotation of 0.088 and 0.080 radians at 11% and 10% lateral drifts, respectively. These rotations indicate that the plastic deformations of these specimens took place within the 150 mm region from the specimen base.

3.8. Variation of FRP tube hoop strains along beam length

The variation in FRP tube hoop strains was recorded by strain gauges placed on the FRP tube at eight locations along the specimen length. Fig. 15 illustrates the strain profiles of the specimens showing the maximum hoop strains recorded along their lengths. As evident from the figure, the specimens with inner tubes of a smaller diameter developed significantly higher hoop strains than those with larger inner steel tubes, with DSTBs 3 and 4 developing 3080 and 5480 microstrains, respectively, compared to 1180 and 1690 microstrains of DSTBs 1 and 2. This can be attributed to the larger concrete area of the specimens with smaller inner steel tubes, which experienced lateral expansion under compression, resulting in the generation of larger hoop strains and confining pressures on the FRP tubes. The results also illustrate that the concrete filling of the inner steel tube and

the provision of mechanical connectors both resulted in an increase in the hoop strains, attributable to the aforementioned concrete expansion and confinement mechanism.

The hoop strain distributions shown in Fig. 15 also indicate that the plastic deformations experienced by the specimens with larger inner steel tubes (i.e. DSTB-1 and DSTB-2) were highly localized and occurred within a short region that did not extend beyond the quarter of the specimen diameter (i.e. $D/4$ = 37.5 mm) beyond the specimen base. This observation is supported by the measured base rotations specimens, which, as discussed previously, suggested that the majority of the plastic deformations took near the specimen base. As can be seen in Fig. 15, hoop strains of DSTBs 3 and 4, with smaller inner steel tubes, were less localized to the specimen base and they extended up to the regions that were $D/2$ = 75 mm away the specimen base. This observation, which is also supported by the previously discussed failure locations of the specimens, suggests that plastic deformation region of these specimens propagated further along the beam length compared to those of DSTBs 1 and 2. This, as noted previously, was one of the main reasons that contributed to the higher lateral drift capacities observed in the specimens of the present study with smaller inner steel tubes. Additional tests are required to gain further insight into the influence of the specimen parameters on this highly important aspect of the beam behavior.

4. Effects of test parameters on observed beam behavior

4.1. Effect of inner steel tube size

A comparison of the behaviors of DSTB-1 and DSTB-3 illustrate that an increase in the diameter and thickness of the inner steel tube resulted in an increase in the lateral load capacity but a decrease in the lateral displacement capacity of the specimen. The results

also indicate both the initial stiffness (K) and energy dissipation capacity (E) of the specimen increased with an increase in the size of the inner steel tube. An increase in the size of the inner steel tube also resulted in a decrease in both the hoop strains recorded on the FRP tube of the specimen and the slippage observed at the steel tube-concrete interface. It is worth noting that the steel tube used in the present study had fairly high D_s/t_s ratios that ranged from 19 to 24. It is expected that an increase in D_s/t_s would result in an increased likelihood of the inner steel tubeto experience localized plastic deformations, especially in the case of hollow DSTB. Therefore, to clearly establish and be able to model the influence of different failure modes of inner steel tubes on the behavior of DSTBs, future studies that examine the behavior of specimens with larger D_s/t_s are recommended.

4.2. Effect of concrete-filling inner steel tube

The effect of concrete-filling the inner steel tube can be investigated by comparing the behaviors of the companion specimens DSTB-1 and DSTB-2. The results show that the presence of an inner concrete core led to a higher specimen initial stiffness and lateral load capacity. On the other hand, the results also indicate that concrete filling the inner steel tube resulted in a slight decrease in the lateral drift and plastic rotation capacities of DSTBs. No significant influence of the concrete-filling was evident on the energy dissipation capacity of DSTBs, but the presence of inner concrete core resulted in the development of higher hoop strains on the FRP tubes of specimens.

4.3. Effect of using mechanical connectors

The influence of using mechanical connectors on the beam behavior can be investigated through the comparison of the behaviors of the companion specimens DSTB-3 and DSTB-4. The results show that the use of mechanical completely eliminated the slippage at the steel tube-concrete interface, and resulted in a significant increase in the specimen lateral load capacity. This increase can be attributed to both: i) the change in partial interaction behavior caused by slippage at concrete-inner steel tube interface to full interaction behavior through the prevention of the slippage, ii) an increase in the overall cross-sectional area of the steel reinforcement. The use mechanical connectors also slightly increased the beam stiffness (K) between 2% and 9% lateral drift cycles, but had no noticeable influence on the trend of the energy dissipation (E) curve of the specimen. The elimination of the interface slips and resulting slip displacements through the use of mechanical connectors resulted in a slightly reduced specimen lateral displacement capacity. Likewise, the elimination of the rotations due to slip by the mechanical connectors resulted in lower specimen base rotations.

5. Comparisons with other structural systems

To gain some insight into the relative performance of the cantilever DSTB system investigated in this study, the behavior of the specimens of the present study is compared with those of the other structural systems reported in the literature. As shown in Table 6, these included: i) a DST beam-column system consisting of an FRP tube that is manufactured with bi-directional carbon fibers (C-0-2 and S-0-2) [34], and ii) a conventional reinforced concrete member (RC-0) [35]. It is worth noting that due to the limitations of the existing literature it was not possible to compare the specimens of the

present study directly with companion cyclically loaded cantilever beam specimens. Instead the comparisons were made with specimens that were designed as beam-columns and loaded under a low level of axial compression (refer to P/P_o in Table 6) and hence were expected to exhibit a behavior that resembles that of a beam under pure bending. In the selection of the comparison specimens it was ensured that these specimens exhibited a flexure dominant behavior and had member aspect ratios (L/D) that are similar to that of the specimens of the present study.

All the specimens shown in Table 6 were tested under reversed cyclic loading and their lateral drift capacities (δ_{max}) were used to evaluate their overall performance under this loading condition. The comparison of the lateral drift capacities of the specimens shown in Table 6 with those of the specimens of the present study indicates that the DSTBs of the present study developed higher drift capacities than both the companion DSTBs manufactured with FRP tubes with bi-directional fibers (C-0-2 and S-0-2) and the conventional reinforced concrete member (RC-0). The performance difference was particularly significant for the specimens of the present study with smaller inner steel tubes (i.e. DSTB-3 and DSTB-4). The better performance of the DSTBs investigated in this study over that of the conventional reinforced concrete member was expected and it is contributed by higher level and efficiency of confinement provided by the external FRP tube compared to that of the discrete transverse reinforcements used in the latter system. Much lower drift capacities of specimens C-0-2 and S-0-2, on the other hand, appear surprising at first glimpse, as these specimens were manufactured using a similar structural system to that was investigated in the present study. However, upon closer investigation of the results it becomes evident that the lower drift capacities of these specimens were caused by the rupture of the longitudinal fibers used in external FRP tubes of these specimens. These ruptures resulted in a significant drop in the load carrying capacity of

these specimens, and hence marked the practical failure of the specimens, with corresponding displacements used in the calculation of their lateral drift capacities.

Results of these comparisons indicate that the composite FRP-HSC-steel DSTBs can be designed to exhibit significantly higher lateral deformation capacities compared to those of the conventional reinforced concrete beams. The results also indicate that DSTBs with FRP tubes manufactured with fibers aligned in lateral direction exhibit a significantly better performance than that of DSTBs with FRP tubes having fibers in both axial and lateral directions. It is worth noting, however, that these observations were derived from the comparisons of the spcimens that had a number of differences in their geometric and material properties. Therefore, additional targeted studies need to be undertaken in the future before definitive conclusion on relative performances of different systems can be reached.

6. Conclusions

This paper has presented the results of an experimental study on the behavior of FRP-HSC-steel DSTBs under reversed-cyclic lateral loading. Based on the results and discussions presented in the paper, the following conclusions can be drawn:

1. FRP-HSC-steel DSTBs exhibit a very ductile behavior under reversed-cyclic lateral loading.
2. An increase in the diameter and thickness of the inner steel tube results in an increase in the lateral load capacity but a decrease in the lateral displacement capacity of DSTBs.

3. An increase in the size of the inner steel tube results in a decrease in both the hoop strains recorded on FRP tubes of DSTBs and the slippage observed at their steel tube-concrete interface.
4. The presence of an inner concrete core leads to a higher specimen initial stiffness and lateral load capacity, but results in a slight decrease in the lateral drift and plastic rotation capacities of DSTBs. The presence of an inner concrete core also results in development of higher hoop strains on FRP tubes of DSTBs.
5. The slippage at the steel-tube concrete interface of DSTBs can be fully eliminated through the use of mechanical connectors welded on the steel tube of DSTBs along their length. It is found that the presence of mechanical connectors also leads to an increase in the lateral load capacity of DSTBs.

Acknowledgement

The authors would like to thank Messrs. Cai, Wang, Xie and Ms. Tu, who have undertaken the tests reported in this paper as part of their undergraduate theses. This research is part of an ongoing program at the University of Adelaide on FRP-concrete composite members.

References

[1] Ozbakkaloglu, T., Lim, J. C., and Vincent, T. (2013). "FRP-confined concrete in circular sections: Review and assessment of stress-strain models." *Engineering Structures*, 49:1068-1088.

[2] Lignola, G. P., Prota, A., Manfredi, G., and Cosenza E. (2007). "Experimental performance of RC hollow columns confined with CFRP." *Journal of Composite for Construction, ASCE*, 11(1): 42–49.

[3] Ilki, A., Peker. O., Karamuk, E., Demir, C., and Kumbasar, N. (2008). “FRP retrofit of low and medium strength circular and rectangular reinforced concrete columns.” *J. Mater. Civ. Eng.*, 20(2): 169–188.

[4] Rousakis, T., and Karabinis, A. (2008). “Substandard reinforced concrete members subjected to compression: FRP confining effects.” *Materials and Structures*, 41(9): 1595 – 1611.

[5] Kusumawardaningsih, Y., and Hadi, M. N. S. (2010). “Comparative behavior of hollow columns confined with FRP composites.” *Composite Structures*, 93(1): 198-205.

[6] Wu, Y. F., and Wei, Y. Y. (2010). “Effect of cross-sectional aspect ratio on the strength of CFRP-confined rectangular concrete columns.” *Engineering Structures*, 32: 32-45.

[7] Fam, A. Z., and Rizkalla, S.H. (2001), “Confinement model for axially loaded concrete confined by circular fiber-reinforced polymer tubes.” *ACI Structural Journal*, 98(4): 451-61.

[8] Park, J. H., Jo, B. W., Yoon, S. J., and Park, S. K. (2011). “Experimental investigation on the structural behavior of concrete filled FRP tubes with/without steel re-bar.” *KSCE J. Civ. Eng*., 15(2): 337-45.

[9] Ozbakkaloglu, T. (2013). “Behavior of square and rectangular ultra high-strength concrete-filled FRP tubes under axial compression.” *Composites Part B: Engineering*, 54: 97-111.

[10] Ozbakkaloglu, T. and Vincent, T. (2013),”Axial compressive behavior of circular high-strength concrete-filled FRP tubes” *Journal of Composites for Construction*, ASCE, 18(2): 04013037.

[11] Vincent, T. and Ozbakkaloglu, T. (2013),”Influence of concrete strength and confinement method on axial compressive behavior of FRP confined high-and ultra high-strength concrete.” *Composites Part B*, 50 : 413-28.

[12] Vincent, T. and Ozbakkaloglu, T. (2013),”Influence of fiber orientation and specimen end conditions on axial compressive behavior FRP-confined concrete.” *Construction and Building Materials*, 47: 814-26.

[13] Lim, J. C., and Ozbakkaloglu, T. (2014),"Influence of silica fume on stress-strain behavior of FRP-confined HSC." *Construction and Building Materials*, 63: 11-24.

[14] Davol, A., Burgueno, R., and Seible, F. (2001), "Flexural Behavior of Circular Concrete Filled FRP Shells." *Journal of Structural Engineering*, 127(7): 810-7.

[15] Fam, A. Z., and Rizkalla, S. H. (2002), "Flexural behavior of concrete filled fiber-reinforced polymer circular tubes." *Journal of Composite for Construction, ASCE*, 6(2):123-32.

[16] Cole, B., and Fam, A. (2006), "Flexural load testing concrete filled FRP tubes with longitudinal steel and FRP rebar." *Journal of Composite for Consturction, ASCE*, 10(2):161-71.

[17] Ozbakkaloglu, T. and Saatcioglu, M. (2006),"Seismic Behavior of High Strength Concrete Columns Confined by Fiber-Reinforced Polymer Tubes." *Journal of Composite Construction, ASCE*, 10(6): 538 – 49.

[18] Ozbakkaloglu, T. and Saatcioglu, M. (2007),"Seismic Performance of Square High Strength Concrete Columns in FRP stay in place formwork." *Journal of Structural Engineering, ASCE*, 133(1): 44-56.

[19] ElGawady, M., Booker, A., and Dawood, H. (2010), "Seismic behavior of posttensioned concrete-filled fiber tubes." *Journal of Composites for Construction, ASCE*, 14(5): 616-28.

[20] Zaghi, A. E., Saiidi, M.S., and Mirmiran, A. (2012). "Shake table response and analysis of a concrete-filled FRP tube bridge column." *Composite Structures*, 94(5): 1564-74.

[21] Idris, Y., and Ozbakkaloglu, T. (2013). "Seismic behavior of square high –strength concrete-filled FRP tube columns." *Journal of Composites for Construction, ASCE*, 17(6): 04013013.

[22] Teng, J. G., Yu, T., Wong, Y. L., and Dong, S. L. (2007). "Hybrid FRP concrete steel tubular columns: concept and behavior." *Construction and Building Materials*, 21: 846-54.

[23] Wong, Y.L., Yu, T., Teng, J.G., and Dong, S.L. (2008). "Behavior of FRP-Confined Concrete in Annular Section Columns." *Composites: Part B*, 39: 451-66.

[24] Yu, T. and Teng, J. G. (2013). “Behavior of hybrid FRP-Concrete-Steel double-skin tubular columns with a square outer tube and a circular inner tube subjected to axial compression.” *Journal of Composites for Construction, ASCE*, 17(2): 271-79.

[25] Louk Fanggi, B.A., and Ozbakkaloglu, T. (2013). “Compressive behavior of aramid FRP-HSC-Steel double-skin tubular columns.” *Construction and Building Materials*, 48: 554-65.

[26] Ozbakkaloglu, T., and Louk Fanggi, B. A. (2013). “FRP–HSC–steel composite columns: behavior under monotonic and cyclic axial compression.” *Materials and Structures.* doi: 10.1617/s11527-013-0216-0

[27] Ozbakkaloglu, T., and Louk Fanggi, B. A. (2014). “Axial compressive behavior of FRP-concrete-steel double-skin tubular columns made of normal- and high-strength concrete.” *Journal of Composites for Construction, ASCE,* 18(1): 04013027.

[28] Ozbakkaloglu, T., and Idris, Y. (2014), “Seismic behavior of FRP-high-strength concrete-steel double skin tubular columns.” *Journal of Structural Engineering, ASCE,* 140(6): 04014019.

[29] Idris, Y., and Ozbakkaloglu, T. (2014).”Flexural behavior of FRP-HSC-steel composite beams.” *Thin-Walled Structures,* 80: 207-16.

[30] Yu, T., Wong, Y., Teng, J., Dong, S., and Lam, E. (2006). ”Flexural Behavior of Hybrid FRP-Concrete-Steel Double-Skin Tubular Members.” *J. Compos. Constr.*, 10(5): 443–452.

[31] ASTM D3039/D3039M-8. (2008). “Standard test method for tensile properties of polymer matrix composite materials.” *ASTM D3039/D3039M-8,* West Conshohocken, PA, 13.

[32] Dong, C. X., and Ho, J. C. M (2012),”Uni-axial behaviour of normal-strength CFDST columns with external steel rings.” *Steel Compos. Struct.*, 13(6): 587-606.

[33] Lai, M. H., Tao, Z., Liao, F. Y., and Xu, Y. (2014),”Behaviour of uni-axially loaded concrete-filled-steel-tube columns confined by external rings.” *Struct. Des. Tall. Spec Build*, 23(6): 403-426.

[34] Han, L.H., Tao, Z., Liao, F.Y., and Xu, Y (2010). “Test on cyclic performance of FRP-concrete-steel double-skin tubular columns.” *Thin-Walled Structures,* 48(6): 430-439.

[35] Cho, C.G., Kim, Y.Y., Feo, L., and Hui, D. (2012). “Cyclic responses of reinforced concrete composite columns strengthened in the plastic region by HPFRC mortar.” *Composite Structures*, 94:2246-2253.

Table 1. Properties of test specimens

Specimens	f'_c (MPa)	FRP tube		Inner steel tube				A_s/A_c
		Shape	n	Shape	D_s (mm)	t_s (mm)	Inner void	
DSTB-1	100	Circular	2	Circular	114.3	6.0	Empty	0.28
DSTB-2	100	Circular	2	Circular	114.3	6.0	Filled	0.13
DSTB-3	112	Circular	2	Circular	76.1	3.2	Empty	0.06
DSTB-4	112	Circular	2	Circular	76.1	3.2	Empty	0.07[a]

f'_c = test-day unconfined concrete strength, n = number of FRP layers, D_s = diameter of steel tubes, t_s = thickness of steel tubes, A_s/A_c = reinforcement ratio.

[a]total steel area includes the additional area of steel rings

Table 2. Material properties of fiber sheets and epoxy resin used in FRP tubes

Type	Nominal thickness t_f (mm/ply)	Provided by manufacturers			Obtained from flat FRP coupon tests		
		Tensile strength f_f (MPa)	Ultimate tensile strain, ε_f (%)	Elastic modulus E_f (GPa)	Tensile strength f_{frp} (MPa)	Ultimate tensile strain, ε_{frp} (%)	Elastic modulus E_{frp} (GPa)
Aramid	0.200	2600	2.20	118.0	2390	1.86	128.5
Epoxy Resin		>50	2.50	>3			

Table 3. Concrete mixing proportions

Cement (kg/m^3)	Silica fume (kg/m^3)	Sand (kg/m^3)	Coarse Aggregate (kg/m^3)	Water (kg/m^3)	Superplasticizer[a] (kg/m^3)	w/c[b]	Slump flow (mm)
506	44	710	1065	135	20	0.27	620

[a]Contained 70% water by weight

[b]Water-cementitious binder ratio

Table 3. Material properties of inner steel sections

Tube	Shape	D (mm)	Yield Stress, f_y (MPa)	Ultimate Tensile Stress, f_u (MPa)	Ultimate Tensile Strain, ε_u (%)	Rupture strain, ε_r (%)
Tube 1	Circular	114.3	436	490	9.5	19.4
Tube 2	Circular	76.1	398	483	6.9	22.0
Steel rings	Steel bar	8	546	612	8.1	18.5

Table 4. Observed behavior of DSTBs

Specimen	F_{max} (kN)	Δ_{Fmax} (mm)	δ_{Fmax} (%)	$F_{\Delta max}$ (kN)	Δ_{max} (mm)	δ_{max} (%)
DSTB-1	31.9	60	6	31.8	70	7
DSTB-2	33.9	60	6	33.8	60	6
DSTB-3	11.8	40	4	9.6	120	12
DSTB-4	14.9	40	4	12.7	100	10

F_{max} = maximum lateral load, Δ_{Fmax} = displacement at maximum load, δ_{Fmax} = lateral drift at maximum load, $F_{\Delta max}$= load at maximum displacement, Δ_{max} = maximum lateral displacement, δ_{max} = maximum lateral drift.

Table 6. Performance of other structural systems under cyclic loading

Study	Specimen	D (mm)	L (mm)	Cross-section	f'_c (MPa)	External tube	Internal Reinforcement	P/P_o	$\delta_{0.8Mmax}$ (%)
Han et al. [34]	C-0-2	150	750	Circular	49.6[a]	Carbon FRP[b]	CST[c]	0.02	3.0
	S-0-2	150	750	Square	49.6[a]	Carbon FRP[b]	CST[c]	0.02	3.3
Cho et al. [35]	RC-0	300	1740	Square	28.7	NA	Steel bars[d]	0.07	5.3

D = cross-sectional sectional dimension, L = shear span length, P/P_o = axial load level ($Po = 0.85 f'_c A_c + f_y A_s$), A_c = cross-sectional area of concrete, A_s = cross-sectional area of inner steel tube or reinforcing bars

[a] Cube strength

[b] 2 layers of bi-directional carbon FRP sheets (t_f = 0.17 mm/layer, f_f = 3950 MPa)

[c] Circular steel tube: D_s = 75 mm, t_s = 2.2 mm.

[d] 8 × 13-mm longitudinal bars, and 10-mm bars placed at 100 mm spacing as transverse reinforcement.

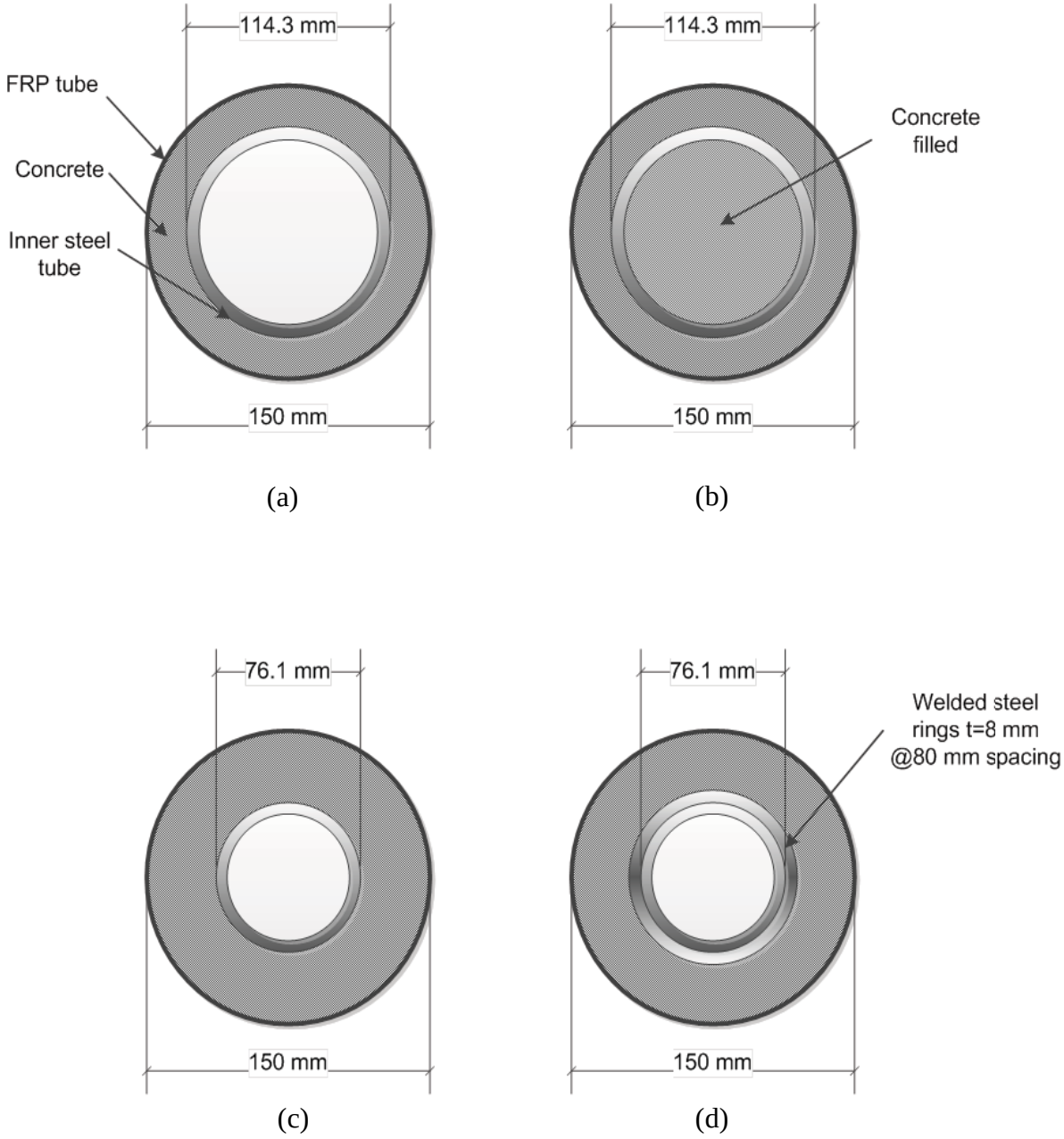

Fig. 1 Beam cross-sections: (a) DSTB-1, (b) DSTB-2, (c) DSTB-3, (d) DSTB-4

Fig. 2. Manufacturing process: (a) Steel tubes; (b) Manufacturing of FRP tubes; (c) Specimens after concrete pouring

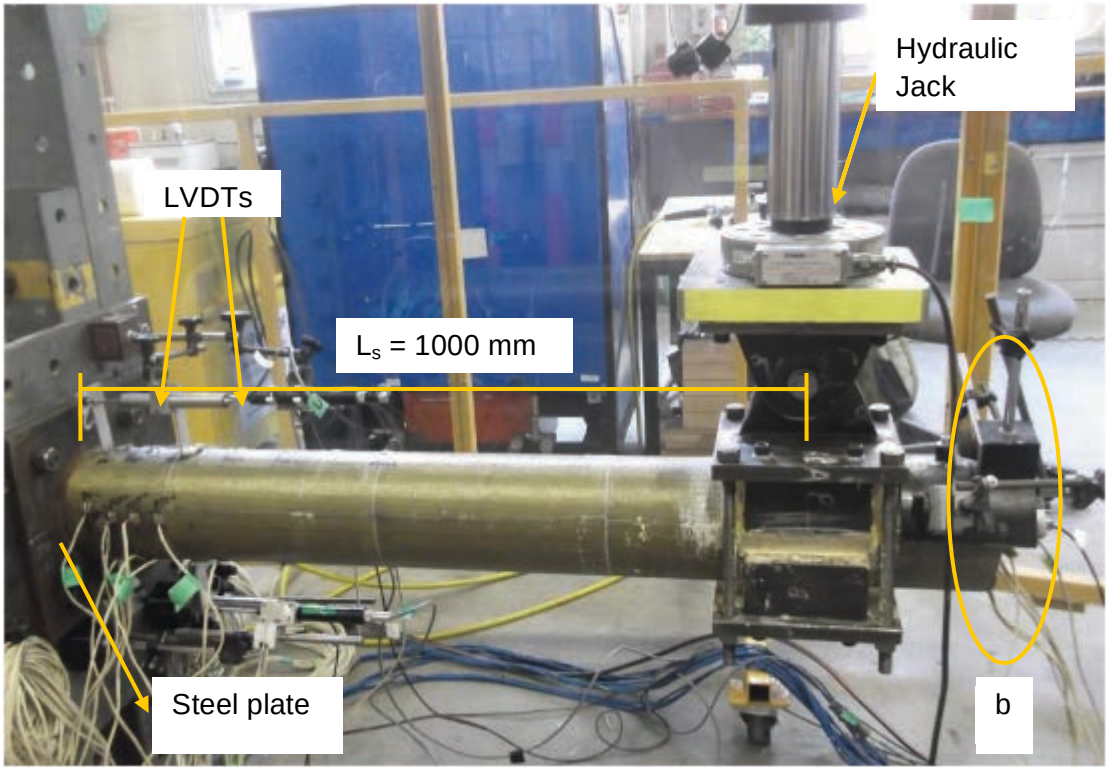

(a)

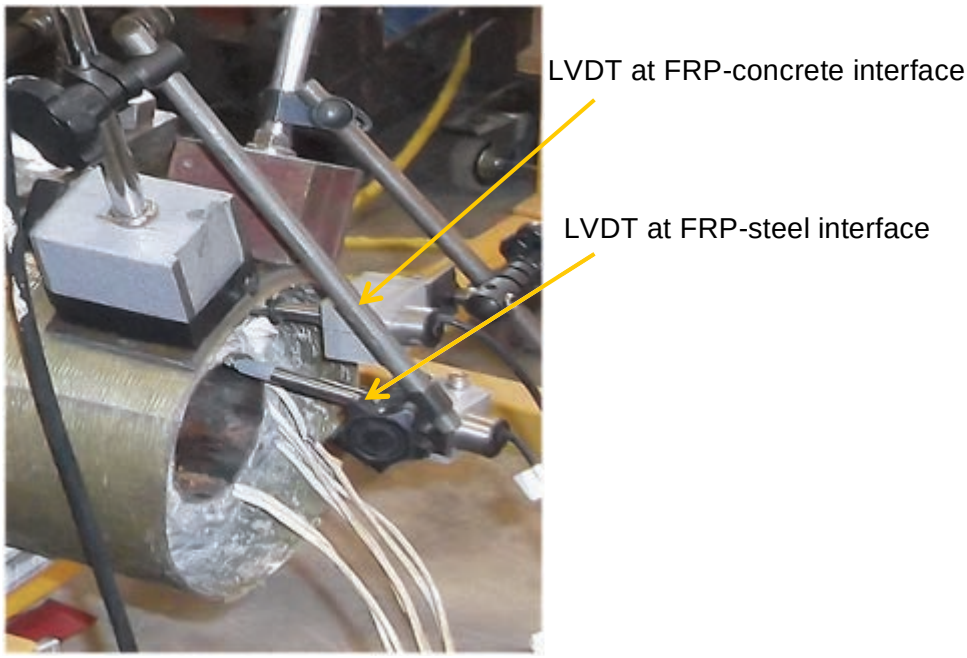

(b)

Fig. 3. (a) Cantilever beam test setup, (b) LVDTs for measuring slips

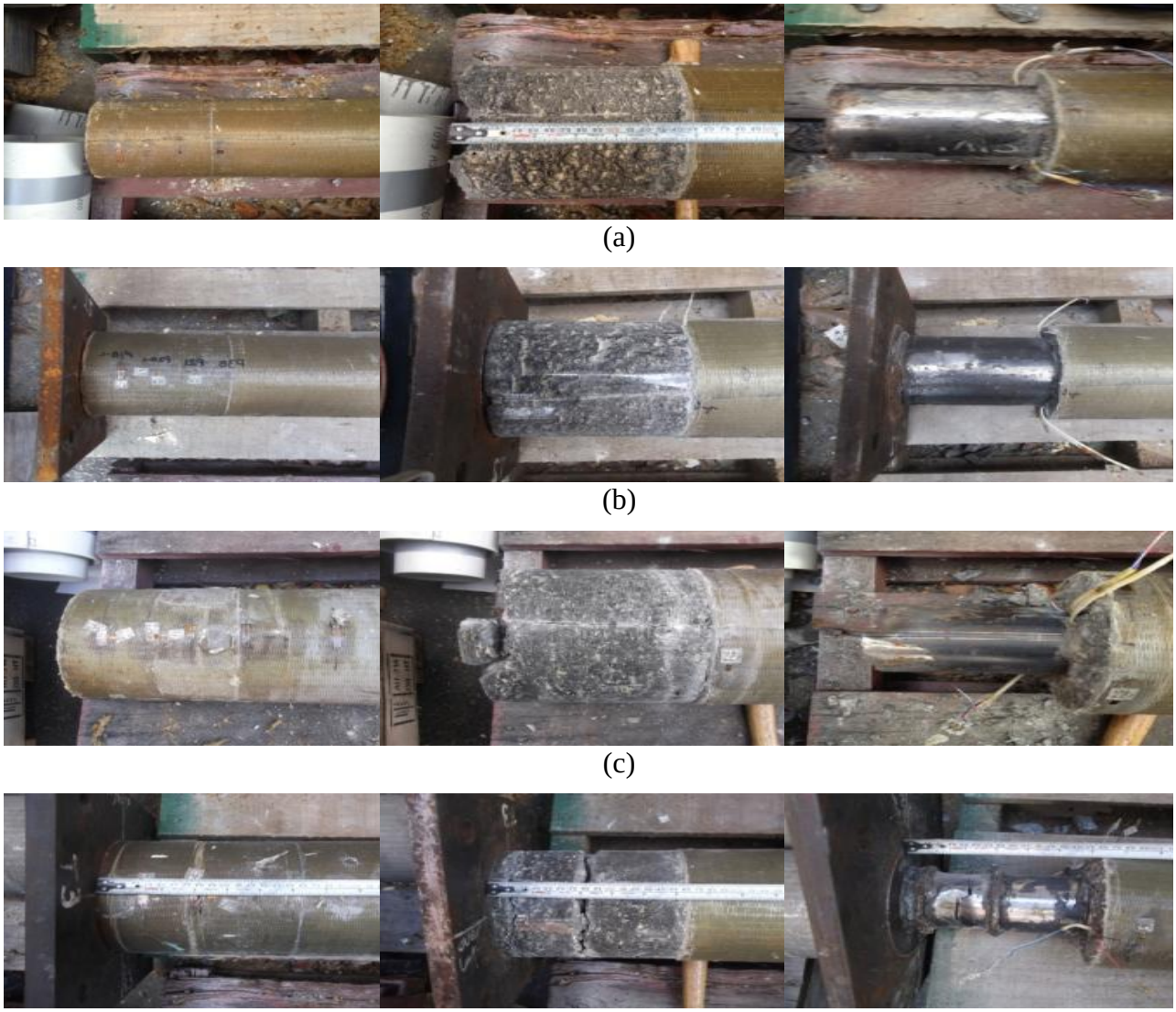

Fig. 4. Specimen damage regions: (a) DSTB-1, (b) DSTB-2, (c) DSTB-3, (d) DSTB-4

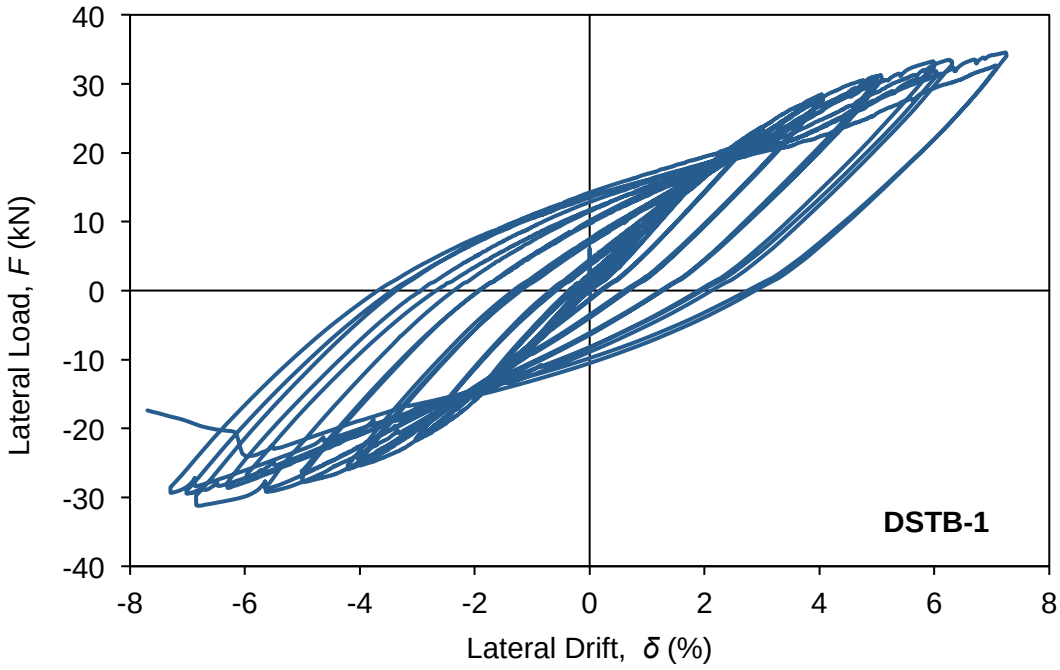
40
30
20
10
0
-10
-20
-30
-40
-8
-6
-4
-2
0
2
4
6
8
Lateral Load, F (kN)
Lateral Drift, δ (%)
DSTB-1

(a)

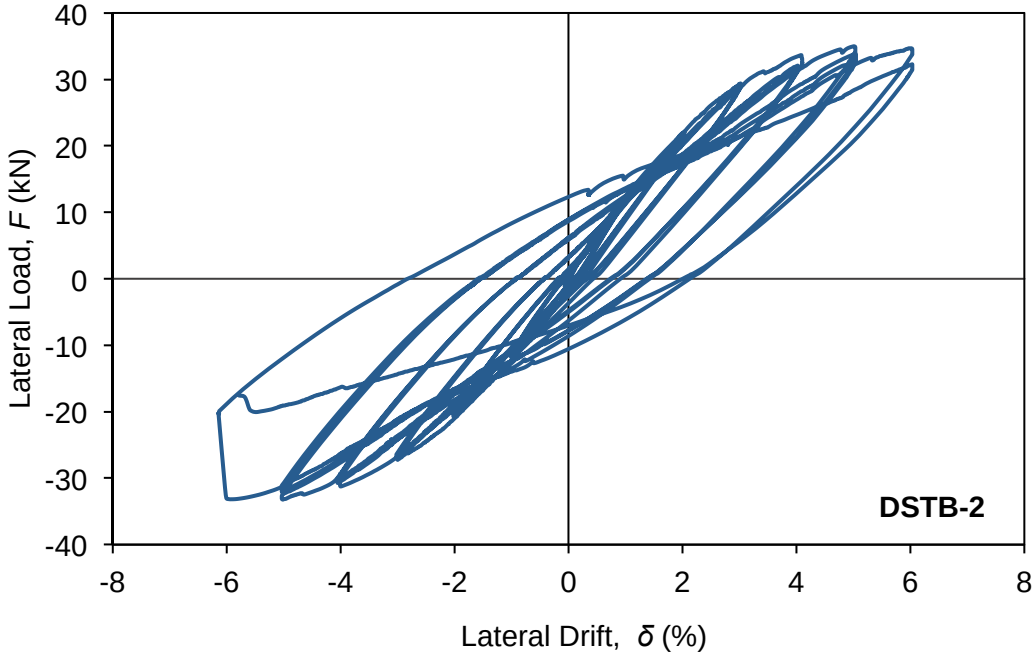
40
30
20
10
0
-10
-20
-30
-40
-8
-6
-4
-2
0
2
4
6
8
Lateral Load, F (kN)
Lateral Drift, δ (%)
DSTB-2

(b)

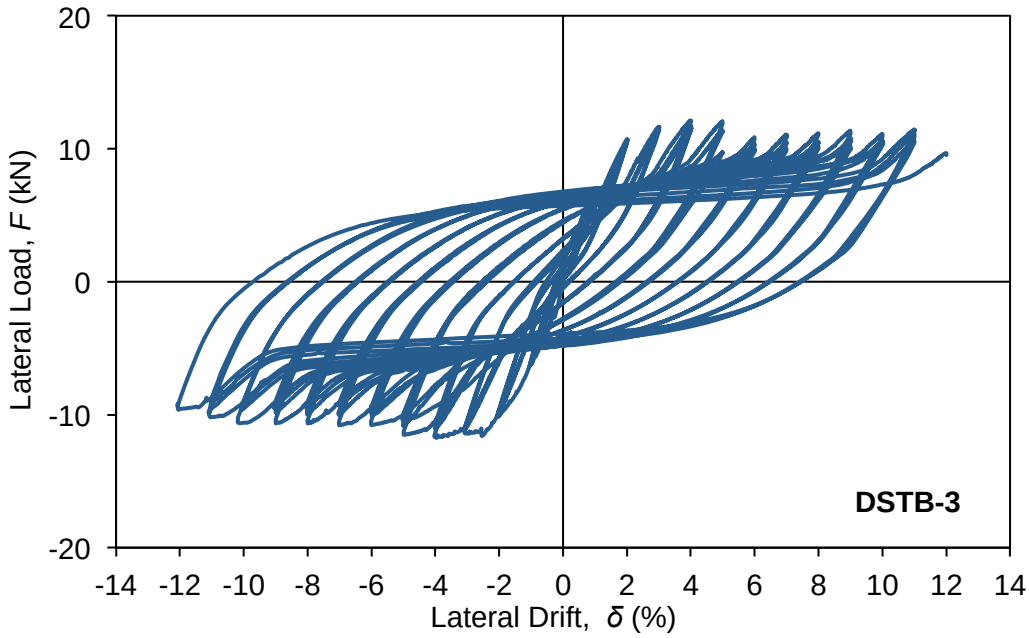

(c)

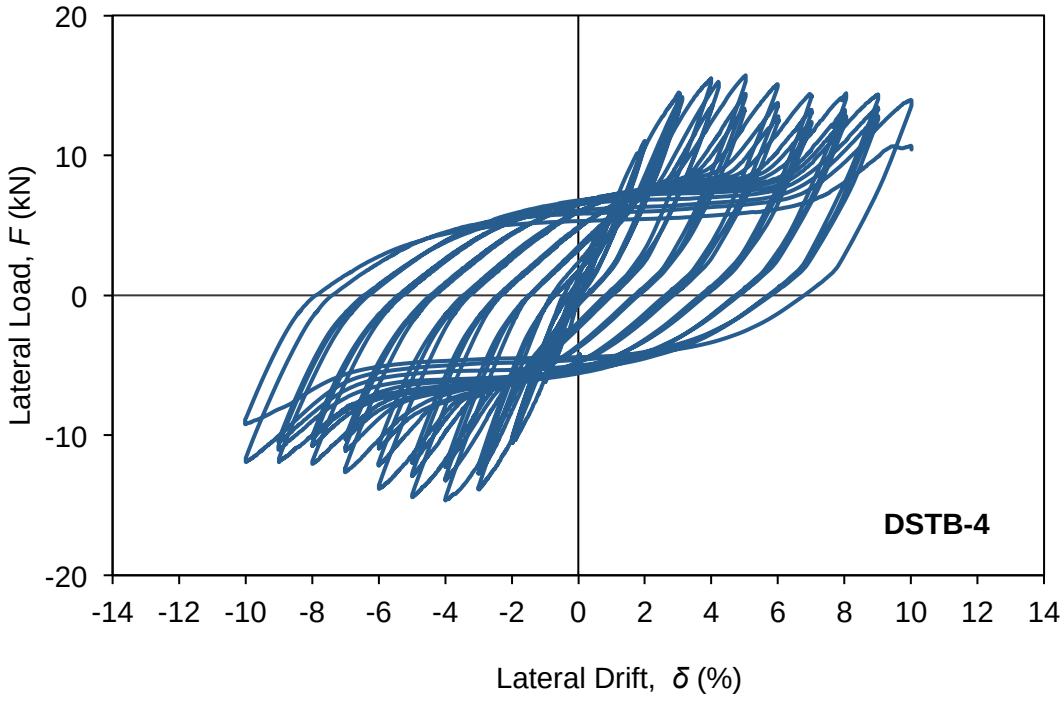

(d)

Fig. 5. Hysteretic lateral load-lateral drift relationships (a) DSTB-1, (b) DSTB-2, (c) DSTB-3, (d) DSTB-4

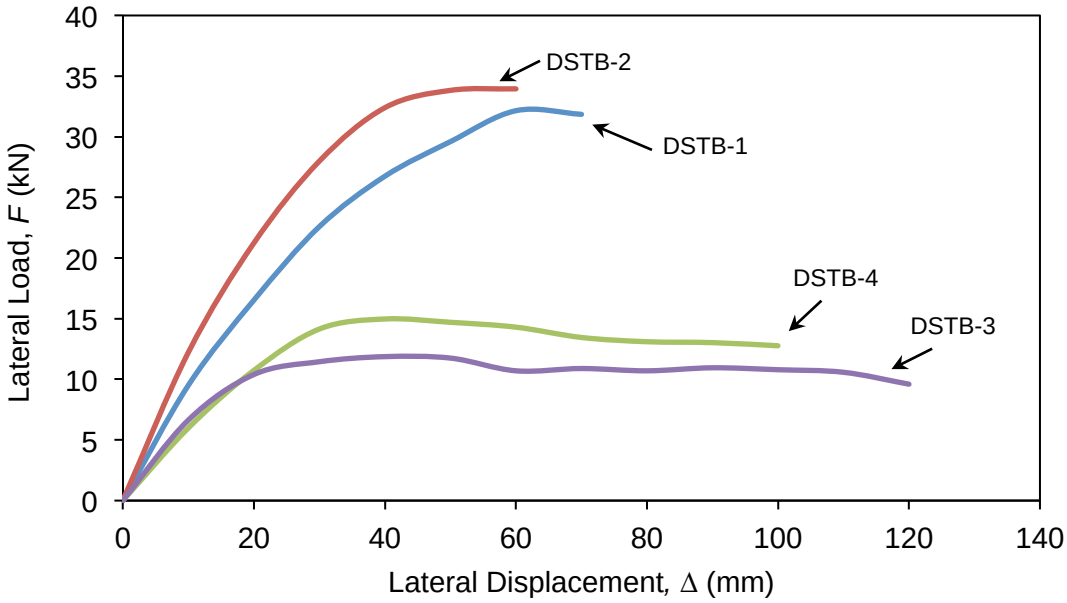

Fig. 6. Envelope curves of beam lateral load-displacement relationships

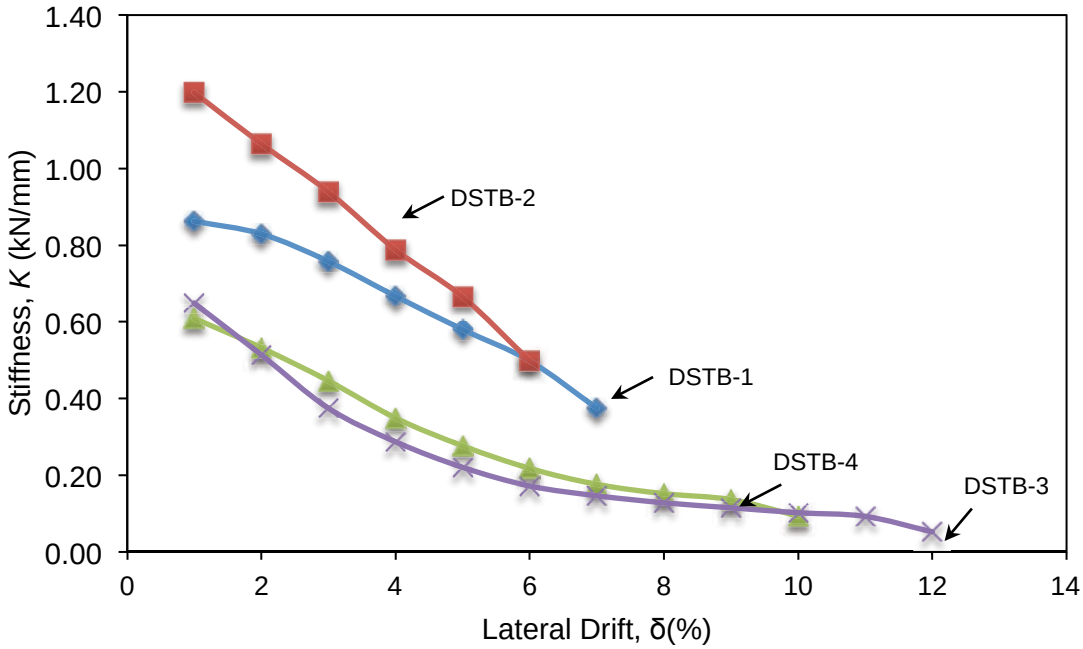

Fig. 7. Variation of beam stiffnesses with lateral drifts

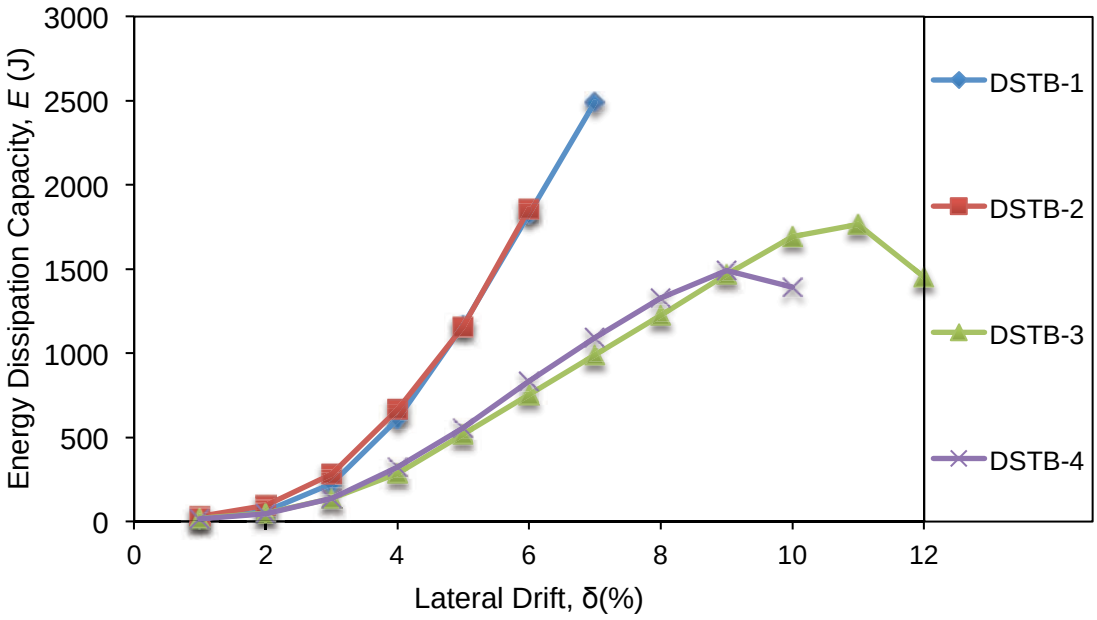

Fig. 8. Specimen energy dissipation capacities

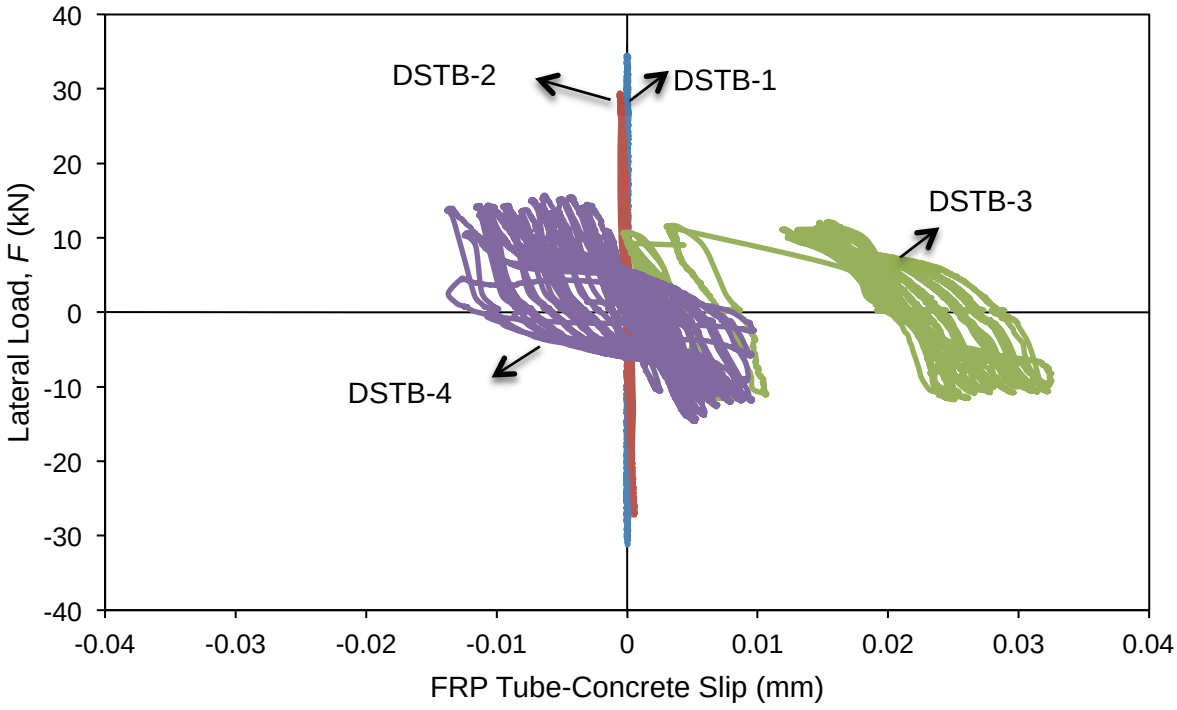

Fig. 9. Load–slip relationships measured between FRP tube and concrete

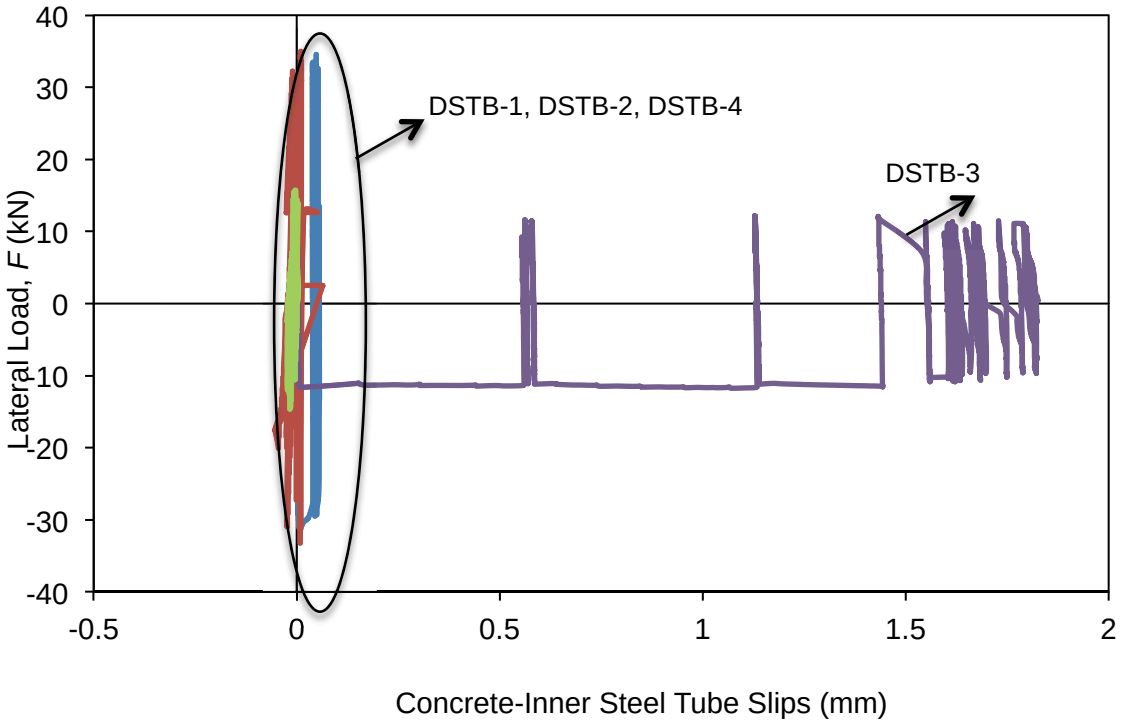

Fig. 10. Load-slip relationships measured between inner steel tube and concrete

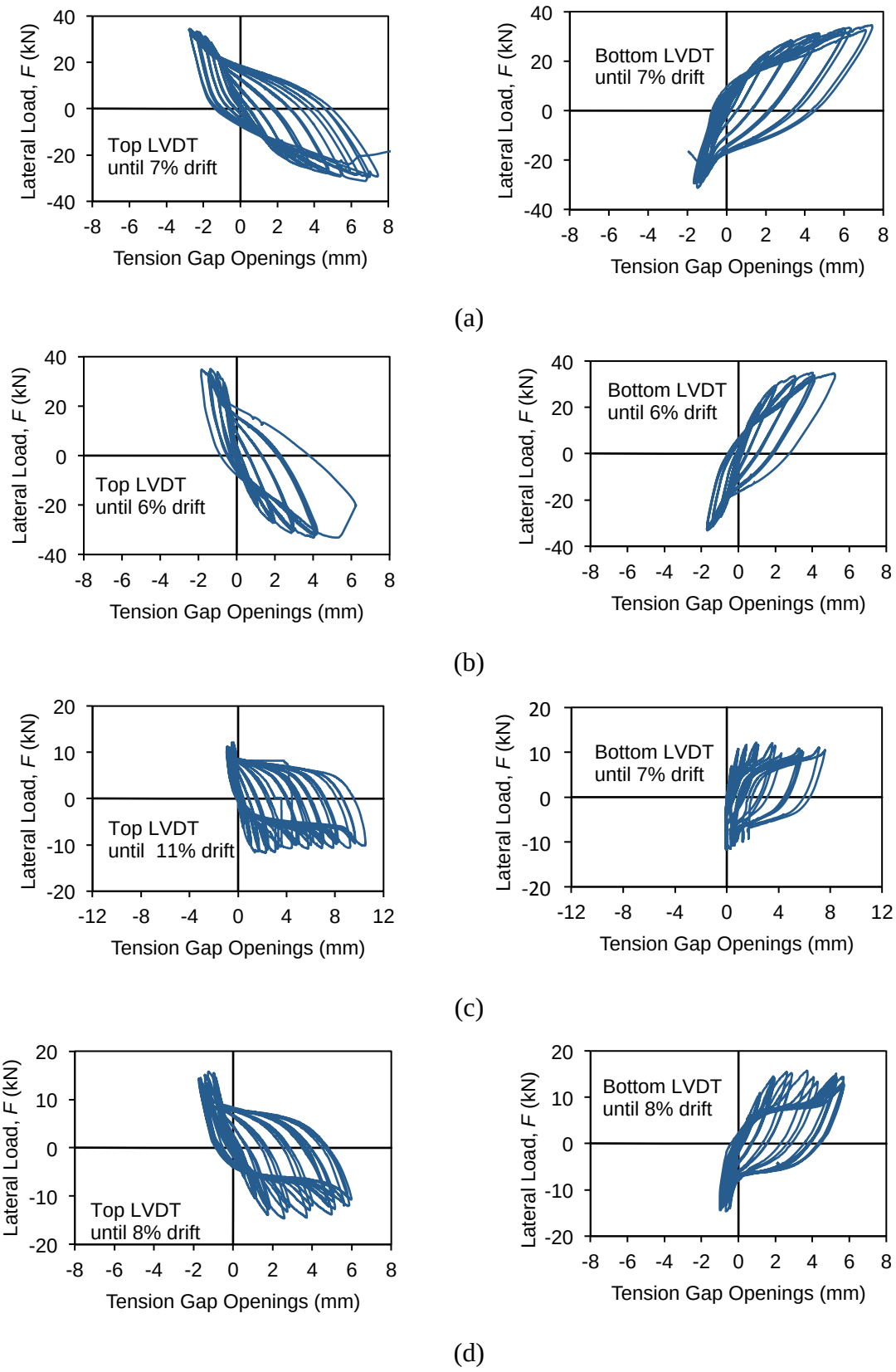

Fig. 11. Tension gap openings measured at beam face: (a) DSTB-1, (b) DSTB-2, (c) DSTB-3, (d) DSTB-4

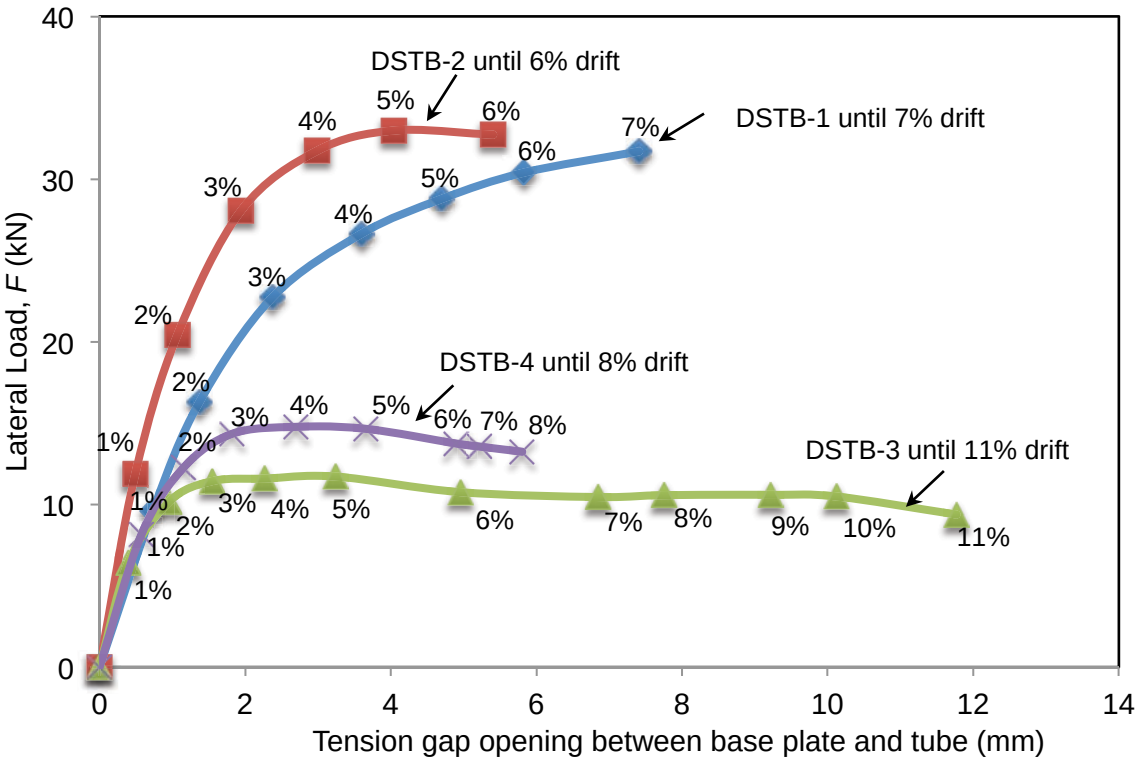

Fig. 12. Lateral load-tension gap opening relationship at specimen base

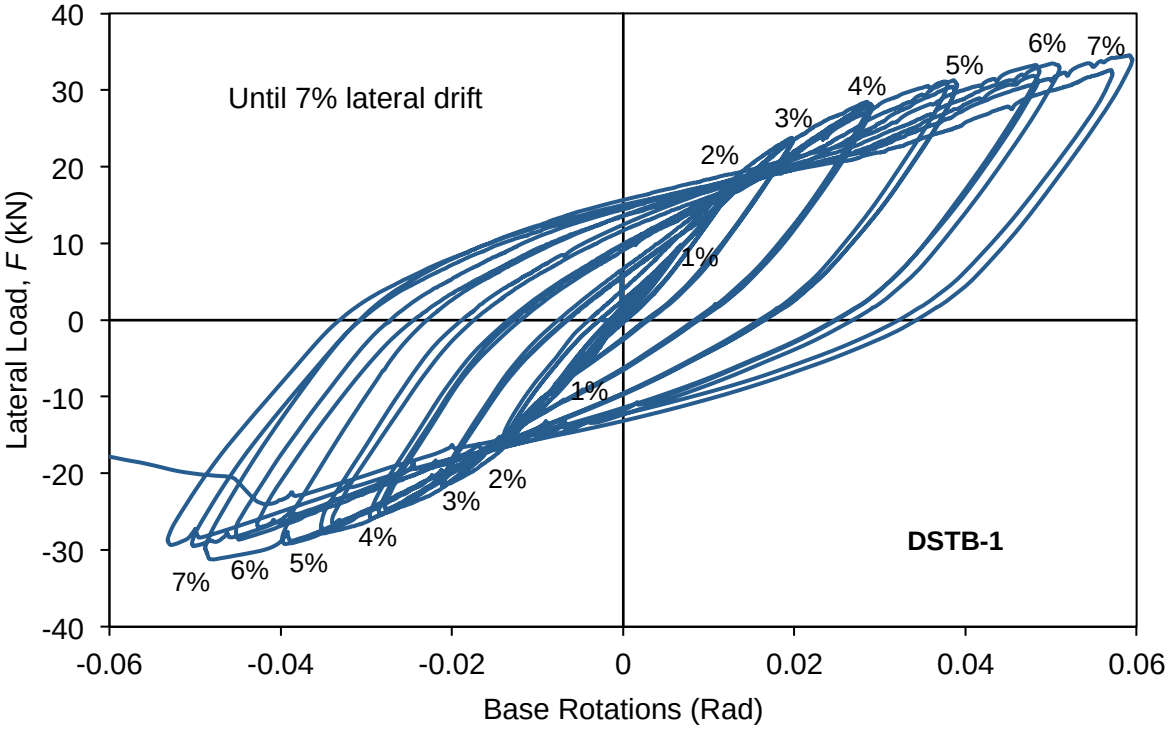
Until 7% lateral drift
Lateral Load, F (kN)
Base Rotations (Rad)
DSTB-1
1%
2%
3%
4%
5%
6%
7%

(a)

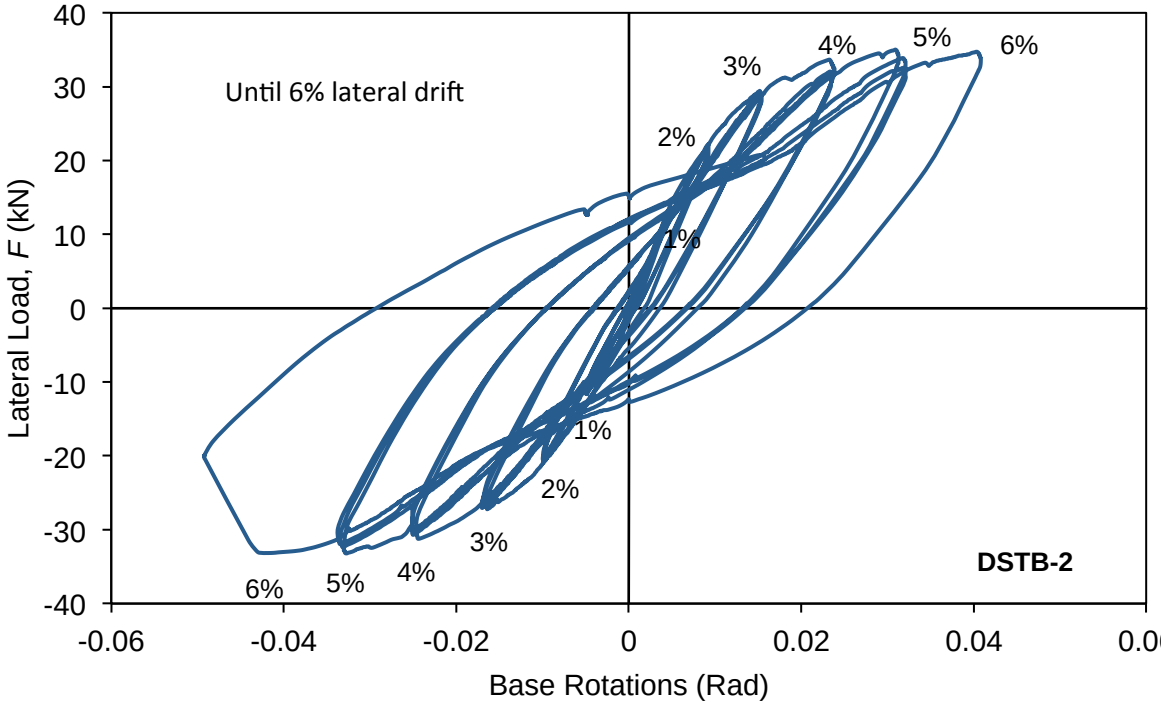
Until 6% lateral drift
Lateral Load, F (kN)
Base Rotations (Rad)
DSTB-2
1%
2%
3%
4%
5%
6%

(b)

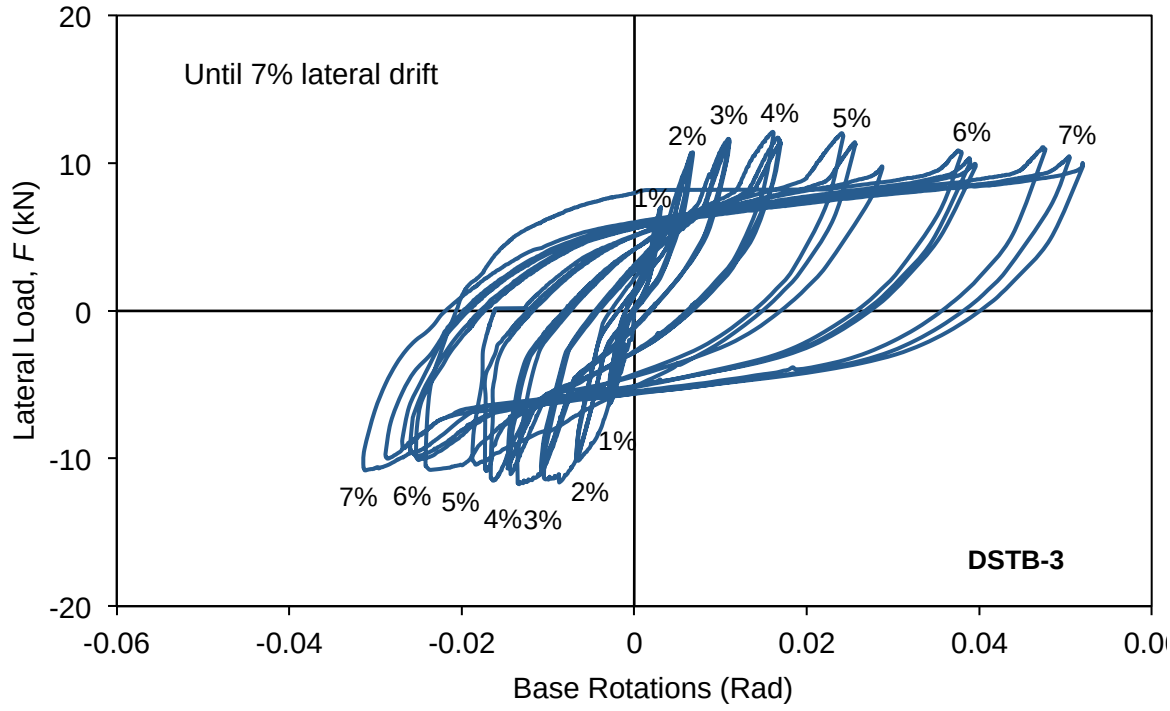

(c)

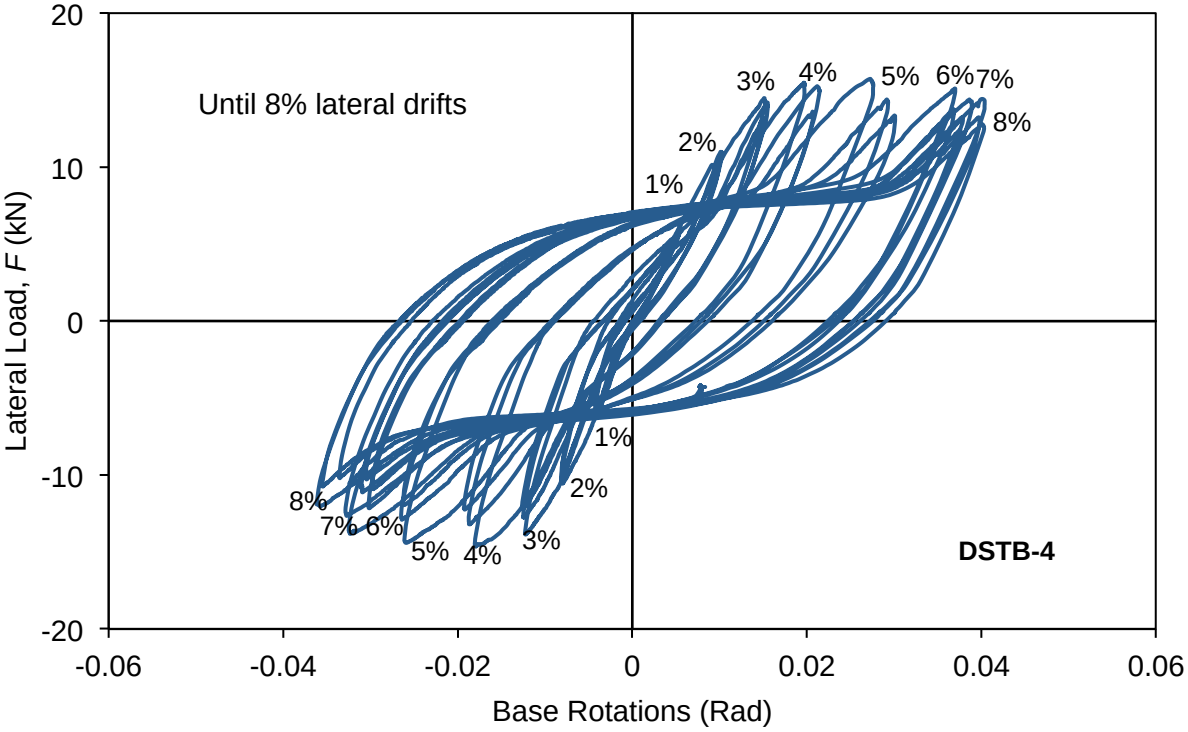

(d)

Fig. 13. Lateral load-base rotation relationships: (a) DSTB-1, (b) DSTB-2, (c) DSTB-3, (d) DSTB-4

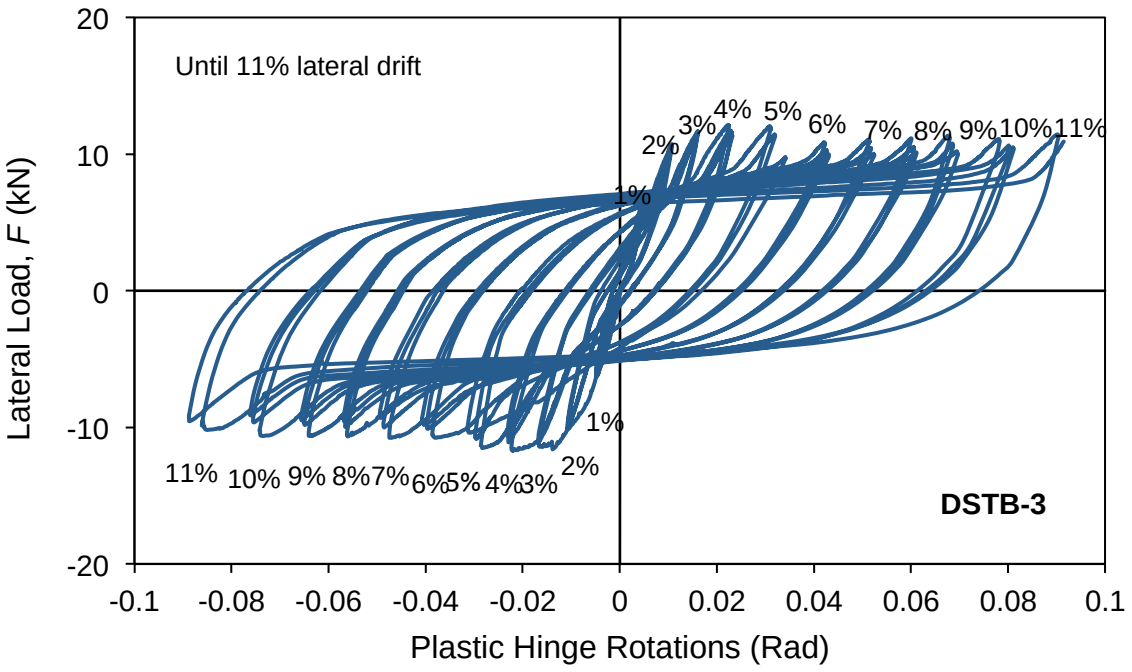

(a)

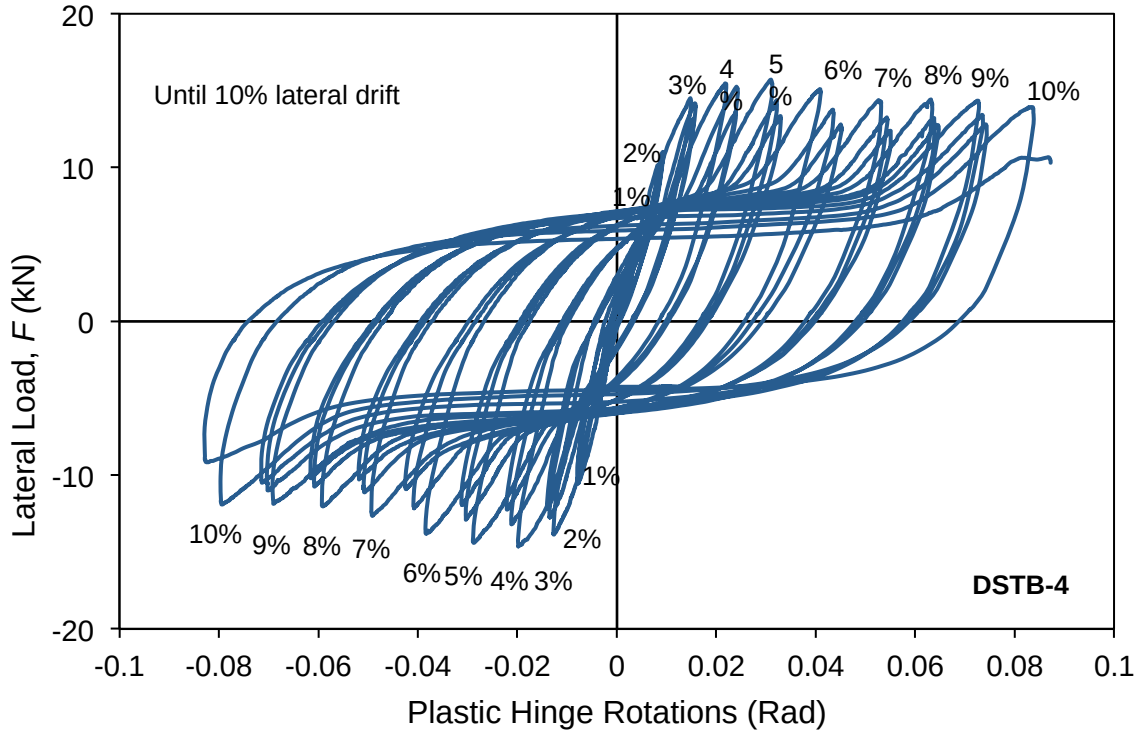

(b)

Fig. 14. Lateral load-plastic hinge rotation relationships: (a) DSTB-3, (b) DSTB-4

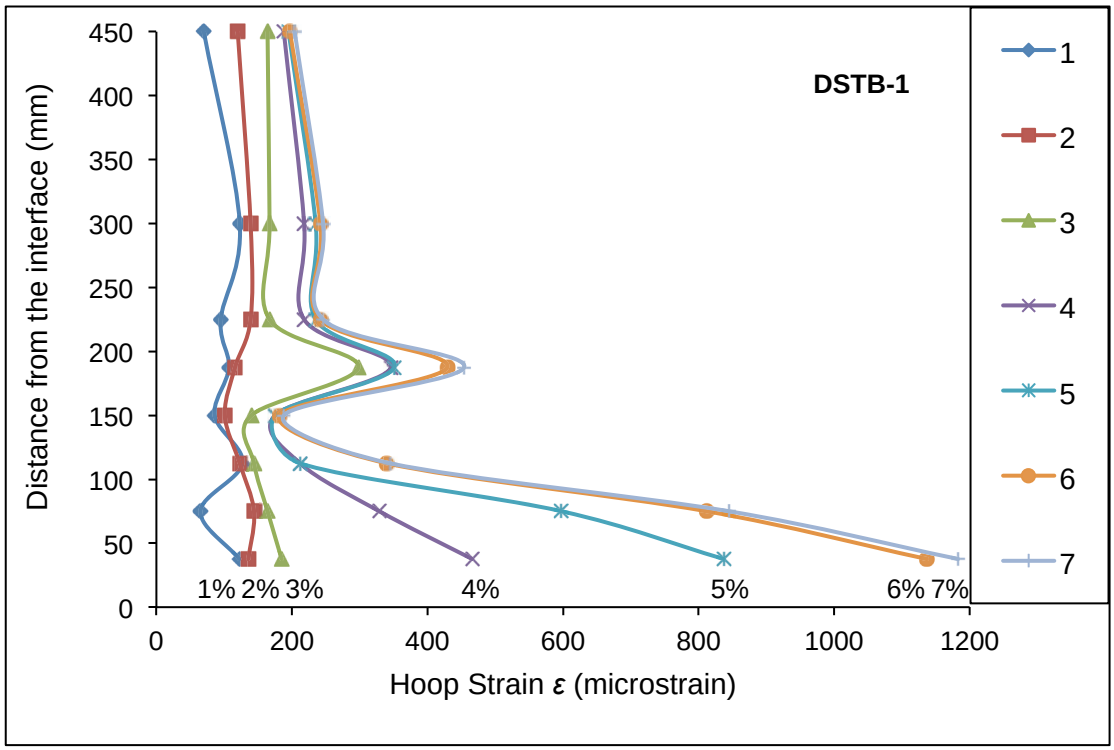
DSTB-1
Distance from the interface (mm)
Hoop Strain ε (microstrain)
1% 2% 3% 4% 5% 6% 7%
1
2
3
4
5
6
7

(a)

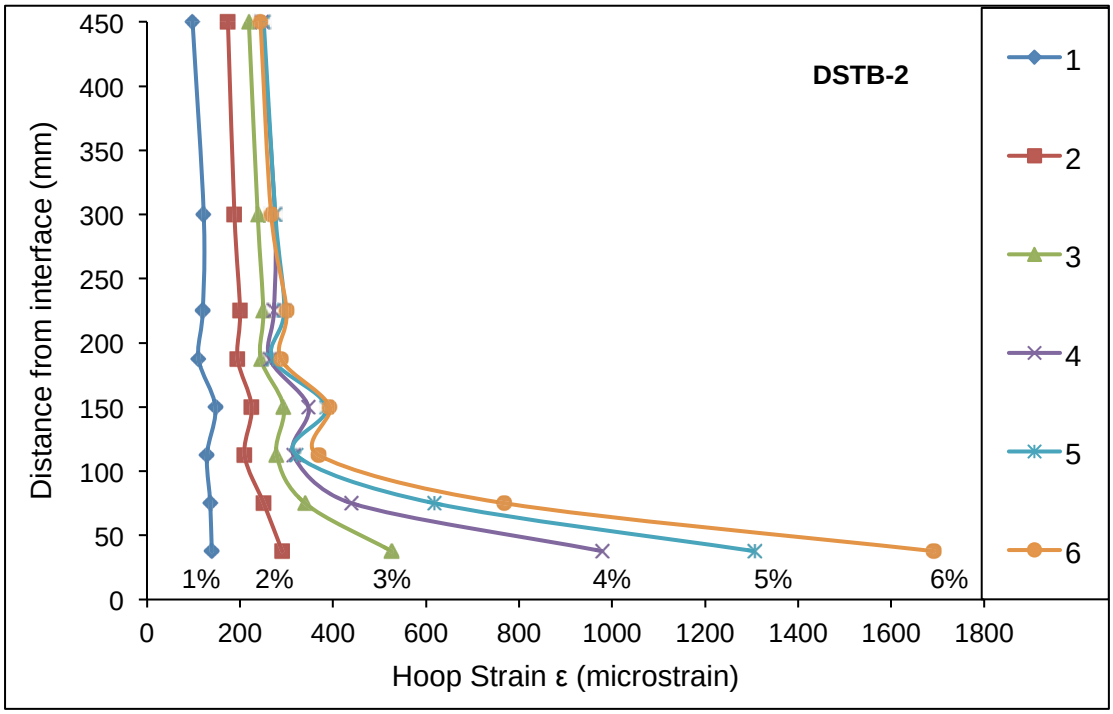
DSTB-2
Distance from interface (mm)
Hoop Strain ε (microstrain)
1% 2% 3% 4% 5% 6%
1
2
3
4
5
6

(b)

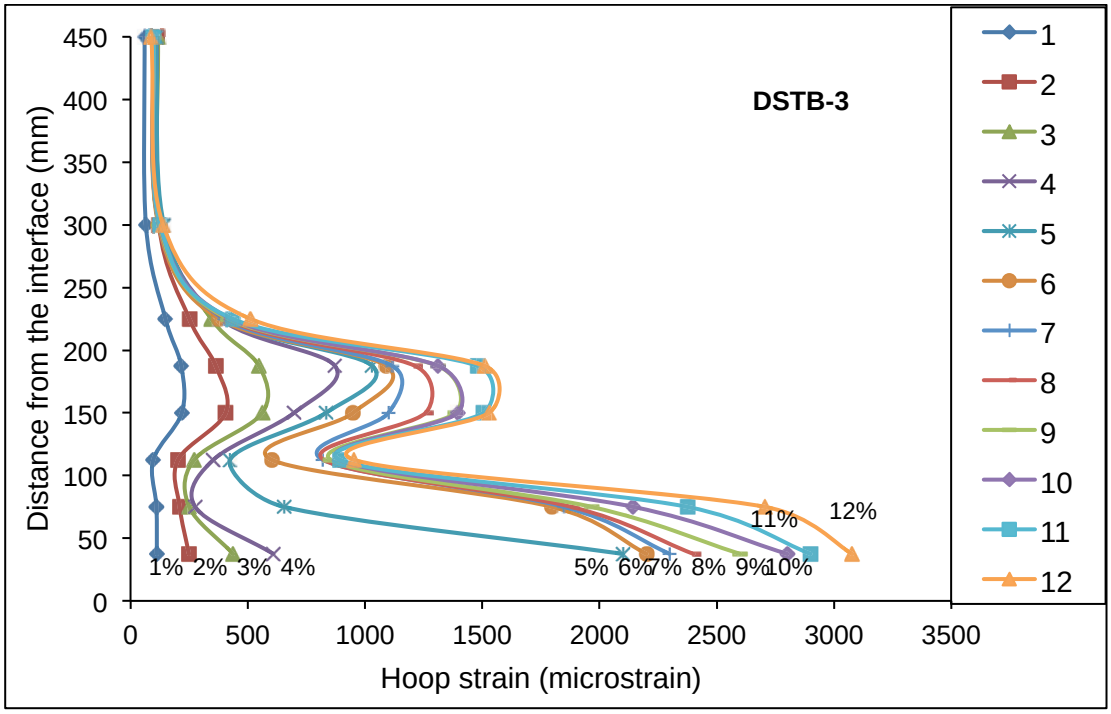

(c)

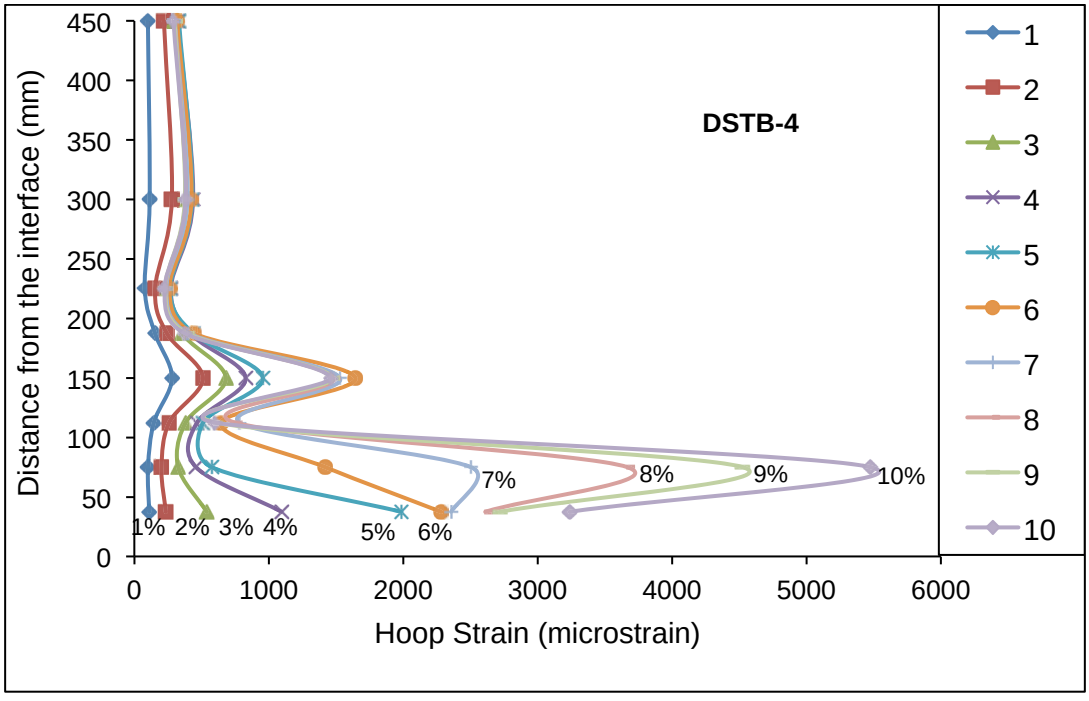

(d)

Fig. 15. Variation of FRP tube hoop strains along the length of beams: (a) DSTB-1, (b) DSTB-2, (c) DSTB-3, (d) DSTB-4

CHAPTER 7

CONCLUSIONS

This thesis has presented a comprehensive study on the behaviour of FRP-concrete-steel composite structural members, namely CFFTs, DSTCs and DSTBs. First, the most influential parameters on the structural behaviour of these composite members were identified, which included the: i) concrete strength, ii) axial load level of columns, iii) presence/absence of a concrete-filling inner steel tube, iv) cross-sectional shape of members, and v) installation of mechanical connectors. Subsequently, a series of experimental studies were undertaken to investigate the behaviour of FRP-concrete-steel composite members under various loading conditions. The results of these studies have demonstrated that DST structural members exhibit a very ductile behaviour under both monotonic and cyclic loading conditions. Findings of this research indicate that DST beams and columns offer an attractive alternative to other composite structural members for use in earthquake-resistant construction of new structures.

Research contributions

This study contributes to improving the understanding on the seismic behaviour of CFFTs and DSTCs, as well as the flexural behaviour of hybrid DSTBs. The specific contributions made by each of the publications presented in this thesis [1-5] are summarized in Table 1. In addition to the journal articles, the work resulted from this research have been shared with the field through three refereed conference papers [6-8].

Recommendations for future research

Further research on the behaviour of DST structural members is suggested. Additional experimental studies are recommended to expand the database of test results, thus accurate empirical models to predict the behaviour of DST structural members can be developed. Analytical and numerical studies are also recommended to gain additional insights into various aspects of the behaviour of DST members including the interactions among each component of the system (i.e. FRP and steel tubes and concrete)

Table 1. Summary of publications and research contributions

Publications	Contributions
Idris and Ozbakkaloglu [1]	This paper reports on an experimental program that investigated the seismic behaviour of high-strength concrete (HSC)-filled fibre reinforced-polymer (FRP) tubes (HSCFFTs), designed as building columns. Five square and one circular CFFT columns were tested under constant axial compression and reversed-cyclic lateral loading simulating seismic loading. This was the first experimental study on the seismic behaviour of HSCFFTs manufactured with aramid FRP (AFRP) tubes.
Ozbakkaloglu and Idris [2]	This paper presents an experimental study on the seismic behaviour of FRP-concrete-steel double-skin tubular (DST) columns. Nine circular DST and one circular concrete-filled FRP-tube (CFFT) columns that were manufactured with HSC were tested under constant axial compression and reversed-cyclic lateral loading. The experimental study reported in this paper was first to investigate the seismic behaviour of Aramid FRP (ARFP) confined high-strength concrete (HSC) DST columns.
Idris and Ozbakkaloglu [3]	This paper presents an experimental investigation, which was designed to study the behaviour of square FRP-HSC-steel DSTCs under simulated seismic loading. Six FRP-concrete-steel DST columns that were manufactured using HSC were tested under combined axial compression and reversed-cyclic lateral loading. This was the first experimental study reported to date on the seismic behaviour of square high-strength concrete (HSC) DST columns.
Idris and Ozbakkaloglu [4]	This paper reports on an experimental study on the flexural behaviour of FRP-HSC-steel composite beams. Seven double-skin tubular beams (DSTBs) and a concrete-filled FRP tube (CFFT) beam with an internal steel I-beam were tested as simply supported beams in four-point bending. The study presented in this paper was the first experimental study on the flexural behaviour of HSC DSTBs.
Idris and Ozbakkaloglu [5]	This paper presents an experimental study on the cyclic behaviour of FRP-concrete-steel DSTBs. Four DSTBs constructed of HSC were tested under reversed-cyclic lateral loading. This was the first study to investigate the behaviour of DSTBs under lateral cyclic loading.

REFERENCES

[1] Idris, Y., and Ozbakkaloglu, T. (2013). "Seismic behavior of square high-strength concrete-filled FRP tube columns." *Journal of Composites for Construction, ASCE,* 17(6): 04013013.

[2] Ozbakkaloglu, T., and Idris, Y. (2014), "Seismic behavior of FRP-high-strength concrete-steel double skin tubular columns." *Journal of Structural Engineering, ASCE,* 140(6): 04014019.

[3] Idris, Y., and Ozbakkaloglu, T. (2014). "Flexural behavior of FRP-HSC-steel composite beams." *Thin-Walled Structures*, 80: 207-16.

[4] Idris, Y., and Ozbakkaloglu, T. (2015). "Flexural behavior of FRP-HSC-steel tubular beams under reversed cyclic loading." *Thin-Walled Structures*, 87: 89-101.

[5] Idris, Y., and Ozbakkaloglu, T. (2015). "Behavior of square FRP-HSC-Steel double-skin tubular columns under combined axial compression and reversed-cyclic lateral loading." *(submitted to Engineering Structures).*

[6] Idris, Y., and Ozbakkaloglu, T. (2013). "Behavior of high-strength concrete-filled FRP tube columns under simulated seismic loading: an experimental study." *Advanced Materials Research*, 743: 39-44.

[7] Idris, Y., and Ozbakkaloglu, T. (2014). "Flexural behavior of hybrid double-skin-tubular beams." *Advanced Materials Research*, 838: 525-529

[8] Idris, Y., and Ozbakkaloglu, T. (2014). "FRP-concrete-steel double skin tubular cantilever beams: behaviour under cyclic loading." *Applied Mechanics and Materials*: 752-753.